Early-Age Behavior of Lightweight Aggregate Concrete

by

Benjamin Edwin Byard

A dissertation submitted to the Graduate Faculty of
Auburn University
in partial fulfillment of the
requirements for the Degree of
Doctor of Philosophy

Auburn, Alabama
December 12, 2011

Keywords: earl-age concrete, cracking, autogenous shrinkage, relaxation, compliance, lightweight aggregate, internal curing

Approved by

Anton K. Schindler, Chair, Associate Professor and Director of the
Highway Research Center
Robert W. Barnes, James J. Mallett Associate Professor of Civil Engineering
James S. Davidson, Associate Professor of Civil Engineering
George T. Flowers, Dean of Graduate School

Abstract

Early-age cracking can be a severe problem in concrete as it can reduce the service life of the structure. In this project the early-age behavior of concrete was measured, evaluated, and modeled. The early-age stress development of concrete was measured with rigid cracking frames. The free strain was measured with a free-shrinkage frame and corrugated tubes. Rigid cracking frames measure the stress development of concrete due to thermal and autogenous effects from setting until the onset of cracking. The stress and strain development of match-cured concretes with various water-cement ratios, densities, and curing temperatures were measured. Mixtures with various proportions of expanded clay, shale, and slate lightweight coarse and fine aggregates were examined, and their behavior was compared to that of normalweight control mixtures. The effects that mechanical properties and internal curing have on cracking tendency, stress development due to autogenous stress, and stress relaxation were examined. The B3 compliance model was modified to accurately model the early-age stress development, and the effect of lightweight aggregates on relaxation was examined.

Increasing the amount of pre-wetted lightweight aggregate in the concrete systematically decreases the density, modulus of elasticity, coefficient of thermal expansion, and thermal diffusivity of the concrete. When compared to a normalweight control concrete, the use of lightweight aggregates in concrete effectively delays the occurrence of cracking at early ages in bridge deck applications. The use of pre-wetted

lightweight aggregates in concrete can reduce or eliminate the stress development caused by autogenous shrinkage. The decrease in autogenous stresses is due to internal curing, because water desorbed from the lightweight aggregates fills capillary voids formed by chemical shrinkage. The B3 Model is a compliance model that was designed and calibrated to estimate the instantaneous and time-dependent strain behavior of mature concrete with an age of one day or more. Modifications to the B3 Model were made that provide a better fit to early-age stress data. Using the Modified B3 Model, it was found that the reduced modulus of elasticity of the lightweight aggregate increases the amount of relaxation compared to normalweight aggregates; and decreasing the water-cement ratio, with constant paste volume, increased the paste quality and decreased relaxation. A simplified version of the Modified B3 Model is proposed that has minimal loss of accuracy compared to the Modified B3 Model.

Acknowledgments

I sincerely thank Dr. Anton Schindler for his endless technical guidance, time, and friendship. I would also like to thank Dr. Robert Barnes and Dr. James Davidson for their time and contribution to this dissertation. Billy Wilson, Matt Peters, Kevin Keith, Richard Weakly, Paul Coulston, Adam Wilkinson, John Moss, Patrick Kimmons, and Jason Meadows deserve thanks for without them this this project could not have been completed.

I would also like to thank the members of the Expanded Shale, Clay and Slate Institute for their financial support. I would like to specifically thank John Ries, Ken Harmon, Reid Castrodale, Jody Wall, Ernest Cubit, George Grygar, Don Reeves, and Andrew Mackie for all their technical support, time, and guidance.

I would like to recognize my mother- and father-in-law Diane and Terry Hughes for their encouragement and allowing me to take their daughter out of Vol country. I would like to thank my family, Clyde, Barbara, Adam, and Amanda, for their infinite support, keeping me grounded, and reminding me that I will, in fact, have to get a real job one day. I would also like to thank my son Augustus for giving me perspective through the process of finishing a dissertation. I would like to thank most of all, my best friend and wife Tera who agreed to move into a trailer in Alabama with me. Without her support, encouragement, and advice I would have never started, let alone finished this project.

Table of Contents

List of Tables

List of Figures

CHAPTER 1

INTRODUCTION

1.1 Background

Cracking of hardening concrete occurs when the induced tensile stress exceeds the tensile strength of the concrete. The development of in-place stresses is affected by the coefficient of thermal expansion, setting characteristics, restraint conditions, stress relaxation (creep-adjusted modulus of elasticity), capillary stresses, and temperature history of the hardening concrete. The tensile strength (and tensile strain capacity) increases as the hydration of the cementitious system progresses. The tensile strength is impacted by the cementing materials, the water-cement ratio *(w/c)*, the aggregate type and gradation, the degree of curing (internal/external) provided, and the temperature history of the hardening concrete. Quantification of many of the mechanisms mentioned above is quite complicated at early ages, and many of these variables have complex interactions.

Early-age cracking of concrete bridge decks, typically caused by thermal effects, drying shrinkage, and autogenous shrinkage, can have detrimental effects on long-term behavior and durability. Darwin and Browning (2008) reported that "by controlling early age cracking, the amount of cracking at later ages should remain low," and that early-age cracking can significantly increase the rate and amount of chloride penetration (from deicing salts), which may accelerate the corrosion rate of embedded reinforcing steel.

Transverse deck cracking occurs in most geographical locations and climates, and in many types of bridge superstructures (Krauss and Rogalla 1996). The National Cooperative Highway Research Program (NCHRP) Report 380 (Krauss and Rogalla 1996) reported results of a survey sent to all U.S. Departments of Transportation (DOTs) and several transportation agencies overseas to evaluate the extent of deck cracking. 62 percent of the responding agencies considered early-age transverse cracking to be problematic. A survey conducted by the Federal Highway Administration (FHWA) found that more than 100,000 bridges suffer from early-age cracking (FHWA 2008). Given the abundance of cracking observed in bridge decks, and the impact of early-age cracking on long-term performance and durability, it is imperative that bridge deck concrete be proportioned and placed to minimize early-age cracking and to optimize hardened properties.

Optimizing hardened properties requires proper curing to promote hydration. However, with lower *w/c* bridge deck mixtures that have lower permeability, topical curing or sealing techniques are often not effective enough to maintain adequate internal moisture to maximize hydration and minimize self-desiccation (Rilem TC 196 2007).

Internal curing is the maintenance of high moisture contents in the placed concrete by incorporating pre-wetted absorptive materials into the mixture during batching. The pre-wetted materials act like internal reservoirs that release their water as drying occurs. The release of the internal curing water increases cementing material hydration and reduces capillary stress caused by self-desiccation (Jensen and Hansen 2001). Decreasing the capillary stress reduces, the stress developed from autogenous

shrinkage. The increased hydration increases the strength of the hardened concrete (Mehta and Monteiro 2006).

There are many models in literature to estimate the creep of mature concrete including the B3 (Bažant and Baweja 2000), ACI 209R-92 (ACI 209 1992), CEB MC90 (CEB 1999), and the GL2000 (Gardner and Lockman 2001). These models were calibrated with mature, well hardened concrete. Because of this, the initial loading age that these models were calibrated for is 1-day or later. Concrete at early ages behaves much differently than mature concrete. Immediately after setting, concrete undergoes a rapid change in mechanical properties. Early-age concrete has significantly greater elastic and viscoelastic behavior (Emborg 1989; Westman 1999; Gutch and Rostásy 1995). For concrete placed in restrained conditions such as bridge decks, culverts, tunnels, retaining walls, and tanks, the early-age relaxation properties are essential to determine so that designers can minimize early-age cracking. By minimizing early-age cracking, the durability of structures can be improved.

1.2 Research Approach

In this project, the effect that the use of lightweight aggregate (LWA) has on the early-age stress development and cracking tendency of concrete was evaluated by cracking frame testing techniques. Cracking frames can measure the development of stresses due to thermal and autogenous shrinkage effects from setting until cracking (Mangold 1998). The combined effect of modulus elasticity, relaxation, coefficient of thermal expansion, thermal conductivity, autogenous shrinkage, and tensile strength on the cracking potential in a specific application is thus directly captured and quantified by this unique test setup.

Since the specimen is sealed against water loss, the effect of drying shrinkage is not measured with this setup.

A rigid cracking frame as developed by Dr. Rupert Springenschmid at the Technical University of Munich, Germany was utilized in this research project. The two rigid cracking frames used at Auburn University during this project are shown in Figure 1-1. These cracking frames were designed to produce restraint for 6 x 6 x 50 in. concrete specimens from placement to approximately six days. Each cracking frame consists of two crossheads and a pair of stiff Invar steel sidebars. The crossheads are designed to grip the concrete specimen while the sidebars provide restraint as the concrete hardens. The Invar steel sidebars are sized to provide approximately 80 percent restraint to movement for the hardened concrete and strain gauges are used to continuously measure the stress state in the concrete specimen as it hardens in the frame. The frame is designed to allow fresh concrete to be cast into temperature-controlled formwork attached to the frame. With this unique formwork, the concrete can be subjected to a variety of temperature profiles that simulate in-place conditions of bridge decks, elevated slabs, pavements, mass concrete structures, etc.

Due to the increased insulation ability of lightweight aggregate, its use in concrete mixtures has been reported to increase the temperature rise due to hydration measured during the construction of the new Benecia-Martinez Bridge (Maggenti 2007). This increase in temperature rise may not translate to increased thermal cracking risk, because thermal cracking risk is also a function of the concrete strength and stress development. Lightweight aggregate has a lower modulus of elasticity, lower coefficient of thermal expansion, and provides internal curing to the concrete. These characteristics may reduce

the stress and counter the effects caused by its increased temperature development (Byard et al. 2010).

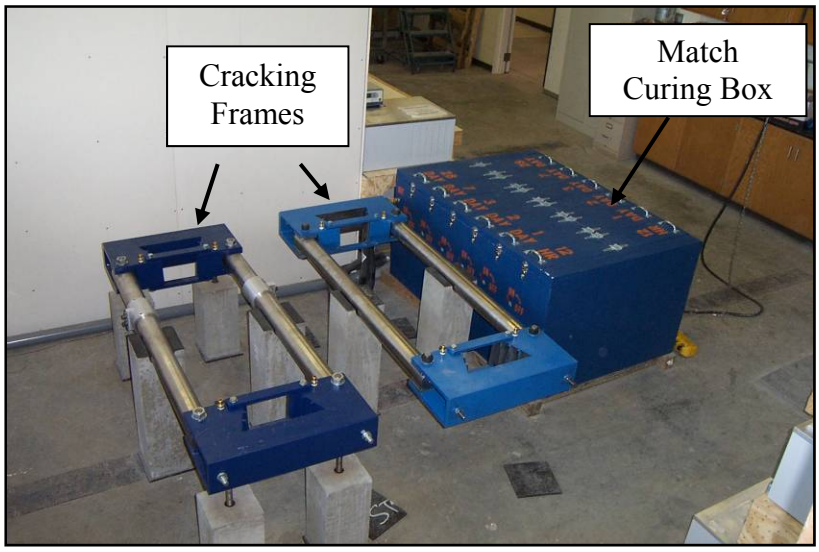

Figure 1-1: Test equipment to assess the early-age stress development of concrete mixtures

1.3 Lightweight Aggregates

Rotary kilns are commonly used to produce lightweight aggregate (LWA) under controlled conditions (Chandra and Berntsson 2002). Historically, LWA have been used to reduce the density of concrete. However, LWA can be used to alter more than just the density of concrete. Because lightweight aggregates have high absorption capacities when compared to conventional aggregates, they provide internally stored water that may become available if needed. These internal water supplies can provide additional water for hydration as well as reduce the effects of self-desiccation and thus autogenous shrinkage effects (Henkensiefken 2008). Limited work has been done to determine the cracking tendency of bridge deck concrete with lightweight aggregate. It is thus

necessary to determine the effect of lightweight aggregate on the cracking tendency of bridge deck concrete. The effect of different amounts of internal curing water provided by lightweight aggregate needs to be evaluated to determine the appropriate proportion of LWA in the mixture.

1.4 Research Objectives

The primary objective of the research is to evaluate the effect lightweight aggregate has on early-age concrete behavior. This was done by first determining the early-age stress development and cracking tendency of various density concretes. Then, the development of autogenous effects was determined for mixtures with lower *w/c*. Finally, an early-age relaxation compliance model was modified to determining the effect of lightweight aggregate on early-age stress relaxation. The research presented in this dissertation is divided into three stand-alone parts. The research described in Part I had the following objectives:

- Develop and evaluate the cracking tendency of three types of lightweight aggregate bridge deck concretes relative to a typically used normalweight concrete mixture,
- Evaluate the effect of placement and curing temperature on the cracking tendency of concrete,
- Determine the mechanical properties of lightweight aggregate concrete and determine their effect on the early-age cracking tendency,

- Evaluate the effect of three different sources of lightweight aggregates (shale, clay, and slate) on the development of mechanical properties and the cracking tendency of bridge deck concrete,

The focus of Part II is to evaluate the behavior of different internal curing mixtures compared to a control mixture. The research described in Part II was focused on the following objectives:

- Evaluate the effect of water-cement ratio and internal curing on the development of stresses and occurrence of cracking at early ages,
- Evaluate the effect of various amounts of internal curing water on the degree of hydration and compare the degree of hydration to some published models,
- Evaluate the effect of water-cement ratio and different amounts of internal curing water on autogenous shrinkage and stress development of concrete specimens, in addition to autogenous shrinkage development of mortar specimens.

The focus of Part III is to develop a model to estimate the stress development of early-age concrete. The research described in Part III include the following specific objectives:

- Model the early-age stress development from the free-shrinkage strain development to accurately predict the measured early-age stress development ,
- Perform a sensitivity analysis to determine the variables that significantly affect the early-age stress development.
- Determine the effect of density, water-cement ratio, and curing temperature on early-age stress development.

1.5 Dissertation Outline

This dissertation is divided into three parts. Part I focuses on the cracking tendency of bridge deck concretes, Part II on the effect of internal curing on early-age hydration and self-desiccation behavior, and Part III on modeling early-age stress development of concrete. Each part focused on significantly different aspects of early-age behavior; thus, each part was written to be a stand-alone document.

The first part describes an investigation of the cracking tendency of lightweight aggregate concrete. Shale, clay, and slate lightweight aggregates from across the country were evaluated in internal curing, sand-lightweight and all-lightweight bridge deck mixtures, each. The mixtures were tested in rigid cracking frames match-cured to modeled summer and fall placement scenarios. The stress development was measured from placement until the onset of cracking. Another cracking frame measured the isothermal stress development to determine the stress development due to autogenous shrinkage. In addition a free-shrinkage frame that was match cured to the modeled temperature profiles measured the strain due to thermal and autogenous effects. Match-cured cylinders were used to determine the development of compressive strength, splitting tensile strength, and modulus of elasticity of the concrete. Specimens were cast to determine the hardened coefficient of thermal expansion. The mechanical properties were compared to estimation equations to check their applicability for use with lightweight aggregates. The three types of lightweight aggregates were then compared to one another.

Part II investigates the effects of internal curing on concrete mixtures with *w/c* of 0.42, 0.36, and 0.30. Mixtures with different amounts of internal curing water were

proportioned. The effect of internal curing water on cracking tendency, isothermal stress development, isothermal free shrinkage, internal relative humidity, and degree of hydration of the concrete was determined. Mortar was also wet sieved from the concrete mixtures for autogenous shrinkage measurement as per ASTM C 1698. For the internal curing mixtures with *w/c* of 0.42, the maximum amount of lightweight fine aggregate was used to obtain a calculated equilibrium density of 135 lb/ft^3. Shale, clay, and slate lightweight aggregates sources were used for these mixtures. Because each aggregate had different absorption and desorption properties, each mixture provided a different amount of internal curing water. The mixtures with *w/c* of 0.36 and 0.30 used a different source of expanded shale for their testing. The method of providing an equal volume of water as chemical shrinkage was used. For each of the mixtures with *w/c* of 0.36 or 0.30, two levels of internal curing water were provided. Two different degree of hydration models from literature were used to calculate the chemical shrinkage, thus a different amount of internal curing water was provided.

Part III is focused on modeling the early-age stress development and modifying the B3 Model (Bǎzant and Baweja 1995) for early-age compliance behavior. Like most compliance models, the B3 model was calibrated with hardened concrete specimens that had been cured for at least one day. Using rigid cracking frames, free-shrinkage frames and the mechanical property development of various density concrete mixtures, the early-age relaxation was determined. The free-shrinkage frame was match-cured to a modeled temperature profile and the free strain due to thermal and autogenous effects was determined. The compressive, tensile and modulus of elasticity development of the mixtures were evaluated using match-cured cylinders. Using the stiffness and free strain

development, the fully elastic stress development was determined. The B3 model was used to determine the relaxation-adjusted stress. The B3 was modified by using the stress data from the rigid cracking frame that was match cured to the same temperature history as the free-shrinkage frame. The early-age modifications made to the B3 had quickly diminishing effect so; the later-age behavior would still be in calibration with the original B3 model.

PART I:

CRACKING TENDENCY OF LIGHTWEIGHT AGGREGATE CONCRETE

CHAPTER 2

PART I: INTRODUCTION

2.1 Background

Early-age cracking of concrete bridge decks, typically caused by thermal effects, drying shrinkage, and autogenous shrinkage can have detrimental effects on long-term behavior and durability. Darwin and Browning (2008) recently reported that "by controlling early age cracking, the amount of cracking at later ages should remain low," and that early-age cracking can significantly increase the rate and amount of chloride penetration (from deicing salts), which may accelerate the corrosion rate of embedded reinforcing steel. Transverse cracking occurs in most geographical locations and climates, and in many types of bridge superstructures (Krauss and Rogalla 1996). The National Cooperative Highway Research Program (NCHRP) Report 380 (Krauss and Rogalla 1996) reported results of a survey sent to all U.S. Departments of Transportation (DOTs) and several transportation agencies overseas to evaluate the extent of deck cracking. 62 percent of the responding agencies considered early-age transverse cracking to be problematic. A survey conducted by the Federal Highway Administration (FHWA) found that more than 100,000 bridges suffer from early-age cracking (FHWA 2008). Given the abundance of cracking observed in bridge decks, and the impact of early-age cracking on long-term performance and durability, it is imperative that bridge deck concrete be proportioned and placed to minimize early-age cracking.

Cracking of hardening concrete occurs when the induced tensile stress exceeds the tensile strength of the concrete. The development of in-place stresses is affected by the shrinkage, coefficient of thermal expansion, setting characteristics, restraint conditions, stress relaxation (creep-adjusted modulus of elasticity), and temperature history of the hardening concrete. The tensile strength (and strain capacity) increases as the hydration of the cementitious system progresses. The tensile strength is impacted by the cementitious materials, the water-cementitious materials ratio, the aggregate type and gradation, the degree of curing (internal/external) provided, and the temperature history of the hardening concrete. Quantification of many of the mechanisms mentioned above is quite complicated at early ages, and many of these variables have complex interactions.

In this project, the effect that of lightweight aggregate (LWA) on the cracking tendency was evaluated by cracking frame testing techniques. Cracking frames can measure the development of stresses due to thermal and autogenous shrinkage effects from setting until cracking (Mangold 1998). The combined effect of modulus elasticity, creep/relaxation, coefficient of thermal expansion, thermal conductivity, autogenous shrinkage, and tensile strength on the cracking potential in a specific application is thus directly captured and quantified by this unique test setup. Since the specimen is sealed against water loss, the effect of drying shrinkage is not measured with this setup.

A rigid cracking frame as developed by Dr. Rupert Springenschmid at the Technical University of Munich, Germany was utilized in this research project. The two rigid cracking frames used at Auburn University during this project are shown in Figure 1-1. These cracking frames were designed to produce restraint for 6 x 6 x 50 in. concrete specimens from placement to approximately 6 days. Each cracking frame consists of two

crossheads and a pair of stiff Invar sidebars. The crossheads are designed to grip the concrete specimen while the sidebars provide restraint as the concrete hardens. The Invar bars are sized to provide approximately 80 percent restraint to movement for the hardened concrete and strain gauges are used to continuously measure the stress state in the concrete specimen as it hardens in the frame. The frame is designed to allow fresh concrete to be cast into temperature-controlled formwork within the frame. With this unique formwork, the concrete can be subjected to a variety of temperature profiles that simulate in-place conditions of bridge decks, elevated slabs, pavements, mass concrete structures, etc.

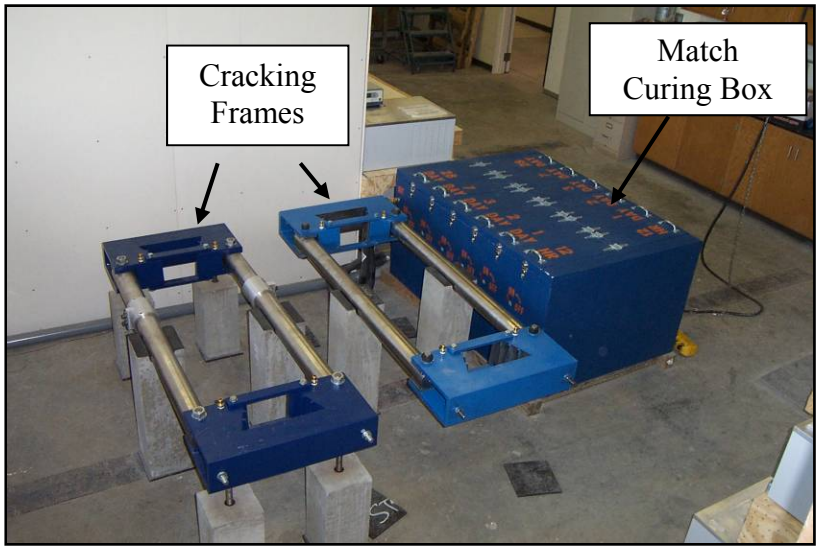

Figure 2-1:Test equipment to assess the early-age stress development of concrete mixtures

Due to increased insulation ability of lightweight aggregate, its use in concrete mixtures has been reported to increase the temperature rise due to hydration measured during the construction of the new Benecia-Martinez Bridge (Maggenti 2007). This increase in temperature rise may not translate to increased thermal cracking risk, simply

since thermal cracking risk is a function of the concrete strength and stress development. Lightweight concrete has a lower modulus of elasticity, lower coefficient of thermal expansion and provides internal curing to the concrete and these characteristics may reduce the stress and counter the effects caused by its increased temperature development (Byard et al. 2010).

2.2 Lightweight Aggregates

Rotary kilns are commonly used to produce LWA under controlled conditions (Chandra and Berntsson 2002). Historically, LWA have been used to reduce the density of concrete. However, LWA can be used to alter more than just the density of concrete. Because lightweight aggregates have high absorption capacities when compared to conventional aggregates, they provide internally stored water that may become available, if needed. These internal water supplies can provide additional water for hydration as well as reduce the effects of self-desiccation and thus autogenous shrinkage effects (Henkensiefken 2008). Limited work has been done to determine cracking tendency of bridge deck concrete with lightweight aggregate. It is thus necessary to determine the effect of lightweight aggregate on the cracking tendency of bridge deck concrete.

2.3 Objectives

The primary objective of this part is to evaluate the influence of lightweight aggregates on the development of stresses and the occurrence of cracking at early ages for bridge deck concrete. The primary objectives of the research described in this part are as follows

- Develop and evaluate the cracking tendency of three types of lightweight aggregate bridge deck concretes relative to a typically used normalweight concrete mixture,
- Evaluate the effect of placement and curing temperature on the cracking tendency of concrete,
- Evaluate the modulus of elasticity, splitting tensile strength, compressive strength, coefficient of thermal expansion, and thermal diffusivity of lightweight aggregate concretes and determine their effect on the early-age cracking tendency,
- Evaluate the effect of three different sources of lightweight aggregate (shale, clay, and slate) on the development of mechanical properties and the cracking tendency of bridge deck concrete, and
- Determine the effectiveness of pre-wetted lightweight aggregate for providing internal curing moisture to mitigate stress development due to autogenous shrinkage.

Secondary objectives of this study include

- Compare the measured modulus of elasticity values to those estimated using the expressions recommended by ACI 318 (2008) and the AASHTO LRFD Bridge Design Specifications (2007), and
- Compare the measured splitting tensile strength to those estimated by the expression recommended by ACI 207.2R (1995) and ACI 207.1R (1996), and evaluate the applicability of the ACI 318 (2008) lightweight concrete coefficient (λ).

2.4 Research Approach

The cracking tendency of the concrete mixtures was determined using rigid cracking frame testing techniques. Three lightweight aggregate sources were evaluated by producing three different concretes with each of these lightweight aggregates and one concrete mixture with normalweight aggregate. Each concrete mixture was subjected to two types of controlled temperature histories while measuring the stress development from setting until the onset of cracking. To assess the effect of placing temperature, each mixture was placed at summer and fall placement conditions. Match-cured concrete cylinders were produced to determine the development of mechanical properties of each concrete mixture under various controlled temperature histories. The effect of the supplied internal curing water from lightweight aggregate was assessed by measuring the restrained stress development of concrete specimens cured under isothermal conditions. In addition, the coefficient of thermal expansion of the hardened concrete was assessed.

2.5 Outline

A summary of literature reviewed pertaining to early-age cracking, lightweight aggregates, properties of lightweight aggregate concrete, autogenous shrinkage, internal curing, and methods to assess early-age concrete behavior is presented in Chapter 3. The experimental testing program used to assess the early-age stress development of concrete is presented in Chapter 4. In addition, Chapter 4 contains the method used to model bridge deck temperatures, and the methods used to assess the fresh and hardened properties of the lightweight and normalweight concretes. The properties of the

lightweight aggregates and the other raw materials are also presented in Chapter 4. The results of the experimental work performed for this project are presented in Chapter 5. A discussion and synthesis of the results are presented in Chapter 6. Conclusions and recommendations resulting from the work documented in this report are presented in Chapter 7.

CHAPTER 3

PART I: LITERATURE REVIEW

The results of a literature review of early-age cracking, autogenous shrinkage, chemical shrinkage, lightweight aggregate production, and lightweight aggregate properties are presented in this chapter. In addition, internal curing and methods for proportioning lightweight aggregate for internal curing purposes in concrete are reviewed in this chapter. Finally, test methods to assess early-age concrete behavior are reviewed and are presented herein.

3.1 Early-Age Cracking

3.1.1 Thermal Effects

The development of thermal stresses can be calculated using the expression presented in Equation 2-1. For an accurate estimate of thermal stress, creep effects during early ages and over the structure's life should be accounted for in Equation 3-1 (Schindler and McCullough 2002).

$$\sigma_T = \Delta T \times \alpha_t \times E_{c,adj} \times K_r \quad \text{Equation 3-1}$$

where σ_T = thermal stress (psi)

ΔT = temperature change = $T_{zero\text{-}stress}$ - T_{min} (°F),

α_t = coefficient of thermal expansion (strain/°F),

$E_{c,adj}$ = creep-adjusted modulus of elasticity (lb/in^2),

K_r = degree of restraint factor,

$T_{zero\text{-}stress}$ = concrete zero-stress temperature (°F), and

T_{min} = minimum concrete temperature (°F).

An illustration of the development of concrete temperatures and thermal stresses over time under summer placement conditions for freshly placed concrete is presented in Figure 3-1. In terms of stress development, the final-set temperature is the temperature at which the concrete begins to resist stresses that result from the restraint of external volume changes. In Figure 3-1, it can be seen that hydration causes the concrete temperature to increase beyond the setting temperature, time (A). Because the expansion of the concrete caused by the temperature rise is restrained, the concrete will be in compression when the peak temperature, time (B), is reached. When the peak temperature is reached, the hydrating paste is still developing structure, its strength is low, and high amounts of early-age relaxation may occur when the concrete is subjected to high compressive stress (Emborg 1989). The phenomenon of gradual decrease in stress when a material is subjected to sustained strain is called stress relaxation (Mehta and Monteiro 2006). As the concrete temperature subsequently decreases, the compressive stress is gradually relieved until the stress condition changes from compression to tension, time (C). The temperature at which this transient stress-free condition occurs is denoted the "zero-stress temperature". Due to the effects of

relaxation, the zero-stress temperature may be significantly higher than the final-set temperature (Emborg 1989). If tensile stresses caused by a further temperature decrease exceed the tensile strength of the concrete, cracking will occur, time (D). Because the thermal stress is proportional to the difference between the zero-stress temperature and the cracking temperature, thermal cracking can be minimized by decreasing the zero-stress temperature. This in turn can be accomplished by (1) minimizing the final-set temperature, (2) minimizing the peak temperature achieved during the high-relaxation phase, or (3) delaying the attainment of the peak temperature.

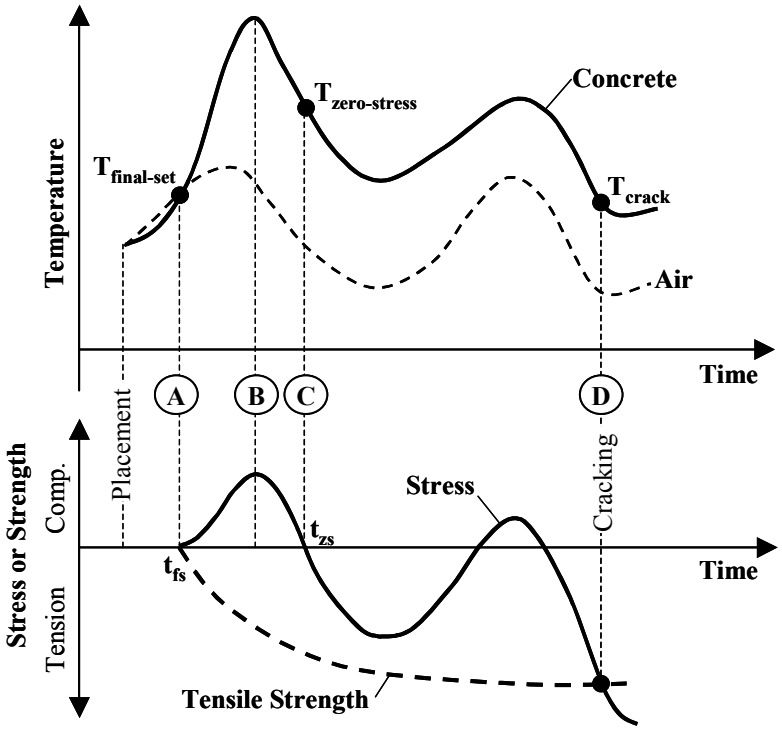

Figure 3-1: Development of early-age thermal stresses (Schindler and McCullough 2002)

3.1.2 Autogenous and Chemical Shrinkage Effects

The reaction products formed from cement hydration occupy a smaller absolute volume than the anhydrous components (L'Hermite 1960). The reduction of the absolute volume of the reactants due to hydration is chemical shrinkage. Before setting, this phenomenon results in a volumetric change but generates no stress as the concrete is still plastic (Holt 2001). At setting, enough hydration products have formed to provide a self-supporting skeletal framework in the paste matrix. In between the framework of solids are water filled capillary voids. As water is consumed by the ongoing hydration process, the voids empty and capillary tensile stresses are generated, which results in a volumetric shrinkage. The concrete volume change that occurs without moisture transfer to the environment and temperature change is called autogenous shrinkage. Before setting, chemical shrinkage and autogenous shrinkage are equal (Holt 2001). The addition of pre-wetted LWA helps mitigate stress due to autogenous stresses by desorbing water from the aggregate particles into the hydrated cement paste pore structure and relieving some or all of the capillary tension (Henkensiefken 2008). Generally, autogenous shrinkage and stress development is not a concern at water-cementitious materials (*w/cm*) ratios above 0.42 (Mindess et al. 2002; Mehta and Monteiro 2006).

Holt (2001) provided the graphic depiction in Figure 3-1of the composition change of a sealed paste due to the cement hydration reactions, where *C* is the cement volume, *W* is the volume of water, H_y is the volume of the hydration products and *V* is the volume of voids. This figure relates how the autogenous shrinkage is a portion of the chemical shrinkage. After set, the chemical shrinkage is an internal volume reduction, whereas the autogenous shrinkage is an external volume change.

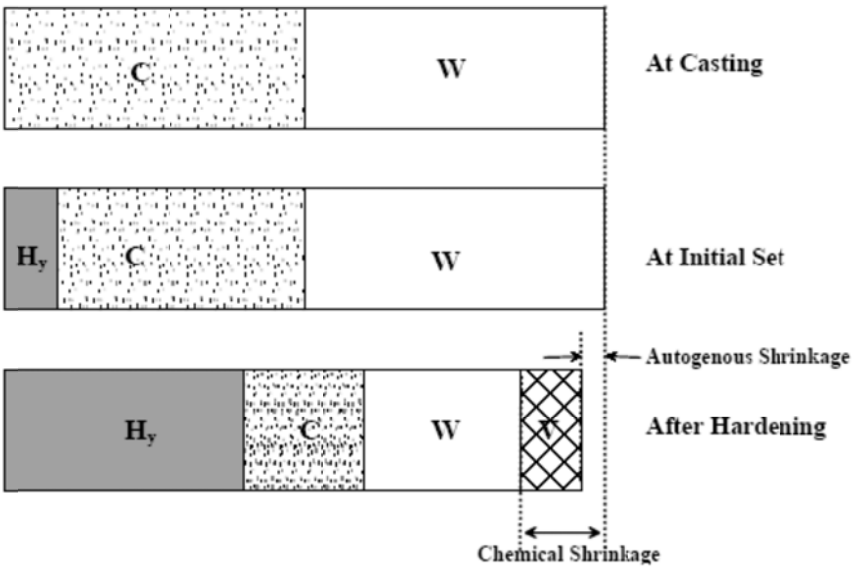

Figure 3-2:Volume reduction due to autogenous shrinkage (Holt 2001)

3.2 Lightweight Aggregate

LWA can be classified as natural or manufactured. Natural LWAs include pumice, scoria, and tuff. Most LWA used in concrete in the United State are manufactured. Manufacturing provides regional availability and more consistency than natural LWA (Chandra and Berntsson 2002). Manufactured LWA includes expanded shale, clay, and slate. In addition to manufactured LWA, some byproducts can serve as LWA including sintered fly ash, expanded slag, and bed ash.

3.2.1 Production

The manufacture of LWA by rotary kiln methods are produced as described in the ESCSI Reference Manual (ESCSI 2007) and illustrated in the flow diagram shown in Figure 3-3. The aggregate is collected from its source by mining in the case of harder materials such as slate or shale or by scraping for softer materials such as clays. The raw materials are

then prepared for the kiln by crushing and sizing. Vibratory screens then size the crushed material. The material is then fed into the upper end of the rotary kiln and it travels down the kiln in 30 to 60 minutes. The travel time depends on the length, diameter, and rotational speed of the kiln. Kiln lengths vary from 60 to 225 ft with diameters of 6 to 12 ft. Heating of the material is gradual for the first two-thirds of the kiln length, but increases rapidly to the maximum in the last third of kiln length. Maximum kiln temperatures vary between 1920 and 2190 °F. The heating of the particle interiors cause gasses to be liberated. The plastic state of the material allows the gasses to form disconnected pores within the material and expansion occurs. As the expanded material cools, the pores remain giving the aggregate its relatively low density and increased ability to absorb water. The materials is then crushed and sieved to various sizes to obtain the desired gradations.

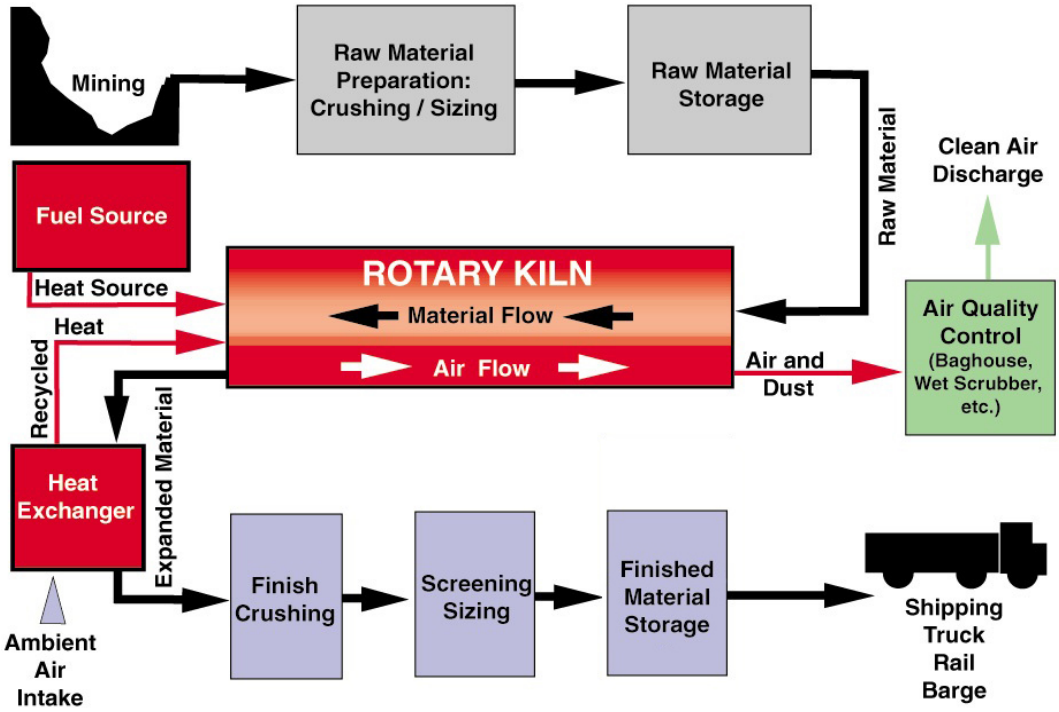

Figure 3-3: Production of rotary kiln lightweight aggregate (ESCSI 2007)

3.2.2 Properties

The impact of using LWA on concrete's coefficient of thermal expansion (α_t), modulus of elasticity, thermal conductivity, and tensile strength are discussed in this section.

3.2.2.1 *Coefficient of Thermal Expansion*

The coefficient of thermal expansion of concrete is primarily affected by the coefficient of thermal expansion of the aggregate, because the aggregate makes up the bulk of the concrete (Mindess et al. 2002). LWAs are reported to have a lower coefficient of thermal expansion compared to siliceous gravel; therefore, concrete made with LWA has a lower coefficient of thermal expansion than its siliceous normalweight counterpart (Mehta and Monteiro 2006).

3.2.2.2 *Modulus of Elasticity*

The modulus of elasticity of the concrete depends heavily on the stiffness of the aggregate (Mehta and Monteiro 2006). LWA has a lower modulus of elasticity because of its increased porosity. Consequently, lightweight concrete has lower modulus of elasticity compared to normalweight concrete (Mindess et al. 2002). Equation 3-2 (ACI 318 2008) can be used to estimate the modulus of elasticity from a known density and compressive strength. This expression indicates that the modulus of elasticity is directly proportional to the density to the 1.5 power and the square root of the compressive strength. This expression also reveals that the concrete's modulus of elasticity will decrease as more LWA is introduced into the mixture.

$$E_c = 33 w_c^{1.5} \sqrt{f_c}$$ .....Equation 3-2

where E_c = modulus of elasticity (lb/in^2),

w_c = density of normal concrete or equilibrium density of lightweight concrete (lb/ft^3), and

f_c = concrete compressive strength (psi).

3.2.2.3 *Thermal Conductivity*

Due to LWA's increased porosity, it has a lower thermal conductivity or greater insulating ability compared to normalweight concrete (Mehta and Montero 2006; Mindess et al. 2002; Chandra and Berntsson 2002). Maggenti (2007) measured the temperature development in mass concrete piers, and concluded that LWA concrete has a greater temperature rise due to hydration compared to normalweight concrete with identical cementing materials, water, and fine aggregate contents.

3.2.2.4 *Tensile Strength*

Tensile strength of concrete develops due to the same factors as compressive strength; however, concrete's tensile strength is much lower than its compressive strength, due to ease of crack propagation under tensile stresses (Mindess et al. 2002). The rate of development and magnitude of the tensile strength play an important role in early-age cracking.

Aggregate characteristics influence the tensile strength of concrete (Mehta and Monteiro 2006). Aggregate texture has a substantial impact on the tensile strength of concrete. Concretes with rough textured or crushed aggregates have been shown to have

higher tensile strengths, especially at early ages, than smoother aggregates (Mehta and Monteiro 2006).

The Interfacial Transition Zone (ITZ) is formed when water films form around aggregate particles in the fresh concrete leading to an increased water to cement ratio in the hydrated paste surrounding the aggregate particles (Mehta and Monteiro 2006). The ITZ is primarily composed of the porous, weak, water-soluble calcium hydroxide (CH). The ITZ is the strength-limiting phase in concrete (Mehta and Monteiro 2006). LWAs have been shown to improve the quality of the ITZ, because of their slight pozzolanic surface, which consumes the CH, and their absorptive surface that reduces the water film around the aggregate (Chandra and Berntsson 2002).

Equation 3-3 (ACI 207.2R 1995) and Equation 3-4 (ACI 207.1R 1996) can be used to estimate the splitting tensile strength from a known compressive strength.

$$f_{ct} = 6.7\sqrt{f_c} \quad \text{.....Equation 3-3}$$

$$f_{ct} = 1.7(f_c)^{2/3} \quad \text{.....Equation 3-4}$$

where f_{ct} = splitting tensile strength (psi), and

f_c = concrete compressive strength (psi).

ACI 318 (2008) provides a lightweight modification factor (λ), presented in Equation 3-5, as a multiplier of the square root of the design compressive strength (f'_c) in all applicable design equations. The AASHTO LRFD Bridge Design Specifications (AASHTO 2007) contains a similar approach to account for the effect lightweight

aggregate on the concrete strength. For sand-lightweight and all-lightweight mixtures, λ is set equal to 0.85 and 0.75, respectively. Linear interpolation between 0.85 and 1.0 is permitted for mixtures with a blend of normalweight and lightweight coarse aggregate. If the splitting tensile strength of the lightweight concrete is known or specified, λ can be calculated using equation 3-5.

$$\lambda = \frac{f_{ct}}{6.7\sqrt{f'_c}} \quad \text{..... Equation 3-5}$$

where λ = lightweight modification factor (unitless),

f_{ct} = splitting tensile strength (psi), and

f'_c = design compressive strength of concrete (psi).

3.3 Internal Curing

Historically, LWA have been used to reduce the density of concrete. In recent years; however, LWAs have been added to concrete to take advantage of the high absorption capacity of the aggregates, which may provide internal water for hydration.

When cement hydrates, capillary pores are created. As the water in the capillary pores is consumed by continuing hydration or by atmospheric desiccation, the internal relative humidity decreases and stresses are induced. Pre-wetted high absorption particles can desorb water into the cement pore structure, thus reducing capillary stresses and providing water for hydration. The process of providing additional water for capillary pore stress reduction and additional cement hydration through pre-wetted particles is called *internal curing*.

High absorption materials such as perlite, wood pulp, super-absorbent particles (SAP), and LWA are some materials that have been used in concrete for internal curing purposes. LWA is used more frequently as an internal curing material (Delatte et al. 2008).

Lightweight fine aggregates are generally used for internal curing purposes due to their greater dispersion compared to coarse aggregates. It has been shown that water from LWA can move 0.07 in. into paste around the aggregate particle (Henkensiefken 2008).

Bentz (Bentz et al. 2005) provides a simplified method for proportioning lightweight fine aggregate for internal curing purposes as shown in Equation 3-6. The unit chemical shrinkage is calculated based on the composition of the cement and the densities of the hydration products is then normalized with water's density. The coefficients suggested by Bentz et al. (2005) for chemical shrinkage due to cement hydration are presented in Table 3-1. The total chemical shrinkage is determined by using the cement content and maximum degree of hydration of the mixture. The maximum degree of hydration can be estimated as *w/cm*/0.36 if the *w/cm* is less than or equal to 0.36. For *w/cm* greater than 0.36, the maximum degree of hydration is assumed to be 1.0. Next, the volume of water equal to the total chemical shrinkage is determined and this amount water is provided by the lightweight aggregate. The volume of water provided by the lightweight fine aggregate is calculated using the absorption capacity of the aggregate and the saturation of the aggregate. This volume of water prevents the capillary voids from emptying, which should prevent capillary stresses from developing.

$$M_{LWA} = \frac{C_f \times CS \times \alpha_{\max}}{S \times \phi_{LWA}}$$ .....Equation 3-6

where M_{LWA} = oven-dry weight of lightweight aggregate (lb),

C_f = cement content for the mixture (lb/yd^3),

CS = chemical shrinkage (lb of water/lb of cement),

α_{max} = maximum degree of cement hydration,

S = degree of saturation of aggregate (0 to 1), and

Φ_{LWA} = absorption of lightweight aggregate (lb water / lb dry LWA).

Table 3-1: Coefficients for chemical shrinkage (Bentz et al. 2005)

Cement Phase	Coefficient (Pound of water / Pound of solid cement phase)
C_2S	0.0704
C_3S	0.0724
C_3A	0.115*
C_4AF	0.086*

* assuming total conversion of the aluminate phases to monosulfate.

Equation 3-6 uses the volume of absorbed water within the LWA as internal curing water to balance the anticipated chemical shrinkage demand. It is known that not all of the absorbed water within the LWA will be desorbed for early-age internal curing (RILEM TC 196 2007). The amount of water desorbed from the LWA will be a function of the aggregate pore size distribution, the spacing of the LWA in the concrete, the pore size distribution of the paste matrix, permeability of the paste and the internal relative humidity around the aggregate particle (RILEM TC 196 2007).

As cement hydrates and consumes water from capillary pores in the paste matrix capillary tensile stresses develop. Water is then desorbed from the pores of the LWA into the paste capillary pores. Available water is more easily removed from larger pores than from smaller pores. LWA with large amounts of smaller pores do not as readily release their internal water. The lower limit of useful pore size may be considered around 100 nm (RILEM TC 196). Due to different pore size distribution within various LWAs, they can have significantly different desorption properties. For internal curing purposes, the desorption properties are more important than absorption properties (Lura 2003; Bentz et al. 2005).

It is necessary that the lightweight aggregate release moisture at a high relativity humidity so the moisture will be available at early-ages within the concrete. Castro et al. (2011) tested the desorption of a variety of lightweight materials at 93 percent relative humidity. A summary of the desorption coefficients relevant to the LWA tested in this study is presented in Table 3-2. The desorption response is thus different for the expanded shale, clay, and slate and this needs to be accounted for when determining the amount of internal curing water available from these LWAs.

Table 3-2: Desorption coefficients at 93% relativity humidity (Castro et al. 2011)

Item	Lightweight Aggregate Type		
	Slate	**Clay**	**Shale**
Supplier	Stalite	TXI	Buildex
Source	Gold Hill, NC	Frazier Park, CA	New Market, MO
Desorption coefficient at 93% relative humidity	0.962	0.887	0.976

3.4 Methods to Assess Early-Age Concrete Behavior

3.4.1 Restrained Stress Development

The rigid cracking frame (RCF), shown in Figure 3-4, is comprised of two mild steel crossheads and two 4-in. diameter Invar sidebars. The test setup was adapted from the configuration developed by Dr. Rupert Springenschmid as documented by RILEM Technical Committee 119 (1998). The RCF test is a relative index of cracking sensitivity. According to Springenschmid and Breitenbücher (1998), a mixture with increased cracking time and decreased cracking temperature will have improved cracking performance in the field. This increased performance may be in the form of increased crack spacing, decreased crack widths or fewer cracks.

Fresh concrete is consolidated in the RCF, and its stress development is measured continuously until cracking occurs. The 6 × 6 × 49 in. concrete specimen is restrained by dovetailed crossheads at each end. The dovetail is gradually tapered to reduce stress concentrations and has multiple teeth that grip the concrete. To further prevent slippage of the concrete, crosshead braces are used at the end of the crosshead to restrain opening of the crosshead as the concrete goes into tension. The formwork includes 0.5-in. diameter copper tubing throughout. A mixture of water and ethylene glycol is circulated from a temperature-controlled water bath through the formwork to control the curing temperature of the concrete sample. The formwork of the RCF is lined with sheeting to reduce friction between the concrete and the form and to seal the concrete specimen on all surfaces. Because of the presence of the sealed plastic layer around the concrete

specimen, no moisture is lost and drying shrinkage effects do not contribute to the stress development while the forms are in place.

a)

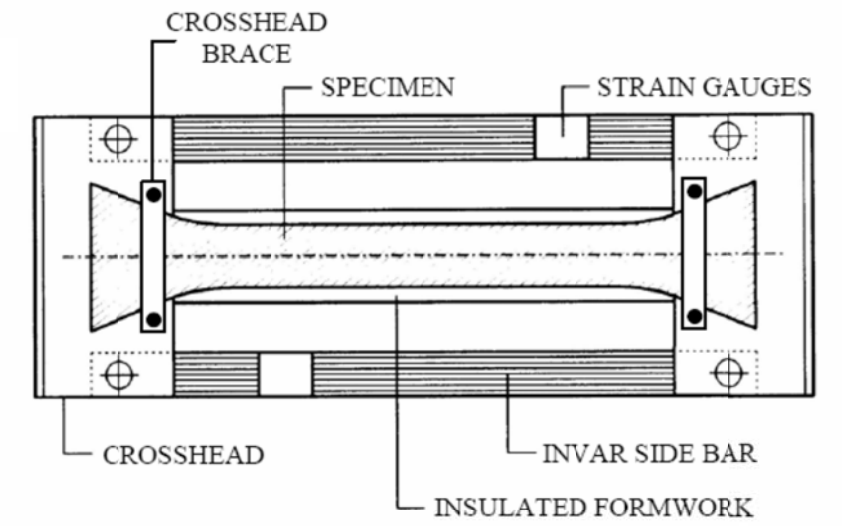

b)

Figure 3-4: Rigid cracking frame test setup: a) Schematic of test (Mangold 1998) b) Actual equipment used

When concrete in the RCF starts to hydrate and volume changes due to temperature and autogenous shrinkage effects develop, the Invar bars provide restraint against movement and stress develops in the concrete. The concrete's stress development is monitored using strain gauges mounted on the Invar bars, that are calibrated to the bar forces, which equilibrate the concrete stresses.

The stress developed by the RCF under an isothermal condition is a function of the modulus of elasticity, the autogenous shrinkage, and the relaxation. The stress developed by the RCF under a match-cured condition is a function of the concrete's coefficient of thermal expansion, temperature history, modulus of elasticity, autogenous shrinkage, and relaxation.

It has been observed that the cracking frame stress at failure is less than the splitting tensile strength measured on molded concrete cylinders (Meadows 2007). This is due to the differences in test specimen size, the rate of loading, and the type of loading (Meadows 2007). The section of concrete subjected to the highest tensile stress is much larger in the cracking frame than in a 6 × 12 in. cylinder. The larger volume of concrete subjected to the highest tensile stress in the cracking frame provides a higher probability of a significant flaw in the sample and therefore it has a lower apparent strength. In addition, the rate of loading can affect the strength results. Slow load rates yield a lower apparent strength and conversely higher load rates yield a higher apparent strength (Wight and MacGregor 2009). The splitting tensile strength specimens were loaded to failure in less than 5 minutes, whereas the cracking frames were loaded for 23 to 109 hours, thus the concrete in the cracking frame will exhibit a lower apparent tensile strength. In addition, the cracking frame is a direct tension test; whereas the splitting tension is an indirect tensions test. Meadows (2007) reports that the ratio of cracking frame stress at failure to splitting tensile strength generally falls between 50 to 80 percent.

3.4.2 Unrestrained Length Change Assessment

Bjøntegaard (1999) developed a free-shrinkage frame (FSF) to determine the unrestrained uniaxial length change of a curing *concrete* specimen. A FSF similar to the one developed by Bjøntegaard was constructed by Auburn University and is shown in Figure 3-5.

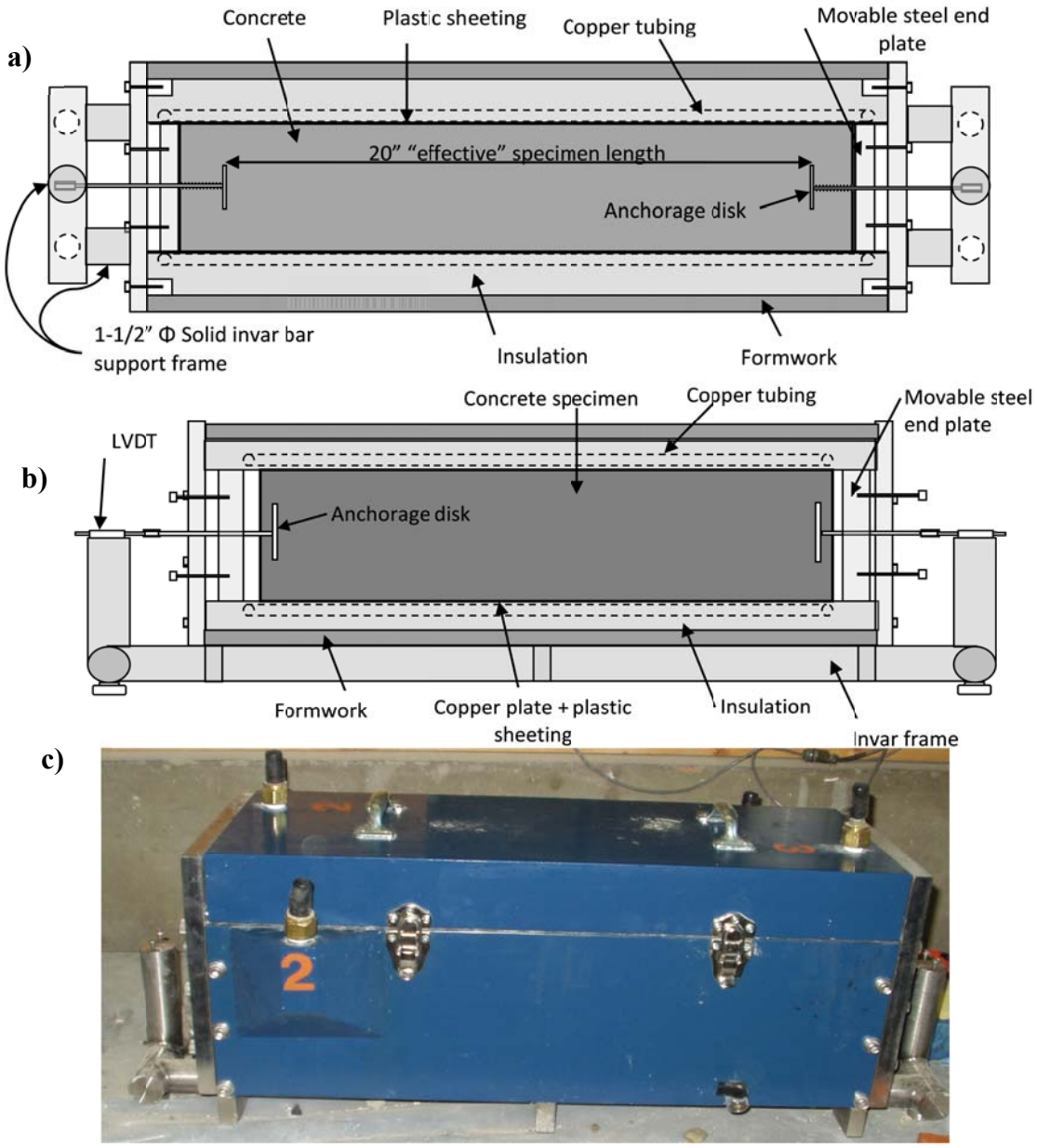

Figure 3-5: Free-shrinkage frame test setup: a) Plan view schematic of test equipment, b) Section view schematic, and c) Actual equipment used

The FSF consists of a box that is thermally controlled with 0.5 in. diameter copper tubing, and a supporting Invar steel frame. The box serves as the formwork for the freshly placed concrete and the system to match cure the concrete to any temperature profile. A 6 × 6 × 24 in. concrete specimen is cast with two sacrificial steel plates connected with an Invar rod to a linear variable displacement transducer (LVDT) to measure linear expansion and contraction. The fresh concrete is placed on a double layer of plastic sheeting with a lubricant in between to minimize friction, which facilitates free movement of the concrete specimen. Plastic sheeting is also used to seal the concrete specimen on all surfaces. When concrete in the FSF is cured to a specified temperature history, the measured strain is a function of thermal and autogenous effects. The test specimen is entirely sealed with a plastic layer, so no moisture is lost. Therefore drying shrinkage effects do not contribute to the free movement measured in the FSF. When the concrete is placed, the movable steel end plates support the fresh concrete ends. When initial set is reached, the movable end plates are released and moved back to allow expansion beyond the initial specimen size. Initial set is determined from penetration resistance as per ASTM C 403. The mortar sample for setting is match-cured to the same temperature history of the FSF. The end plates in position prior to placement is shown in Figure 3-5a and the end plates drawn back after setting is shown in Figure 3-5b.

3.4.3 Coefficient of Thermal Expansion

AASHTO T 336 (2009) can be used to determine the coefficient of thermal expansion of the hardened concrete. For this test, a cylindrical concrete specimen is placed in a frame

and submerged in water. A schematic of a typical test frame and specimen are shown in Figure 3-6. A spring-loaded linear variable displacement transformer (LVDT), mounted on a frame, is placed in contact with the top surface of the concrete specimen. The temperature of the water is cycled over a range of 50 °F to 122 °F ± 2 °F, and the subsequent length change of the concrete specimen is measured. From the measured displacement over the known temperature change, the concrete specimen's coefficient of thermal expansion is calculated.

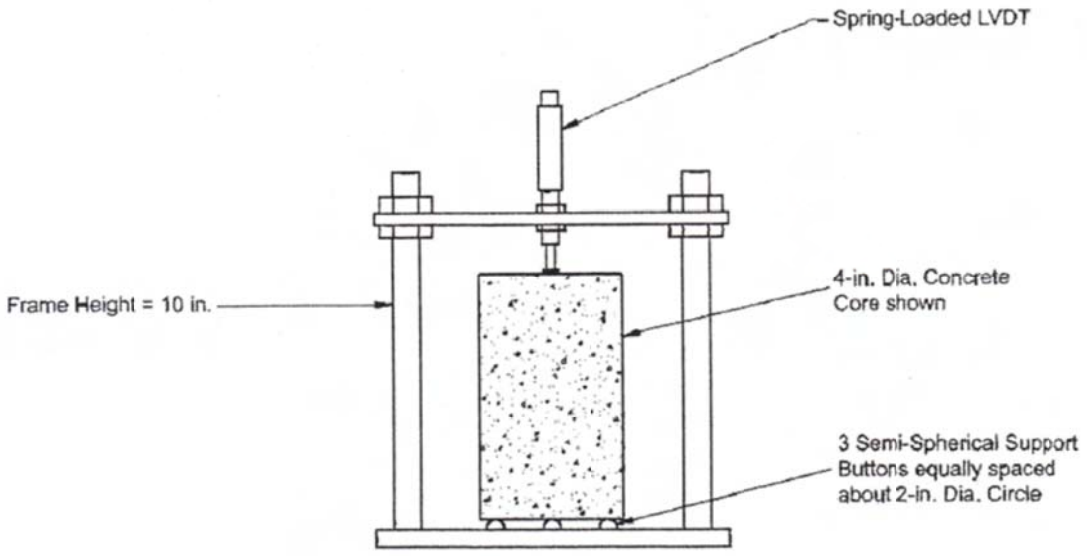

Figure 3-6: Front view of coefficient of thermal expansion test setup (AASHTO T 336 2009)

3.4.4 Semi-Adiabatic Calorimetry

Under adiabatic conditions, a specimen is sealed in a chamber and no heat loss is permitted to occur. Under semi-adiabatic conditions, a small amount of heat loss systematically occurs over time and the heat loss is accounted for by calibration.

Hydration of portland cement is an exothermic reaction. Determining the amount and rate of heat evolved by a particular mixture is essential when modeling early-age in-

place temperatures. Semi-adiabatic calorimetry provides an indirect, convenient means of measuring the heat released during hydration of a concrete sample (Schindler and Folliard 2005). Each concrete mixture has a unique heat of heat of hydration development. Without knowing the rate and amount of heat evolved from a concrete mixture, modeling the early-age in-place temperature is impossible.

Semi-adiabatic calorimetry testing generally involves placing the fresh concrete in an insulated vessel or calorimeter. The calorimeter must be calibrated with a material of known thermal properties to determine the rate that the calorimeter dissipates thermal energy. Normally hot water is used for calibration. Temperature probes are used to measure the concrete temperature and the ambient temperature around the calorimeter. The difference between the ambient temperature and temperature inside the calorimeter affects the rate the calorimeter dissipates thermal energy. As the cement hydrates, the heat evolution is captured by the temperature probe positioned in the concrete specimen. Knowing the amount and rate of heat loss from the calorimeter, the amount of heat evolved from the concrete can be calculated. A schematic view of the semi-adiabatic calorimeter used on this project is shown in Figure 3-7.

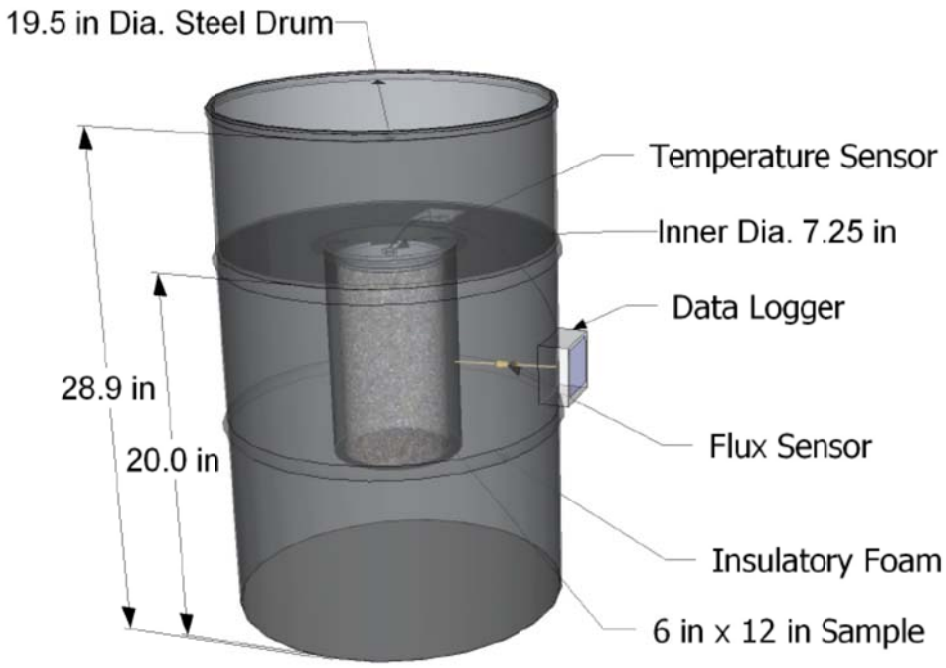

Figure 3-7: **Semi-adiabatic calorimeter (adapted from Weakley 2009)**

CHAPTER 4

PART I: EXPERIMENTAL WORK

4.1 Experimental Program

Concretes proportioned with varying amounts and types of lightweight aggregates were tested to determine their cracking tendency compared to a control mixture using rigid cracking frame (RCF) testing techniques. A mixture using river gravel was tested as a control concrete and all mixtures were proportioned for bridge deck applications. Temperature profiles were modeled to determine the temperature history that concrete in an 8-in thick bridge deck would experience in both summer and fall placement scenarios with the mixtures used. Two rigid cracking frames were used for match-cured and isothermal temperature conditions as schematically shown in Figures 3-1 and 3-2, respectively. Additional tests that were performed on match-cured concrete specimens are shown in Figure 4-1.

Concrete in RCF A was *match cured* (Figure 4-1) to the modeled bridge deck temperature profiles to determine the concrete stress generated due to thermal effects and autogenous shrinkage effects. A free-shrinkage frame (FSF) was also used to determine the free strain of the mixtures. The FSF was tested using the same *match-cured* temperature profile that simulates bridge deck conditions to determine the free strain due to thermal and autogenous effects. Molded cylinders were also *match cured* to the

modeled bridge deck temperature to determine the concrete strength and modulus of elasticity development. Concrete in RCF B was cured under *isothermal* temperatures (Figure 4-2) and the stress generated is due to only autogenous shrinkage effects.

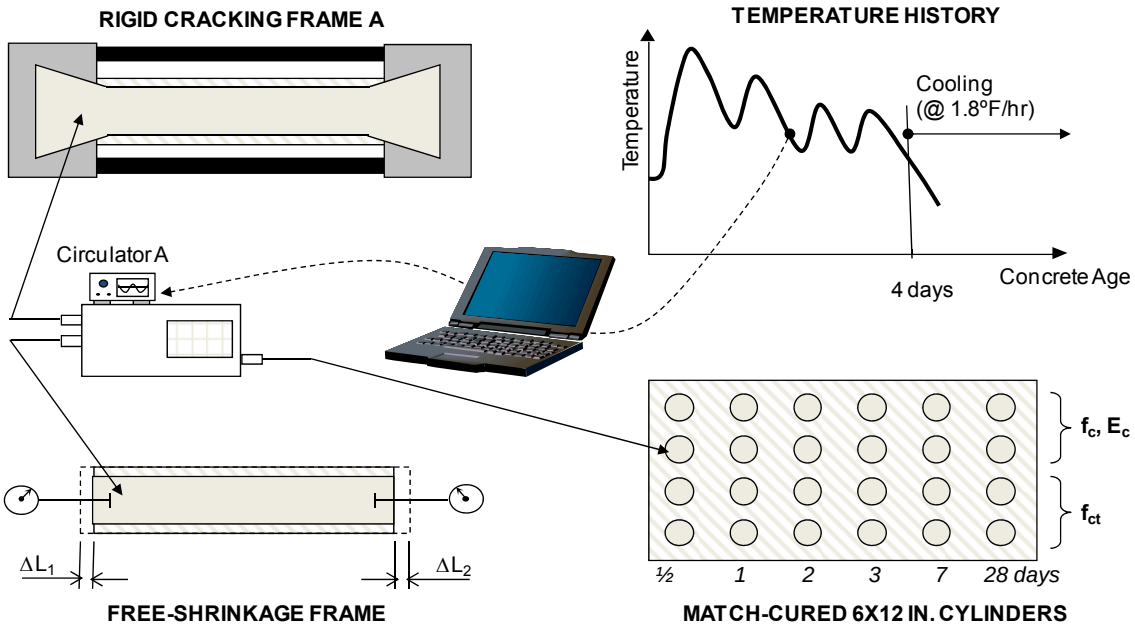

Figure 4-1:Match curing testing setup

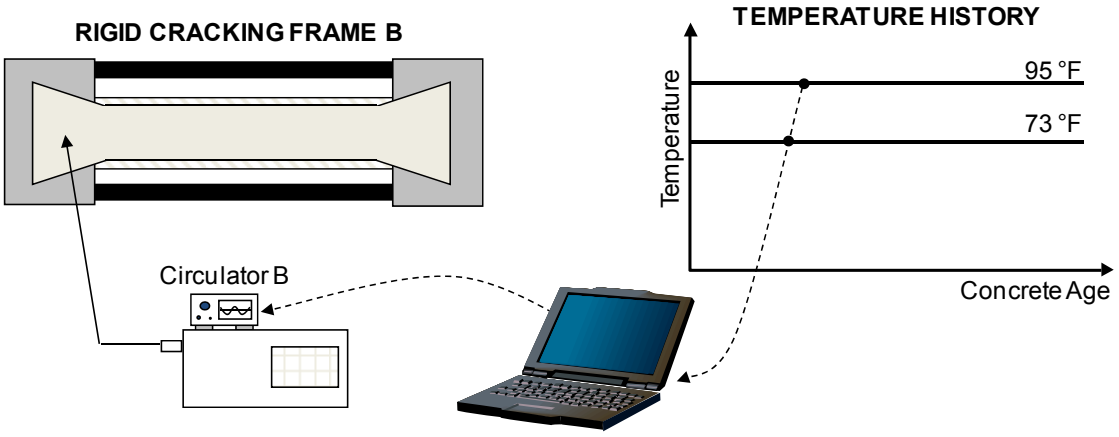

Figure 4-2: Isothermal curing testing setup

Curing temperatures have a major impact on the rate of hydration, rate of development of mechanical properties, and the rate of stress development in concrete. Cracking tendency data collected at typical laboratory temperatures often do not represent the worst-case scenario, as it is well known that early-age cracking is exacerbated under warm-weather conditions (Schindler and McCullough 2002). Each mixture was thus tested under the following two placement scenarios:

- **Summer placement scenario**: Concrete placement temperature ≈ 95 °F, and ambient air temperature cycling between 85 and 95 °F.
- **Fall placement scenario**: Concrete placement temperature ≈ 73 °F, and ambient air temperature cycling between 70 and 77 °F.

The use of these two placement scenarios allows one to determine the effect of placement and curing temperature on the cracking sensitivity of the lightweight and control concrete mixtures. The ConcreteWorks software program (Poole et al. 2006) was used to predict the concrete temperature history of each specific mixture as it would develop in an 8-in. thick bridge deck for both summer and fall placement scenarios. The development of the temperature profile is discussed in Section 4.5.

All constituent materials for the summer placement scenario were placed in an environmental chamber and preconditioned so that the fresh concrete temperature would be approximately 95 °F. All the constituent materials for the fall placement scenario were conditioned at room temperature so that the fresh concrete temperature would be approximately 73 °F.

After 96 hours, the modeled temperature profile essentially followed the prevailing diurnal cycle typical of the simulated placement month. The temperature

peaks and valleys were the same from day-to-day, because the effect of the cement hydration had dissipated and only environmental effects affect the temperature change. Therefore, if cracking had not occurred before 96 hours it would not likely occur without additional temperature decrease. If cracking had not occurred at 96 hours, the temperature was decreased by 1.8 °F/hr until the onset of cracking, which is also the practice used by Breitenbücher and Mangold (1994).

4.2 Lightweight Aggregates

4.2.1 Sources

Expanded shale, clay, and slate lightweight coarse and fine aggregates were evaluated. The lightweight aggregates were selected to represent those available in different regions of the United States and to include the three raw materials used in the United States for LWA: shale, clay, and slate. The type and source of LWA used in the experimental work are shown in Table 4-1. It should be noted that two gradations of *clay* fine aggregates were used; the coarser gradation will be called "*Maximizer*" as per the terminology used by this supplier. In addition, two *slate* fine aggregates were used. The coarser fine aggregate will be called "D Tank" and the other will be called "MS 16" Fine aggregate. Suppliers directly shipped all of the lightweight aggregates to Auburn University's Concrete Materials Laboratory.

Table 4-1: Lightweight material source type, location, and properties

Item		Lightweight Aggregate Type				
		Slate		Clay		Shale
Supplier		Stalite		TXI		Buildex
Source		Gold Hill, NC		Frazier Park, CA		New Market, MO
Coarse Aggregate	Gradation	#4 to 3/4 in.		#4 to 3/8 in.		#4 to 1/2 in.
	Pre-wetted Absorption §	6.4 %		25.5 %		32.0 %
	Relative Density*	1.52		1.72		1.59
Fine Aggregate	Gradation	0 to #4	0 to #4	0 to #4	0 to 3/8 in.	0 to #4
	Pre-wetted Absorption §	9.0 %	9.0 %	19.0 %	19.0 %	19.3 %
	Relative Density *	1.84	1.84	1.81	1.81	1.80
	Fineness Modulus	2.83	3.37	3.07	4.32	2.99

Notes: * Relative density at surface dry state after 7 days of soaking in water for slate and clay aggregates and 14 days of soaking for shale aggregates.
§ Measured water absorbed after pre-wetting aggregates for either 7 or 14 days.

4.2.2 Properties

The lightweight aggregates were shipped in super sacks and were stored in Auburn University‘s Structural Engineering laboratory. Upon arrival, the aggregates were sampled and sieve analyses were performed to obtain the gradations as per ASTM C 136. The specific gravity and pre-wetted absorption of the coarse and fine aggregate were determined in accordance with ASTM C 127 and ASTM C 128, respectively. The materials were pre-wetted for 7 or 14 days prior to absorption and relative density testing. The slate and clay samples were pre-wetted for 7 days and the shale for 14 days. For the lightweight fine aggregates, Provisional Method 2 of ASTM C 128 (the rubber mat method) was used to determine when the sample was at surface dry condition. The sieve

analysis, pre-wetted absorption, relative density, and fineness modulus results are presented in Table 4-1. The gradations for all aggregates are listed in Appendix A.

4.2.3 Lightweight Aggregate Preconditioning

The lightweight aggregates were placed in plastic barrels and submerged in water for moisture preconditioning. The preconditioning time for the materials was based on recommendations provided by each supplier. The slate and clay materials were preconditioned for at least 7 days and the shale material for at least 14 days prior to batching. Valves were installed in the bottom of plastic, 55-gallon barrels to allow the water to be drained from the aggregates. For the lightweight fine aggregate materials, a 6-in. thick filter layer of normalweight coarse aggregate was placed in the bottom to prevent clogging of the valve during draining. Illustrations of the barrel setup are shown in Figure 4-3. After the material was preconditioned, it was drained slowly to reduce the amount of fines lost. The lightweight coarse and fine aggregate material were then shoveled onto a clean plastic sheet in separate piles where the excess surface moisture was allowed to run out. Then the aggregates were shoveled into separate 5-gallon buckets for temperature conditioning and batching.

Temperature preconditioning was achieved by placing the sealed 5-gallon buckets at room temperature or in a heated environmental chamber for the fall or summer placement scenarios, respectively. On the morning of mixing, after 24 hours of temperature preconditioning, samples of aggregates were taken to assess their moisture contents to allow moisture corrections to be made for batching. Once the final moisture-

adjusted batch weights were determined, the 5-gallon buckets of materials were taken from the temperature preconditioning area and weighed for mixing.

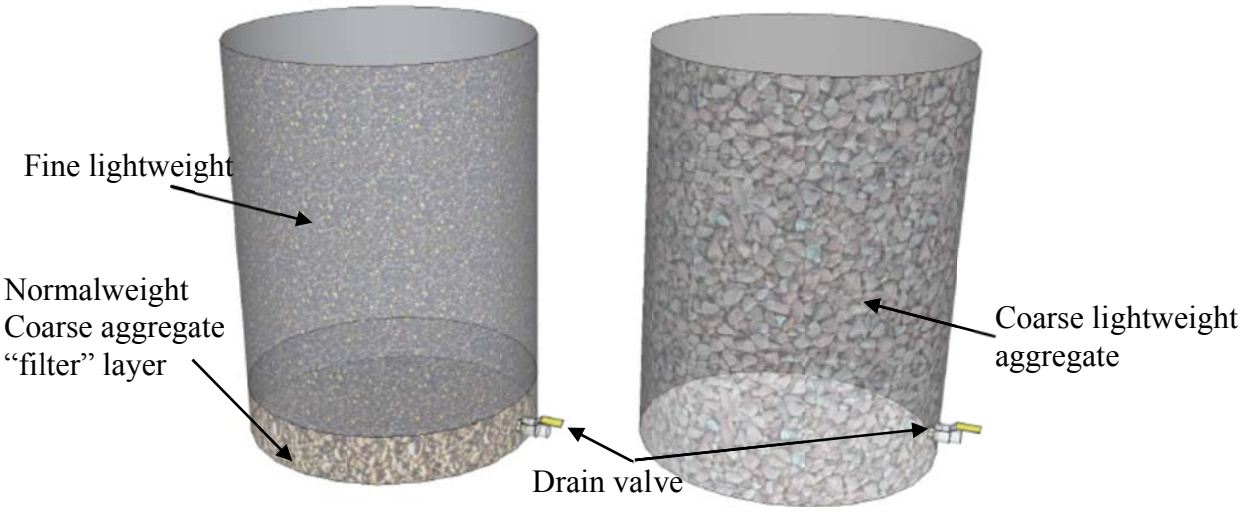

Figure 4-3: Illustration of barrel setup used for lightweight aggregate preconditioning

4.3 Mixture Proportions

Normalweight (CTRL), internal curing (IC), sand-lightweight (SLW), and all-lightweight (ALW) concretes were evaluated. The mixture proportions used for testing the shale, clay, and slate lightweight aggregates are shown in Table 4-2, Table 4-3, and Table 4-4, respectively. For comparison purposes, the mixture proportions for the normalweight concrete are also shown in these tables. Because LWA may never reach a state of saturation, the term saturated surface dry (SSD) is not used with LWA. Therefore, the LWA batch weights are for the pre-wetted surface dry (SD) condition. Pre-wetting of the aggregates is described in Section 4.2.3.

For convenience, a mixture identification system is used in this report to refer to a specific type of LWA, mixture type, and simulated placement season. The identification system used is as follows:

LWA Type	Mixture Type	(Simulated Placement Season)
↑	↑	↑
Slate	CTRL	Fall (Fall *match-cured* conditions)
Clay	IC	Sum (Summer *match-cured* conditions)
Shale	SLW	73°F (Fall *isothermal* temperature)
	ALW	95°F (Summer *isothermal* temperature)

Example: **Slate SLW (Fall)**, represents the sand-lightweight concrete with slate LWA that is made and cured under *match-cured* fall conditions.

Table 4-2: **Expanded slate and normalweight mixture proportions and properties**

Item	CTRL	Slate IC	Slate SLW	Slate ALW
Water Content (lb/yd^3)	260	260	276	276
Cement Content (lb/yd^3)	620	620	658	658
SSD Normalweight Coarse Aggregate (lb/yd^3)	1,761	1,761	0	0
SD Slate Lightweight Coarse Aggregate (lb/yd^3)	0	0	875	896
SSD Normalweight Fine Aggregate (lb/yd^3)	1,210	818	1,381	0
SD Slate Lightweight D Tank Fine Aggregate (lb/yd^3)	0	276	0	0
SD Slate Lightweight MS 16 Fine Aggregate (lb/yd^3)	0	0	0	945
Water-Reducing Admixture (oz/yd^3)	31.0	34.1	0.0	0.0
High-Range Water-Reducing Admixture (oz/yd^3)	0.0	0.0	39.5	8.2
Rheology-Controlling Admixture (oz/yd^3)	0.0	0.0	0.0	52.6
Air-Entraining Admixture (oz/yd^3)	0.8	0.8	6.6	7.4
Target Total Air Content (%)	5.5	5.5	5.5	5.5
Water-cement ratio (w/c)	0.42	0.42	0.42	0.42

Table 4-3: Expanded clay and normalweight mixture proportions and properties

Item	CTRL	Clay IC	Clay SLW	Clay ALW
Water Content (lb/yd^3)	260	260	276	276
Cement Content (lb/yd^3)	620	620	658	658
SSD Normalweight Coarse Aggregate (lb/yd^3)	1,761	1,761	0	0
SD Clay Lightweight Coarse Aggregate (lb/yd^3)	0	0	1,029	948
SSD Normalweight Fine Aggregate (lb/yd^3)	1,210	878	1,316	0
SD Clay Lightweight Maximizer (lb/yd^3)	0	230	0	0
SD Clay Lightweight Fine Aggregate (lb/yd^3)	0	0	0	998
Water-Reducing Admixture (oz/yd^3)	31.0	31.0	0.0	0.0
High-Range Water-Reducing Admixture (oz/yd^3)	0.0	0.0	52.6	34.5
Rheology-Controlling Admixture (oz/yd^3)	0.0	0.0	0.0	26.3
Air-Entraining Admixture (oz/yd^3)	0.8	0.8	19.7	2.5
Target Total Air Content (%)	5.5	5.5	5.5	5.5
Water-cement ratio (w/c)	0.42	0.42	0.42	0.42

Table 4-4: Expanded shale and normalweight mixture proportions and properties

Item	CTRL	Shale IC	Shale SLW	Shale ALW
Water Content (lb/yd^3)	260	260	276	276
Cement Content (lb/yd^3)	620	620	658	658
SSD Normalweight Coarse Aggregate (lb/yd^3)	1,761	1,761	0	0
SD Shale Lightweight Coarse Aggregate (lb/yd^3)	0	0	933	948
SSD Normalweight Fine Aggregate (lb/yd^3)	1,210	878	1,354	0
SD Shale Lightweight Fine Aggregate (lb/yd^3)	0	230	0	908
Water-Reducing Admixture (oz/yd^3)	31.0	31.0	0.0	0.0
High-Range Water-Reducing Admixture (oz/yd^3)	0.0	0.0	39.5	16.5
Rheology-Controlling Admixture (oz/yd^3)	0.0	0.0	0.0	79.0
Air-Entraining Admixture (oz/yd^3)	0.8	0.8	6.6	2.9
Target Total Air Content (%)	5.5	5.5	5.5	5.5
Water-cement ratio (w/c)	0.42	0.42	0.42	0.42

The normalweight mixture is a typical bridge deck mixture used in Alabama that meets the specification requirements of the Alabama Department of Transportation. The IC mixture is similar to the normalweight mixture, except that a fraction of the

normalweight fine aggregate was replaced with lightweight fine aggregate. The IC mixture was initially proportioned using the method described in Section 3.3 proposed by Bentz, et al. (2005). However, it was found that the ASTM C 567 calculated equilibrium density of the IC mixture was below 135 lb/ft^3, which did not allow the mixture to be classified as "normalweight concrete" as per the AASHTO LRFD Bridge Design Specifications (2007). It was desired that the mixture be in the "normalweight concrete" category as per AASHTO LRFD Bridge Design Specifications (2007). Because of this, the maximum replacement of normalweight fine aggregate with lightweight fine aggregate was determined to obtain a calculated equilibrium density of 135 lb/ft^3. The IC mixtures thus contained *less* LWA than required by the method proposed by Bentz et al. (2005).

The SLW mixture was proportioned using lightweight coarse aggregate and normalweight fine aggregate. The ALW mixture used both lightweight fine and coarse aggregate. The cement content for the SLW and ALW mixtures was increased to increase the paste content to improve the workability and pumpability of these lightweight concrete mixtures.

The slump and air contents were specified to be 4.0 ± 1.0 in. and 5.5 ± 1.5 percent, which are typical values for bridge deck construction in the southeastern region of the United States. For this project, the measured density of the concrete was produced to be ± 1 lb/ft^3 of the calculated density after correcting for the measured air content of each batch.

As discussed in Section 3.3, not all of the absorbed water will be available for internal curing purposes, because the water held in the smaller pores will not be available

for internal curing. The amount of water required by Bentz et al. (2005) in Equation 3-6 to fill the voids created by chemical shrinkage is presented in Table 4-5 along with the total amount of internal curing water available in the lightweight aggregates for each mixture. The total amount of available water is calculated using the absorption capacity in Table 4-1 and the desorption coefficients presented in Table 3-2. It was further assumed that the normalweight aggregates do not provide water for internal curing, which matches current normalweight concrete proportioning practice (ACI 211.1R 1991). The data in Table 4-5 reveals that the internal curing slate, clay, and shale concretes provide 44, 23, and 16 percent *less* internal curing water, respectively than required by the method proposed by Bentz et al. (2005). All SLW and ALW concretes tested in this study provide more internal curing water than required by the method proposed by Bentz et al. (2005).

Table 4-5: Total absorbed water available from LWA and water required by Equation 3-6

Concrete Type	Internal Curing Water Available From LWA (lb/yd^3)			Water Required by Equation 2-6 (lb/yd^3)
	Slate	Clay	Shale	
Internal curing	24	33	36	43
Sand-lightweight concrete	49	185	221	47
All-lightweight concrete	134	312	367	47

4.4 Test Methods

4.4.1 Restrained Stress Development

Each mixture was placed in the RCF and was cured to a temperature profile developed to reflect the temperature profile of an 8-in. thick concrete bridge deck constructed under summer or fall placement conditions. The development of the temperature profile is discussed in Section 4.5. The mixture was also placed in a RCF that was cured at an isothermal condition at 95 °F or 73 °F for summer or fall placement conditions, respectively. If the specimen had not cracked after 96 hours, the concrete was cooled at a rate of 1.8 °F/hr to induce cracking, which is also the practice used by Breitenbücher and Mangold (1994). Since the response of the specimen was still measured after cooling was started, this approach still allows one to assess the behavior of the concrete up until cracking occurs.

The stress development of a specimen in the RCF cured under an isothermal curing condition is a function of its modulus of elasticity, autogenous shrinkage, and relaxation. The stress development of a specimen in the RCF cured under match-cured conditions is a function of its coefficient of thermal expansion, temperature history, modulus of elasticity, autogenous shrinkage, and relaxation.

4.4.2 Unrestrained Length Change Assessment

Each mixture was tested in the FSF and cured using the same match-cured temperature profile that was used for the RCF A, as shown in Figure 4-1. The FSF captured the strain

the concrete would experience if it were unrestrained. The strain measured is a function of autogenous shrinkage, coefficient of thermal expansion, and temperature history.

4.4.3 Mechanical Properties

For each mixture and placement scenario, twenty-four 6 × 12 in. cylinders were cast as per ASTM C 192. The cylinders were match cured using the same temperature history as the RCF A and the FSF, as shown in Figure 4-1. The cylinders were tested for compressive strength, splitting tensile strength, and modulus of elasticity as per ASTM C 39, ASTM C 496, and ASTM C 469, respectively at ½ , 1, 2, 3, 7, and 28 days. Two cylinders were first tested to determine the splitting tensile strength of the concrete. From the splitting tensile strength, 40 percent of the compressive strength was estimated, which was used for modulus of elasticity testing. The same two cylinders used for modulus of elasticity testing were used for compressive strength testing. After the modulus of elasticity testing was completed, the two cylinders were then tested to failure to determine the compressive strength of the concrete. In no instance was the upper load limit used for modulus of elasticity testing greater than 40 percent of the actual compressive strength of the tested sample.

4.4.4 Coefficient of Thermal Expansion

While the development of coefficient of thermal expansion is difficult to test at very early ages, a test setup similar to the one described in AASHTO T 336 (2009) was used to determine the coefficient of thermal expansion of the hardened concrete after 28 days of

standard curing. The modified AASHTO T 336 setup used for testing is shown in Figure 4-4.

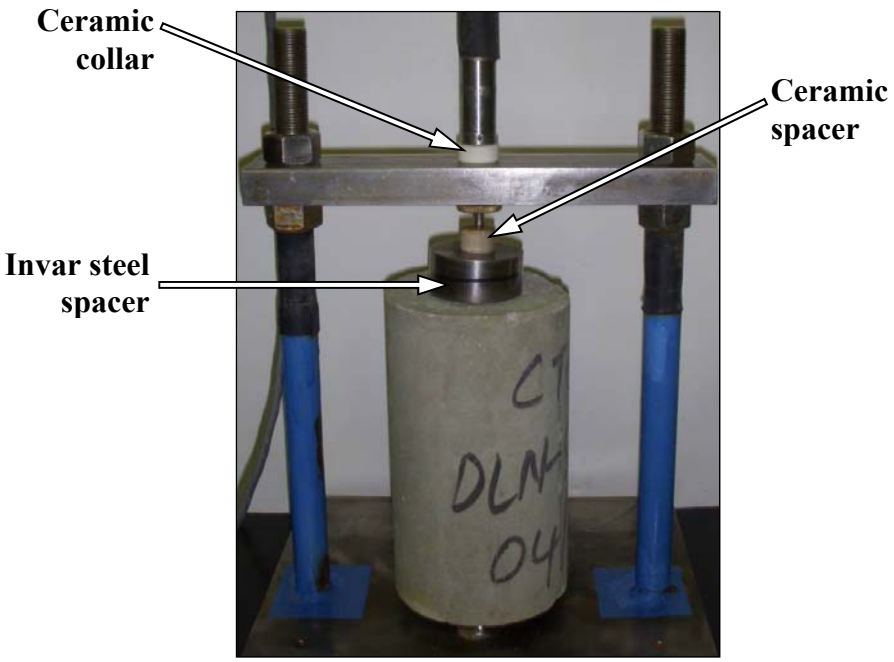

Figure 4-4: Modified AASHTO T 336 setup used for coefficient of thermal expansion testing

The coefficient of thermal expansion test setup used in this study matched the configuration required by AASHTO T 336 (2009) specification; however, slight modifications were made to improve the repeatability of the test. Ceramic inserts were used to provide insulation between the heated components and the LVDT, which reduces the effect of temperature on the readings of the LVDT. Specifically, a smaller ceramic disk was used under the tip of the LVDT and a ceramic collar was used to mount the LVDT to the frame. The purpose of the ceramic collar was to limit the temperature transferred to the LVDT through the mounting crossbar. Additionally, an Invar steel spacer was added on top of the concrete specimen to create additional height above the specimen for fluctuations in water level and to limit heat transfer from the heated water to

the crossbar. The disks and collar were used in the calibration procedure, thus their effects were accounted for in the calibration method of AASHTO T 336 (2009).

4.4.5 Semi-Adiabatic Calorimetry

Semi-adiabatic testing is used to characterize the heat of hydration development of each mixture (Schindler and Folliard 2005). The semi-adiabatic calorimeter (SAC) test equipment used during this project was supplied by Digital Site Systems, Inc., Pittsburgh, Pennsylvania. Since no standardized ASTM test method exists for this procedure, a RILEM draft test procedure was followed (RILEM 119-TCE 1998). The SAC setup consisted of an insulated 55-gallon drum and a 6 × 12 in. cylindrical concrete sample. Probes are used to record the concrete temperature, heat loss through the calorimeter wall, and air temperature surrounding the test setup. The heat loss through the calorimeter was determined by a calibration test performed by using heated water.

4.4.5.1 *Heat of Hydration Characterization*

Trial batches were produced to ensure the slump, total air content, and yield of the concrete met the project requirements. After a trial batch met the slump, air and yield criteria, a 6 × 12 in. cylinder was produced, weighed, and placed in the SAC. The cylinder was cured in the SAC for at least five days. The heat of hydration parameters were determined from the SAC data (Schindler and Folliard 2005).

4.4.5.2 *Thermal Diffusivity Assessment*

After approximately 7 days of curing, a cylinder produced from the sand-lightweight concrete trial batch was placed in an oven, heated to approximately 160 °F, and placed in the SAC. The heat decay was measured over four to five days and the thermal diffusivity of the concrete back-calculated. With the specific heat of the constituents except the lightweight coarse aggregate known (Lamond and Pielert 2006), the thermal diffusivity of the coarse aggregate was back-calculated to fit the measured temperature decay in the SAC. Now with the thermal diffusivity of the coarse aggregate known, the same process was used to determine the thermal diffusivity of the lightweight fine aggregate in the all-lightweight concrete mixture. With the adiabatic heat curve and the thermal diffusivities known, two temperature profiles were generated with the ConcreteWorks software package (Poole et al. 2006). One temperature profile simulates the temperature history a concrete bridge deck would experience during summer placement conditions (95°F) and the other was for fall placement conditions (73°F).

4.4.6 Setting Testing

Setting of concrete is the gradual transition from liquid to solid. Final setting of concrete relates to the point where stress and stiffness start to develop in freshly placed concrete. It is caused by the formation of sufficient hydration products (Schindler 2004b). According to ASTM C 403, initial set is achieved when the concrete paste reaches a penetration resistance of 500 psi, and final set is achieved when the concrete paste reaches a penetration resistance of 4,000 psi.

In this project, one - 6 × 8 in. container was filled with mortar that was wet-sieved from the concrete. This specimen was placed in a chamber that is match-cured to the temperature profile of the free-shrinkage frame. Penetration resistance testing is performed on this specimen in accordance with ASTM C 403. When initial setting is reached, the supporting plates in the free-shrinkage frame are released to allow free movement to occur.

4.4.7 Other Fresh Quality Control Tests

All concrete was mixed as per ASTM C 192 under laboratory conditions. The temperature, slump, and density of the fresh concrete were measured as per ASTM C 1064, ASTM C 143, and ASTM C 138, respectively, for each batch of concrete. The total air content for the all normalweight aggregate mixtures was measured by the pressure method as per ASTM C 231. The total air content for all mixtures containing lightweight aggregate was measured by the volumetric method as per ASTM C 173. All ASTM tests were performed by a technician certified as an ACI Field Testing Technician - Grade I.

4.5 Concrete Temperature Modeling

The temperature profile that an in-place concrete element experiences is a function of the geometry of the element, the concrete mixture proportions, the chemical composition of the cementing materials, the placement temperature, the thermal conductivity of the aggregate, and environmental effects such as ambient temperature, wind speed, and incoming solar radiation.

To assess the effect of placement and curing temperature, the concrete modeling software ConcreteWorks (Poole et al. 2006) was used to determine the temperature profile that an 8-in thick bridge deck constructed on stay-in-place metal forms would experience. Two placement scenarios were investigated: summer and fall conditions. Bridge deck temperatures for summer and fall placements were determined for Montgomery, Alabama on construction dates of August 15 and October 15, respectively. Semi-adiabatic calorimetry was used to determine the hydration parameters of each mixture (Schindler and Folliard 2005). Using the hydration parameters, as well as the placement date, city, bridge geometry, aggregate type, thermal diffusivity, mixture proportions, placement temperature, wind speed, ambient relative humidity, and percent cloud cover, two concrete temperature profiles were generated for each simulated placement season. Note that this practice captures the unique temperature profile that each mixture would experience due to its own heat of hydration and thermal properties should it be placed in an 8-in. thick bridge deck. The match-cured temperature profile used for each mixture is thus unique to that mixture.

The mixtures were tested at each of the temperature scenarios to evaluate the effect of placement temperature and curing temperature on time to initial cracking. When summer scenarios mixtures were tested, the raw materials were placed in an environmental chamber and conditioned to obtain fresh concrete temperatures of approximately 95 °F.

4.6 Other Raw Concrete Materials

4.6.1 Portland Cement

An adequate quantity of Type I portland cement was donated by TXI to complete all testing associated with this project. The properties of the portland cement are shown in Table 4-6.

Table 4-6:Portland cement properties

C_3S	C_2S	C_3A	C_4AF	Free CaO	SO_3	MgO	Blaine Fineness
60.3 %	18.2 %	5.4 %	11.3 %	0.9 %	2.6 %	1.3 %	351 (m^2/kg)

4.6.2 Normalweight Aggregates

The coarse aggregate for the project was an ASTM C 33 No. 67 siliceous river gravel. The fine aggregate used throughout the project was siliceous river sand. Both aggregate types were obtained from the quarry of Martin Marietta Materials located in Shorter, Alabama. The aggregates were sampled and sieve analyses were performed to obtain the gradations as per ASTM C 136. Samples were also obtained for specific gravity and absorption capacity testing of the coarse and fine aggregate as per ASTM C 127 and ASTM C 128, respectively. The sieve analysis results are presented in Appendix A. The specific gravity and absorption capacity for the normalweight coarse and fine aggregates were 2.63, 0.52 percent and 2.61, 0.41 percent, respectively. The fineness modulus of the normalweight sand was 2.45.

4.6.3 Chemical Admixtures

Chemical admixtures were used as needed in the concrete mixtures to control the slump and the total air content of the fresh concrete. All chemical admixtures were supplied by BASF Admixtures, Inc.

The air-entraining admixture (AEA) used for this research was MB AE 90 which meets the requirements of ASTM C 260. The AEA dosage was determined based on multiple trial batches to obtain the target total air content.

The normal-range water-reducing admixture was Pozzolith 322N which meets the requirements for an ASTM C 494 Type A admixture. A polycarboxylate-based high-range water-reducing (HRWR) admixture was also used for some mixtures as shown in Table 4-2 to Table 4-4. The HRWR admixture was Polyheed 1025, which meets the requirements for an ASTM C 494 Type F admixture. The dosages of the water-reducing admixtures were determined by trial batches to obtained fresh concrete that met the project slump requirements.

For the ALW mixtures, a rheology-controlling admixture was used. Without the rheology-controlling admixture, the slump test of all ALW mixtures exhibited a shear failure and this concrete was very harsh. Representatives of BASF Admixtures, Inc. recommended the use of Navitas 33 to counter the harshness of the ALW mixtures and this admixture significantly improved the workability of these mixtures. The rheology-controlling admixture can be classified as an ASTM C 494 Type S admixture.

CHAPTER 5

PART I: EXPERIMENTAL RESULTS

The results collected from the experimental work performed for this part are presented in this chapter. A discussion and synthesis of the results are provided in Chapter 6. Three lightweight aggregates were tested: expanded slate, expanded clay, and expanded shale. The mixture proportions, thermal properties, fresh properties, temperature profiles, restrained stress development, unrestrained length change, and mechanical property development for both the summer and fall placement scenarios were evaluated for each mixture. The results for concretes made with expanded shale, clay, and slate aggregates are compared to the normalweight aggregate concrete mixture in Sections 5.1, 5.2, and 5.3, respectively.

5.1 Expanded Slate Results

5.1.1 Mixture Gradations and Proportions

Three concretes containing expanded slate LWA were produced and tested at two temperature scenarios. The three concretes used were an internal curing (IC), a sand-lightweight (SWL), and an all-lightweight (ALW) concrete. The proportions for the concretes made with this LWA are shown in Table 4-2. The combined aggregate gradations for the mixtures are presented on a 0.45 power curve in Figure 5-1 and Figure

5-2. The 0.45 power curve gives an indication of the particle packing of a blended aggregate gradation (Mindess et al. 2002).

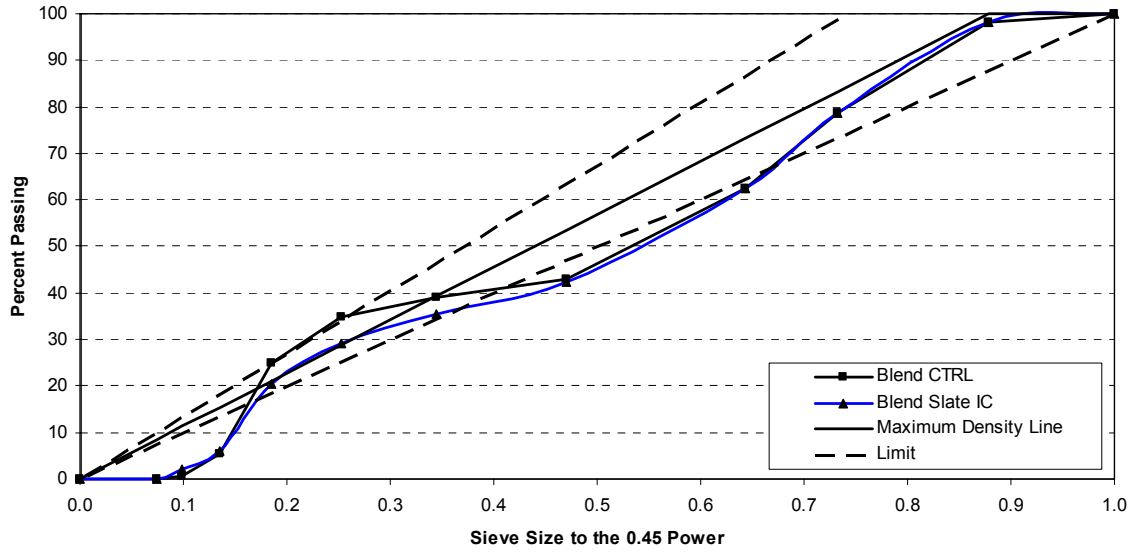

Figure 5-1: Combined gradation of CTRL and Slate IC mixtures on the 0.45 power curve

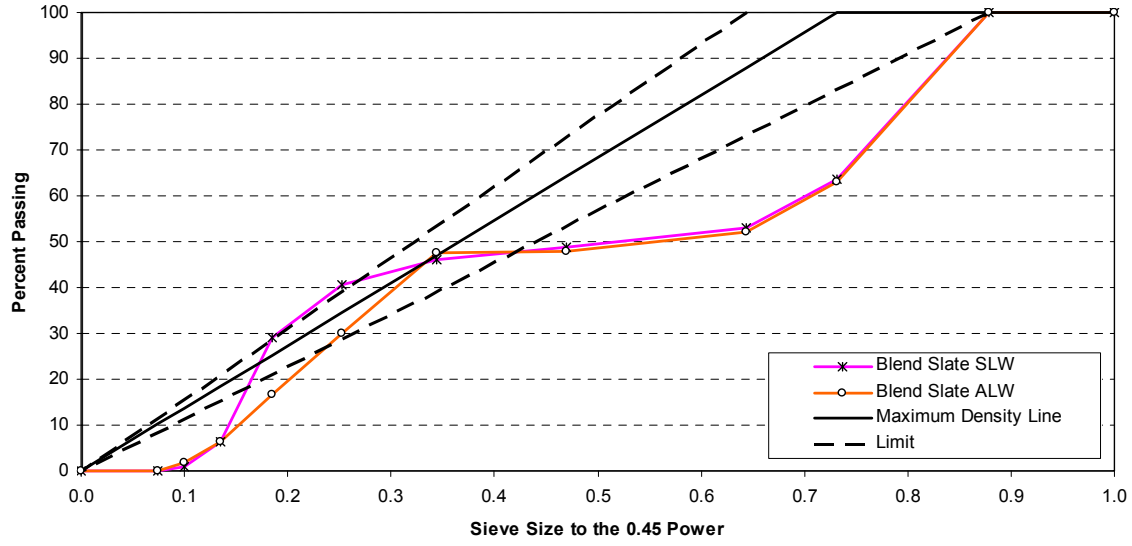

Figure 5-2: Combined gradation of Slate SLW and ALW mixtures on the 0.45 power curve

5.1.2 Fresh Concrete Properties

For each mixture and placement scenario, two batches were produced. The first batch was used to produce the concrete cylinders for mechanical property testing and the second batch was for RCF and FSF testing. The fresh properties for each mixture, batch, and placement scenario are presented in Table 5-1. The "Δ Density" column in Table 5-1 is the difference between the measured density and the calculated density after correcting for the measured air content of each batch. A positive sign for the "Δ Density" indicates the measured density was greater than the calculated density and vice versa.

5.1.3 Miscellaneous Properties

The calculated equilibrium density as per ASTM C 567, coefficient of thermal expansion measured from the modified AASHTO T 336 setup, and the thermal diffusivity determined from semi-adiabatic calorimetry are summarized in Table 5-2.

5.1.4 Curing Temperatures

The curing temperature profiles for the fall and summer placement scenarios for the expanded slate aggregate concretes and the normalweight control concrete are presented in Figure 4-3. The temperature profiles are truncated at the time of cracking.

Table 5-1: Measured fresh concrete properties of expanded slate and control mixtures

Mixture and Placement Scenario	Batch No.	Fresh Concrete Test Results				Calculated
		Slump (in.)	Temp. (°F)	Air (%)	Density (lb/ft^3)	Δ Density (lb/ft^3)
CTRL (Fall)	1	3.25	74	5.0	143.8	0.3
	2	4.5	73	6.25	141.9	0.6
CTRL (Sum)	1	2.5	100	4.75	143.0	-0.3
	2	2.0	100	5.25	141.9	-0.6
Slate IC (Fall)	1	3.25	74	5.75	137.8	-0.2
	2	3.5	75	5.75	138.6	0.6
Slate IC (Sum)	1	2.0	97	4.5	140.6	0.8
	2	2.5	97	4.75	140.1	0.8
Slate SLW (Fall)	1	3.5	74	4.5	119.0	0.3
	2	3.75	74	4.5	119.2	0.1
Slate SLW (Sum)	1	2.0	97	4.25	119.8	0.2
	2	2.5	95	4.25	120.0	0.4
Slate ALW (Fall)	1	5.0	70	5.0	104.0	0.8
	2	4.5	68	5.25	103.8	0.8
Slate ALW (Sum)	1	2.25	92	4.5	104.3	0.6
	2	2.5	95	4.25	104.8	0.8

Table 5-2: Miscellaneous properties of expanded slate and control mixtures

Property	CTRL	Slate IC	Slate SLW	Slate ALW
Calculated Equilibrium Density (lb/ft^3)	140.0	135.0	113.6	95.5
Coefficient of Thermal Expansion (με/°F)	6.2	5.9	5.1	4.3
Thermal Diffusivity (ft^2/hr)	0.046	0.042	0.033	0.029

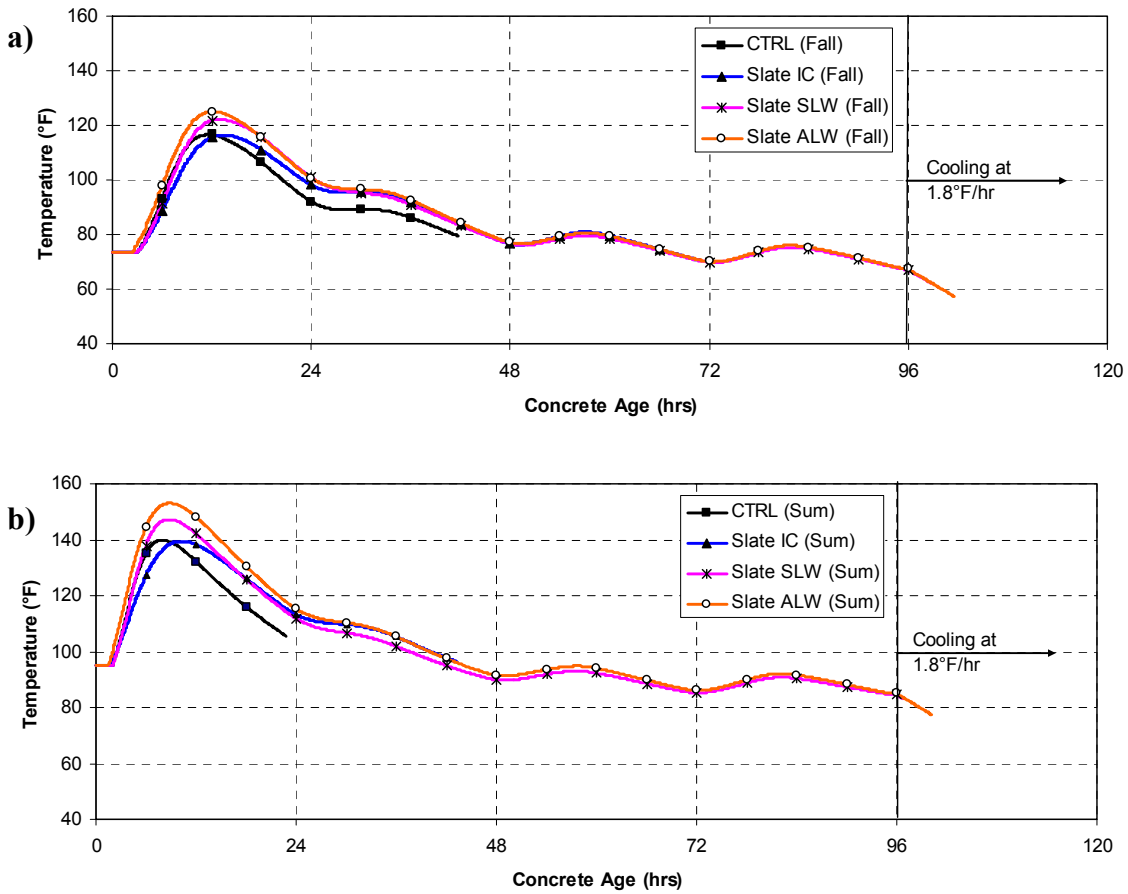

Figure 5-3: Modeled temperature profile for slate and control mixtures: a) Fall and b) Summer placement scenarios

5.1.5 Restrained Stress Development

The restrained stress development is presented in Figure 5-4 and Figure 5-5 for the match cured and isothermal cured conditions, respectively. The restrained stress development data for the match-cured condition end at the time of cracking. The restrained stress development for the isothermal curing conditions was measured for 96 hours.

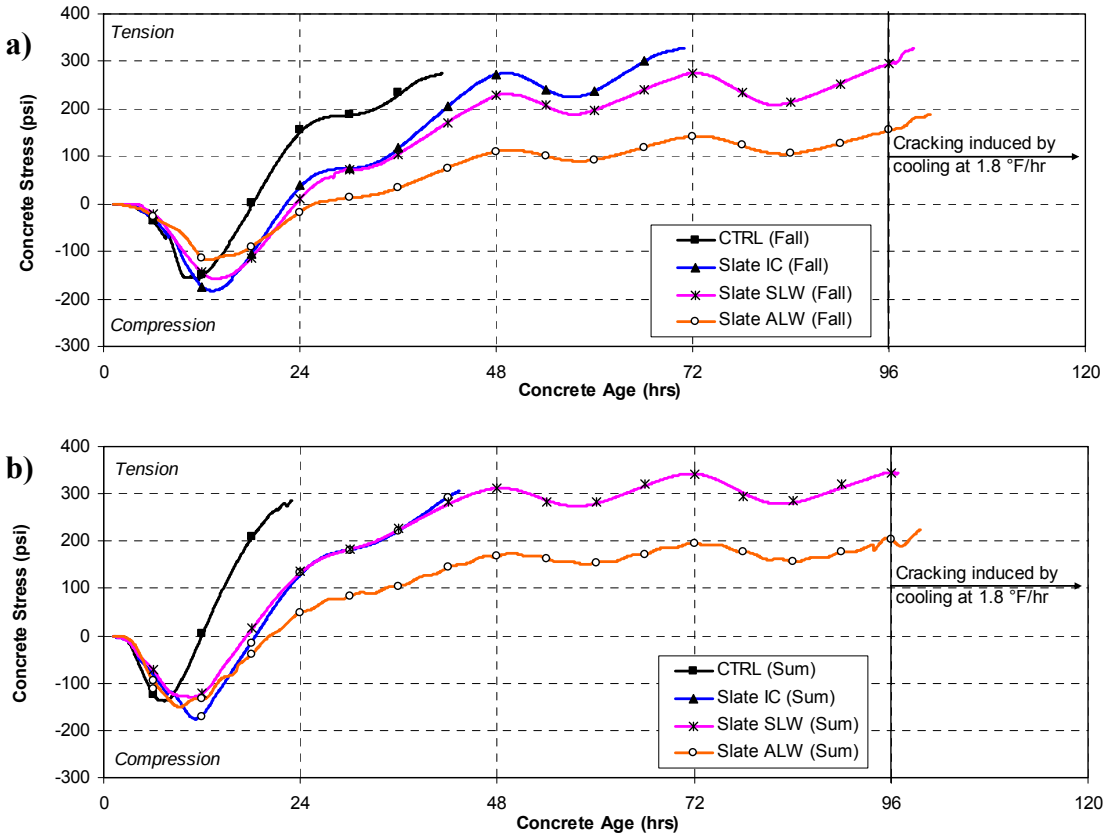

Figure 5-4: Restrained stress development for slate and control mixtures: a) Fall and b) Summer placement scenarios

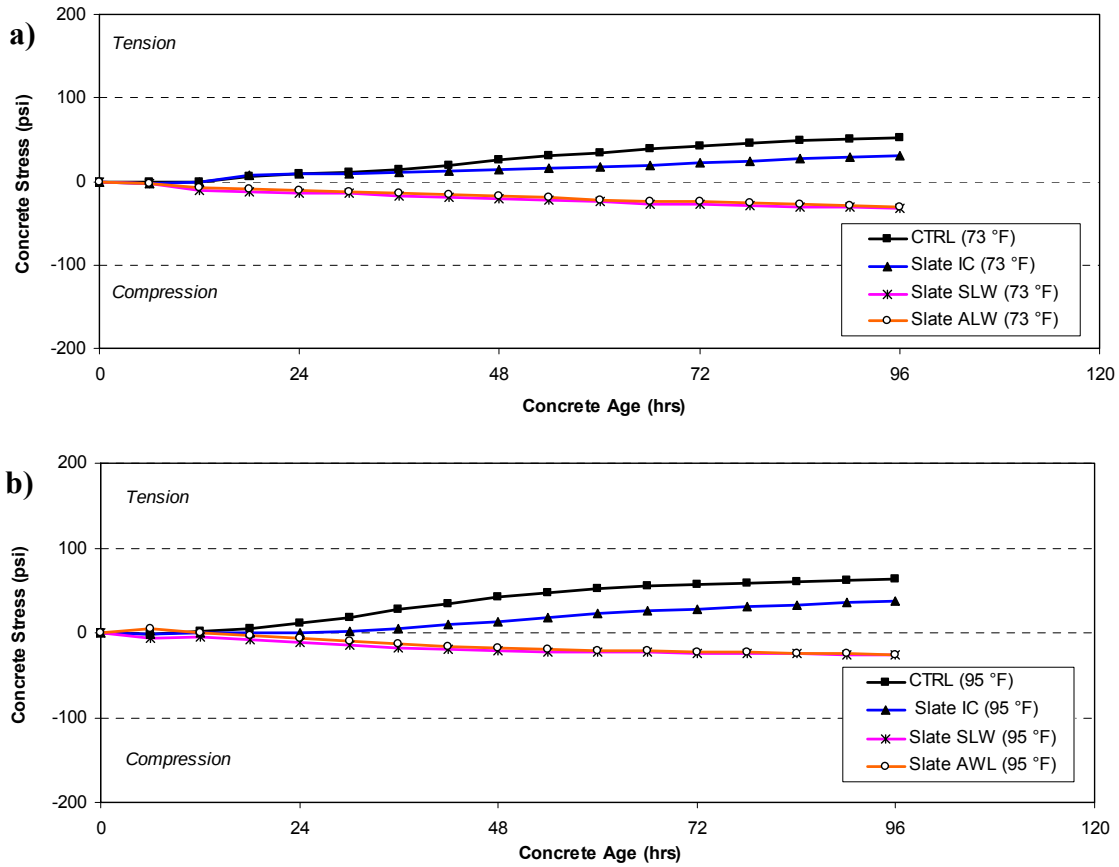

Figure 5-5: Restrained stress development for slate and control mixtures under: a) 73 °F and b) 95 °F isothermal conditions

5.1.5.1 *Time to zero stress and cracking*

The time and temperature to the zero stress and cracking condition for each mixture and curing scenario are summarized in Table 5-3.

Table 5-3: Time and temperature at zero stress and cracking of slate and control mixtures

Mixture	Zero Stress		Cracking	
	Time (hrs)	Temp. (°F)	Time (hrs)	Temp. (°F)
CTRL (Fall)	18.7	104.8	41.7	79.5
CTRL (Sum)	12.4	131.0	22.8	105.5
Slate IC (Fall)	22.3	101.6	70.8	70.6
Slate IC (Sum)	18.4	125.1	43.3	96.4
Slate SLW (Fall)	23.3	102.5	98.9 *	61.9
Slate SLW (Sum)	17.4	127.3	96.9 *	82.8
Slate ALW (Fall)	23.5	101.6	100.3 *	59.7
Slate ALW (Sum)	17.9	131.0	99.6*	78.5

* Note: Cracking induced by cooling at 1.8 °F/hr after 96 hours

5.1.6 Measured Unrestrained Length Change

The strain measurements from the unrestrained specimens in the FSF are presented in Figure 5-6. The concrete specimens were match cured using the modeled temperature profile of the 8-in. thick bridge deck. The data are truncated at the time of cracking to help illustrate the strain developed in concrete until cracking occurred.

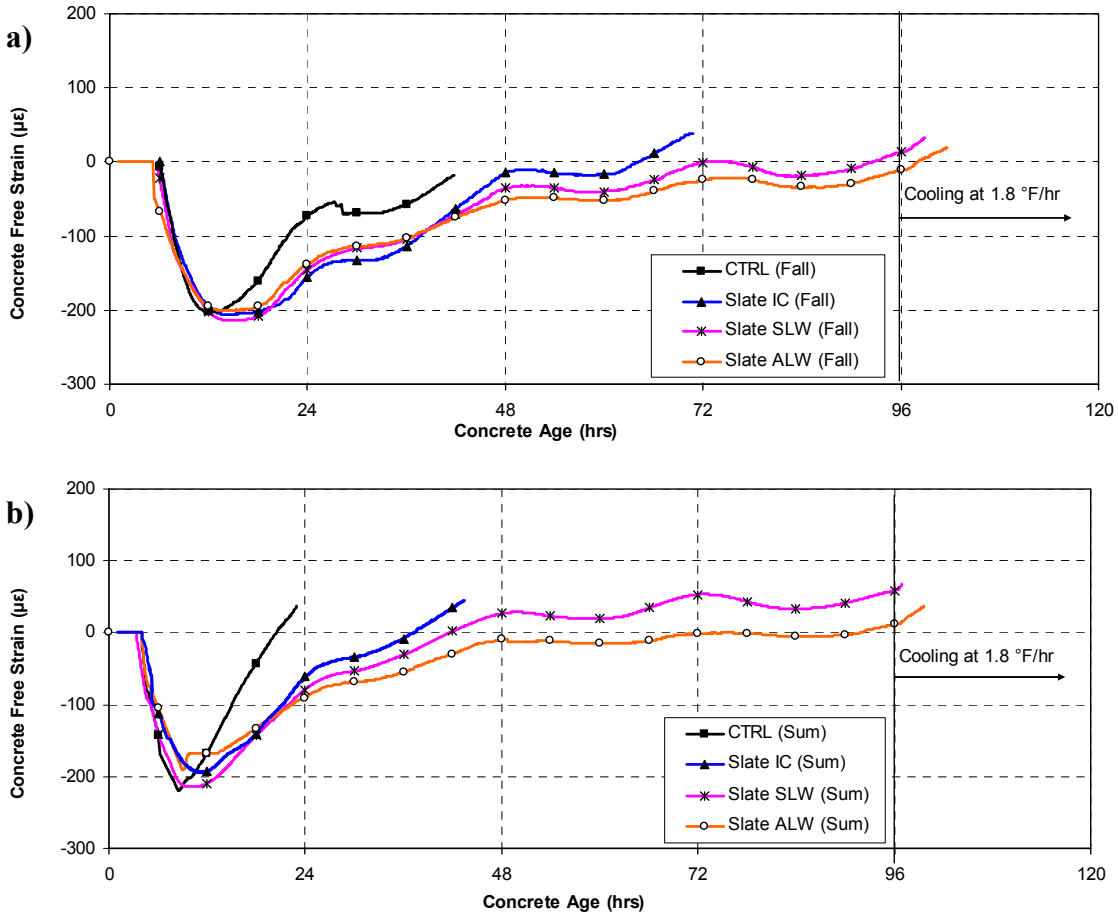

Figure 5-6: Free shrinkage strains for slate and control mixtures: a) Fall and b) Summer placement scenarios

5.1.7 Mechanical Properties

The compressive strength, splitting tensile strength, and modulus of elasticity development were measured by testing cylinders match cured to the bridge deck temperature profile for each mixture and placement scenario. A regression analysis was performed on the discrete data points with the exponential function recommended by ASTM C 1074. The resulting best-fit curves for each property are shown in Figure 5-7and Figure 5-8 for fall and summer placement scenarios, respectively. The average of the two test cylinders for each mechanical property is summarized in Appendix B.

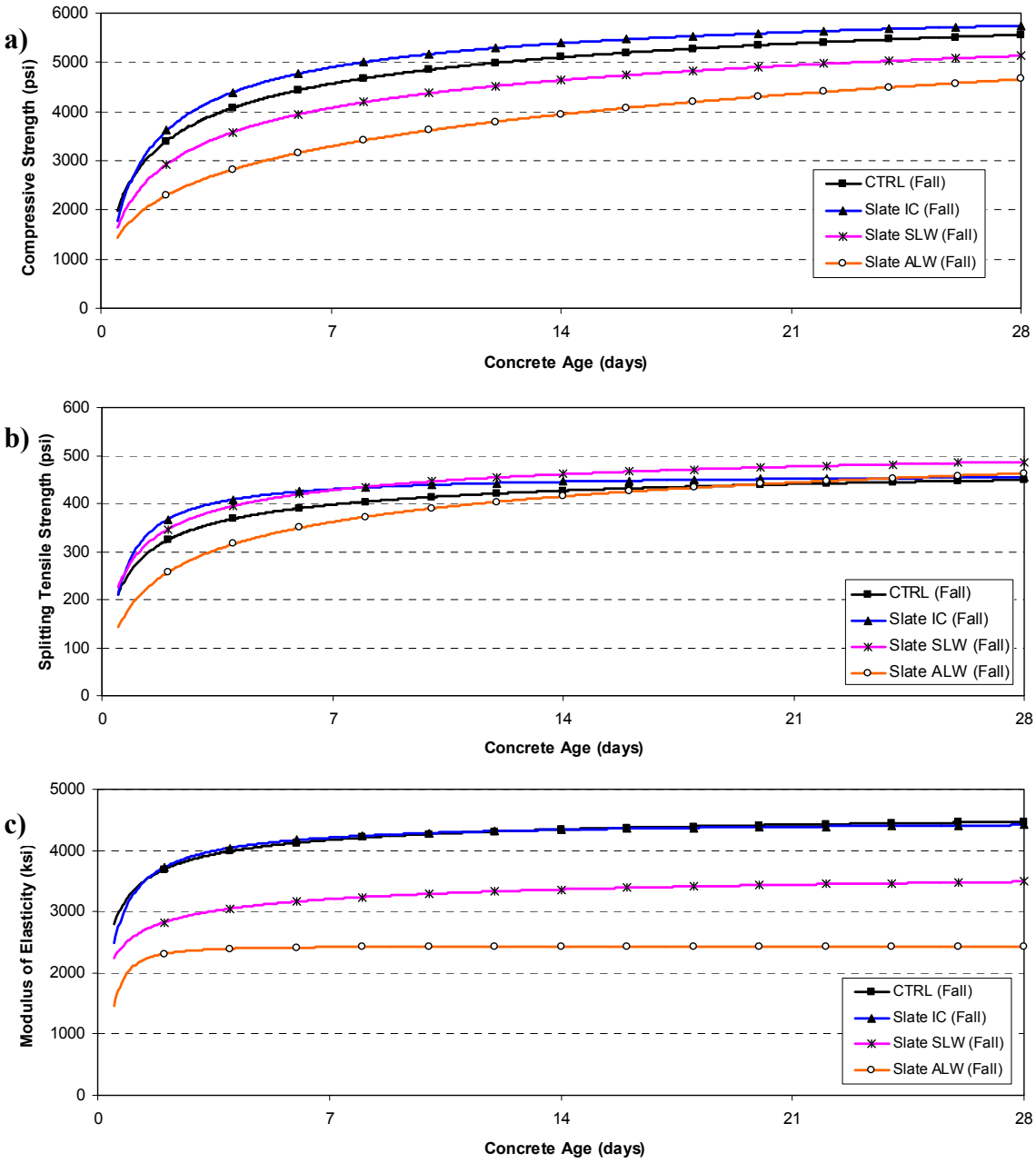

Figure 5-7: Fall placement scenario for slate and control mixtures: a) Compressive strength, b) Splitting tensile strength, and c) Modulus of elasticity development

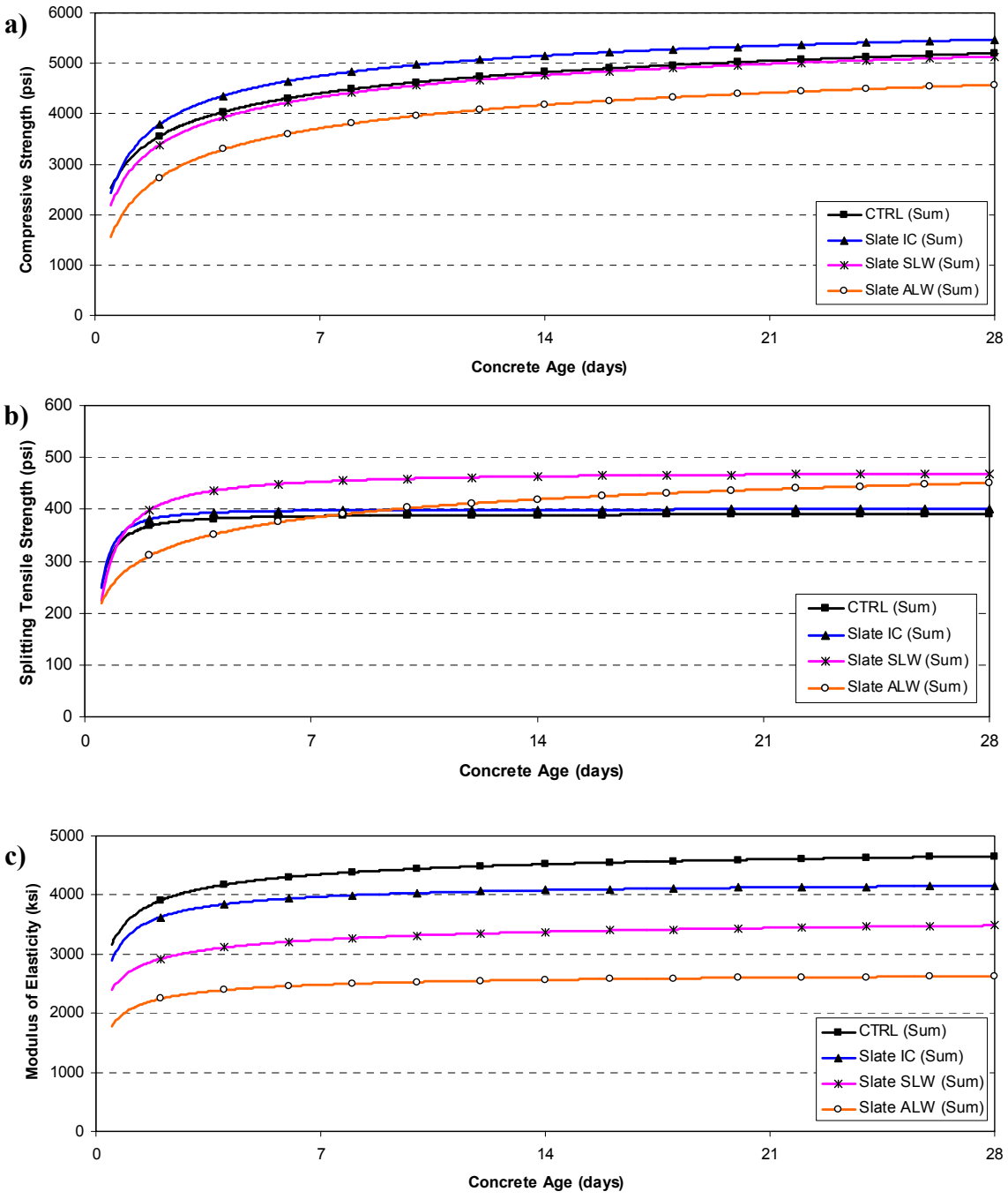

Figure 5-8: Summer placement scenario for slate and control mixtures: a) Compressive strength, b) Splitting tensile strength, and c) Modulus of elasticity development

5.2 Expanded Clay Results

5.2.1 Mixture Gradations and Proportions

Three concretes containing expanded clay LWA were produced and tested at two temperature scenarios. The three concretes were an internal curing (IC), a sand-lightweight (SWL) and an all-lightweight (ALW) concrete. The proportions for the concretes made with this LWA are shown in Table 4-3. The combined aggregate gradations of each mixture presented on a 0.45 power curve are presented in Figure 5-9 and Figure 5-10.

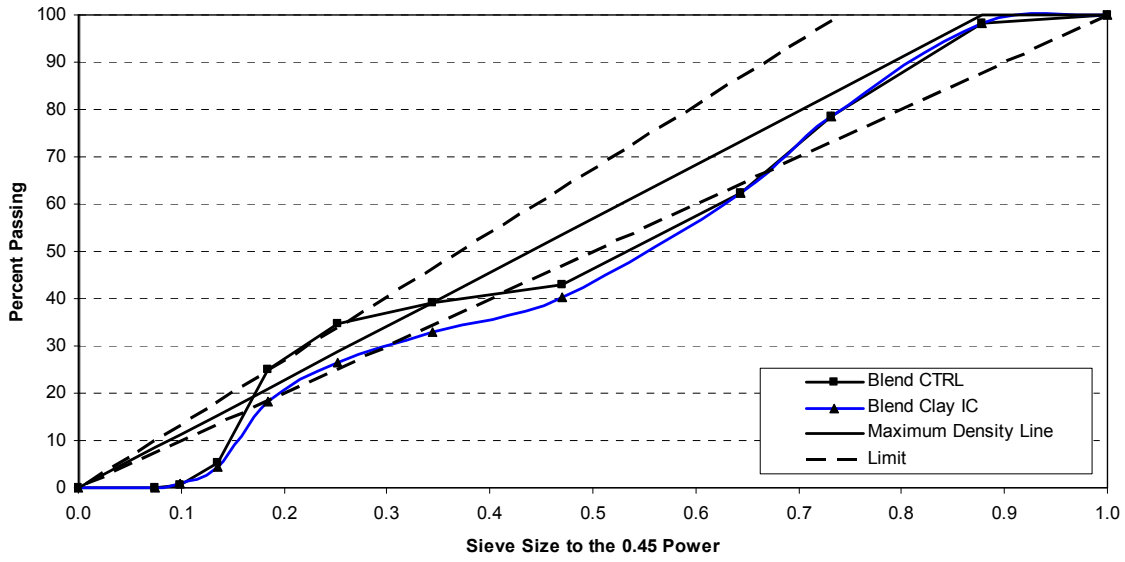

Figure 5-9: Combined gradation of CTRL and Clay IC mixtures on the 0.45 power curve

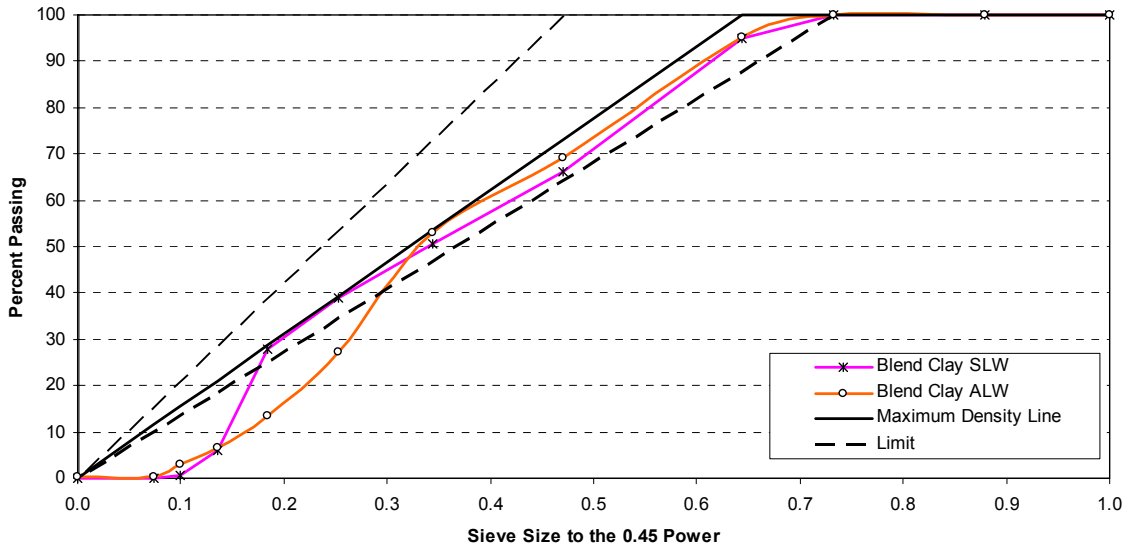

Figure 5-10: Combined gradation of Clay SLW and ALW mixtures on 0.45 power curve

5.2.2 Fresh Concrete Properties

For each mixture and placement scenario, two batches were produced. The first batch was used to produce the concrete cylinders for mechanical property testing and the second batch was for RCF and FSF testing. The fresh properties for each mixture, batch, and placement scenario are presented in Table 5-4. As mentioned previously, the "Δ Density" column in Table 5-4 is the difference between the measured density and the calculated density after correcting for the measured air content of each batch.

Table 5-4: Measured fresh concrete properties of expanded clay and control mixtures

Mixture and Placement Scenario	Batch No.	Fresh Concrete Test Results				Calculated
		Slump (in.)	Temp. (°F)	Air (%)	Density (lb/ft^3)	Δ Density (lb/ft^3)
CTRL (Fall)	1	3.25	74	5.0	143.8	0.3
	2	4.5	73	6.25	141.9	0.6
CTRL (Sum)	1	2.5	100	4.75	143.0	-0.3
	2	2.0	100	5.25	141.9	-0.6
Clay IC (Fall)	1	3.25	73	4.5	140.4	0.1
	2	4.75	73	5.25	136.4	0.2
Clay IC (Sum)	1	2.25	95	4.25	141.4	0.8
	2	2.5	96	4.5	140.6	0.3
Clay SLW (Fall)	1	3.75	74	5.0	122.1	0.0
	2	4.0	74	5.25	121.7	0.1
Clay SLW (Sum)	1	2.5	97	5.0	122.8	0.7
	2	2.25	97	4.5	123.4	0.7
Clay ALW (Fall)	1	3.0	73	6.0	105.6	0.6
	2	3.5	72	6.5	106.5	0.3
Clay ALW (Sum)	1	2.0	95	4.5	108.6	0.8
	2	2.25	95	4.75	107.4	-0.1

5.2.3 Miscellaneous Properties

The calculated equilibrium density as per ASTM C 567, coefficient of thermal expansion measured from the modified AASHTO T 336 setup, and the thermal diffusivity determined from semi-adiabatic calorimetry are summarized in Table 5-5.

Table 5-5: Miscellaneous properties of expanded clay and control mixtures

Property	CTRL	Clay IC	Clay SLW	Clay ALW
Calculated Equilibrium Density (lb/ft^3)	140.0	135.0	111.2	91.3
Coefficient of Thermal Expansion (με/°F)	6.2	5.8	5.1	4.0
Thermal Diffusivity (ft^2/hr)	0.046	0.042	0.035	0.030

5.2.4 Curing Temperatures

The curing temperature profiles for fall and summer placement scenarios for the expanded clay aggregate concretes and the normalweight aggregate control concrete are presented in Figure 5-11. The temperature profiles are truncated at the time of cracking.

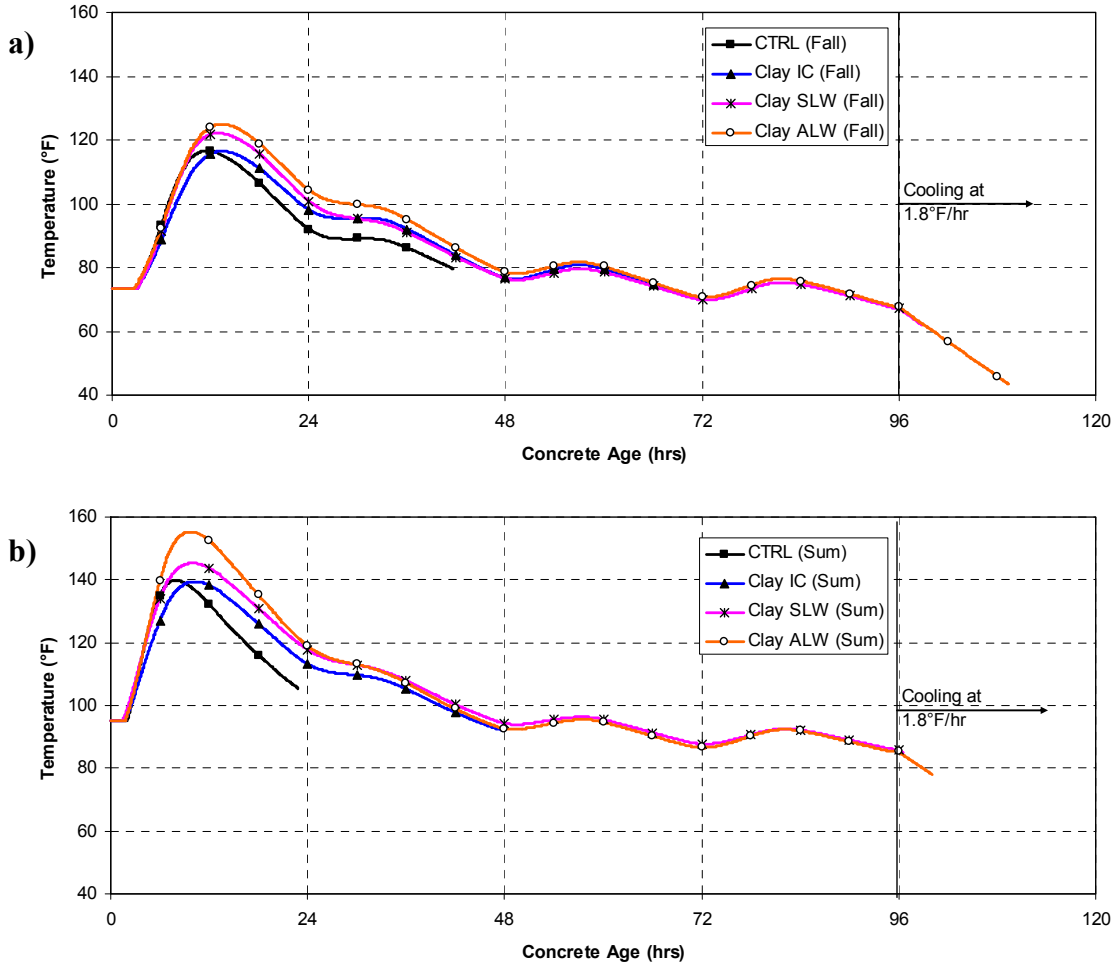

Figure 5-11: Modeled temperature profile for clay and control mixtures:a) Fall and b) Summer placement scenarios

5.2.5 Restrained Stress Development

The restrained stress development is presented in Figure 5-12 and Figure 5-13 for the match cured and isothermal cured conditions, respectively. The restrained stress

development data for the match-cured condition end at the time of cracking. The restrained stress development for the isothermal curing conditions was measured for 96 hours.

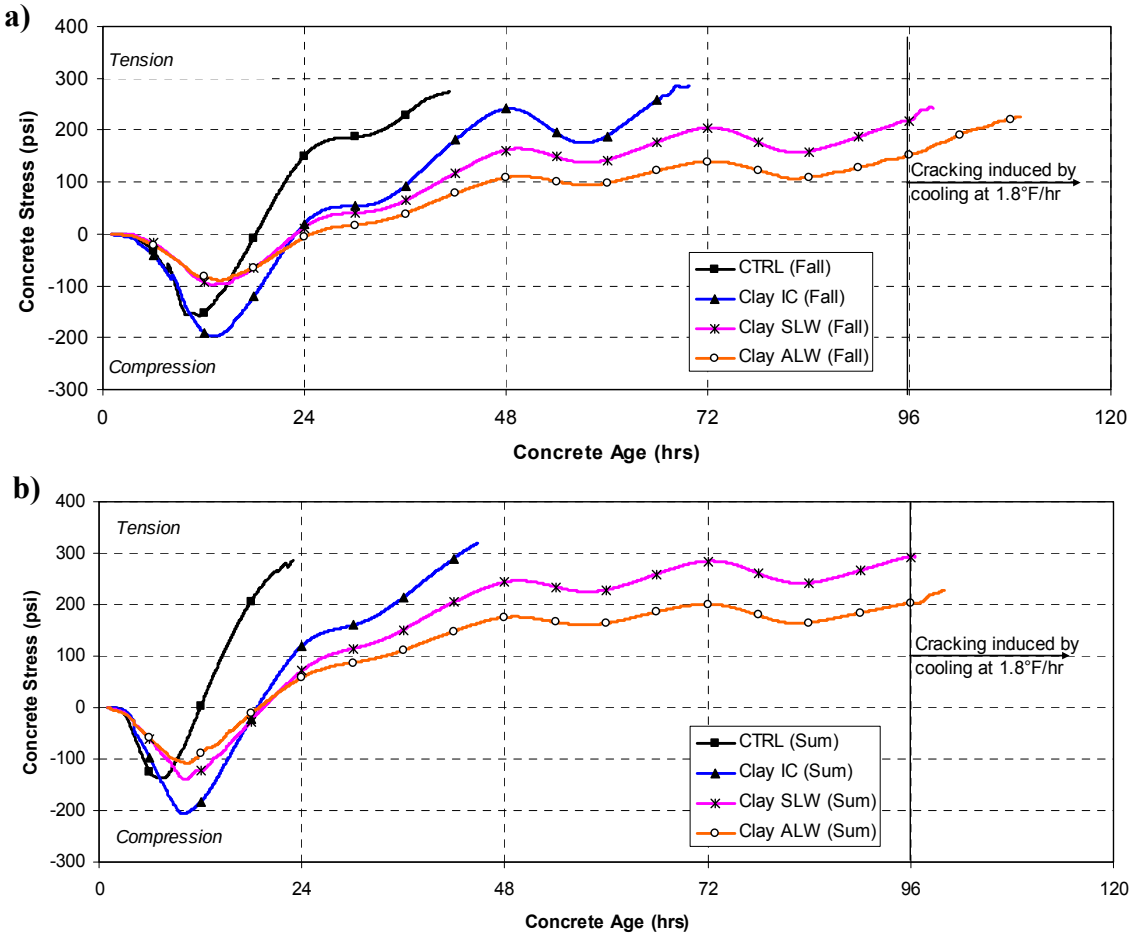

Figure 5-12: Restrained stress development for clay and control mixtures: a) Fall and b) Summer placement scenarios

5.2.5.1 *Time to Zero Stress and Cracking*

The time and temperature to the zero stress and cracking for each mixture and curing scenario is presented in Table 5-6.

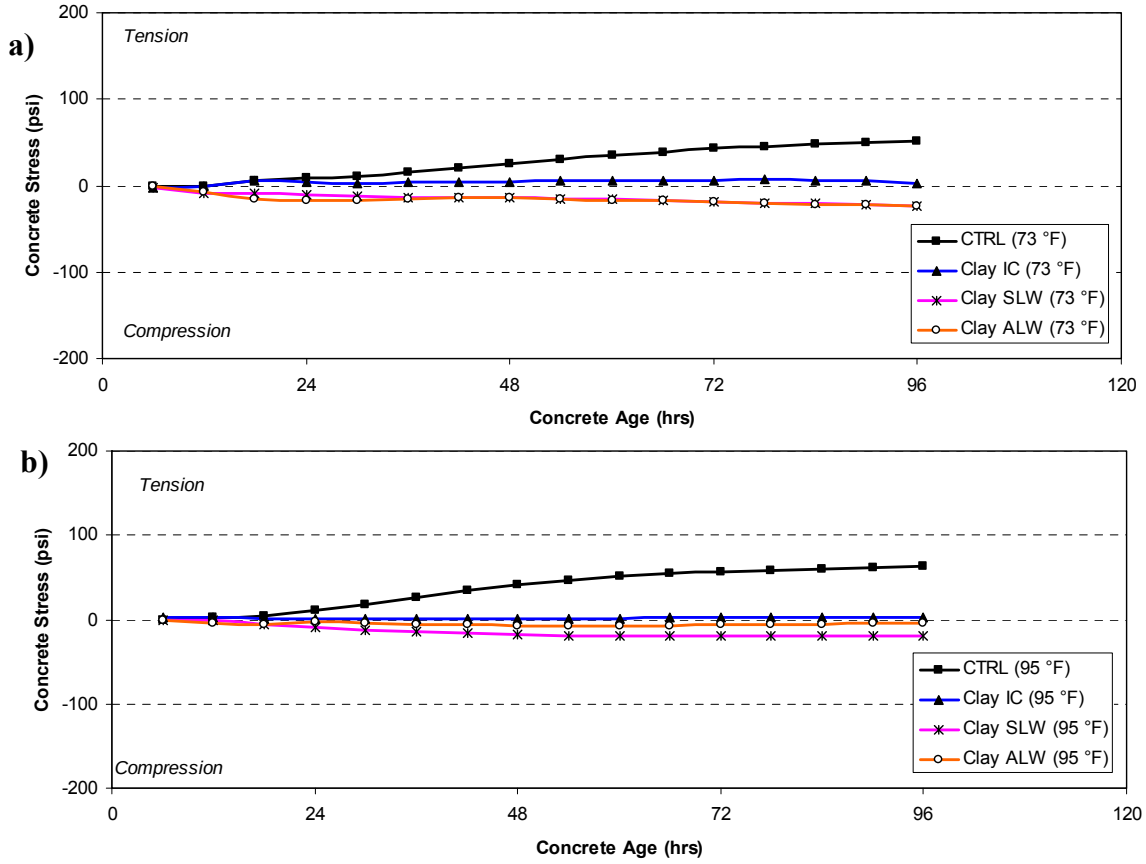

Figure 5-13: Restrained stress development for clay and control mixtures under: a) 73 °F and b) 95 °F isothermal conditions

Table 5-6: Time and temperature at zero stress and cracking of clay and control mixtures

Mixture	Zero Stress		Cracking	
	Time (hrs)	Temp. (°F)	Time (hrs)	Temp. (°F)
CTRL (Fall)	18.7	104.8	41.7	79.5
CTRL (Sum)	12.4	131.3	22.8	105.5
Clay IC (Fall)	22.8	100.3	69.8	71.4
Clay IC (Sum)	18.8	124.3	44.8	94.7
Clay SLW (Fall)	22.5	104.3	98.8 *	62.0
Clay SLW (Sum)	19.5	127.4	96.6 *	85.0
Clay ALW (Fall)	24.8	103.0	109.3 *	43.5
Clay ALW (Sum)	18.9	132.5	100.0 *	78.0

* Note: Cracking induced by cooling at 1.8 °F/hr after 96 hours

5.2.6 Measured Unrestrained Length Change

The strain measurements from the unrestrained specimens in the FSF are presented in Figure 5-14. The concrete specimens were match cured to the modeled temperature profile of the 8-in. thick bridge deck. The data are truncated at the time of initial cracking to help illustrate the strain developed in concrete until cracking occurred.

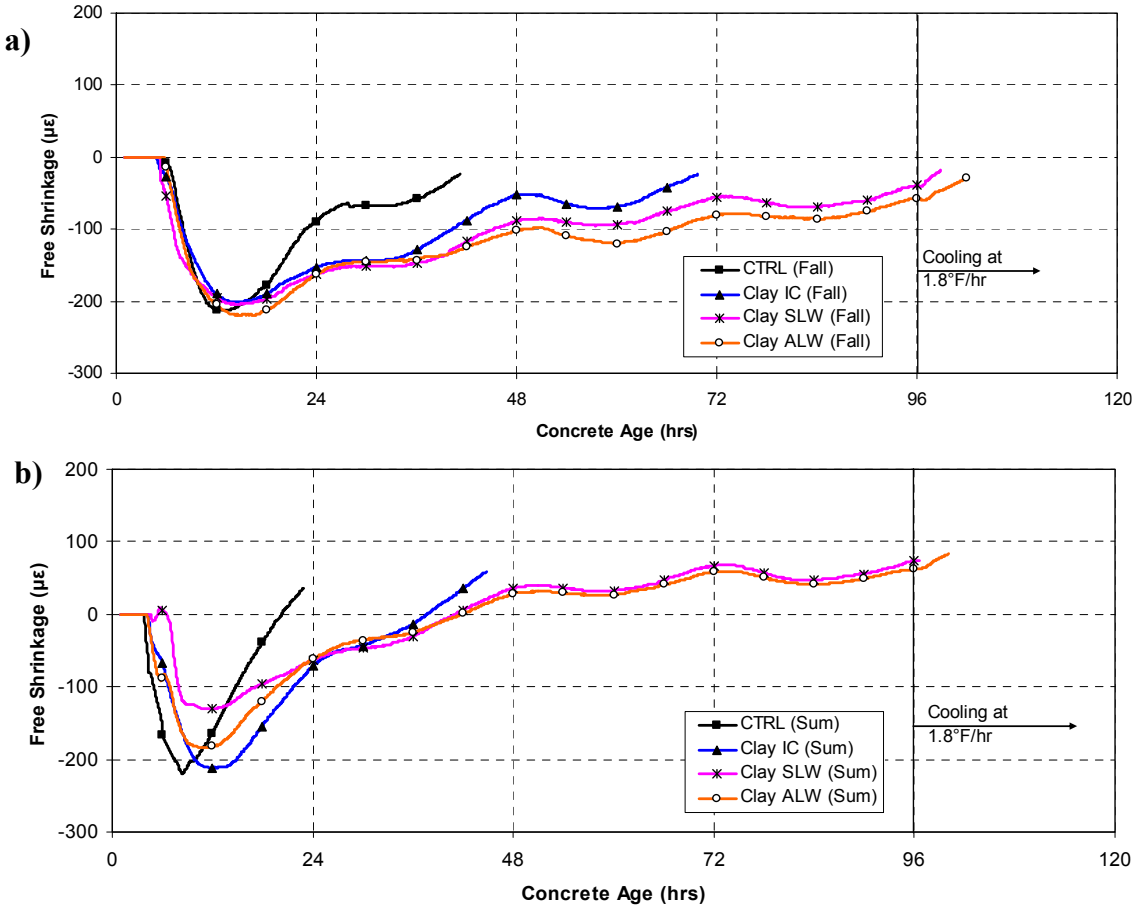

Figure 5-14: Free shrinkage strains for clay and control mixtures: a) Fall and b) Summer placement scenarios

5.2.7 Mechanical Properties

The compressive strength, splitting tensile strength, and modulus of elasticity development were measured by testing cylinders match cured to the bridge deck

temperature profile for each mixture and placement scenario. A regression analysis was performed on the discrete data points with the exponential function recommended by ASTM C 1074. The resulting best-fit curves for each property are shown in Figure 5-15 and Figure 5-16 for fall and summer placement scenarios, respectively. The average of the two test cylinders for each mechanical property is summarized in Appendix B.

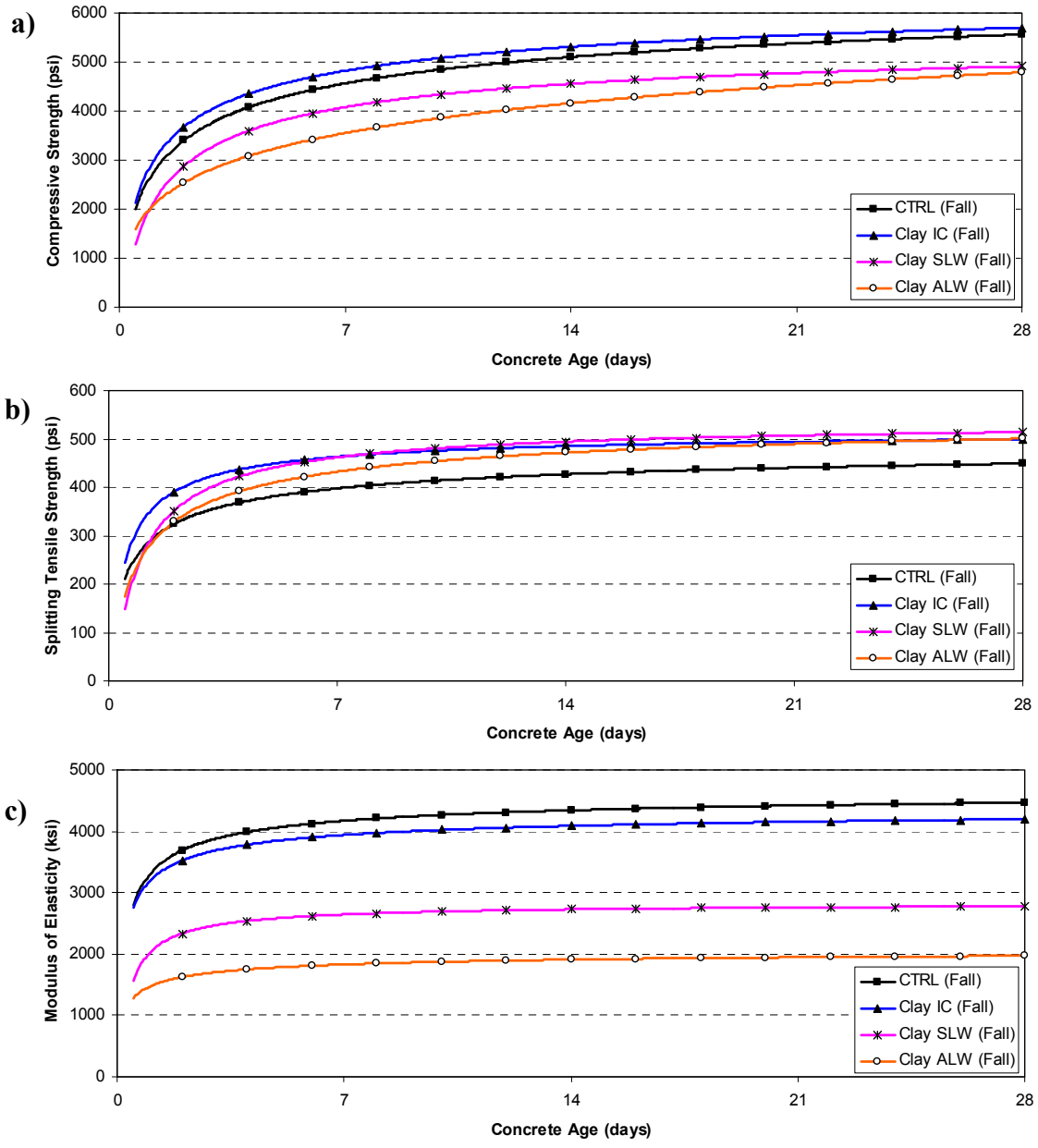

Figure 5-15: Fall placement scenario for clay and control mixtures: a) Compressive strength, b) Splitting tensile strength, and c) Modulus of elasticity development

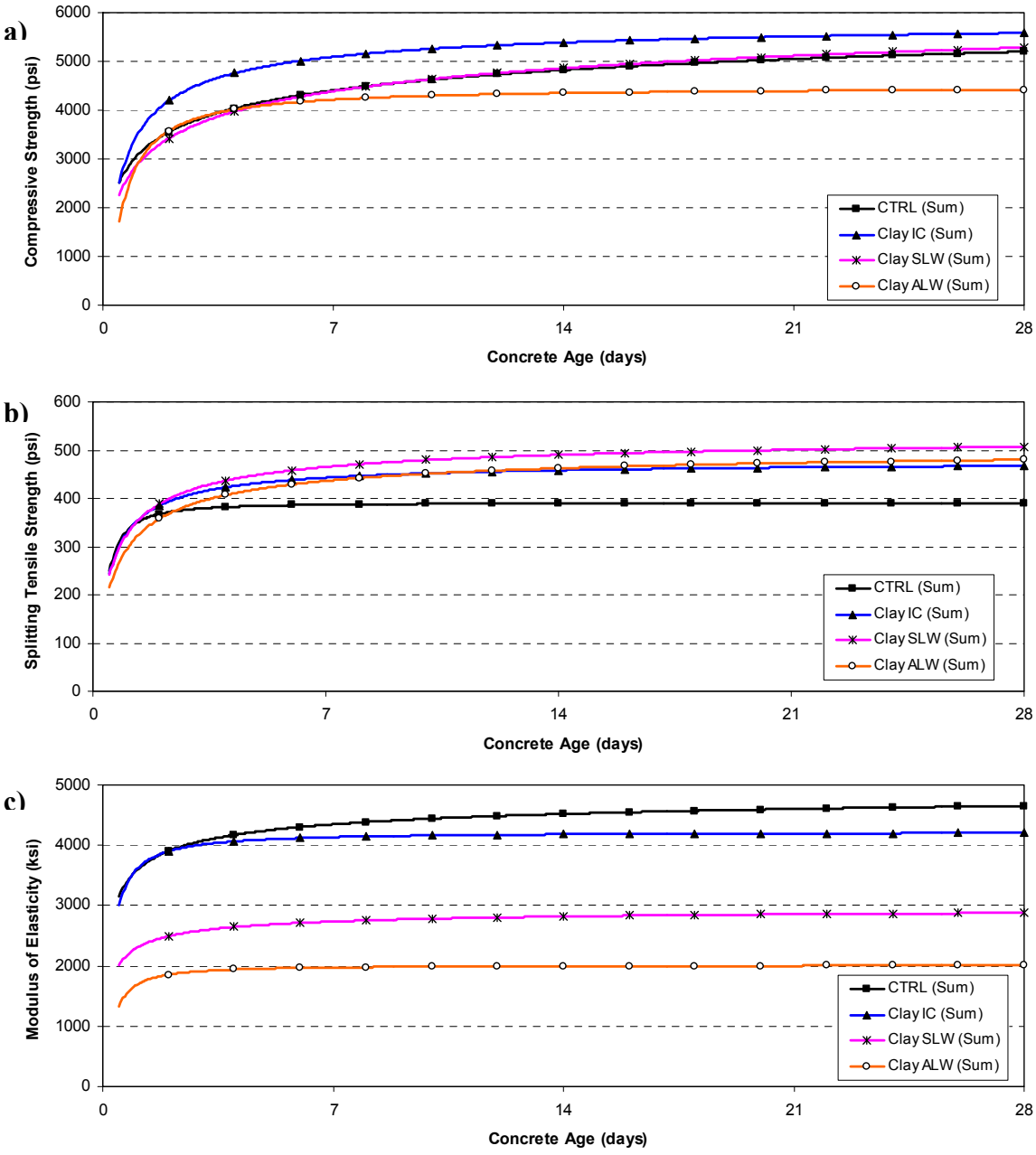

Figure 5-16: Summer placement scenario for clay and control mixtures: a) Compressive strength, b) Splitting tensile strength, and c) Modulus of elasticity development

5.3 Expanded Shale Results

5.3.1 Mixture Gradations and Proportions

Three concretes containing expanded shale LWA were produced and tested at two temperature scenarios. The three concretes used were an internal curing (IC), a sand-lightweight (SWL), and an all-lightweight (ALW) concrete. The proportions for the concretes made with this LWA are shown in Table 4-4. The combined aggregate gradations for the mixtures are presented on a 0.45 power curve in Figure 5-17 and Figure 5-18.

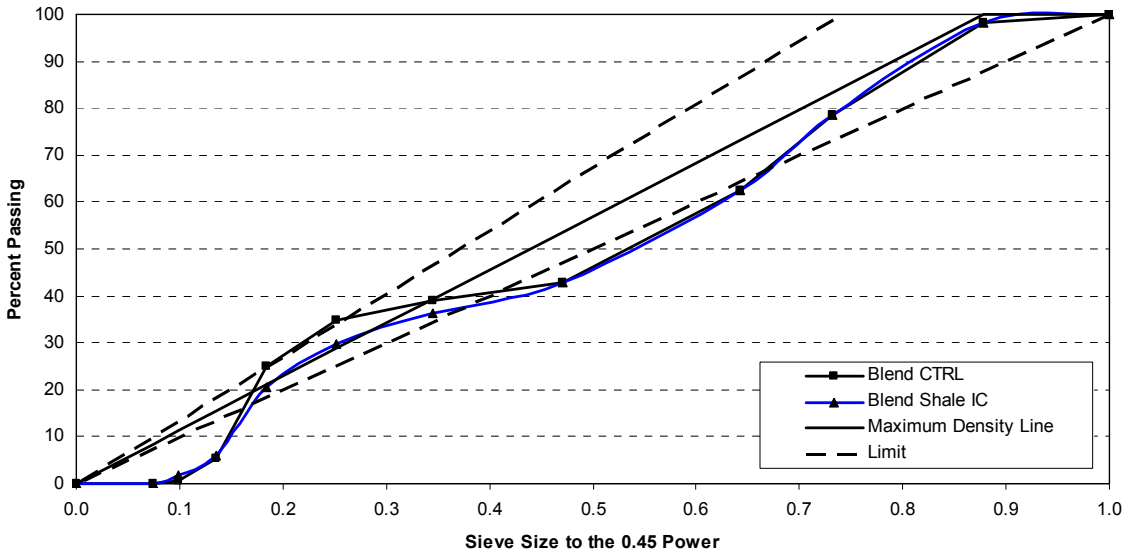

Figure 5-17: Combined gradation of CTRL and Shale IC mixtures on the 0.45 power curve

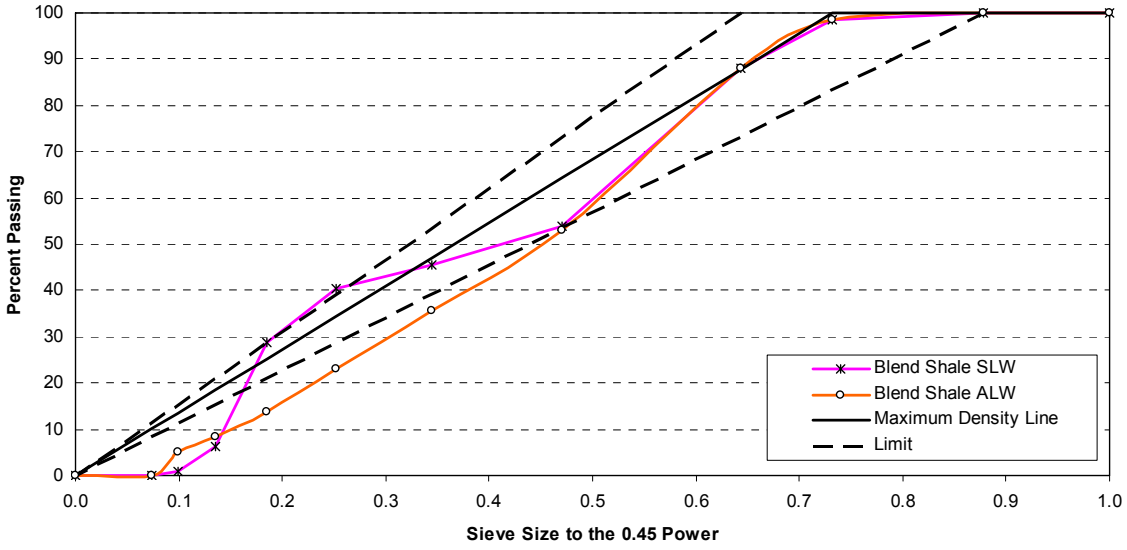

Figure 5-18: Combined gradation of Shale SLW and ALW mixtures on the 0.45 power curve

5.3.2 Fresh Concrete Properties

For each mixture and placement scenario, two batches were produced. The first batch was used to produce the concrete cylinders for mechanical property testing and the second batch was for RCF and FSF testing. The fresh properties for each mixture, batch and placement scenario is presented in Table 5-7. As mentioned previously, the "Δ Density" column in Table 5-7 is the difference between the measured density and the calculated density after correcting for the measured air content of each batch.

Table 5-7: Measured fresh concrete properties of expanded shale and control mixtures

Mixture and Placement Scenario	Batch No.	Fresh Concrete Test Results				Calculated
		Slump (in.)	Temp. (°F)	Air (%)	Density (lb/ft^3)	Δ Density (lb/ft^3)
CTRL (Fall)	1	3.25	74	5.0	143.8	0.3
	2	4.5	73	6.25	141.9	0.6
CTRL (Sum)	1	2.5	100	4.75	143.0	-0.3
	2	2.0	100	5.25	141.9	-0.6
Shale IC (Fall)	1	5.5	69	6.0	138.0	-0.3
	2	5.0	69	4.75	140.1	-0.2
Shale IC (Sum)	1	5.25	93	4.25	141.0	0.7
	2	3.5	97	4.0	141.0	-0.1
Shale SLW (Fall)	1	3.5	74	6.0	117.9	-0.8
	2	3.5	75	6.0	117.8	-1.0
Shale SLW (Sum)	1	2.0	94	4.25	120.5	-0.3
	2	2.0	95	4.25	120.4	-0.5
Shale ALW (Fall)	1	2.75	76	5.5	103.2	-0.4
	2	2.5	75	4.5	104.4	-0.2
Shale ALW (Sum)	1	3.0	94	5.0	104.6	0.5
	2	5.5	97	5.25	103.4	-0.4

5.3.3 Miscellaneous Properties

The calculated equilibrium density as per ASTM C 567, coefficient of thermal expansion measured from the modified AASHTO T 336 setup, and the thermal diffusivity determined from semi-adiabatic calorimetry are summarized in Table 5-8.

Table 5-8: Miscellaneous properties of expanded shale and control mixtures

Property	CTRL	Shale IC	Shale SLW	Shale ALW
Calculated Equilibrium Density (lb/ft^3)	140.0	135.0	110.6	87.1
Coefficient of Thermal Expansion (με/°F)	6.2	6.0	5.2	4.0
Thermal Diffusivity (ft^2/hr)	0.046	0.042	0.035	0.029

5.3.4 Curing Temperatures

The curing temperature profiles from for fall and summer placement scenarios for the expanded shale aggregate concretes and the normalweight control concrete are presented in Figure 5-19. The temperature profiles end when cracking occurred in RCF A.

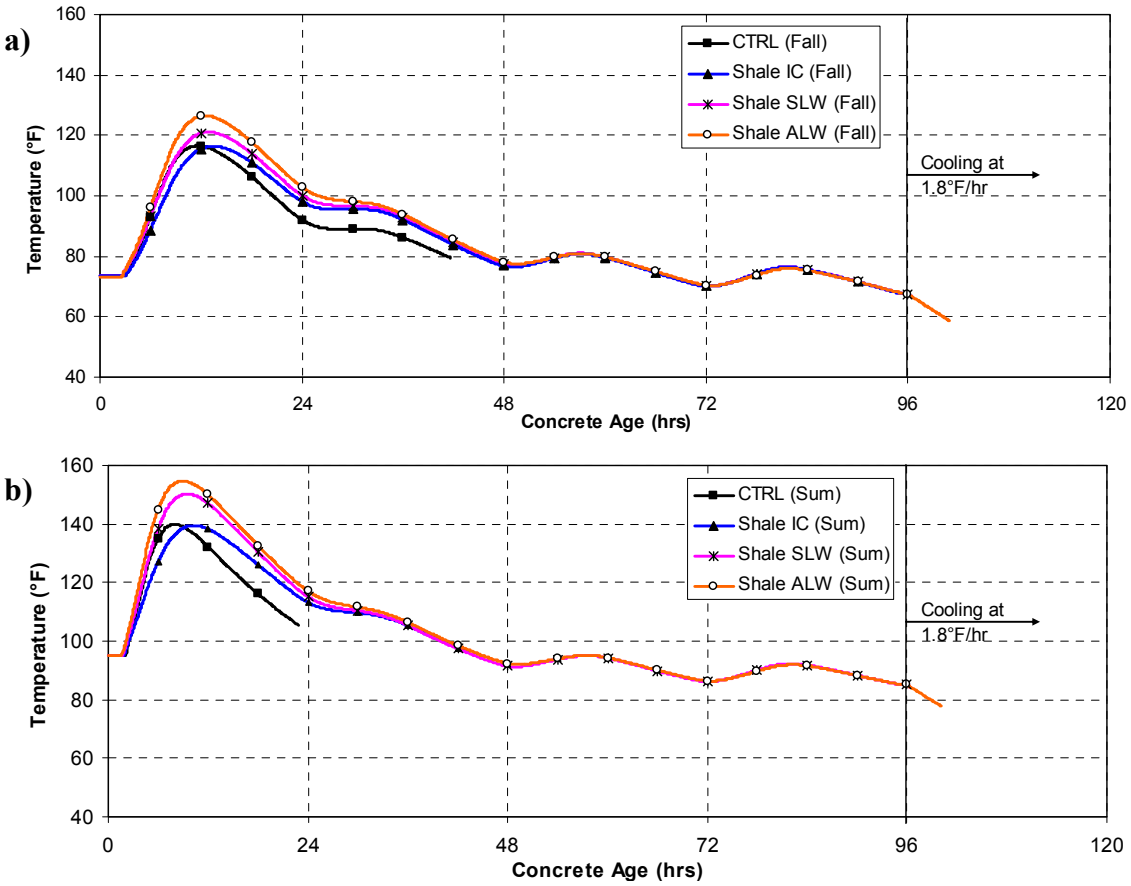

Figure 5-19: Modeled temperature profile for expanded shale and control mixtures: a) Fall and b) Summer placement scenarios

5.3.5 Restrained Stress Development

The restrained stress development is presented in Figure 5-20 and Figure 5-21 for the match-cured and isothermal cured conditions, respectively. The restrained stress development data for the match-cured condition end at the time of cracking. The

restrained stress development for the isothermal curing conditions was measured for 96 hours.

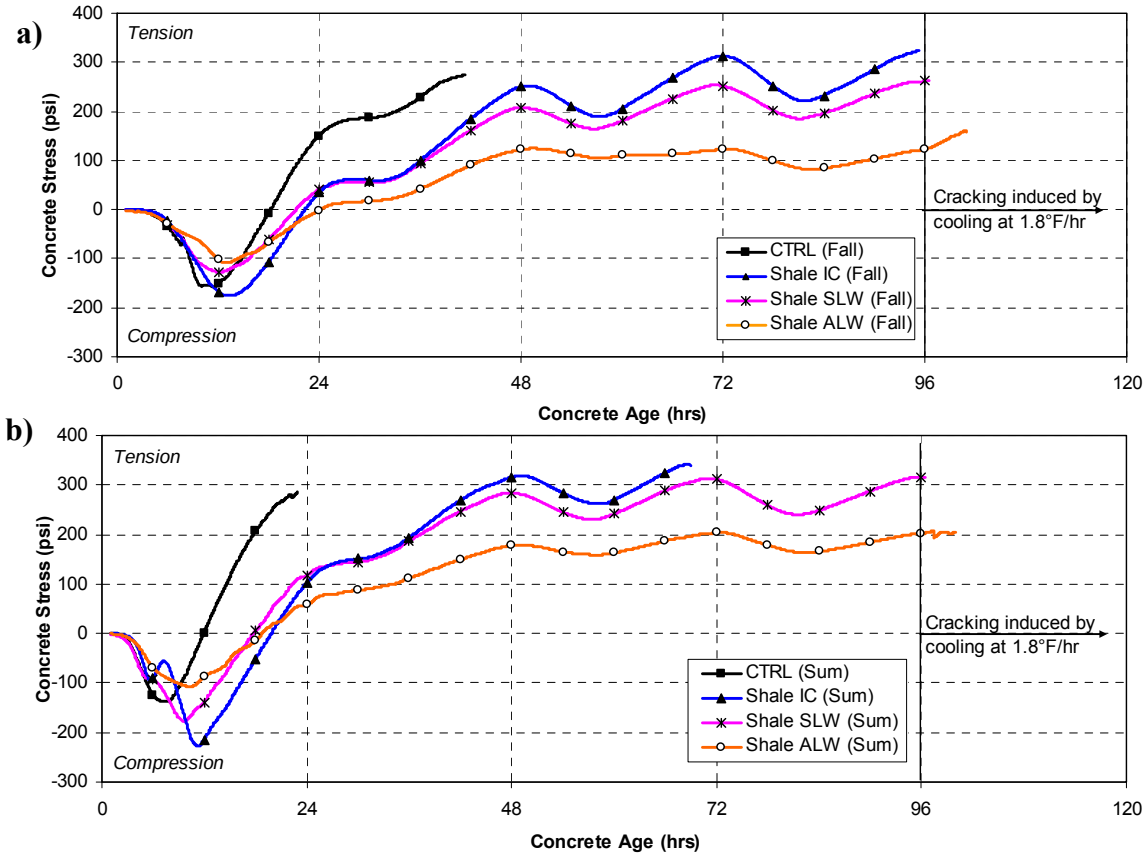

Figure 5-20: Restrained stress development for expanded shale and control mixtures: a) Fall and b) Summer placement scenarios

5.3.5.1 *Time to zero stress and cracking*

The time and temperature to the zero stress and cracking for each mixture and curing scenario is presented in Table 5-9.

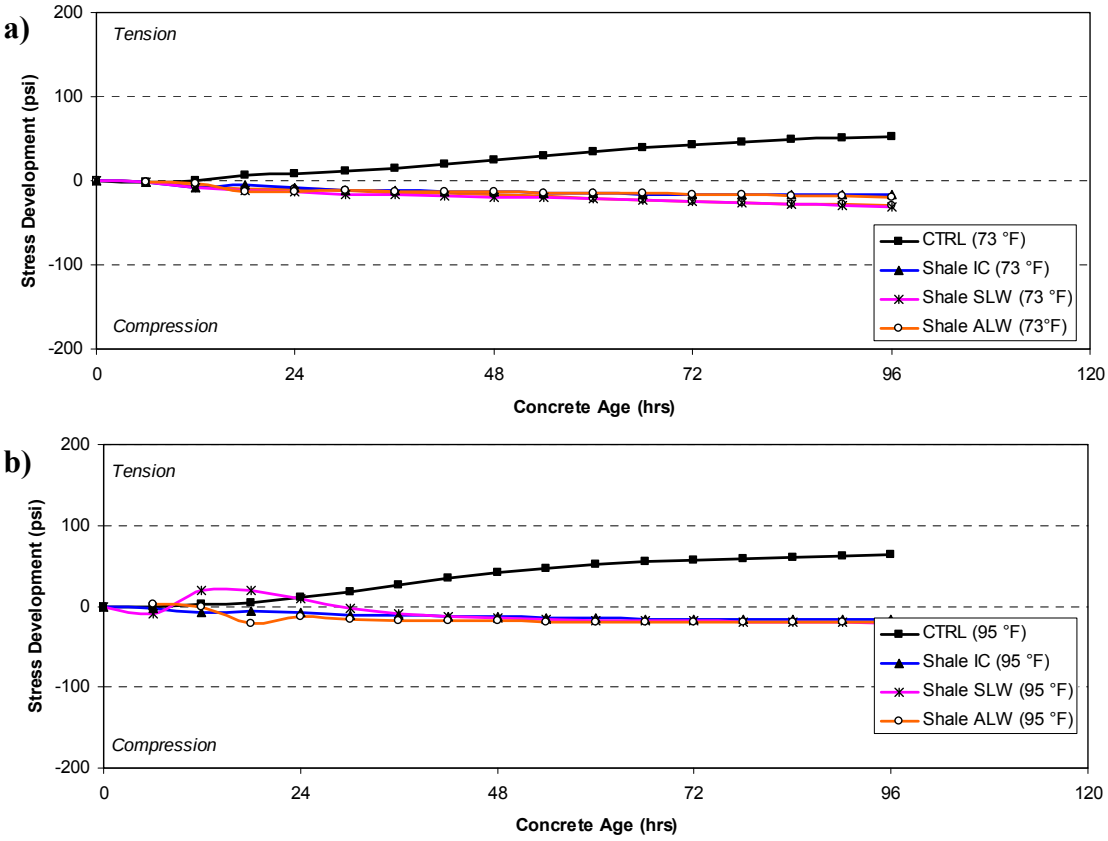

Figure 5-21: Restrained stress development for expanded shale and control mixtures under: a) 73 °F and b) 95°F isothermal conditions

Table 5-9: Time and temperature to zero stress and cracking of shale and control mixtures

Mixture	Zero Stress		Cracking	
	Time (hrs)	Temp. (°F)	Time (hrs)	Temp. (°F)
CTRL (Fall)	18.7	104.8	41.7	79.5
CTRL (Sum)	12.4	131.3	22.8	105.5
Shale IC (Fall)	24.3	99.7	95.3	67.6
Shale IC (Sum)	19.0	127.6	68.9	88.4
Shale SLW (Fall)	21.3	103.9	96.5 *	66.5
Shale SLW (Sum)	17.8	126.6	96.4 *	84.5
Shale ALW (Fall)	22.3	104.6	101.0 *	58.5
Shale ALW (Sum)	19.8	125.6	100.1 *	77.7

* Note: Cracking induced by cooling at 1.8 °F/hr after 96 hours

5.3.6 Measured Unrestrained Length Change

The strain measurements from the unrestrained specimens in the FSF are presented in Figure 5-22. The concrete specimens were match cured to the modeled temperature profile of the 8-in. thick bridge deck. The data are truncated at the time of initial cracking to help illustrate the strain developed in concrete until cracking occurred.

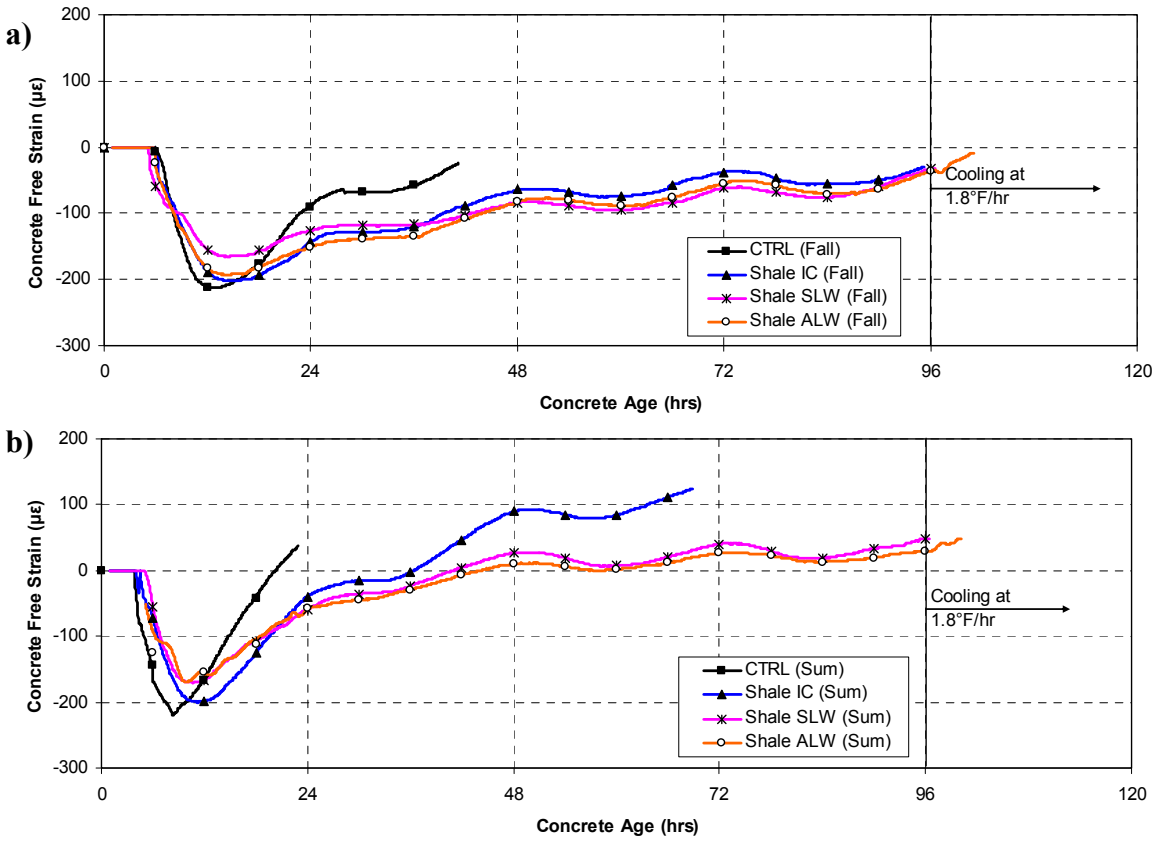

Figure 5-22: Free shrinkage strains for expanded shale and control mixtures: a) Fall and b) Summer placement scenarios

5.3.7 Mechanical Properties

The compressive strength, splitting tensile strength, and modulus of elasticity development were measured by testing cylinders match cured to the bridge deck

temperature profile for each mixture and placement scenario. A regression analysis was performed on the discrete data points with the exponential function recommended by ASTM C 1074. The resulting best-fit curves for each property are shown in Figure 5-23 and Figure 5-24 for fall and summer placement scenarios, respectively.

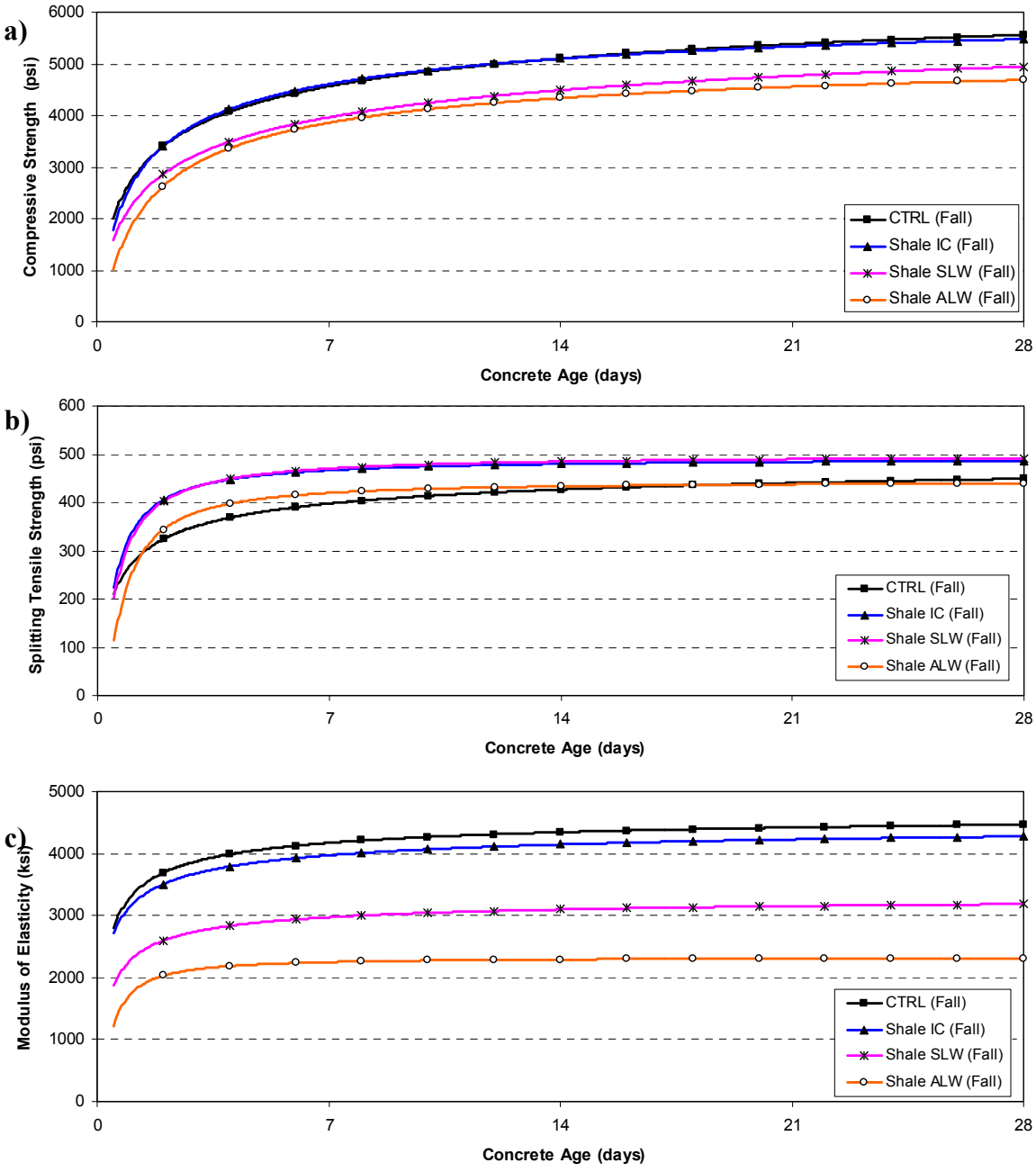

Figure 5-23: Fall placement scenario for shale and control mixtures: a) Compressive strength, b) Splitting tensile strength, and c) Modulus of elasticity development

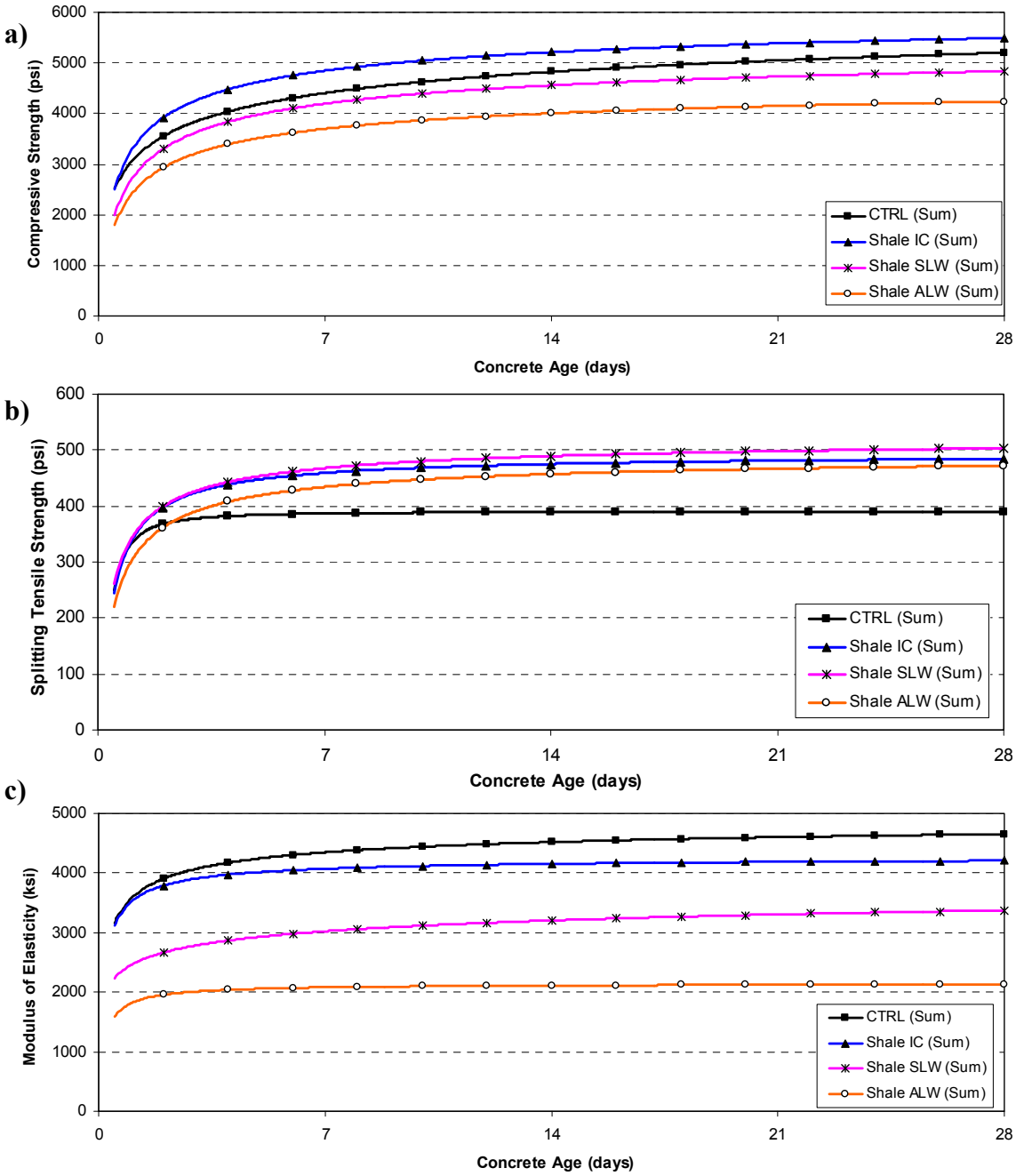

Figure 5-24: Summer placement scenario for shale and control mixtures: a) Compressive strength, b) Splitting tensile strength, and c) Modulus of elasticity development

CHAPTER 6

PART I: DISCUSSION OF RESULTS

A discussion and synthesis of the results are presented in this chapter. The changes in concrete properties when lightweight aggregates are introduced are evaluated in Section 6.1of this chapter. The effects of placement and curing temperature are discussed in Section 6.2. The effect of using various lightweight aggregates on the cracking tendency, autogenous shrinkage, and peak hydration temperature is then evaluated. The mechanisms by which the altered concrete properties affect early-age stress are discussed in Section 6.6. The applicability of the ACI 318 (2008) expression to estimate the modulus of elasticity and ACI 207.2R and ACI 207.1R to estimate the splitting tensile strength of the concretes made with LWAs are assessed at the end of this chapter.

6.1 Effect of Lightweight Aggregates on Concrete Properties

6.1.1 Modulus of Elasticity

The modulus of elasticity development for all concretes and both placement scenarios is presented in Part (c) of Figure 5-7, Figure 5-8, Figure 5-15, Figure 5-16, Figure 5-23, and Figure 5-24. It can be seen that the ALW concrete has a significantly lower modulus of elasticity than the other concretes. In all cases, except for Slate IC (Fall), the modulus of elasticity is reduced when lightweight aggregate is added to the mixture. This reduction

in modulus of elasticity is due to the reduced stiffness of the LWA. The reduction in modulus of elasticity was expected, as the addition of LWA lowers the density of the concrete as compared to its control concrete, which as per Equation 3-2 will lower the modulus of elasticity. The results for the Slate IC (Fall) test seem similar to that of the normalweight concrete; however, this is not the case for the Slate IC (Sum) results. Since the Slate IC (Fall) modulus of elasticity results are the only ones not reduced by the addition of LWA, these results may be a slight anomaly and not the norm.

6.1.2 Compressive Strength

The compressive strength development for all concretes are presented in Part (a) of Figure 5-7, Figure 5-8, Figure 5-15, Figure 5-16, Figure 5-23, and Figure 5-24. All internal curing (IC) mixtures, except Shale IC (Fall), have slightly higher compressive strengths at all ages than the normalweight control concrete. The compressive strength of the Shale IC (Fall) is similar to that of the normalweight control concrete. The compressive strength of the SLW concretes is similar to that of the normalweight control concrete. Whereas, the compressive strength for all ALW concretes is approximately 13 to 19 percent lower when compared to that of the normalweight control concrete. The ALW mixtures could have been proportioned with a lower water-cement ratio to have strength equivalent to the control concrete. However, since the 28-day compressive strength level of the ALW mixtures sufficiently exceeded 4,000 psi, it was decided to proportion the SLW and ALW concretes with the same water-cement ratio and paste volume.

6.1.3 Splitting Tensile Strength

The splitting tensile strength development for all concretes are presented in Parts (b) of Figure 5-7, Figure 5-8, Figure 5-15, Figure 5-16, Figure 5-23, and Figure 5-24. All internal curing concretes exhibited an increase in tensile strength when compared to the normalweight control concrete. Furthermore, the increase in tensile strength for the clay and shale internal curing concretes was more. This occurs because these IC concretes provide more internal curing water, which promotes increased cement hydration. An interesting finding is that the splitting tensile strength of all the SLW concretes is either higher or similar to that of the IC concretes, even though their compressive strengths are lower. In all cases, the splitting tensile strength of the SLW concretes exceeds that of the normalweight control concrete. The increase in tensile strength of the SLW concrete as compared to the normalweight control concrete is partly attributable to the replacement of river gravel with an angular porous lightweight aggregate as well as increased cement hydration. The increased cement hydration is promoted by the availability of additional water desorbed from the LWA.

Mixed trends can be observed from the splitting tensile strength results of the ALW concretes. The slate ALW concrete has a decreased splitting tensile strength up to an age of approximately 7 days when compared to the normalweight control concrete. Whereas, both the clay and shale ALW concretes have a similar or slightly increased splitting tensile strength when compared to the normalweight control concrete. The difference in the splitting tensile strength results of the ALW concretes may be related to the poor particle packing of the slate ALW mixture, as shown in Figure 5-2. The particle

packing was closer to the maximum density line for the clay and shale concretes, as shown in Figure 5-10 and Figure 5-18. Further research is necessary to confirm the cause of the reduced tensile strength of the slate ALW concrete used in this study as compared to the clay and shale ALW concretes.

6.1.4 Coefficient of Thermal Expansion

The measured coefficient of thermal expansion values for all concretes are summarized in Table 5-2, Table 5-5, and Table 5-8. In all cases, the concretes in ascending order of coefficient of thermal expansion are ALW, SLW, IC, and normalweight. There is a significant reduction of approximately 30 percent in coefficient of thermal expansion for all of the all-lightweight concretes when compared to the normalweight control concrete. The coefficient of thermal expansion is reduced by about 15 percent for all the sand-lightweight concretes when compared to the normalweight control concrete.

The finding that the addition of lightweight aggregate lowers the coefficient of thermal expansion of concrete made with river gravel aggregate is significant in applications where thermal cracking occurs, as is the case in bridge decks or pavements. Equation 3-1 indicates that the magnitude of thermal stress is proportional to the coefficient of thermal expansion; therefore, any reduction in coefficient of thermal expansion will reduce the magnitude of thermal stress that develops.

6.1.5 Thermal Diffusivity

The measured thermal diffusivity values for all concretes are summarized in Table 5-2, Table 5-5, and Table 5-8. Concrete with high thermal diffusivity, more rapidly adjusts its

temperature to that of its surroundings than a concrete with a low thermal diffusivity. In all cases, the concretes in ascending order of thermal diffusivity are ALW, SLW, IC, and CTRL. The thermal diffusivity decreases as the amount of lightweight aggregate added to mixture is increased.

6.2 Effect of Placement Season

The cracking times for each mixture for fall and summer placement scenario are shown in Figure 6-1 and Figure 6-2, respectively. From comparison of the results on Figure 5-4, Figure 5-12, Figure 5-20, Figure 6-1, and Figure 6-2 and the data presented in Table 5-3, Table 5-6, and Table 5-9, it can also be concluded that increasing the placement and curing temperature increases the zero-stress temperature and decreases the time to cracking. As shown in Equation 2-1, the higher the zero-stress temperature, the greater the thermal stresses become. Breitenbücher and Mangold (1994) also found that decreasing the temperature of the fresh concrete significantly increased the time to cracking. These results confirm that the thermal stresses that develop during summer placement conditions are much higher than those that develop during fall placement conditions.

A comparison of the results in Figure 6-1 and Figure 6-2 reveal that the time to cracking for all concretes made with LWA when placed under *summer* placement conditions, is *greater* than the time to cracking of the normalweight concrete when placed under *fall* conditions. This indicates that the use of pre-wetted LWA may be especially beneficial during summer time placement conditions to minimize the occurrence of cracking at early ages in bridge deck applications.

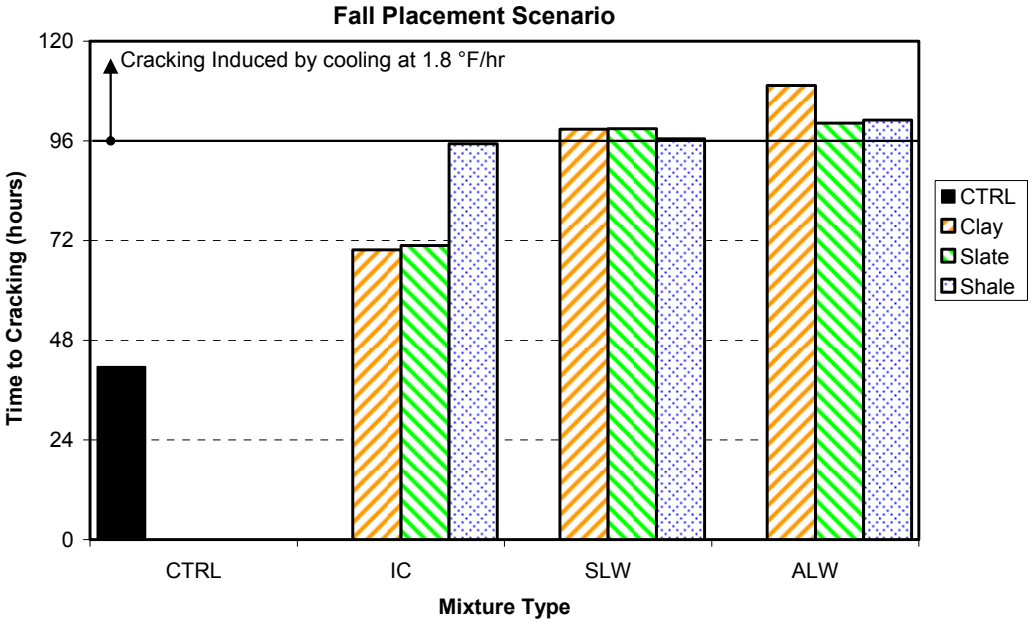

Figure 6-1: Time to cracking for the fall placement scenario

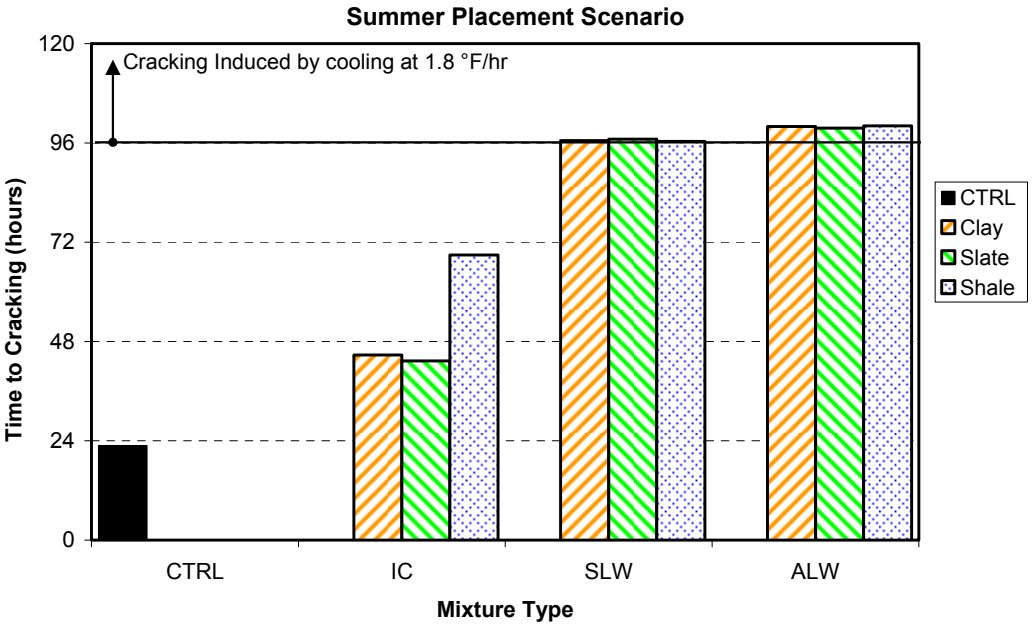

Figure 6-2: Time to cracking for the summer placement scenario

6.3 Effect of Internal Curing Water on Autogenous Stress Development

The internal curing water provided by each mixture containing LWA is summarized in Table 4-5. The SLW and ALW concretes have more water available because of the greater proportion of LWA in these mixtures. The stress development due to autogenous shrinkage effects are shown for all concretes in Figure 5-5, Figure 5-13, and Figure 5-21. The stress developed due to autogenous shrinkage effects is reduced in all cases by the introduction of lightweight aggregates when compared to the behavior of the normalweight control concrete. The decrease in autogenous stresses is due to the availability of water from the LWA to fill capillary voids formed by chemical shrinkage and the reduction in modulus of elasticity. The IC concretes experienced reduced autogenous shrinkage compared to the control concrete due to the fraction of fine LWA replacement and its reduced modulus of elasticity. The SLW and ALW concretes have an even greater reduction in autogenous tensile stress than the IC concretes. It can be concluded that both the SLW and ALW concretes completely prevent the development of tensile stresses caused by autogenous shrinkage effects. These SLW and ALW concretes thus contain sufficient amounts of internal curing water to mitigate the effects of autogenous shrinkage.

6.4 Comparison of the Behavior of Various Types of Lightweight Concretes

The early-age behavior of the internal curing, sand-lightweight, and all-lightweight concretes with the various sources of lightweight aggregate are compared to the behavior of a normalweight control concrete in this section.

6.4.1 Response of Internal Curing Concretes

The modeled temperature profiles, the match-cured restrained stress development, and the isothermal restrained stress development for the internal curing concretes for all three sources of lightweight aggregates are compared to the response of the control concrete for the fall placement scenario in Figure 6-3. The amount of internal curing water provided by each internal curing mixture is shown in Figure 6-3c. The internal curing water provide was calculated using the absorbed water in the LWA and the desorption coefficients presented in Table 3-2. The modeled temperature profiles for the three IC concretes were nearly identical, as shown in Figure 6-3a.

The effect of using LWA for internal curing purposes is evident in Figure 6-3c, which show the stress development under isothermal curing conditions. All three internal curing mixtures experienced *reduced* stress development due to autogenous shrinkage effects when compared to the normalweight concrete (CTRL). The decrease in autogenous stresses is due to the availability of water from the LWA to fill capillary voids formed by chemical shrinkage and the reduction in modulus of elasticity. The Shale IC and Clay IC concretes reduce the autogenous stress more than the Slate IC concrete as they contain more internal curing water available from the LWA. The fact that the stress development of Shale IC remains in compression, simply indicates that sufficient internal curing water is provided to negate the development of tensile stresses.

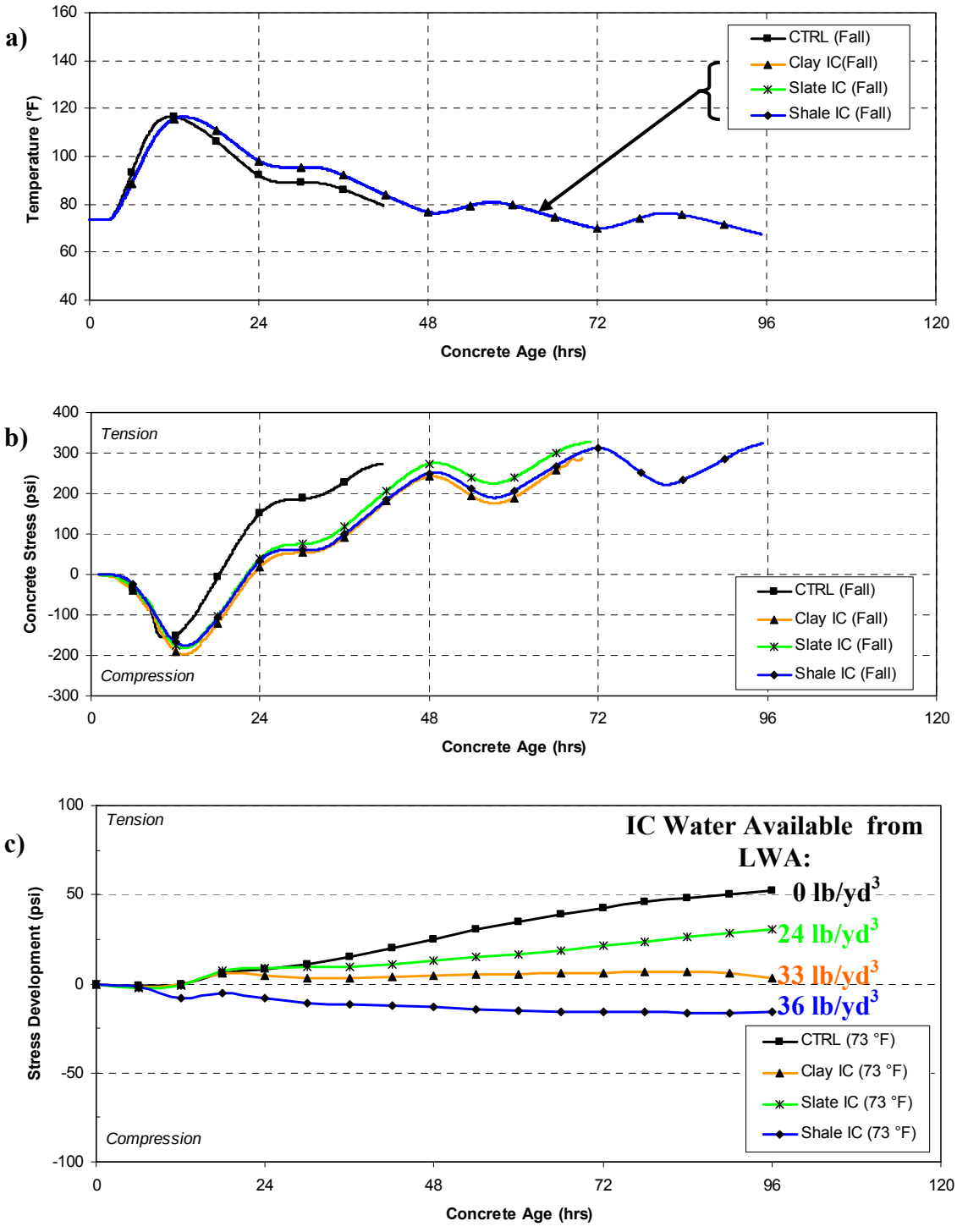

Figure 6-3: Fall placement scenario: a) Temperature profiles, b) Match-cured restrained stress development, and c) Isothermal restrained stress development for internal curing mixtures

It is clear from the results shown in Figure 6-3b that the use of lightweight aggregates in these internal curing concretes delays the occurrence of cracking at early ages in bridge deck concrete applications. As stated in Section 6.2, the results shown in Figure 5-4, Figure 5-12, Figure 5-20, Figure 6-1, and Figure 6-2 reveals that the use of LWA in *summer* conditions, improves the time to cracking of the concrete to exceed the time of cracking of the control concrete placed under *fall* conditions. This improvement in cracking behavior is attributed to the *increased* tensile strength and *decrease* in modulus of elasticity, coefficient of thermal expansion, and autogenous shrinkage of the internal curing concretes when compared to the normalweight control concrete.

It can be seen in Figure 6-3b that all three IC concretes cracked at a similar level of tensile stress; however, the shale concrete did not crack at the 96-hour temperature low, thereby delaying its cracking an additional 24 hours. Of the internal curing concretes, the slate LWA had the lowest absorption capacity and did not fully mitigate the isothermal stress as seen in Figure 6-3c. This difference in the degree of autogenous stress mitigation, may explain the slight difference in measured tensile stress between the Slate IC mixture and the other two IC mixtures

6.4.2 Response of Sand-Lightweight Concretes

The modeled temperature profiles, the match-cured restrained stress development, and the modulus of elasticity development for the sand-lightweight concretes for all three sources of lightweight aggregates are compared to the response of the control concrete for the fall placement scenario in Figure 6-4.

It is clear from the results shown in Figure 6-4b that the use of lightweight aggregates in these sand-lightweight concretes significantly reduces the tensile stress and delays the occurrence of cracking at early ages in bridge deck concrete applications. This improvement in cracking behavior is caused by the *decreased* modulus of elasticity, coefficient of thermal expansion, and autogenous shrinkage of the SLW concretes when compared to the normalweight control concrete.

The SLW concretes have similar coefficient of thermal expansion values and curing temperature profiles. Because of these factors and the fact that autogenous shrinkage effects are not present in these SLW concretes, the difference in stress development shown in Figure 6-4b is primarily attributable to differences in modulus of elasticity values of these SLW concretes as shown in Figure 6-4c. For example, because the Clay SLW concrete has the lowest modulus of elasticity, the stresses that develop from the same change in temperature are the least, as seen in the test results. However, all three SLW concretes cracked at very similar times, which indicate that they provide similar levels of improvement to the cracking response of the normalweight control concrete.

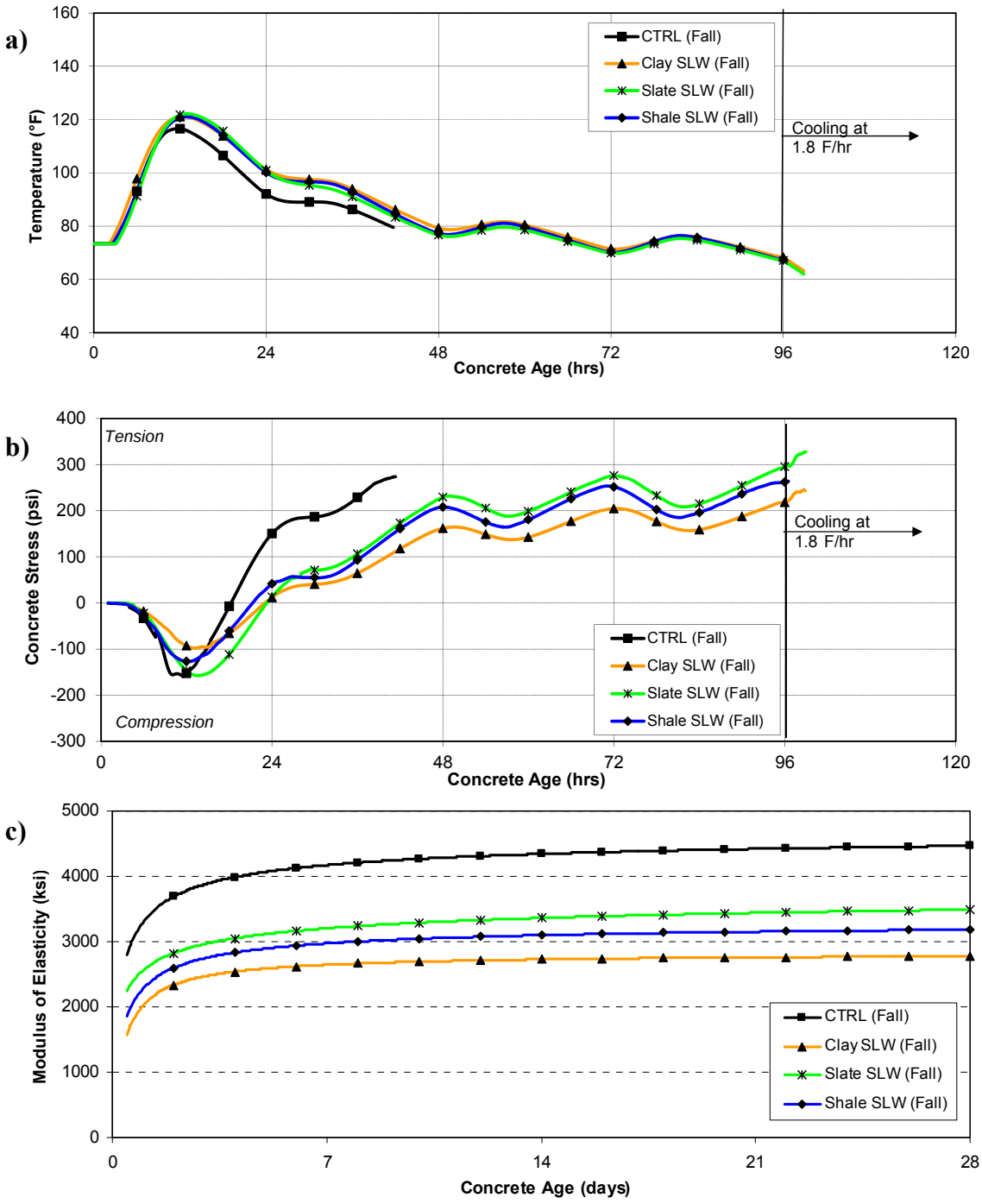

Figure 6-4: Fall placement scenario a) Temperature profiles, b) Match-cured restrained stress development, and c) Modulus of elasticity development for SLW mixtures

6.4.3 Response of All-Lightweight Concretes

The modeled temperature profiles, the match-cured restrained stress development, and the modulus of elasticity development for the all-lightweight concretes are compared to the response of the control concrete for the fall placement scenario in Figure 6-5.

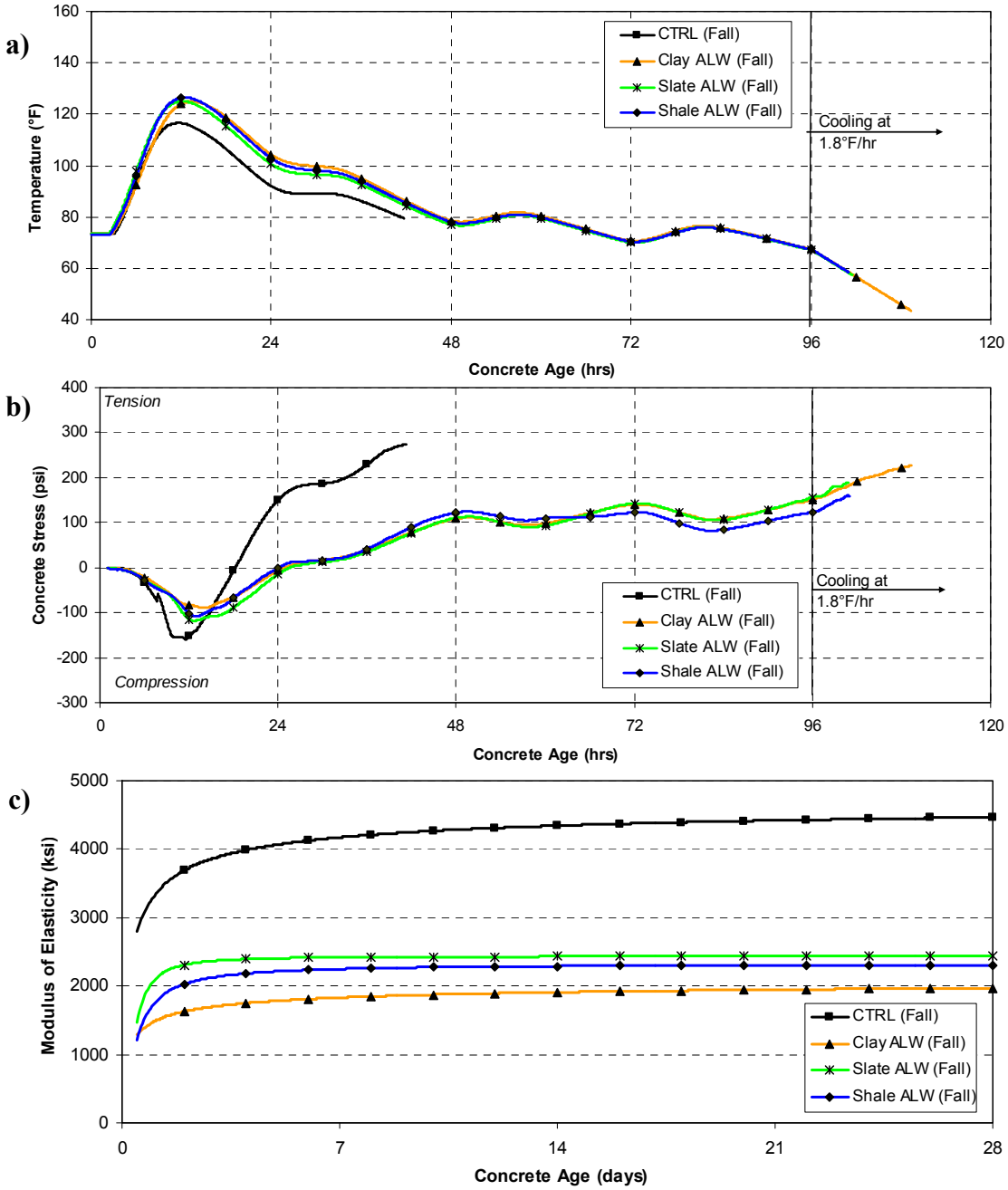

Figure 6-5: Fall placement scenario a) Temperature profiles, b) Match-cured restrained stress development, and c) Modulus of elasticity development for ALW mixtures

The results shown in Figure 6-5b indicate that the use of lightweight aggregates in these all-lightweight concretes significantly delays the occurrence of cracking at early ages in bridge deck concrete applications. The magnitudes of the early-age stresses in all three ALW concretes are significantly reduced when compared to that of the normalweight control concrete. Note that when the control concrete cracks in tension, the tensile stress developed in the ALW concretes is one-third of the stress in the control concrete. This improvement in cracking behavior is caused by the *significant decrease* in modulus of elasticity, coefficient of thermal expansion, and autogenous shrinkage of the ALW concretes when compared to the normalweight control concrete.

The ALW concretes have similar coefficient of thermal expansion values and curing temperature profiles. As was the case for the SLW concretes, the difference in stress development shown in Figure 6-5b is mostly attributable to differences in modulus of elasticity values of these ALW concretes as shown in Figure 6-5c. For example, because the clay ALW concrete has the lowest stiffness, it requires the most cooling to induce cracking. However, the stress levels measured for all three ALW concretes are very similar, which indicate that they provide similar levels of improvement to the cracking response of the normalweight control concrete.

6.5 Effect of LWA on Peak Temperatures

The temperature profiles simulated for an 8-in. thick bridge deck for all the concretes evaluated in this project are shown inFigure 5-3, Figure 5-11, and Figure 5-19. It can be seen that the peak temperatures of the ALW concretes, followed by the SLW concretes,

for both placement scenarios and all lightweight aggregate sources are higher than the peak temperatures of the CTRL and IC concretes. This is because the ALW concretes have the lowest thermal diffusivity followed by the SLW concretes, and these concretes have slightly increased portland cement contents. The decrease in thermal diffusivity has an insulating effect that retains the heat of cement hydration causing a greater peak temperature as noted by Maggenti (2007). The temperature peaks of the CTRL and IC concretes are similar, but the peak temperatures of IC concretes are slightly retarded when compared to the CTRL concrete.

6.6 Effect of Lightweight Concrete Properties on Early-Age Stress Development

The restrained stress development results shown in Figure 5-4, Figure 5-12 and Figure 5-20 reveal that the magnitude of the peak temperature alone does not provide a direct indication of the cracking tendency of the concretes. While the magnitude of the peak temperature is important, the decreased coefficient of thermal expansion of the LWA concretes causes a reduced strain per unit temperature change, and the reduced modulus of elasticity of the LWA concretes causes a reduced stress for a given strain. Although the SLW and ALW concretes experience greater peak temperatures, the significant reduction in coefficient of thermal expansion and modulus of elasticity lead to a reduction in stress and a significant overall delay in early-age cracking in bridge deck concrete applications.

6.7 Modulus of Elasticity Behavior Compared to ACI 318 and AASHTO LRFD Estimates

The ACI 318 (2008) and the AASHTO LRFD Bridge Design Specifications (2007) modulus of elasticity estimation equation was used to calculate the modulus of elasticity of each concrete based on the average measured compressive strength at each testing age and temperature scenario. ACI 318 (2008) clearly states that the density of the concrete should be the calculated based on the equilibrium density, which may be an attempt to obtain a lower-bound estimate of the concrete's modulus of elasticity for design purposes. The estimated compared to the measured modulus of elasticity for the 0.5, 1, 2, 3, 7, and 28-day results, when both the equilibrium density and fresh density are used, are shown in Figure 6-6 and Figure 6-7, respectively.

From the results shown in Figure 6-6, it can be concluded that the ACI 318 (2008) modulus of elasticity equation using the fresh density estimated the stiffness of all the concretes reasonably well. The ACI 318 (2008) modulus of elasticity estimation equation in general underestimates the modulus when the equilibrium density is used, as shown in Figure 6-7. Using the fresh density, the ACI 318 (2008) modulus estimation equation generally underestimates the concretes made with slate, slightly over estimates the stiffness of the concretes made with clay, and estimates the modulus of the shale concrete reasonably well. This is due to the modulus of the slate being the highest, followed by the shale and then the clay.

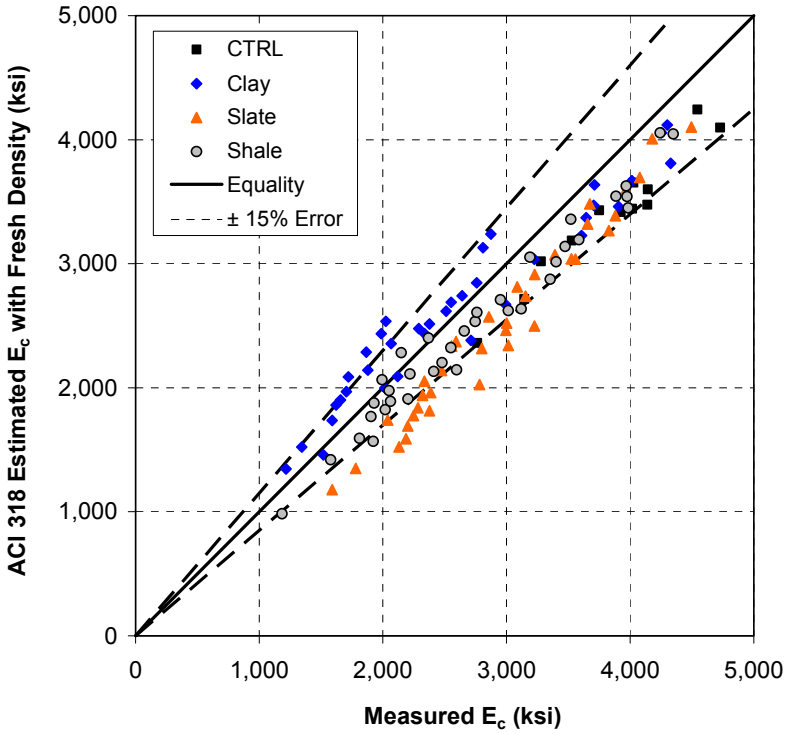

Figure 6-6: Measured modulus of elasticity compared to ACI 318 predicted with *fresh density*

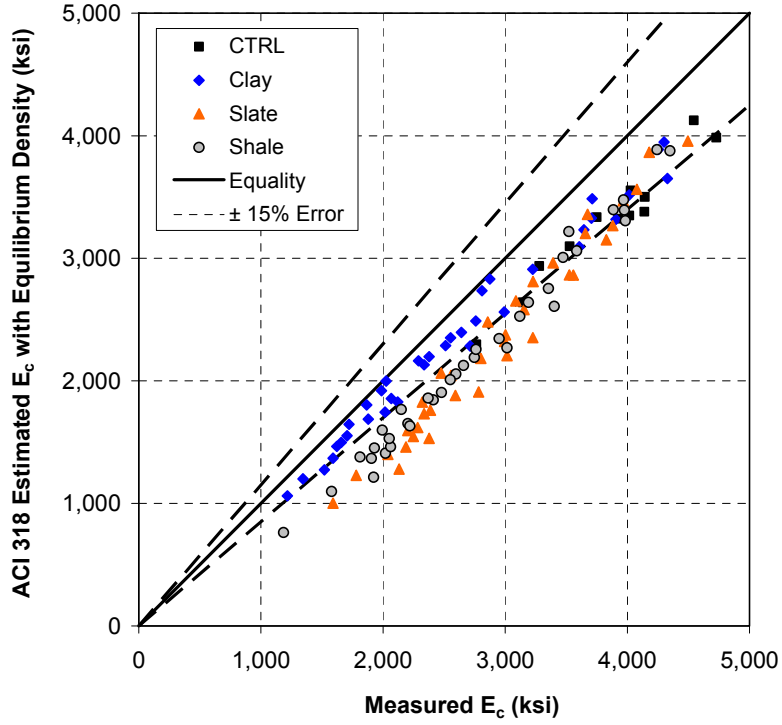

Figure 6-7: Measured modulus of elasticity compared to ACI 318 predicted with *equilibrium density*

The unbiased estimate of the standard deviation of the absolute error can be determined as shown in Equation 6-1 (McCuen 1985). The unbiased estimate of the standard deviation of the absolute error when using the ACI 318 (2008) and the AASHTO LRFD Bridge Design Specifications (2007) modulus of elasticity equation using both the fresh and calculated equilibrium density is presented in Table 6-1 and Table 6-2. It can be seen from Table 6-1 and Table 6-2 that using the *fresh density* in the ACI 318 (2008) and the AASHTO LRFD Bridge Design Specifications (2007) modulus of elasticity estimation equation produces a lower absolute error and thus better predicts the modulus of elasticity of all the mixtures.

$$S_j = \sqrt{\frac{1}{n-1}\sum_i^n \Delta_i^2} \quad \text{..... Equation 6-1}$$

where S_j = unbiased estimate of the standard deviation (ksi),

n = number of data points (unitless), and

Δ_i = absolute error (ksi).

Table 6-1: Unbiased estimate of standard deviation of absolute error for modulus of elasticity estimation equations per source material

Density used for E_c Estimate	S_j for E_c Estimate (ksi)			
	CTRL	Slate	Clay	Shale
E_c Estimated with Fresh Density	484	456	277	290
E_c Estimated with Equilibrium Density	579	624	303	553

Table 6-2: Unbiased estimate of standard deviation of absolute error for modulus of elasticity estimation equations per mixture type

Density used for E_c Estimate	S_j for E_c Estimate (ksi)			
	CTRL	IC	SLW	ALW
E_c Estimated with Fresh Density	484	361	364	326
E_c Estimated with Equilibrium Density	579	488	538	629

6.8 Splitting Tensile Strength Behavior Compared to ACI Estimates

The ACI 207.2R (1995) and ACI 207.1R (1996) splitting tensile strength estimation equations were used to estimate the measured splitting tensile strength based on the measured compressive strength test results. The 1, 2, 3, 7 and 28-day measured splitting tensile strengths compared to the results obtained from both ACI 207 estimation equations are shown in Figure 6-8.

The unbiased estimate of the standard deviation of the absolute error when using both ACI 207 estimation equations are presented in Table 6-3 and Table 6-4. Because the control concrete contained coarse aggregate that was smooth river gravel, the splitting tensile strength estimated with both ACI 207 expressions is generally greater than the measured strength. For the same reason, the measured splitting tensile strengths of the IC concrete are also generally overestimated. As the amount of LWA used in the concrete is increased, the predictions of ACI 207.2R and ACI 207.1R improve, as shown in Table 6-4. From Table 6-3 and Table 6-4 it can be seen that the splitting tensile strength formulations of ACI 207.2R and ACI 207.1R both provide adequate estimates of the splitting tensile strength of all the concretes made with LWA.

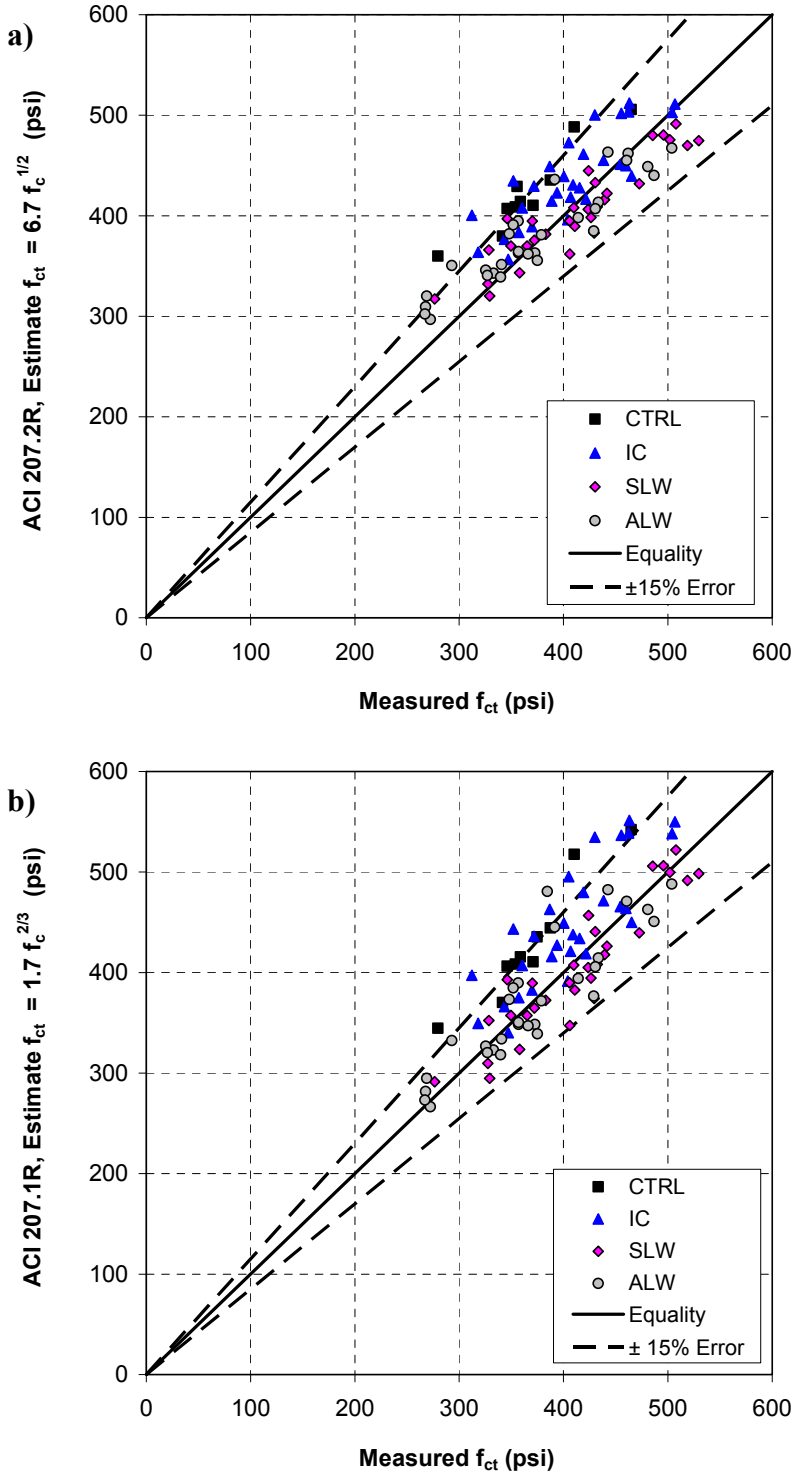

Figure 6-8: Measured splitting tensile strength compared to a) ACI 207.2R and b) ACI 207.1R estimates

Table 6-3: Unbiased estimate of standard deviation of absolute error for splitting tensile strength estimation equations for each source material

Splitting Tensile Strength Estimation Model	S_j for f_{ct} Estimate (psi)			
	CTRL	Slate	Clay	Shale
$6.7\times f_c^{0.5}$	43	26	39	38
$1.7\times f_c^{2/3}$	47	30	40	46

Table 6-4: Unbiased estimate of standard deviation of absolute error for splitting tensile strength estimation equations for each mixtures type

Splitting Tensile Strength Estimation Model	S_j for f_{ct} Estimate (psi)			
	CTRL	IC	SLW	ALW
$6.7\times f_c^{0.5}$	43	42	33	28
$1.7\times f_c^{2/3}$	47	54	31	27

The 1, 2, 3, 7 and 28-day splitting tensile strength data compared to the ACI 318 lightweight modification factor (λ) is presented in Figure 6-9. The lines on Figure 6-9 represent the ACI 318 (2008) and AASHTO (2007) specified lightweight modification factors for SLW (λ = 0.85) and ALW (λ = 0.75) concretes when the splitting tensile strength data are unavailable. From Figure 6-9, it can be seen that the measured splitting tensile strength results for all SLW concretes are above the 0.85 modification factor line and the measured splitting tensile strength results for all ALW concrete are above the 0.75 modification factor line. The average calculated lambda values for each mixture type is shown in Table 6-5. Based on these results, it may be concluded that the ACI 318 (2008) and AASHTO (2007) lightweight modification factors are very conservative for the lightweight aggregate concretes tested in this study.

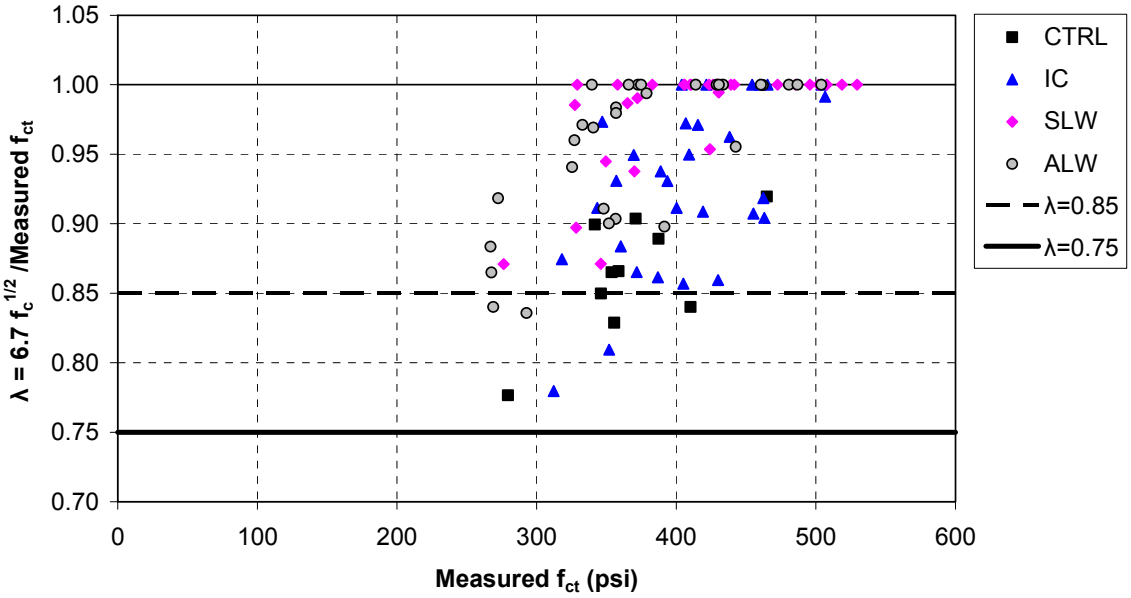

Figure 6-9: Measured splitting tensile strength compared to ACI 318 (2008) and AASHTO (2007) lightweight modification factors

Table 6-5: Average lightweight modification (λ) of each mixture type

Lightweight Modification Factor	Mixture Type			
	CTRL	IC	SLW	ALW
ACI 318 and AASHTO Specified without f_{ct} Data	1.00	1.00	0.85	0.75
Average Lightweight Modification Factor (λ)	0.86	0.93	0.98	0.96

CHAPTER 7

PART I: CONCLUSIONS AND RECOMMENDATIONS

7.1 Summary of Work

Early-age cracking in bridge decks is a severe problem that may reduce functional life of the structure. In this project, the effect of using lightweight aggregate on the cracking tendency of bridge deck concrete was evaluated by cracking frame testing techniques. Cracking frames measure the development of stresses due to thermal and autogenous shrinkage effects from setting until the onset of cracking. Restrained and unrestrained concrete specimens were tested under temperature conditions that match those in an 8-in. thick bridge deck and under isothermal curing conditions.

Expanded shale, clay, and slate lightweight coarse and fine aggregates were evaluated in this study. Normalweight, internal curing (IC), sand-lightweight (SLW), and all-lightweight (ALW) concretes were made in the laboratory and their early-age behavior evaluated. The normalweight concrete used is a typical 0.42 water to cement ratio mixture used in bridge deck applications in the Southeastern United States. The IC mixture is similar to the normalweight mixture, except that a fraction of the normalweight fine aggregate was replaced with pre-wetted lightweight fine aggregate. Note that the amount of lightweight aggregate added to the IC mixture was selected to obtain a concrete with an equilibrium density of 135 lb/ft^3, which allows this mixture to be

classified as “normalweight concrete” as per the AASHTO LRFD Bridge Design Specifications (2007).

Each concrete was made and cured under conditions that simulate summer and fall placement conditions in the southeastern parts of the United States. Ten different concretes were produced and tested at two different curing conditions. Additionally, for each mixture and placement condition, 24 cylinders were cast and tested for compressive strength, splitting tensile strength, and modulus of elasticity to assess the development of these properties over time. The coefficient of thermal expansion of the hardened concrete was also assessed with a test setup similar to that required by AASHTO T 336 (2009).

7.2 Conclusions

7.2.1 Effect of Using Lightweight Aggregates on Concrete Properties

From this research, the following conclusions can be made about the effect of using lightweight aggregate on concrete properties:

1. Increasing the amount of pre-wetted lightweight aggregate in the concrete systematically decreases the density and thus the modulus of elasticity of the concrete. By using the *fresh* density and Equation 3-2 found in ACI 318 (2008), the density and compressive strength can be used to estimate, with reasonable accuracy, the modulus of elasticity of all the concretes made with lightweight aggregate.
2. In general, the compressive strength of the internal curing concretes was slightly higher at all ages than that of the normalweight control concrete. The

compressive strength development of the sand-lightweight concretes was similar to that of the normalweight control concrete. Whereas, the compressive strength for the all-lightweight concretes were approximately 13 to 19 percent lower when compared to that of the normalweight control concrete.

3. All internal curing and sand-lightweight concretes exhibited an increase in splitting tensile strength when compared to the normalweight control concrete.
4. The slate all-lightweight concrete has a decreased splitting tensile strength up to an age of approximately 7 days when compared to the normalweight control concrete. Whereas, both the clay and shale all-lightweight concretes have a similar or slightly increased splitting tensile strength when compared to the normalweight control concrete. The difference in the splitting tensile strength results of the all-lightweight concretes may be related to the particle packing of the slate all-lightweight mixture used in this study.
5. The equations of ACI 207.2R (1995) and ACI 207.1R to estimate the splitting tensile both provide accurate estimates for all of the concretes made with lightweight aggregate.
6. The ACI 318 (2008) and AASHTO (2007) lightweight modification factor (λ factor) to estimate the splitting tensile strength from a known compressive strength is very conservative for the lightweight aggregate concretes tested in this study.
7. Increasing the amount of pre-wetted lightweight aggregate in the concrete systematically decreases the coefficient of thermal expansion. There is a reduction of 15 and 30 percent in coefficient of thermal expansion for the sand-

lightweight and all-lightweight concretes, respectively, when compared to the normalweight control concrete.

8. Increasing the amount of lightweight aggregate in the mixture decreases the concrete's thermal diffusivity, which resulted in an increase in peak hydration temperatures.

7.2.2 Early-Age Concrete Behavior

From this research, the following conclusions can be made about the effect of using lightweight aggregate on the cracking tendency and autogenous shrinkage of concrete:

1. Higher placement and curing temperatures result in higher thermal stresses. Decreasing the placement and curing temperature can reduce tensile stresses and delay cracking.
2. The time to cracking for all concretes made with LWA when placed under *summer* placement conditions is *greater* than the time to cracking of the normalweight concrete when placed under *fall* conditions. This indicates that the use of pre-wetted LWA may be especially beneficial during summer time placement conditions to minimize the occurrence of cracking at early ages in bridge deck applications.
3. The use of pre-wetted lightweight aggregates in concrete can reduce or eliminate the stress development caused by autogenous shrinkage. The decrease in autogenous stresses is due to internal curing, because water is desorbed from the lightweight aggregates to fill capillary voids formed by chemical shrinkage.

4. Internal curing concrete made with pre-wetted lightweight aggregate experienced *reduced* stress development due to autogenous shrinkage effects when compared to the normalweight concrete. Since the sand-lightweight and all-lightweight concretes can supply more internal curing water, they cause a greater reduction in tensile stresses due to autogenous shrinkage effects than the internal curing concretes. The sand-lightweight and all-lightweight concretes used in this study completely prevented the development of tensile stresses due to autogenous shrinkage effects.
5. The use of lightweight aggregates to produce internal curing concretes with a density of 135 lb/ft^3 delays the occurrence of cracking at early ages in bridge deck concrete applications when compared to the normalweight control concrete. This improvement in cracking behavior is attributed to the *increased* tensile strength and *decrease* in modulus of elasticity, coefficient of thermal expansion, and autogenous shrinkage of the internal curing concretes when compared to the normalweight control concrete.
6. The use of sand-lightweight and all-lightweight concretes significantly delays the occurrence of cracking at early ages in bridge deck concrete applications when compared to the normalweight control concrete. Although the sand-lightweight and all-lightweight concretes experience greater peak temperatures, the significant reduction in coefficient of thermal expansion and modulus of elasticity lead to a significant overall delay in early-age cracking in bridge deck concrete applications.

7. When compared to a normalweight control concrete, the introduction of lightweight aggregates in concrete effectively delays the occurrence of cracking at early ages in bridge deck applications.

PART II:

EARLY-AGE BEHAVIOR OF INTERNALLY CURED CONCRETE

CHAPTER 8

PART II: INTRODUCTION

8.1 Background

With increasing demand for bridge deck concretes with excellent long-term performance, it is necessary to maximize the performance of concrete mixtures. Optimizing hardened properties requires proper curing practice. However, with lower water-cement ratio (*w/c)* bridge deck mixtures that feature lower permeability, topical curing or sealing techniques are often not effective enough to maintain adequate internal moisture to maximize hydration and minimize self-desiccation (Rilem TC 196 2007).

Internal curing is the maintenance of high moisture contents in the placed concrete by incorporating pre-wetted absorptive materials into the mixture during batching. The pre-wetted materials act like internal reservoirs that release their water as drying occurs. The release of the internal-curing water increases cementing material hydration and reduces capillary stress caused by self-desiccation (Jensen and Hansen 2001). Decreasing the capillary stress decreases the stress developed from autogenous shrinkage. The increased hydration increases the strength of the hardened concrete (Mehta and Monteiro 2006).

Cracking of concrete occurs when the tensile stress exceeds the tensile strength. Reducing the autogenous shrinkage stress development and increasing the tensile strength reduces the risk of early-age cracking. Effective control of early-age cracking can result

in limited later-age cracking and can reduce chloride penetration and corrosion potential (Darwin and Browning 2008). Early age is generally defined as the time after setting where the properties are changing rapidly. For most mixtures this is within the first 7 days (ACI 231 2010).

8.2 Research Significance

Sixty-two percent of surveyed transportation agencies consider early-age transverse cracking to be problematic (Krauss and Rogalla 1996). More than 100,000 bridges suffer from early-age cracking (FHWA 2008). Considering the impact of early-age cracking on long-term performance and durability, it is imperative that bridge deck concrete be proportioned and placed to minimize early-age cracking. The investigation described in this part evaluated the effectiveness of using LWA and internal curing to mitigate early-age cracking of bridge deck concretes.

8.3 Research Objectives

The focus of this part is to determine the early-age behavior of internally-cured concrete. The objectives of the research presented in this part are as follows

- Evaluate the effect of water-cement ratio and internal curing on the development of stresses and occurrence of cracking at early ages,
- Evaluate the effect of various amounts of internal-curing water on the degree of hydration and compare the degree of hydration those estimated by published models,

- Evaluate the effect of water-cement ratio and internal-curing water on the internal relative humidity during early ages,
- Determine the effect of lightweight fine aggregate replacement of normalweight fine aggregate on the compressive strength, splitting tensile strength, and modulus of elasticity, and
- Evaluate the effect of water-cement ratio and different amounts of internal curing water on autogenous shrinkage and stress development of concrete and mortar specimens.

CHAPTER 9

PART II: LITERATURE REVIEW

The results of a literature review of early-age thermal effects, chemical shrinkage, autogenous shrinkage, degree of hydration models, methods for determining degree of hydration, methods for proportioning internal-curing mixtures, and test methods for determining early-age properties are presented in this chapter.

9.1 Concrete Volume Change

Tensile stresses are induced in bridge decks when concrete volume changes are restrained by the girders. Early-age volume changes occur due to temperature changes, autogenous shrinkage, and drying shrinkage. The amount of stress produced when volume changes are restrained is a function of the extent of volume change, the modulus of elasticity, degree of restraint, stress concentrations, and relaxation of the concrete, which all vary with the maturity of the concrete.

9.1.1 Thermal Effects

The development of thermal stress at cracking can be calculated using the expression presented in Equation 9-1. For accurate estimation of thermal stress, creep effects during early ages and over the service life should be accounted for in Equation 9-1 (Schindler and McCullough 2002).

$$\sigma_T = \Delta T \times \alpha_t \times E_{c,adj} \times K_r \quad \text{Equation 9-1}$$

where σ_T = thermal stress (psi)

ΔT = temperature change = $T_{zero\text{-}stress}$ - T_{min} (°F),

α_t = coefficient of thermal expansion (strain/°F),

$E_{c,adj}$ = creep-adjusted modulus of elasticity (lb/in^2),

K_r = degree of restraint factor,

$T_{zero\text{-}stress}$ = concrete zero-stress temperature (°F), and

T_{min} = minimum concrete temperature (°F).

An illustration of the development of concrete temperatures and thermal stresses for freshly placed concrete under summer placement conditions is presented in Figure 9-1. In terms of stress development, the final-set temperature is the temperature at which the concrete begins to resist stresses that result from the restraint of external volume changes. Hydration causes the concrete temperature to increase beyond the setting temperature, time (A). Because the expansion of the concrete caused by the temperature rise is restrained, the concrete will be in compression when the peak temperature, time (B), is reached. When the peak temperature is reached, the hydrating paste is still developing structure, its strength is low, and high amounts of early-age relaxation may occur when the concrete is subjected to high compressive stress (Emborg 1989). The phenomenon of gradual decrease in stress when a material is subjected to sustained strain is called stress relaxation (Mehta and Monteiro 2006). As the concrete temperature subsequently decreases, the compressive stress is gradually relieved until the stress condition changes

from compression to tension, time (C). The temperature at which this transient stress-free condition occurs is denoted the "zero-stress temperature". Due to the effects of relaxation, the zero-stress temperature may be significantly higher than the final-set temperature (Emborg 1989). If tensile stresses caused by a further temperature decrease exceed the tensile strength of the concrete, cracking will occur, time (D). Because the thermal stress is proportional to the difference between the zero-stress temperature and the cracking temperature, thermal cracking can be minimized by decreasing the zero-stress temperature. This in turn can be accomplished by (1) minimizing the final-set temperature, (2) minimizing the peak temperature achieved during the high-relaxation phase, or (3) delaying the attainment of the peak temperature (Breitenbücher and Mangold 1994).

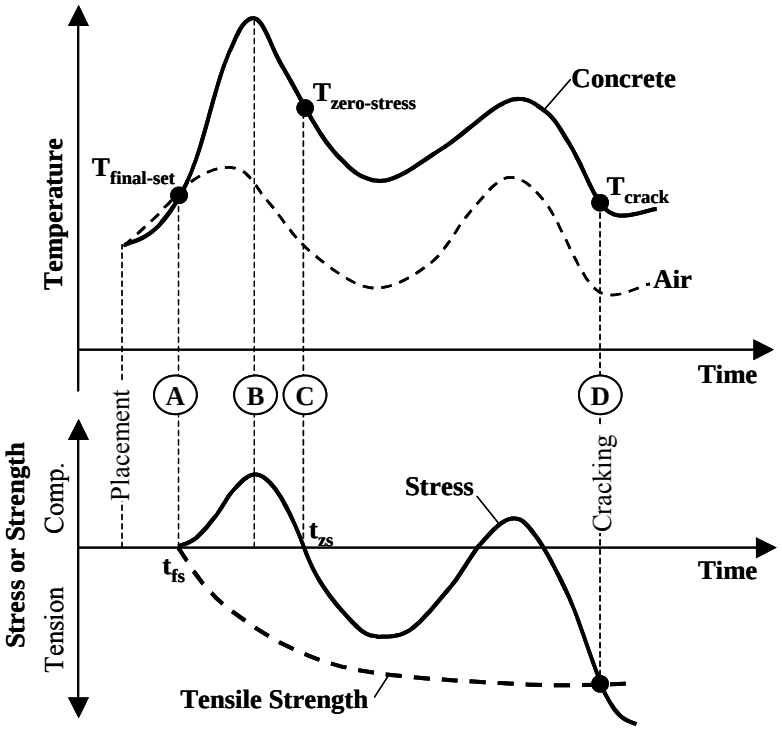

Figure 9-1: Development of early-age thermal stresses (Schindler and McCullough 2002)

9.1.2 Autogenous and Chemical shrinkage

The reaction products formed from cement hydration occupy a smaller absolute volume than the anhydrous components (L'Hermite 1960). The reduction of the absolute volume of the reactants due to hydration is chemical shrinkage. Before setting, this phenomenon results in a volumetric change but generates no stress because the concrete is still plastic (Holt 2001). At setting, enough hydration products have formed to provide a self-supporting skeletal framework in the paste matrix. Within the framework of solids are water-filled capillary voids. As water is consumed by the ongoing hydration process, the voids empty and capillary tensile stresses are generated, which results in a volumetric shrinkage. The concrete volume change that occurs without moisture transfer to the environment or temperature change is called autogenous shrinkage. Before setting, chemical shrinkage and autogenous shrinkage are equal (Holt 2001). After setting, autogenous shrinkage is a function of capillary stresses induced by self-desiccation as illustrated in Figure 9-2. An illustration of setting, chemical shrinkage, and autogenous shrinkage is shown in Figure 9-3.

9.2 Degree of Hydration

The degree of hydration (α) is a measure of the reaction between the cementitious materials and water. It is defined as the ratio of hydrated cementing material to the original quantity of cementing material. The degree of hydration varies from 0 at the start to 100% when all the cementing material is hydrated. However, a 100% degree of hydration may never be reached (Mills 1966).

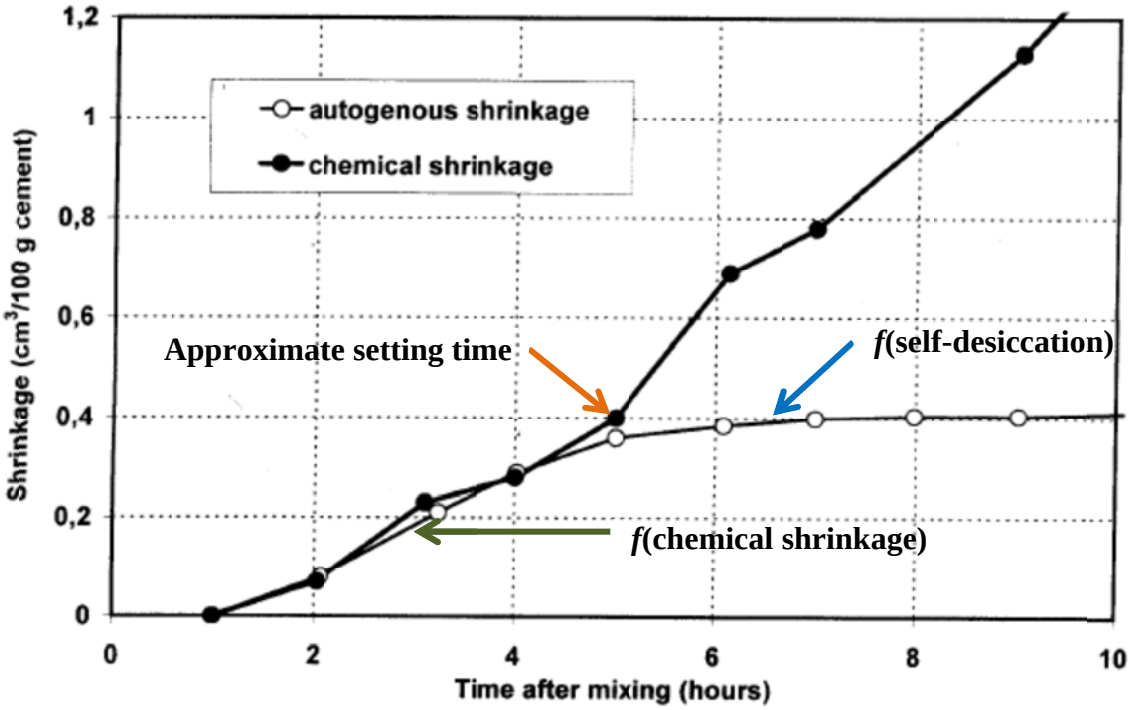

Figure 9-2: Chemical and autogenous shrinkage test results as well as illustration of hydrating cement (adapted from Hammer 1999)

The degree of hydration can be measured directly or indirectly. Direct methods measure the quantity of hydration products that have formed, but as RILEM Commission 42-CEA (1981) states, it is "almost impossible to make a direct determination of the quantity of cement gel formed or the quantity of hydrated cement." Indirect methods based on the heat development during hydration can be used to estimate the degree of hydration. The heat released divided by the heat available provides a good measure of the degree of hydration (RILEM 119-TCE 1999; Van Brugel 1997). The total heat of hydration available is generally determined from the chemical makeup of the cementing materials (Schindler and Folliard 2005).

t=0, water meets cement

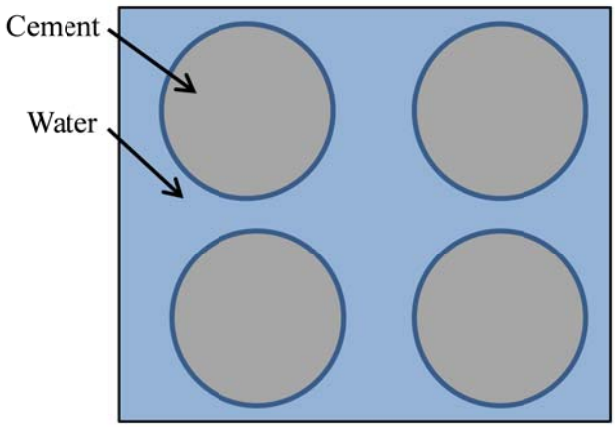

t = initial set, hydration products form skeleton

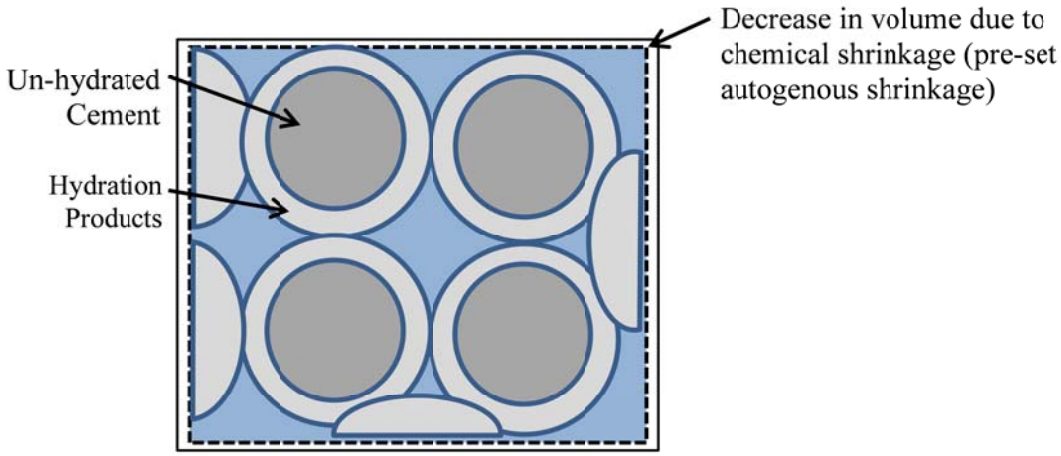

t=after set, hydration continues and cement consumes capillary pore water and induce capillary stresses

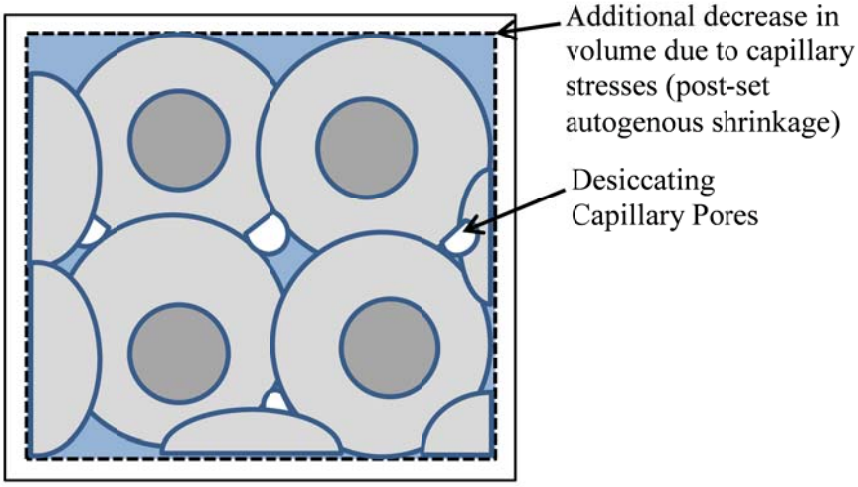

Figure 9-3: Illustration of autogenous shrinkage, chemical shrinkage, and setting

Mills (1966) performed a study on a wide range of cement materials to determine the ultimate degree of hydration (α_u) based on the amount of chemically bound water after hydration was complete. Ultimate degree of hydration is strongly affected by the *w/c* (Mills 1966; Hansen 1986). Mills (1966) developed Equation 9-2 to estimate the ultimate degree of hydration based on *w/c*.

$$\alpha_u = \frac{1.031 \cdot w/c}{0.194 + w/c} \quad \text{..... Equation 9-2}$$

If additional water is provided from external sources, Hansen (1986) derived the limiting factor is the space available for hydration products, based on consideration of the fundamental behavior of hydrating cement. In this case, the ultimate degree of hydration can be estimated using Equation 9-3.

$$\alpha_u = \frac{w/c}{0.36} \leq 1.0 \quad \text{..... Equation 9-3}$$

9.3 Internal Relative Humidity

The relative humidity (RH) of an air water system is defined as the ratio of the partial pressure of water vapor to the saturated vapor pressure of pure water at a prescribed temperature as shown in Equation 9-4 (Coussy 2010). When water is removed from capillary pores a reduction in internal RH takes place. Water can be removed from the

concrete system by external drying when the ambient environment has a lower RH than the system or by self-desiccation.

$$RH = \frac{\rho_w}{\hat{\rho}_w} \times 100\% \quad \text{Equation 9-4}$$

where RH = relative humidity (%),

ρ_w = partial pressure of vapor, and

$\hat{\rho}_w$ = saturated vapor pressure of water.

Water is removed from larger capillary pores first then progressively smaller ones (Coussy 2010). As water leaves the saturated pores a meniscus is formed at the vapor to fluid interface. The amount of capillary suction is a function of the radius of the meniscus. Smaller capillary pores have smaller menisci and therefor much greater capillary suction. RH measurements of concrete can capture the capillary suction created by desiccation (Grasley 2006).

The Kelvin equation can be used to capture the relationship between RH and pore radius and is given in Equation 9-5 (Coussy 2010) and illustrated on a log scale in Figure 9-4. The Kelvin and Laplace equations can be combined to show the relationship between RH and capillary pressure. The Kelvin-Laplace equation is given in equation 9-6 (Coussy 2010) and a plot of Kelvin-Laplace equation on a log scale illustrating the relationship between RH and capillary pressure is shown in Figure 9-5.

$$-\ln(RH) = \frac{2\sigma M}{\rho RTr} \quad \text{Equation 9-5}$$

$$-\ln(RH) = \frac{sM}{\rho RT} \quad \text{..... Equation 9-6}$$

where RH = relative humidity expressed as a decimal,

σ = surface tension of air-water interface (≈ 0.074 N/m),

M = molecular weight of water (18 kg/kmol),

ρ = density of water (998 kg/m^3 at 293 °K),

R = universal gas constant (8314 J/(kmol °K),

T = temperature (293 °K),

r = pore radius (m), and

s = capillary suction (Pa).

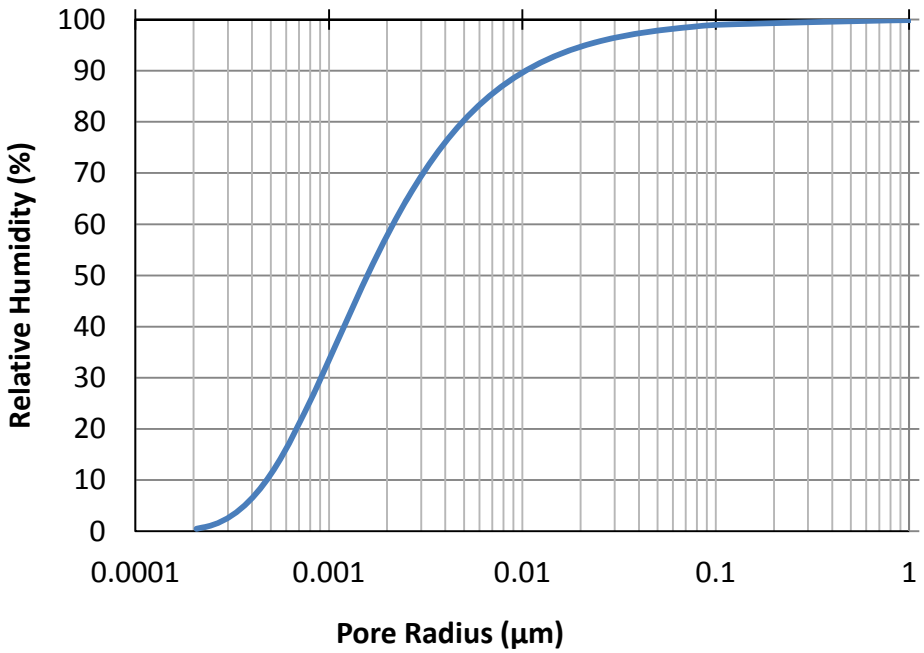

Figure 9-4: Relationship between empty pore radius and relative humidity based on the Kelvin equation

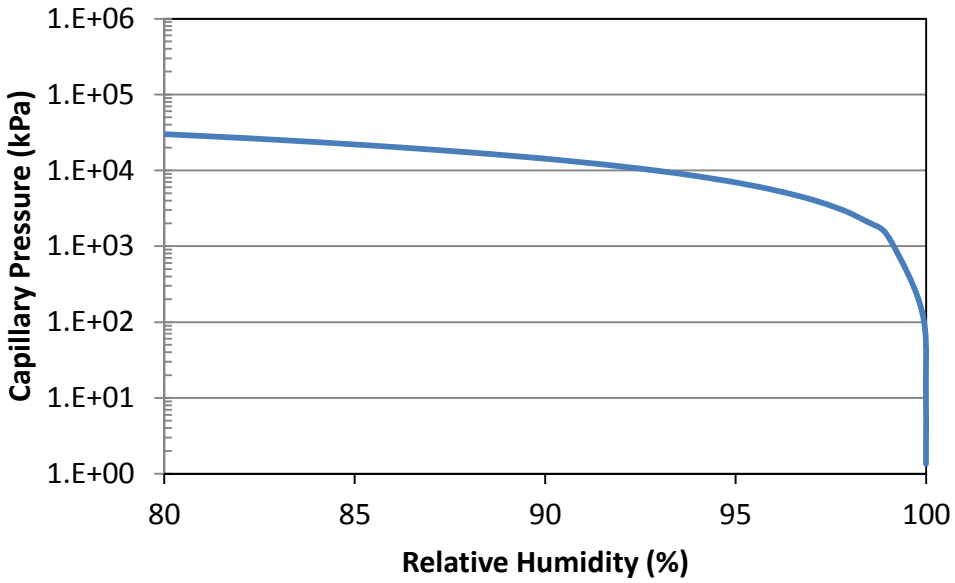

Figure 9-5: Relationship between capillary pressure and relative humidity based on Kelvin-Laplace equation

Figure 9-4 illustrates the relationship between relative humidity and pore size in a porous solid like hardened cement paste. The figure shows that as the relative humidity decreases, the radius of the pore that is drying decreases non-linearly. A RH change from 100% to 90% leads to three orders of magnitude change in empty pore size. As the size of the pore decreases the amount of stress on the capillary pore wall increases as shown in Figure 9-5. Figure 9-5 shows the relationship between capillary stress and RH is non-linear and at RH values above 95% a small change in RH brings about a large change in capillary stress. Therefore, for concrete mixtures with smaller capillary pores small changes in the internal moisture state can lead to relative large changes in stress.

Because concrete has dissolved salts such as potassium and sodium in solution, there is a reduction in vapor pressure, which leads to a reduction in the equilibrium RH. Therefore, the maximum RH of concrete pore solution is less than 100% (Grasley 2006).

9.4 Internal Curing

Historically, lightweight aggregate (LWA) has been used to reduce the density of concrete. In recent years; however, LWA has been added to concrete to take advantage of the high absorption capacity of the aggregates, which may provide internal water for hydration and mitigation of capillary stresses due to self-desiccation.

The addition of pre-wetted LWA helps mitigate stress due to autogenous shrinkage by desorbing water from the aggregate particles into the hydrated cement paste pore structure and relieving some or all of the capillary tension (Henkensiefken 2008). Generally, autogenous shrinkage and stress development is not a concern for mixtures with *w/c* ratios exceeding 0.42 (Mindess et al. 2002; Mehta and Monteiro 2006). An illustration of lightweight aggregate mitigating capillary stresses is shown in Figure 9-6**.**

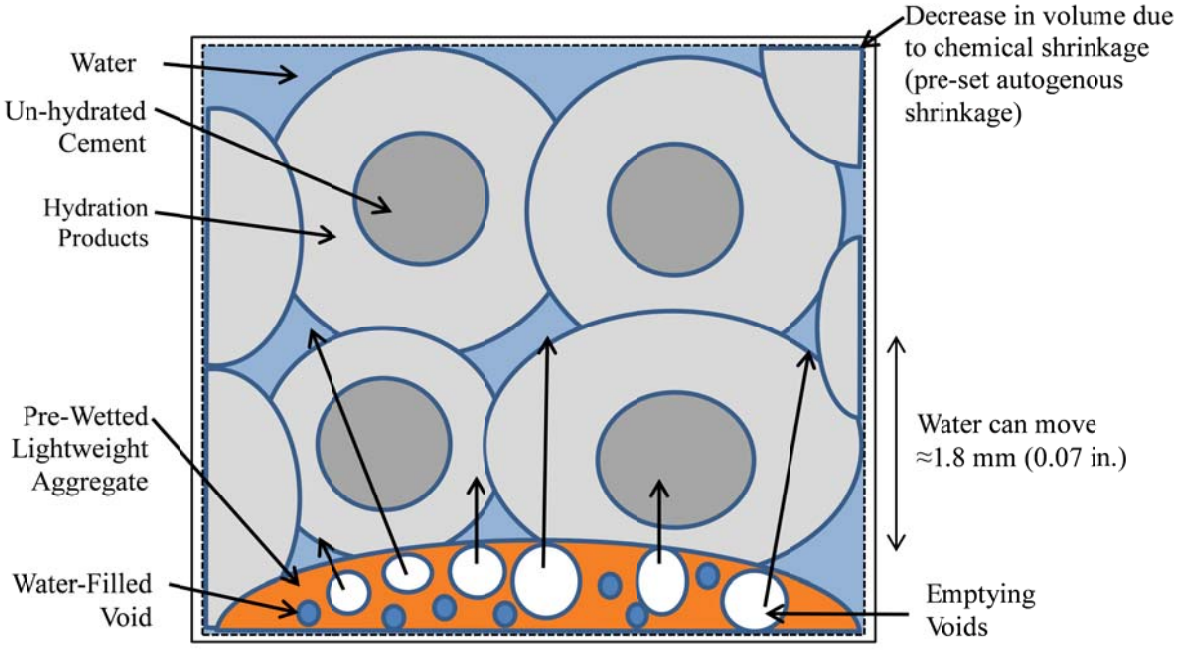

Figure 9-6: Illustration of water movement from lightweight aggregate to capillary pores

Figure 9-6 shows how water can move from pre-wetted lightweight aggregate pores and into the hardened cement paste matrix preventing pores from empting. This additional water can decrease capillary stress caused by self-desiccation and reducing autogenous shrinkage.

High absorption materials such as perlite, wood pulp, super-absorbent particles, and LWA are some materials that have been used in concrete for internal curing purposes. LWA is used more frequently as an internal-curing material (Delatte et al. 2008). Lightweight fine aggregates are generally used for internal curing purposes due to their greater dispersion compared to coarse aggregates. Water from LWA can move 0.07 in. into the paste surrounding the aggregate particles (Henkensiefken 2008).

Bentz et al. (2005) provide a simplified method for proportioning lightweight fine aggregate for internal curing purposes as shown in Equation 9-7. The unit chemical shrinkage (*CS*) is calculated using coefficients that provide the chemical shrinkage in terms of water mass per cement mass. The total chemical shrinkage is determined by using the cement content (C_f) and ultimate degree of hydration of the mixture (α_u). The coefficients suggested by Bentz et al. (2005) for chemical shrinkage due to cement hydration are presented in Table 9-1. Bentz et al. (2005) use Equation 9-3 to estimate the ultimate degree of hydration. The volume of water equal to the total chemical shrinkage is known, and this is the amount of water to be provided by the lightweight aggregate. The volume of water provided by the lightweight fine aggregate is calculated using the absorption (Φ_{LWA}) and the degree of saturation (*S*) of the aggregate. This volume of water prevents the capillary voids from desiccating, which should prevent capillary stresses from developing.

$$M_{LWA} = \frac{C_f \times CS \times \alpha_{\max}}{S \times \phi_{LWA}}$$ ..... Equation 9-7

where M_{LWA} = oven-dry weight of lightweight aggregate (lb),

C_f = cement content for the mixture (lb/yd^3),

CS = chemical shrinkage (lb of water/lb of cement),

α_u = ultimate degree of cement hydration,

S = degree of saturation of aggregate (0 to 1), and

Φ_{LWA} = absorption capacity of lightweight aggregate (lb water / lb dry LWA).

Table 9-1: Coefficients for chemical shrinkage (Bentz et al. 2005)

Cement Phase	Coefficient (Pound of water / Pound of solid cement phase)
C_2S	0.0704
C_3S	0.0724
C_3A	0.115*
C_4AF	0.086*

* assuming total conversion of the aluminate phases to monosulfate.

Equation 9-7 balances the volume of absorbed water within the LWA with the anticipated chemical shrinkage demand. Not all the absorbed water within the LWA will be desorbed for early-age internal curing (Bentz et al. 2005; RILEM TC 196 2007). The amount of water desorbed from the LWA will be a function of the aggregate pore size distribution, the spacing of the LWA in the concrete, the pore size distribution of the paste matrix, permeability of the paste, and the internal RH around the aggregate particle (RILEM TC 196 2007).

Capillary tensile stresses develop as cement hydrates and consumes water from capillary pores in the paste matrix. Water is then desorbed from the pores of the LWA into the paste capillary pores. Available water is more easily removed from larger pores than from smaller pores. LWA with large amounts of smaller pores do not readily release their internal water. The lower limit of useful aggregate pore size is around 100 nm (RILEM TC 196 2007). Due to different pore size distributions, various LWAs can have significantly different desorption properties. For internal curing purposes, desorption properties are more important than absorption properties (Lura 2003; Bentz et al. 2005).

It is necessary that the lightweight aggregate release moisture at a high RH so the moisture will be available at early ages. Castro et al. (2011) tested the desorption of a variety of lightweight materials at 93% RH. A summary of the desorption coefficients found by Castro et al. (2011) relevant to the LWA used in this study are presented in Table 9-2. The desorption coefficient is the percentage of water lost relative to the amount of absorbed water in the aggregate at the surface dry condition. The desorption response is different for expanded shale, clay, and slate; thus, it needs to be accounted for when determining the amount of internal-curing water available from these LWAs.

Table 9-2: Desorption coefficients at 93% relative humidity (Castro et al. 2011)

Item	Lightweight Aggregate Type		
	Slate	**Clay**	**Shale**
Supplier	Stalite	TXI	Buildex
Source	Gold Hill, NC	Frazier Park, CA	New Market, MO
Desorption coefficient at 93% relative humidity	0.962	0.887	0.976

Self-desiccation can also decrease the degree of hydration (Lura et al. 2004). Reducing the water availability around the cement grain diminishes the ability of the cement to hydrate and gain strength. Bazant and Najjar (1972) found that below 80% internal RH the strength development is very minimal. The additional water provided by internal curing generally increases the degree of hydration (Bentz and Weiss 2010).

9.5 Modulus of Elasticity

The modulus of elasticity of the concrete depends heavily on the stiffness of the aggregate (Mehta and Monteiro 2006). The increased porosity of LWA results in smaller modulus of elasticity compared to normalweight concrete (Mindess et al. 2002). ACI 318 (2008) provides Equation 9-8 to estimate the modulus of elasticity from a known density and compressive strength. This expression indicates that the modulus of elasticity will decrease as more LWA is introduced into the mixture.

$$E_c = 33 w_c^{1.5} \sqrt{f_c} \quad \text{..... Equation 9-8}$$

where E_c = modulus of elasticity (psi),

w_c = density of the concrete (lb/ft^3), and

f_c = concrete compressive strength (psi).

CHAPTER 10

PART II: EXPERIMENTAL WORK

10.1 Experimental Program

The early-age stress development of internally cured concretes was investigated using ten different mixtures with three different *w/c*. Four mixtures were proportioned with a *w/c* of 0.42, and three mixtures with *w/c* values of 0.36 and 0.30. Each mixture was tested in two rigid cracking frames (RCF). One RCF was match-cured to a modeled temperature profile, and the concrete stress development was monitored until the onset of cracking. The second RCF was cured at an isothermal condition to determine the concrete stress development due to autogenous shrinkage. All specimens were sealed to prevent drying shrinkage. Mechanical properties were evaluated using 6 × 12 inch cylindrical samples match-cured to the temperature profile of an 8-inch thick bridge deck with stay-in-place metal forms. The temperature modeling, which accounted for the unique heat of hydration development of each mixture, was performed using ConcreteWorks (Poole et al. 2006). The autogenous shrinkage was measured by free-shrinkage frame for concrete and corrugated tubes for mortar specimen. The internal relative humidity (RH) of concrete samples was measured with a setup similar to the one described by Grasley (2006).

10.2 Lightweight Material Preconditioning

The lightweight fine aggregates were placed in water-filled plastic barrels for moisture preconditioning. Valves were installed in the bottom of the plastic barrels for drainage. A river gravel filter layer was placed in the bottom 6 in. of the barrel to prevent clogging of the drain valve. The lightweight materials were soaked for at least 7 days. After the preconditioning period, the barrels were drained slowly to prevent the loss of the fines. The lightweight fine aggregate was then placed on plastic sheets in stockpiles to allow excess surface water to drain. The material was then shoveled into 5-gallon buckets for batching.

Relative density and absorption testing of the lightweight material was performed using ASTM C 128-07. For the lightweight fine aggregates, Provisional Method 2 of ASTM C 128 (the rubber mat method) was used to determine when the sample was at the surface dry condition. The source location, type, and properties of each of the LWA are shown in Table 10-1. Because LWA never reach saturation, the term saturated surface dry is inappropriate (ESCSI 2007). Because of this, the relative density calculations are presented for the pre-wetted surface dry (SD) condition after at least 7 days of preconditioning. The gradations for each aggregate type can be seen in Appendix B.

10.3 Materials and Mixtures

Three *w/c* and several different internal-curing mixtures were evaluated in this part. The three *w/c* evaluated were 0.42, 0.36, and 0.30. The internal-curing (IC) mixtures with *w/c* of 0.42 used expanded shale, clay, or slate LWA. The IC mixtures with *w/c* of 0.36 and 0.30 used only a source of expanded shale that was different from the IC mixture with a

w/c of 0.42. The mixtures in this part are identified by their *w/c* first and then by type of IC, if applicable. The IC types for mixtures with w/c of 0.42 are identified by the variety of lightweight aggregate used (shale, clay, and slate). The IC types provided to mixture with w/c of 0.36 and 0.30 are identified as ICM or ICH. The control mixtures with no internal curing are identified by only their *w/c*.

Table 10-1: Lightweight aggregate source and material properties

Item	Lightweight Aggregate Type			
	Slate	**Clay**	**Shale**	
Supplier	Stalite	TXI	TXI	Buildex
Source	Gold Hill, NC	Frazier Park, CA	Streetman, TX	New Market, MO
Gradation	#4 to 0	3/8 in. to 0	#4 to 0	#4 to 0
Absorption (%)	9.0	19.0	24.5	19.3
Bulk-specific gravity	1.84	1.81	1.8	1.80
Fineness Modulus	2.83	4.32	3.35	2.99
Desorption Coefficent (Castro et al. 2010)	0.962	0.887	0.853	0.976

Concrete mixture proportions are shown in Table 10-2. The control mixture with *w/c* of 0.42 is a typical bridge deck mixture used in the southeastern United States. It uses natural river gravel as coarse aggregate and natural river sand as fine aggregate. IC mixtures were proportioned by replacing a fraction of the normalweight fine aggregate with lightweight fine aggregate. The coarse aggregate, cement, and total aggregate volumes of the IC mixtures remained the same as for the control mixture. Shale, clay, and slate lightweight aggregates were used in the IC mixture testing with *w/c* of 0.42. Because LWA may never be 100% saturated, the batch weights for the lightweight materials are for the SD condition after at least 7 days of soaking in water. The target slump and total air

content for all the mixtures were 4 ± 1 in. and 5.5 ± 1.5 %, respectively, which are typical values for bridge deck construction in the southeastern U.S. For this project, the measured density of the concrete was within ± 1 lb/ft^3 of the calculated density after correcting for the measured total air content.

Each 0.42 IC mixture was proportioned with the maximum amount of LWA to obtain a calculated equilibrium (EQ) density of 135 lb/ft^3, the normalweight concrete density limit according to the AASHTO LRFD Bridge Design Specifications (2007). The equilibrium density was calculated following ASTM C 567. Because the absorption capacity and pore size distribution of each of the three LWA sources are different, they each provided different amounts of IC water. Using the desorption coefficients in Table 9-2 and the absorption capacity from Table 10-1, the internal curing water provided by each mixture was calculated and is shown in Table 10-2.

A control and two IC mixtures were tested at a *w/c* of 0.36 and 0.30. The mixtures with *w/c* of 0.36 and 0.30 have the same paste, fine aggregate, and coarse aggregate volumes as the mixtures with *w/c* of 0.42 . The cement contents were increased accordingly to keep the paste volumes constant for each *w/c*. Only a shale LWA was used to replace the normalweight fine aggregate to provide internal curing for the mixtures with *w/c* of 0.36 and 0.30. Two different levels of internal curing were provided. Both IC mixtures were proportioned using the method of balancing chemical shrinkage demand with internal-curing water as proposed by Bentz et al. (2005). However, one mixture was based on the Hansen (1986) ultimate degree of hydration equation, and this mixture is identified as ICH. The other IC mixture (identified as ICM) was based on the ultimate degree of hydration as computed by Mills (1966). The chemical shrinkage constant used

for lightweight mixture proportioning was 0.0695 grams of water per grams of cement. Which was calculated based on the cement composition and the constants provided by Bentz et al. (2005) assuming full conversion of the aluminates to monosulfate. The LWA were soaked for 7-days before absorption testing and mixing, therefore the saturation term is set equal one.

Table 10-2: Concrete mixture proportions and properties

Component	Concrete Mixture									
	0.42	0.42 IC Shale	0.42 IC Clay	0.42 IC Slate	0.36	0.36 ICM	0.36 ICH	0.30	0.30 ICM	0.30 ICH
Water Content (lb/yd^3)	260	260	260	260	238	238	238	218	218	218
Cement Content (lb/yd^3)	620	620	620	620	677	677	677	738	738	738
No. 67 River Gravel, SSD (lb/yd^3)	1761	1761	1761	1761	1761	1761	1761	1761	1761	1761
Buildex Shale Fine, SD (lb/yd^3)	0	230	0	0	0	0	0	0	0	0
TXI Shale Fine, SD (lb/yd^3)	0	0	0	0	0	184	275	0	188	253
TXI Clay Fine, SD (lb/yd^3)	0	0	230	0	0	0	0	0	0	0
Stalite Slate Fine, SD (lb/yd^3)	0	0	0	276	0	0	0	0	0	0
Natural Sand, SSD (lb/yd^3)	1210	878	878	818	1210	956	823	1210	940	867
Target Air (**%**)	5.5	5.5	5.5	5.5	5.5	5.5	5.5	5.5	5.5	5.5
w/c	0.42	0.42	0.42	0.42	0.36	0.36	0.36	0.30	0.30	0.30
Calculated EQ density (lb/yd^3)	140	135	135	135	143	139	137	145	141	140
Fresh Density (lb/yd^3)	143	139	139	138	144	141	140	145	142	142
Internal-Curing Water Provided (lb/yd^3)	0	36	33	22	0	31	46	0	32	42
Internal-Curing Water Required by Eq.9-7 (lb/yd^3)	43	43	43	43	47	47	47	43	43	43

The coarse aggregate for the project was ASTM C 33 No. 67 siliceous river gravel. The normalweight fine aggregate used throughout the project was siliceous river sand. Both aggregate types were obtained from the quarry of Martin Marietta Materials located in Shorter, Alabama. The aggregates were sampled, and ASTM C 136 sieve analyses were performed to determine the gradations. The specific gravity and absorption capacity for the normalweight coarse (ASTM C 127) and fine (ASTM C 128) aggregates were 2.63, 0.52% and 2.61, 0.41%, respectively. The fineness modulus of the normalweight fine aggregate was 2.45. The gradations of each aggregate can be seen in Appendix B.

An adequate quantity of Type I portland cement was donated by TXI to complete all testing associated with this project. The properties of the portland cement are shown in Table 10-3. Chemical admixtures were used as needed in the concrete mixtures to control the slump and the total air content of the fresh concrete.

Table 10-3: Portland cement properties

C_3S	C_2S	C_3A	C_4AF	Free CaO	SO_3	MgO	Blaine Fineness
60.3 %	18.2 %	5.4 %	11.3 %	0.9 %	2.6 %	1.3 %	351 (m^2/kg)

10.4 Restrained Stress Development

The rigid cracking frame (RCF), shown in Figure 10-1, is comprised of two mild steel crossheads and two 4-in. diameter Invar sidebars. The test setup was adapted from the configuration developed by Dr. Rupert Springenschmid as documented by RILEM Technical Committee 119 (1998). The RCF test is a relative index of cracking sensitivity. According to Springenschmidand Breitenbücher (1998), a mixture with increased cracking

time and decreased cracking temperature will have improved cracking performance in the field. This increased performance may be in the form of increased crack spacing, decreased crack widths or fewer cracks.

a)

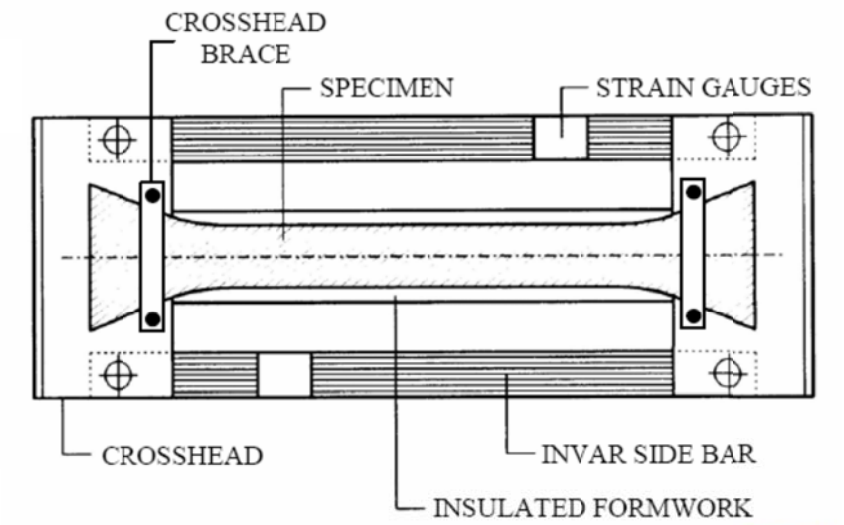

b)

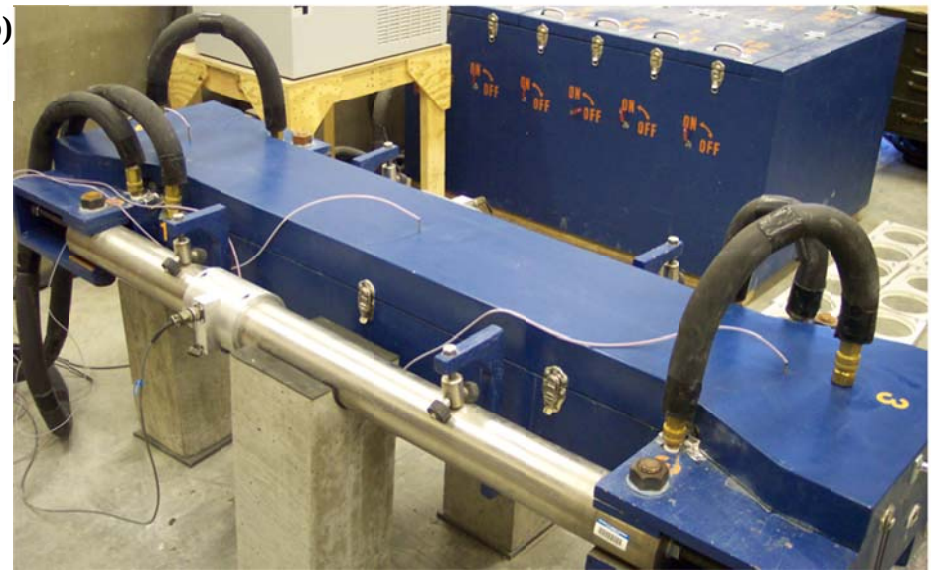

Figure 10-1: Rigid cracking frame test setup: a) Schematic of test (Mangold 1998) b) Actual equipment used

Fresh concrete is consolidated in the RCF, and its stress development is measured continuously until cracking occurs. The 6 × 6 × 49 in. concrete specimen is restrained by dovetailed crossheads at each end. The dovetail is gradually tapered to reduce stress

concentrations and has multiple teeth that grip the concrete. To further prevent slippage of the concrete, crosshead braces are used at the end of the crosshead to restrain opening of the crosshead as the concrete goes into tension. The formwork includes 0.5-in. diameter copper tubing throughout. A mixture of water and ethylene glycol is circulated from a temperature-controlled water bath through the formwork to control the curing temperature of the concrete sample. The formwork of the RCF is lined with sheeting to reduce friction between the concrete and the form and to seal the concrete specimen on all surfaces. Because of the presence of the sealed plastic layer around the concrete specimen, no moisture is lost and drying shrinkage effects do not contribute to the stress development while the forms are in place.

When concrete in the RCF starts to hydrate and volume changes due to temperature and autogenous shrinkage effects develop, the Invar bars provide restraint against movement and stress develops in the concrete. The concrete's stress development is monitored using strain gauges mounted on the Invar bars, that are calibrated to the bar forces, which equilibrate the concrete stresses.

The stress developed by the RCF under an isothermal condition is a function of the modulus of elasticity, autogenous shrinkage, and relaxation. The stress developed by the RCF under a match-cured condition is a function of the concrete's coefficient of thermal expansion, temperature history, modulus of elasticity, autogenous shrinkage, and relaxation.

It has been observed that the cracking frame stress at failure is less than the splitting tensile strength measured on molded concrete cylinders (Meadows 2007). This is due to the differences in test specimen size, the rate of loading, and the type of loading

(Meadows 2007). The section of concrete subjected to the highest tensile stress is much larger in the cracking frame than in a 6 × 12 in. cylinder. The larger volume of concrete subjected to the highest tensile stress in the cracking frame provides a higher probability of a significant flaw in the sample and therefore it has a lower apparent strength. In addition, the rate of loading can affect the strength results. Slow load rates yield a lower apparent strength and conversely higher load rates yield a higher apparent strength (Wight and MacGregor 2009). The splitting tensile strength specimens were loaded to failure in less than 5 minutes, whereas the cracking frames were loaded for 27-95 hours, thus the concrete in the cracking frame will exhibit a lower apparent tensile strength. In addition, the cracking frame is a direct tension test; whereas the splitting tension is an indirect tensions test. Meadows (2007) reports that the ratio of cracking frame stress at failure to splitting tensile strength generally falls between 50 to 80 percent.

10.5 Autogenous Shrinkage

The linear autogenous shrinkage was measured for both concrete and mortar specimen. This was done by using a measuring the unrestrained length change of the *concrete* in a free shrinkage frame and for sieved *mortar* in corrugated tubes as per ASTM C 1698-09. The free shrinkage frame test was used to determine the autogenous strain of the control *concrete* mixtures with *w/c* of 0.30, 0.36, and 0.42. The corrugated tubes were used to determine the autogenous strain of *mortar* sieved from the concrete of all of the mixtures.

10.5.1 Unrestrained Length Change of Concrete

Bjøntegaard (1999) developed a free shrinkage frame (FSF) to determine the unrestrained uniaxial length change of a curing *concrete* specimen. A FSF similar to the one developed by Bjøntegaard was constructed by Auburn University and is shown in Figure 10-2.

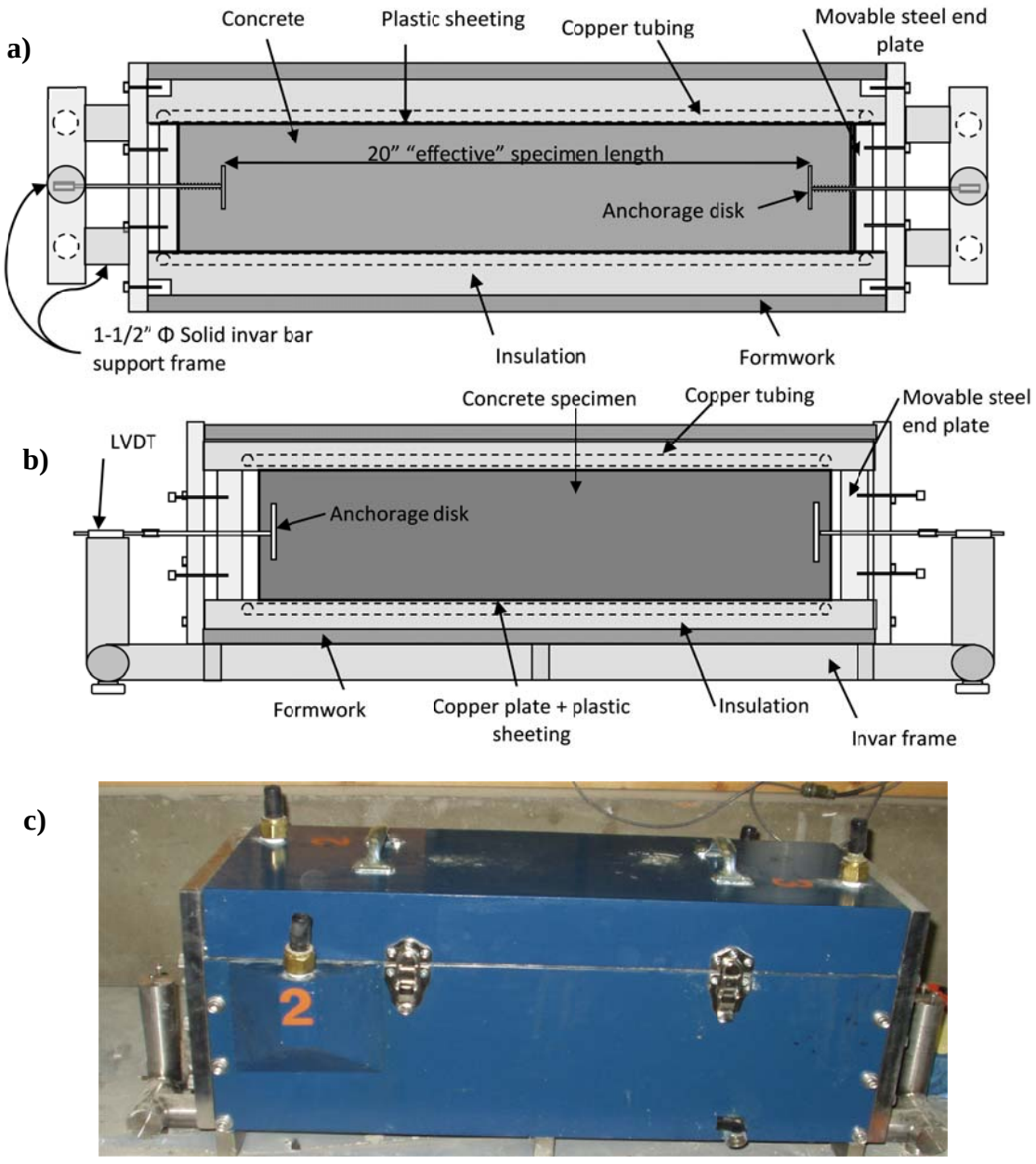

Figure 10-2: Free shrinkage frame test setup: a) Plan view schematic of test equipment, b) Section view schematic, and c) Actual equipment used

The FSF consists of a box that is thermally controlled with 0.5 in. diameter copper tubing, and a supporting Invar steel frame. The box serves as the formwork for the freshly placed concrete and the system to match cure the concrete to any temperature profile. A 6 × 6 × 24 in. concrete specimen is cast with two sacrificial steel plates connected with an Invar rod to a linear variable displacement transducer (LVDT) to measure linear expansion and contraction. The fresh concrete is placed on a double layer of plastic sheeting with a lubricant in between to minimize friction, which facilitates free movement of the concrete specimen. The plastic sheeting is also used to seal the concrete specimen on all surfaces. When concrete in the FSF is cured to a specified temperature history, the measured strain is a function of thermal and autogenous effects. The test specimen is entirely sealed with a plastic layer, so no moisture is lost. Therefore drying shrinkage effects do not contribute to the free movement measured in the FSF. When the concrete is placed, the movable steel end plates support the fresh concrete ends. When initial set is reached, the movable end plates are released and moved back to allow expansion beyond the initial specimen size. Initial set is determined from penetration resistance as per ASTM C 403. The end plates in position prior to placement is shown in Figure 10-2a and the end plates drawn back after setting is shown in Figure 10-2b.

10.5.2 Unrestrained Length Change of Mortar

The linear autogenous shrinkage of *mortar* was measured with corrugated tubes as per ASTM C 1698. The testing deviated from the ASTM C1698 specifications in that mortar was wet sieved from concrete instead of being mixed as per ASTM C 305. Three specimens were cast into corrugated tubes from each mixture and immediately placed in

an environmental chamber that maintained the ambient temperature between 71°F and 72°F. Setting was measured by ASTM C 403. At final set, the tubes were carefully placed in the dilatometer bench and there initial lengths were measured. Subsequent measurements were taken to determine the development of autogenous shrinkage. The dilatometer bench, corrugated tube, reference bar, and a specimen is shown in Figure 10-3.

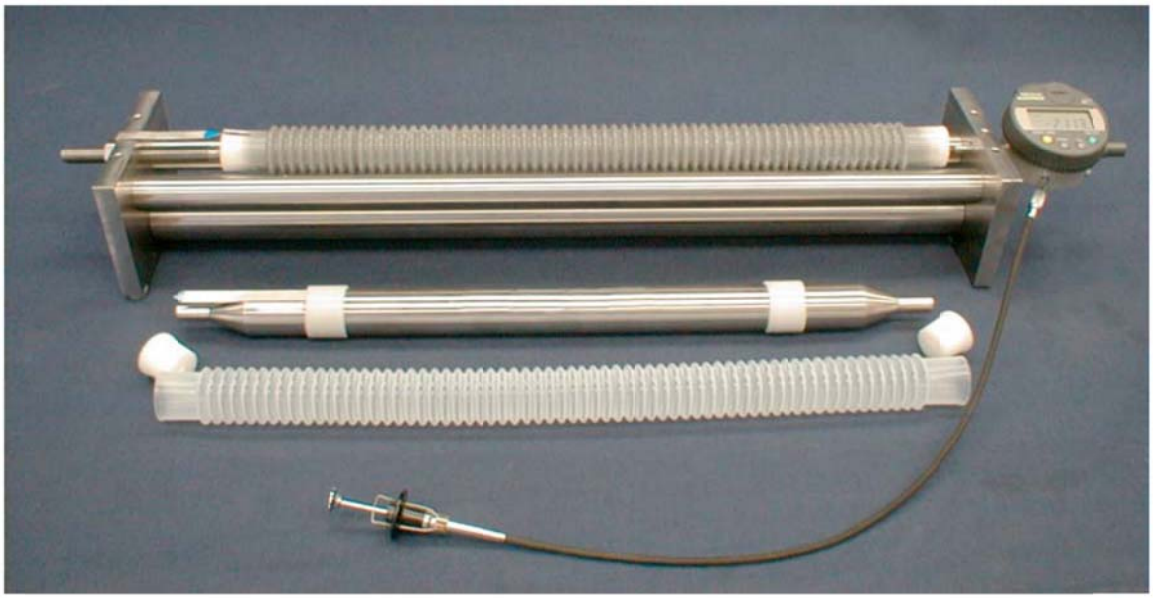

Figure 10-3: Dilatometer bench, corrugated tube, reference bar and specimen (ASTM C 1698 2009)

10.6 Internal Relative Humidity Measurement

A RH probe setup similar to the one described by Grasley (2006) was used to measure the internal RH of each mixture. A commercially available RH sensor was modified to protect the sensor. Sensirion SHT75 sensors were used for the research program. The sensors are capacitive sensors which measure the change in electrical impedance of a hygroscopic material that corresponds to the change in RH. Because of this, the sensors cannot be submerged, but only exposed to water vapor. Therefore, the sensors needed to

be protected so that they could be imbedded into concrete without submerging the sensor in the aqueous pore solution of the concrete. The sensors were placed into rigid 5/16-in. outer diameter styrene tubes with Gore-Tex® filter media affixed to the opposite end. The tube and sensor unit was then sealed with adhesive shrink tubing. The Gore-Tex® material allowed water vapor into the cavity, but not liquid water. Because the cavity is relative small, equilibrium is reached quickly. The modified RH sensor is shown in Figure 10-4.

The modified RH sensors were imbedded in a fresh 4 in. × 8 in. concrete cylinder that was then sealed with silicone caulk and water-resistant aluminum-foil tape. The RH specimens were stored so that the ambient temperature was between 70°F and 74°F. The RH development of each mixture was measured continuously for 96 hours.

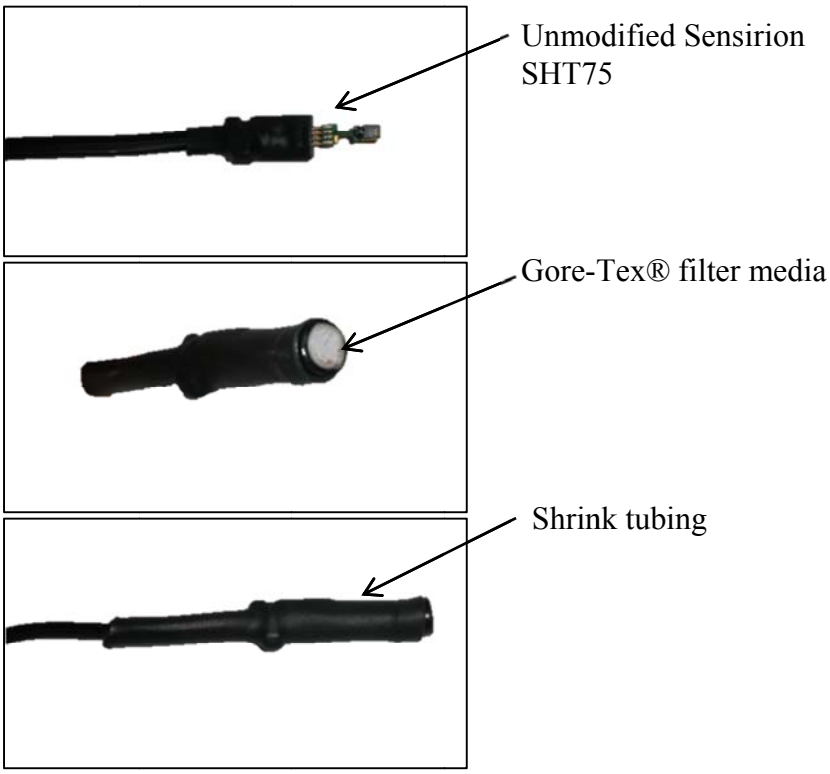

Figure 10-4: Relative humidity sensor modifications

10.7 Mechanical Properties

For each mixture and placement scenario, twenty-four 6 in. × 12 in. test cylinders were cast as per ASTM C 192. The cylinders were match cured to the same modeled temperature profile as the RCF, as shown in Figure 9-1. The cylinders were tested for compressive strength (ASTM C 39), splitting tensile strength (ASTM C 496), and modulus of elasticity (ASTM C 469) at ages of ½, 1, 2, 3, 7, and 28 days. All mechanical property testing met the precision and bias statement of their respective ASTM specification.

10.8 Degree of Hydration

Semi-adiabatic calorimetry was used to indirectly measure the degree of hydration, and to determine the hydration parameters for temperature modeling.

The semi-adiabatic calorimeter (SAC) test equipment used during this project was supplied by Digital Site Systems, Inc., Pittsburgh, Pennsylvania. The SAC setup consisted of an insulated 55-gallon drum and a 6 × 12 in. cylindrical concrete sample. Probes are used to record the concrete temperature, heat loss through the calorimeter wall, and air temperature surrounding the test equipment. The heat loss through the calorimeter was determined by a calibration test performed by using heated water. An illustration of the SAC is shown in Figure 10-5.

The ultimate degree of hydration was indirectly determined in this study using the semi-adiabatic calorimetry methods documented by Schindler and Folliard (2005). A 6

in. × 12 in. cylinder of fresh concrete was placed into the calibrated SAC, and the heat release of the sample was monitored. The degree of hydration was determined by dividing the heat released by the total heat of hydration of the cement. The total heat of hydration of the cement is the maximum heat that a cement, based on its chemical composition, can evolve. The experimental degree of hydration data were then fit to an S-shaped curve to quantify the ultimate degree of hydration as determined by Schindler and Folliard (2005).

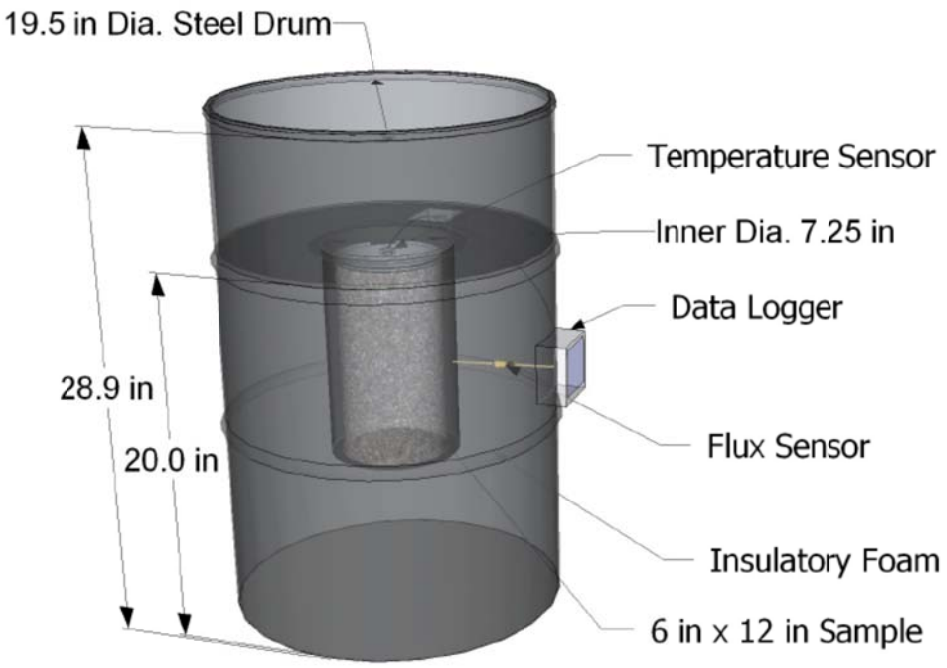

Figure 10-5: **Semi-adiabatic calorimeter (adapted from Weakley 2009)**

10.9 Concrete Temperature Modeling

The temperature profile that an in-place concrete element experiences is a function of the geometry of the element, the concrete mixture proportions, the chemical composition of the cementing materials, the placement temperature, the thermal conductivity of the

aggregate, and environmental effects such as ambient temperature, wind speed, and incoming solar radiation.

To assess the effect of placement and curing temperature, the concrete modeling software ConcreteWorks (Poole et al. 2006) was used to determine the temperature profile that an 8-in. thick bridge deck, constructed on stay-in-place metal forms, would experience. A fall placement scenario was selected. Bridge deck temperatures for fall placements were determined for Montgomery, Alabama on the construction dates of October 15. Semi-adiabatic calorimetry was used to determine the hydration parameters of each mixture (Schindler and Folliard 2005). Using the hydration parameters, as well as the placement date, city, bridge geometry, aggregate type, thermal diffusivity, mixture proportions, placement temperature, wind speed, ambient relative humidity, and percent cloud cover, a concrete temperature profile was generated for the simulated placement season. Note that this practice captures the unique temperature profile that each mixture would experience due to its own heat of hydration and thermal properties should it be placed in an 8-in. thick bridge deck. The match-cured temperature profile used for each mixture is thus unique to that mixture.

10.10 Other Fresh Quality Control Tests

All concrete was mixed as per ASTM C 192 under laboratory conditions. The temperature, slump, and density of the fresh concrete were measured as per ASTM C 1064, ASTM C 143, and ASTM C 138, respectively, for each batch of concrete. The total air content for the all normalweight aggregate mixtures was measured by the pressure method as per ASTM C 231. The total air content for all mixtures containing lightweight

aggregate was measured by the volumetric method as per ASTM C 173. All ASTM tests were performed by a technician certified as an ACI Field Testing Technician - Grade I.

CHAPTER 11

PART II: EXPERIMENTAL RESULTS

The results collected from the experimental work performed for this part are presented in this chapter. The modeled temperature profiles, restrained stress development for modeled and isothermal curing conditions, isothermal concrete and mortar free shrinkage, relative humidity, and degree of hydration results are presented in this chapter. A discussion and synthesis of the results are provided in Chapter 12.

11.1 Temperature Profiles and Stress Development

The modeled temperature profile of the mixture with *w/c* of 0.30, 0.36, and 0.42 is shown in Figure 11-1a, Figure 11-2a and Figure 11-3a, respectively. The measured restrained stresses of the mixture with *w/c* of 0.30, 0.36, and 0.42 can be seen in Figure 11-1b, Figure 11-2b and Figure 11-3b, respectively. The temperature and stress data plots end at the time of initial cracking. The initial cracking times are summarized in Table 11-1. The isothermal stress development of the mixture with *w/c* of 0.30, 0.36, and 0.42 are shown in Figure 11-4, Figure 11-5, and Figure 11-6, respectively. The isothermal stress reached at 96 hours for all the mixtures is summarized in Table 11-1.

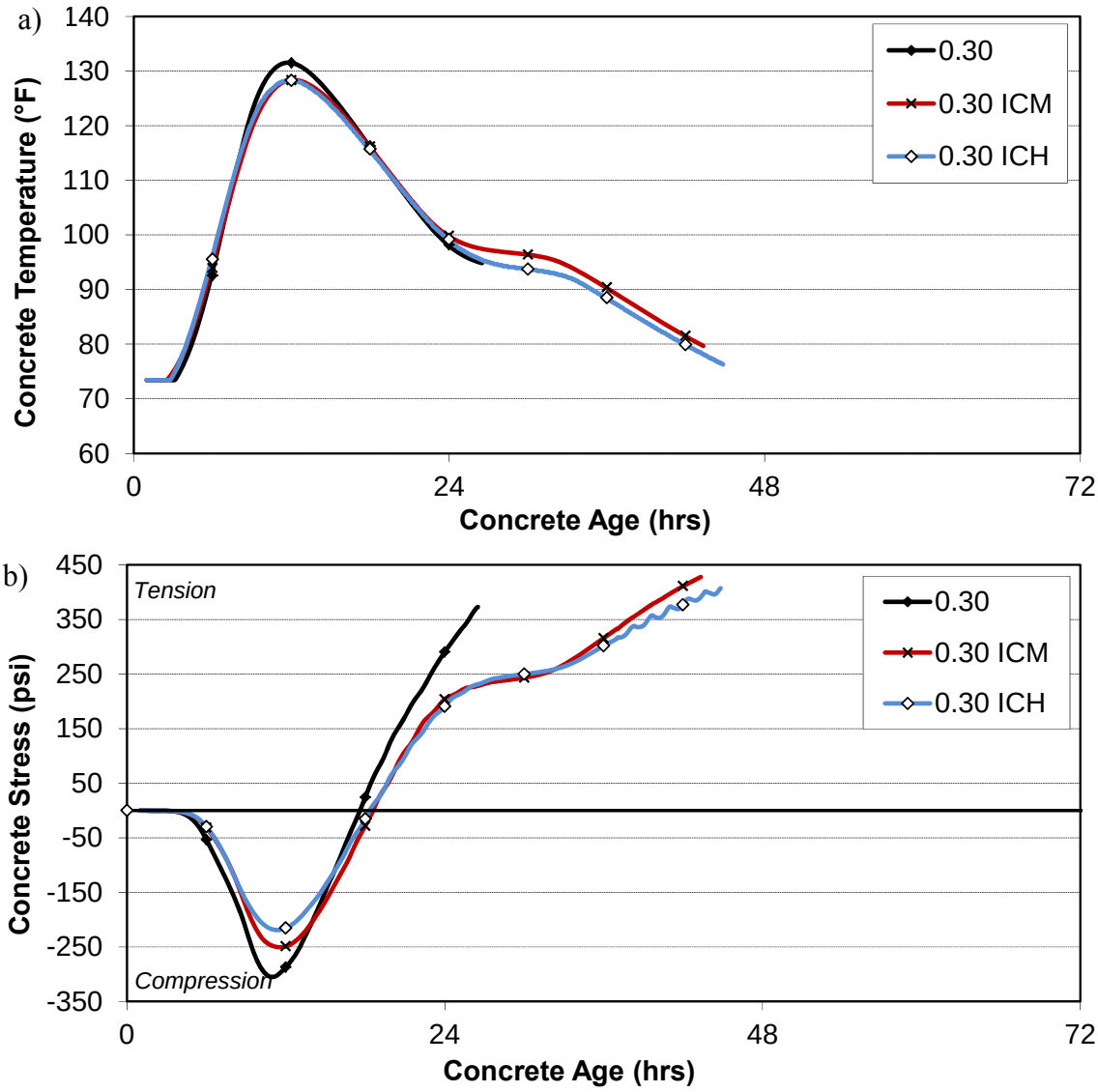

Figure 11-1: 0.30 *w/c* mixtures a) temperature profiles and b) match-cured stress development

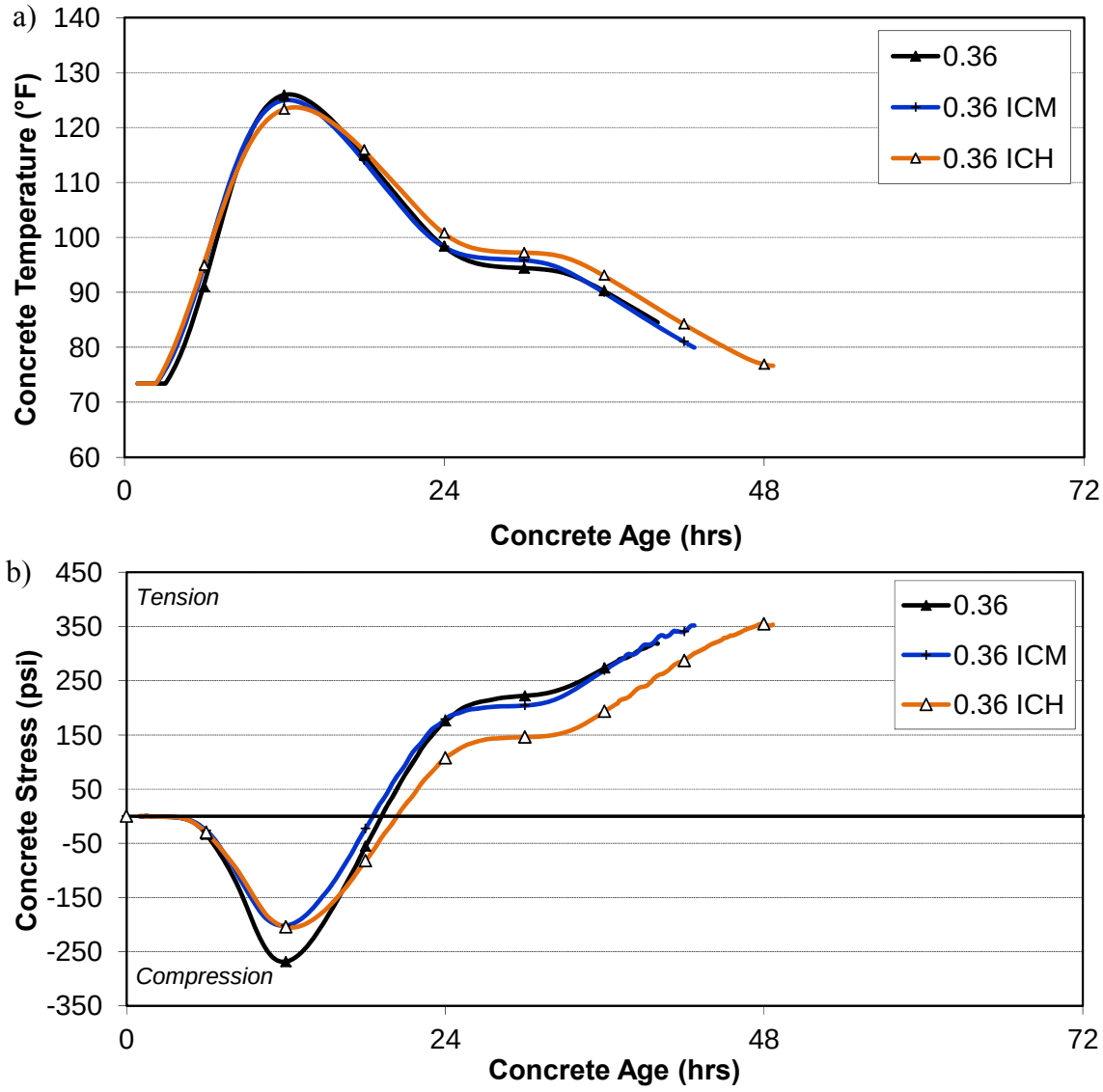

Figure 11-2: 0.36 *w/c* mixtures a) temperature profile and b) match-cured stress development

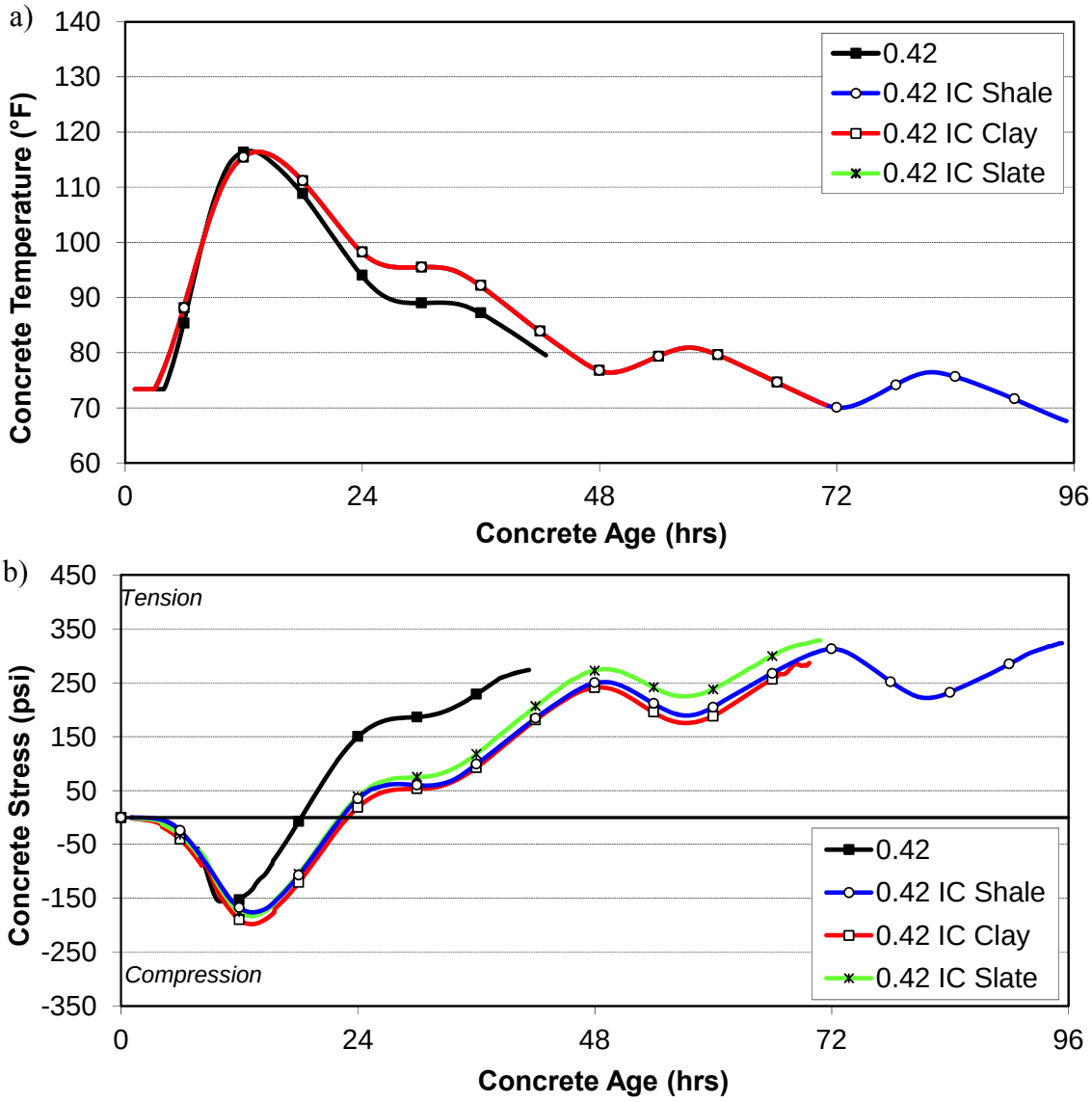

Figure 11-3: 0.42 *w/c* mixtures a) temperature profile and b) match-cured stress development

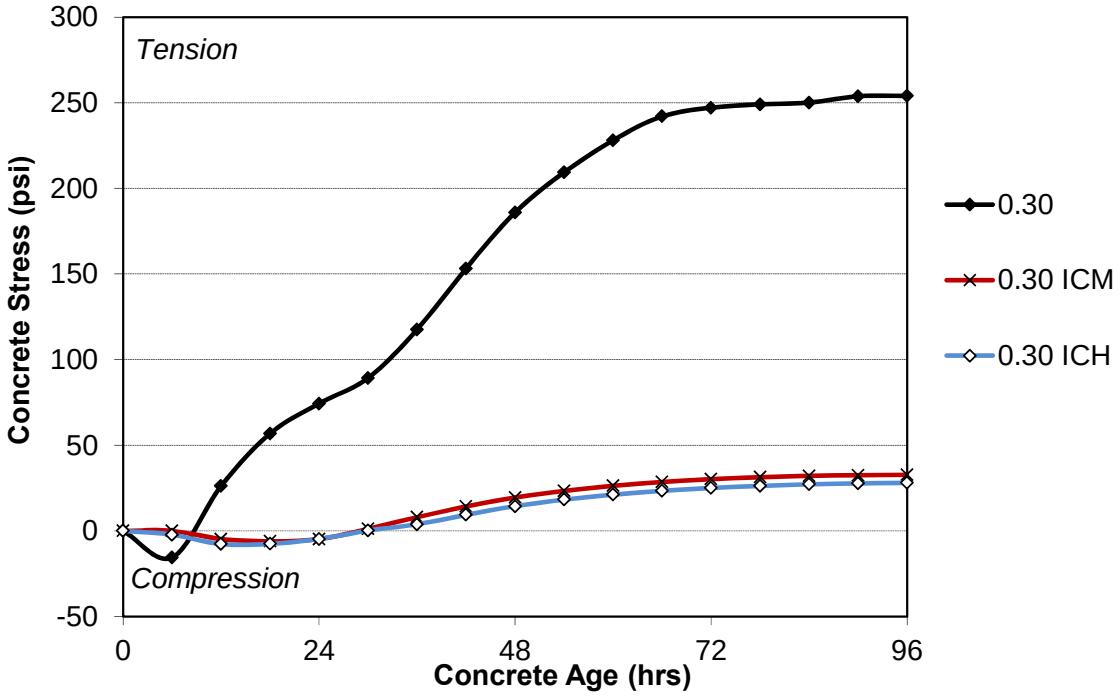

Figure 11-4: Isothermal stress development of 0.30 *w/c* mixtures

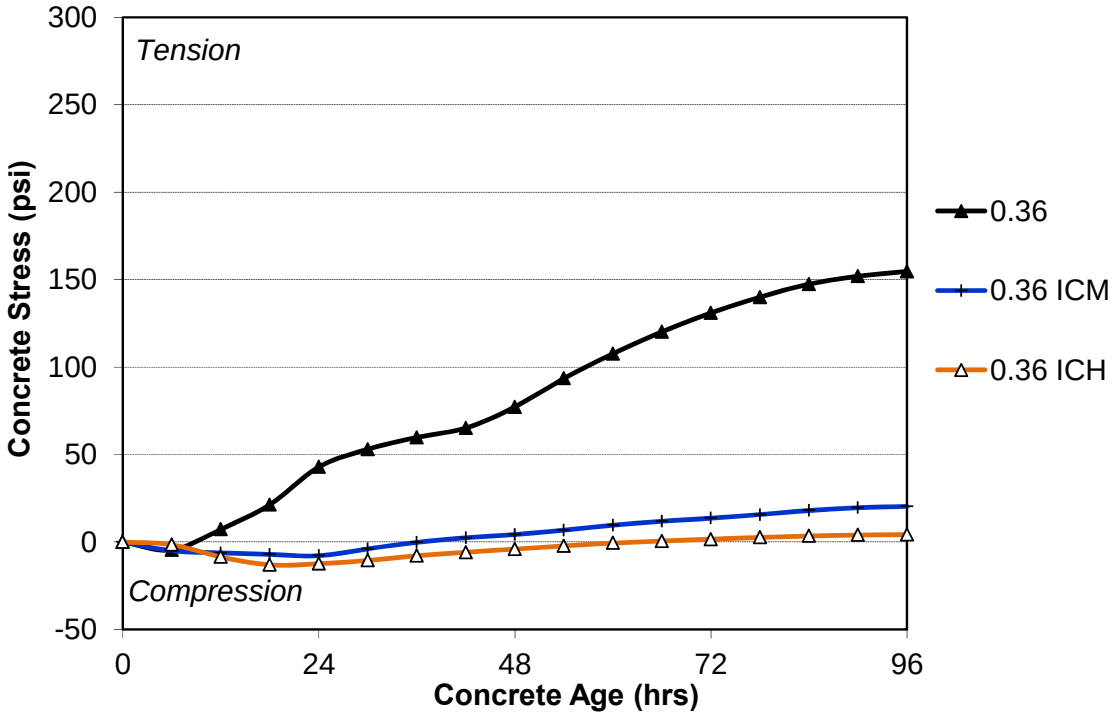

Figure 11-5: Isothermal stress development of 0.36 *w/c* mixtures

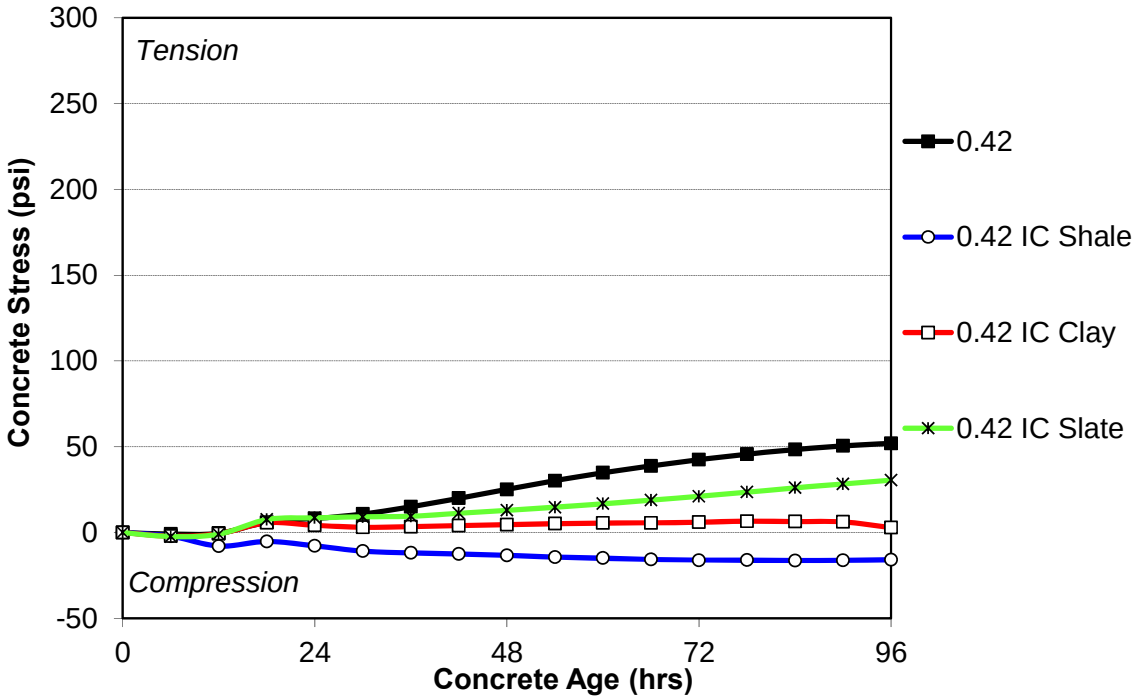

Figure 11-6: Isothermal stress development of 0.42 w/c mixtures

Table 11-1: Initial Cracking times and 96-hour isothermal stress development

Property	Mixture ID									
	0.42	**0.42 IC Shale**	**0.42 IC Clay**	**0.42 IC Slate**	**0.36**	**0.36 ICM**	**0.36 ICH**	**0.30**	**0.30 ICM**	**0.30 ICH**
Initial Cracking Time (hrs)	41.7	95.3	69.8	70.8	40.0	42.8	48.7	26.5	43.3	44.8
96-hr Isothermal Stress development (psi)	52	-16	3	31	155	20	4	254	33	28
Isothermal Stress Reduction Compared to Control (%)	-	131	94	42	-	87	97	-	87	89

11.2 Autogenous Shrinkage

The autogenous shrinkage of the *concrete* control mixtures are shown in Figure 11-7. The autogenous shrinkage of the sieved *mortar* for all of the mixture with *w/c* of 0.30, 0.36, and 0.42 are shown in Figure 11-8, Figure 11-9, and Figure 11-10, respectively. Table 11-2 summarizes the results of the autogenous shrinkage testing of concrete and mortar. Because, isothermal free-shrinkage data was only collected for the non-internally cured concrete mixtures there is no data (ND) for the autogenous strain of the internally cured concrete mixtures.

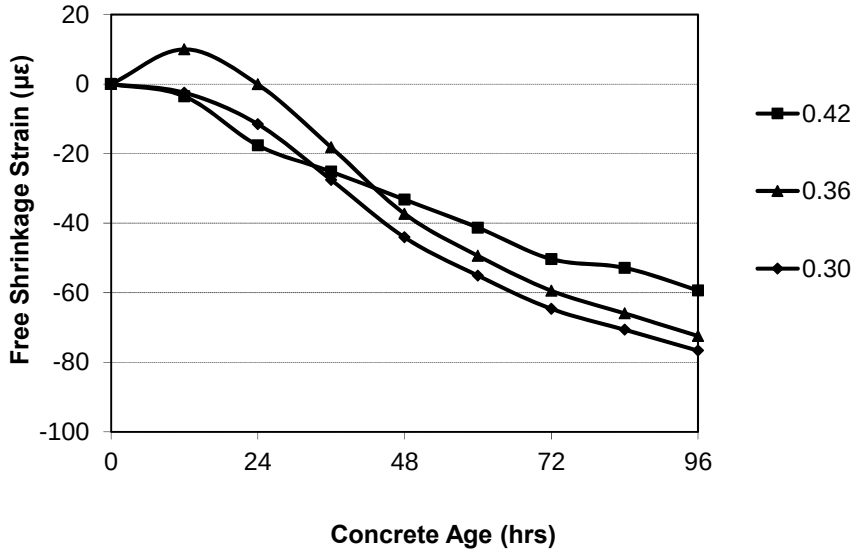

Figure 11-7: Autogenous shrinkage of control concrete mixtures measured in the free shrinkage frame

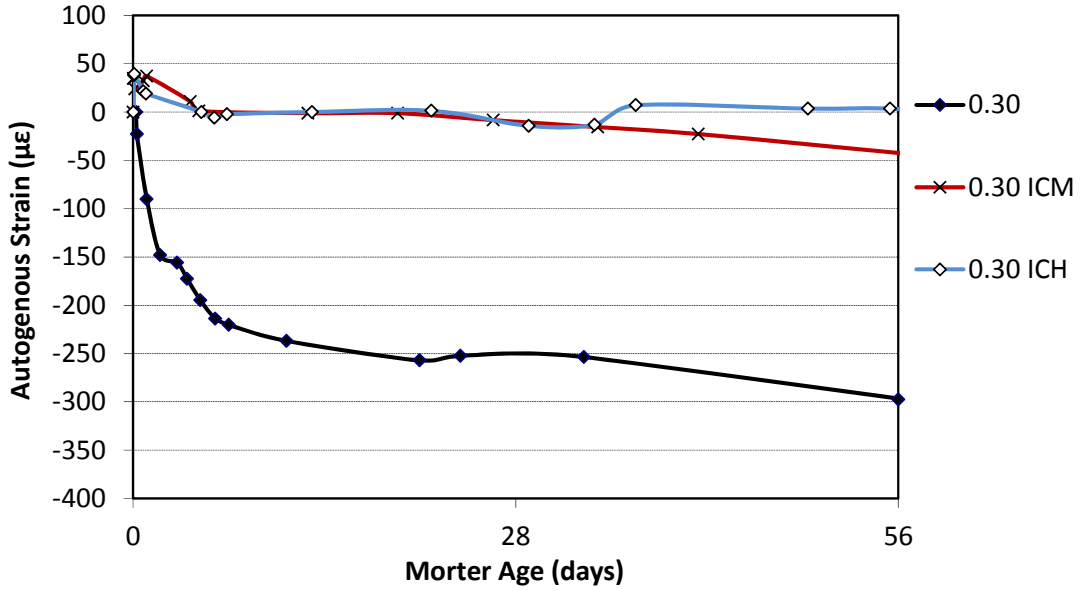

Figure 11-8: Autogenous shrinkage mortar from 0.30 *w/c* mixtures measured with corrugated tube method

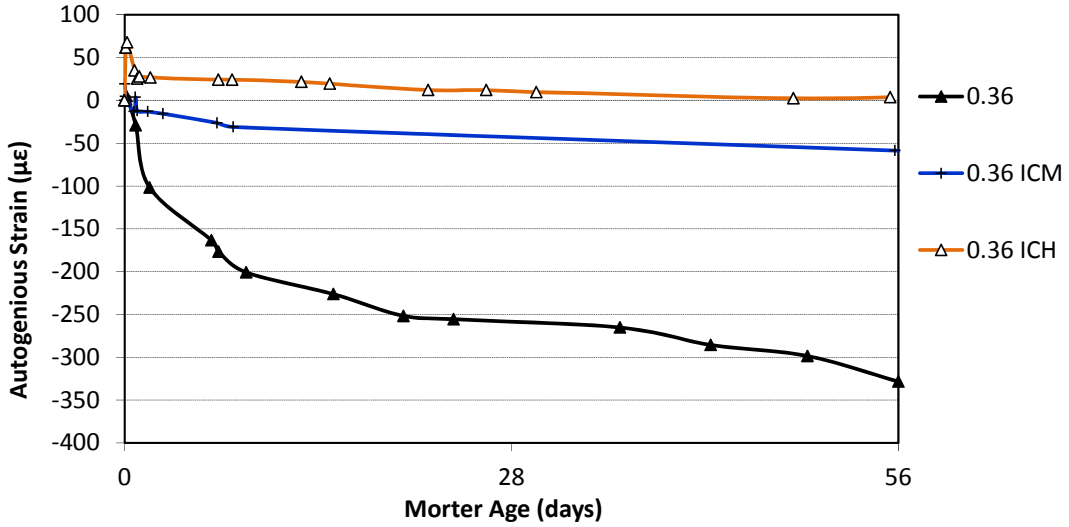

Figure 11-9: Autogenous shrinkage mortar from 0.36 *w/c* mixtures measured with corrugated tube method

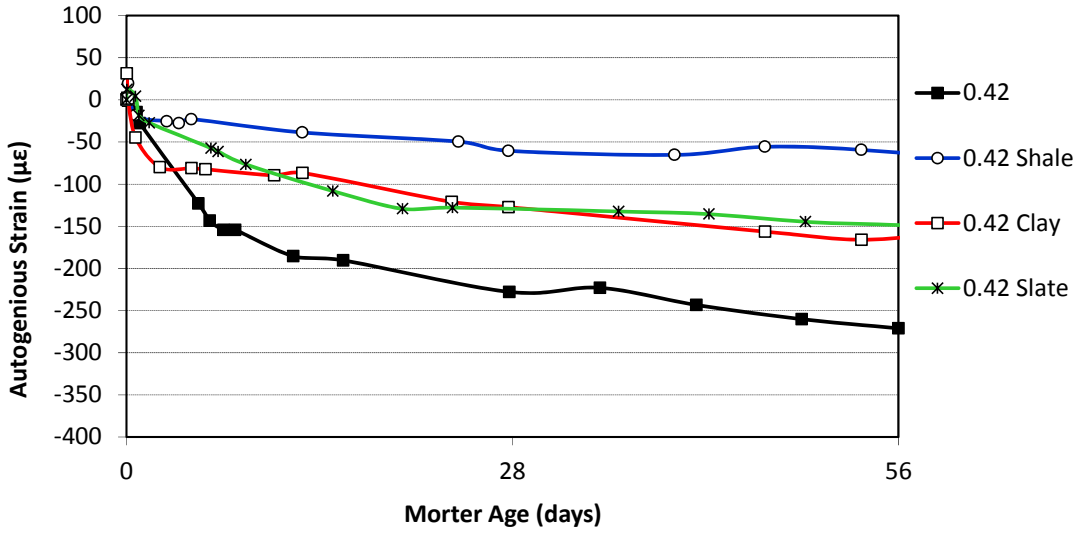

Figure 11-10: Autogenous shrinkage mortar from 0.42 *w/c* mixtures measured with corrugated tube method

Table 11-2: Autogenous strain results for concrete and mortar

Property	Mixture ID									
	0.42	**0.42 IC Shale**	**0.42 IC Clay**	**0.42 IC Slate**	**0.36**	**0.36 ICM**	**0.36 ICH**	**0.30**	**0.30 ICM**	**0.30 ICH**
96-hr Concrete Autogenous Strain (με)	-59	ND	ND	ND	-72	ND	ND	-77	ND	ND
96-hr Mortar Autogenous Strain (με)	-96	-28	-80	-43	-132	-19	25	-174	12	5
56-day Mortar Autogenous Strain (με)	-271	-63	-162	-149	-329	-59	4	-298	-42	3

Note: A negative value indicates a contraction and positive value indicates an expansion.

11.3 Internal Relative Humidity and Degree of Hydration

The internal relative humidity data are presented in Figure 11-11. The data are scaled to 100% at 18 hours to account for dissolved salt in the pore solution and the time for the cavity in the probe to equilibrate to the internal RH of the concrete. None of the internally

cured concrete mixtures showed a decrease in internal RH in the four-day period. Therefore, only the data from the control mixtures are shown. The measured ultimate degree of hydration for each mixture is shown in Table 11-3 along with the Mills and Hansen model estimations.

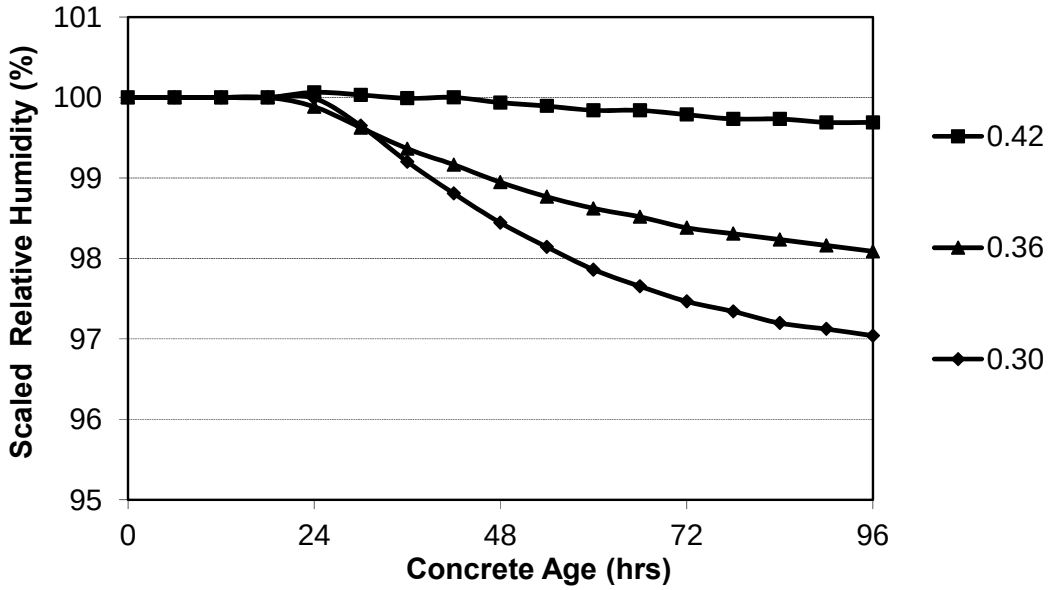

Figure 11-11: Scaled internal relative humidity results for control mixtures

Table 11-3: Measured and predicted ultimate degree of hydration values

Mixture	Ultimate Degree of Hydration			Prediction Error	
	Measured	Predicted with Hansen	Predicted with Mills	Hansen	Mills
0.42	0.78	1.00	0.71	29 %	9 %
0.42 IC Shale	0.85	1.00	0.71	18%	17%
0.42 IC Clay	0.85	1.00	0.71	18 %	17 %
0.42 IC Slate	0.82	1.00	0.71	22 %	14 %
0.36	0.72	1.00	0.67	39 %	7 %
0.36 ICM	0.76	1.00	0.67	32 %	12 %
0.36 ICH	0.87	1.00	0.67	15 %	23 %
0.30	0.66	0.83	0.63	27 %	4 %
0.30 ICM	0.69	0.83	0.63	21 %	9 %
0.30 ICH	0.72	0.83	0.63	17 %	12 %

11.4 Mechanical Properties

The match-cured mechanical properties of each of the mixtures are summarized in Table 11-4.

Table 11-4: Match-cured mechanical properties

Mixture	Concrete Age (days)					
	0.5	1	2	3	7	28
	Compressive Strength (psi)					
0.42	1770	2890	3690	3720	4230	5700
0.42 IC Shale	1580	2830	3500	3870	4310	5610
0.42 IC Clay	1950	3160	3900	4130	4530	5820
0.42 Slate	1590	2950	3700	3980	4740	5840
0.36	2935	4232	4875	4975	5300	6435
0.36 ICM	2780	4420	4810	5245	5675	6890
0.36 ICH	2760	4095	4835	5165	5565	6960
0.30	4830	6115	6570	6760	7330	8115
0.30 ICM	4355	5725	6445	6435	7030	8120
0.30 ICH	3595	5520	5995	6685	7815	8860
Splitting Tensile Strength (psi)						
0.42	200	280	345	355	385	465
0.42 IC Shale	215	345	405	420	465	495
0.42 IC Clay	235	345	405	410	455	505
0.42 Slate	205	320	360	395	420	465
0.36	330	425	450	475	475	485
0.36 ICM	305	505	515	495	515	565
0.36 ICH	315	395	455	495	495	525
0.30	505	550	575	575	600	600
0.30 ICM	465	525	540	580	620	665
0.30 ICH	365	530	555	545	555	610
Modulus of Elasticity (ksi)						
0.42	2750	3300	3900	3750	4050	4550
0.42 IC Shale	2600	3350	3600	3500	3900	4350
0.42 IC Clay	2700	3200	3650	3700	3700	4300
0.42 Slate	2500	3250	3850	3900	4100	4500
0.36	3310	4660	4755	4825	5095	5535
0.36 ICM	3270	4105	4595	4855	4925	5250
0.36 ICH	3380	3945	4375	4515	4520	4865
0.30	4595	5500	5745	5695	5710	5700
0.30 ICM	3740	4605	4840	4875	5040	5265
0.30 ICH	3625	4530	4790	4695	4730	5170

CHAPTER 12

PART II: DISCUSSION OF RESULTS

A discussion and synthesis of the results is presented in this chapter. The effect of internal cuing and water-cement ratio on degree of hydration are evaluated in Section 12.1. The effect of internal-curing water on internal relative humidity, autogenous shrinkage, and stress development due to autogenous shrinkage are presented in Section 12.2. The effects of using mortar or concrete on the measured of autogenous strain are discussed in Section 12.3. The effect of internal curing on mechanical properties is summarized in Section 12.4. In Section 12.5 the effect of the amount of internal cuing water supplied on the cracking tendency is discussed.

12.1 Effect of Internal Curing and Water Cement Ratio on Degree of Hydration

As shown in Figure 12-1, the amount of internal-curing water increased the ultimate degree of hydration. The 0.42 IC Clay and 0.42 IC Shale mixtures have the same ultimate degree of hydration although the shale mixture has slightly higher dosage of internal-curing water; however, these degree of hydration results are within the normal error range of the SAC test method. Alternatively, the degree of hydration may have reached an upper limit where the degree of hydration will not increase, even with additional internal curing water. The increased cement hydration results from the availability of additional

water desorbed from the LWA. This agrees with the results of others (Jensen and Hansen 2001; Golias 2010; Bentz and Weiss 2011).

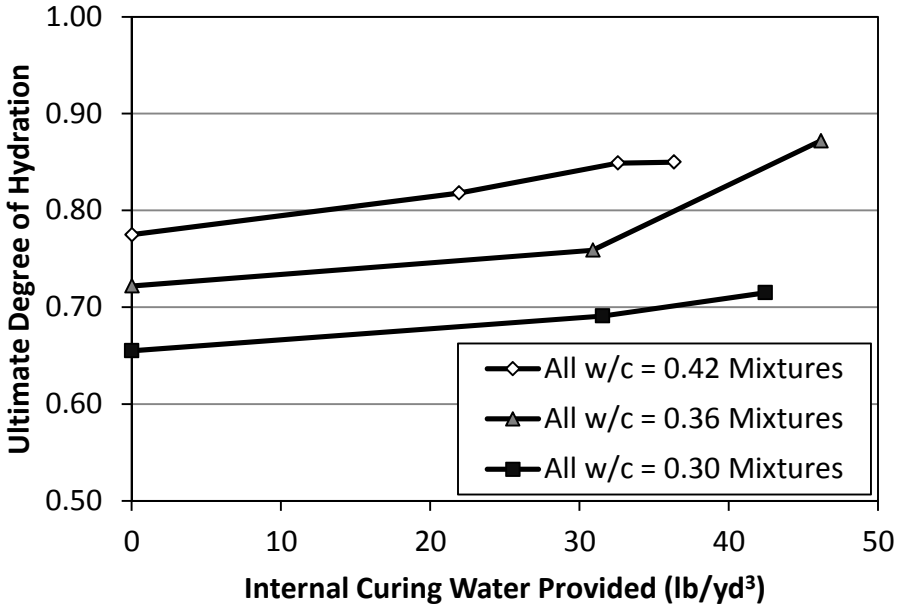

Figure 12-1: Impact of internal-curing water on ultimate degree of hydration

The Mills (1966) model estimates the ultimate degree of hydration of the non-internally cured mixtures with reasonable accuracy. The error of the Mills expression compared to the measured ultimate degree of hydration for the 0.42, 0.36, and 0.30 mixtures is 9.0, 7.2, and 4.4%, respectively. However, it was not calibrated with internally cured mixtures and does not account for additional hydration due to internal curing. Thus, it does not predict the ultimate degree of hydration of the internal-curing mixtures well. The prediction error of ultimate degree of hydration of the internally cured mixtures compared to the Mills expression ranges from 9.4 to 23.1% as shown in Table 11-3. The Hansen (1986) model was based on derivations rather than laboratory testing and provides poor estimates of the ultimate degree of hydration of internally cured and non-internally cured concretes as shown in Table 11-3. However, from an internal curing

standpoint an increased degree of hydration increases the amount of chemical shrinkage predicted using Equation 4, and thus provides additional internal curing water for mitigation of other durability issues such as plastic shrinkage cracking (Bentz and Weiss 2011).

The w/c has a large influence on the degree of hydration. As the *w/c* is decreased the amount of water as well as the space available for hydration products to form is decreased. Decreasing the *w/c* decreases the degree of hydration as shown in Figure 12-1 and Table 11-3. This agrees with the models of Mills (1966) and Hansen (1986).

12.2 Effect of Internal Curing on Autogenous Shrinkage

The effect of internal curing on the unrestrained strain of concrete and mortar is shown in Figure 11-7, Figure 11-8, Figure 11-9, Figure 11-10, and Table 11-2. The addition of pre-wetted LWA for internal curing significantly *reduces* the autogenous strain when compared to non-internally cured control concretes. The decrease in autogenous strains are attributable to the availability of water from the LWA to fill capillary voids formed by chemical shrinkage. Though the 0.42 IC Clay mixture has more internal-curing water than the 0.42 Slate mixture it develops more strain as seen in Figure 11-10. This behavior is attributed to the wet sieving of the concrete to obtain the mortar specimen. The clay aggregate source was a coarser fine aggregate with 3/8 in. particles. The wet sieving removed some of the coarse fraction of the pre-wetted lightweight aggregate and thereby reduced the amount of internal curing in the mortar specimen.

The effect of internal curing on stress development is evident in Figure 11-4, Figure 11-5, Figure 11-6, and Table 11-1, which indicate the stress development under

isothermal curing conditions. All internal-curing mixtures experienced *reduced* stress development due to autogenous shrinkage effects when compared to the non-internally cured control concretes. The decrease in autogenous stress development is due to the decreases autogenous strain and to the reduction in concrete modulus of elasticity. The fact that the developed stresses of 0.42 IC Shale remained in compression indicates that sufficient internal-curing water is provided to preclude the development of tensile stresses.

The reduction in the amount of developed stresses is not linear with respect to the amount of IC water provided as shown in Table 11-1. This is because the removal of water from the smaller pores creates greater stress than removal of water from larger pores (Rilem TC 196 2007). Therefore, providing enough water to keep the smaller pores filled mitigates most of the autogenous shrinkage stresses.

Concretes with lower *w/c* have greater autogenous shrinkage stress as shown in Figure 12-2 and Table 11-1. This is because as the *w/c* decreases, the pores become smaller (Holt 2001). As a result, the lower *w/c* mixtures experience greater capillary stress and autogenous shrinkage when desiccated (Rilem TC 196 2007).

Because the decrease in internal RH is the driving force of autogenous shrinkage after set, the internal RH data will be discussed in this section. Only the control mixtures showed decreased internal RH results. The data in Figure 12-2 shows the isothermal stress development and the scaled internal RH. The similar magnitudes of stress development and RH decreases show the dependence of isothermal stress development on self-desiccation.

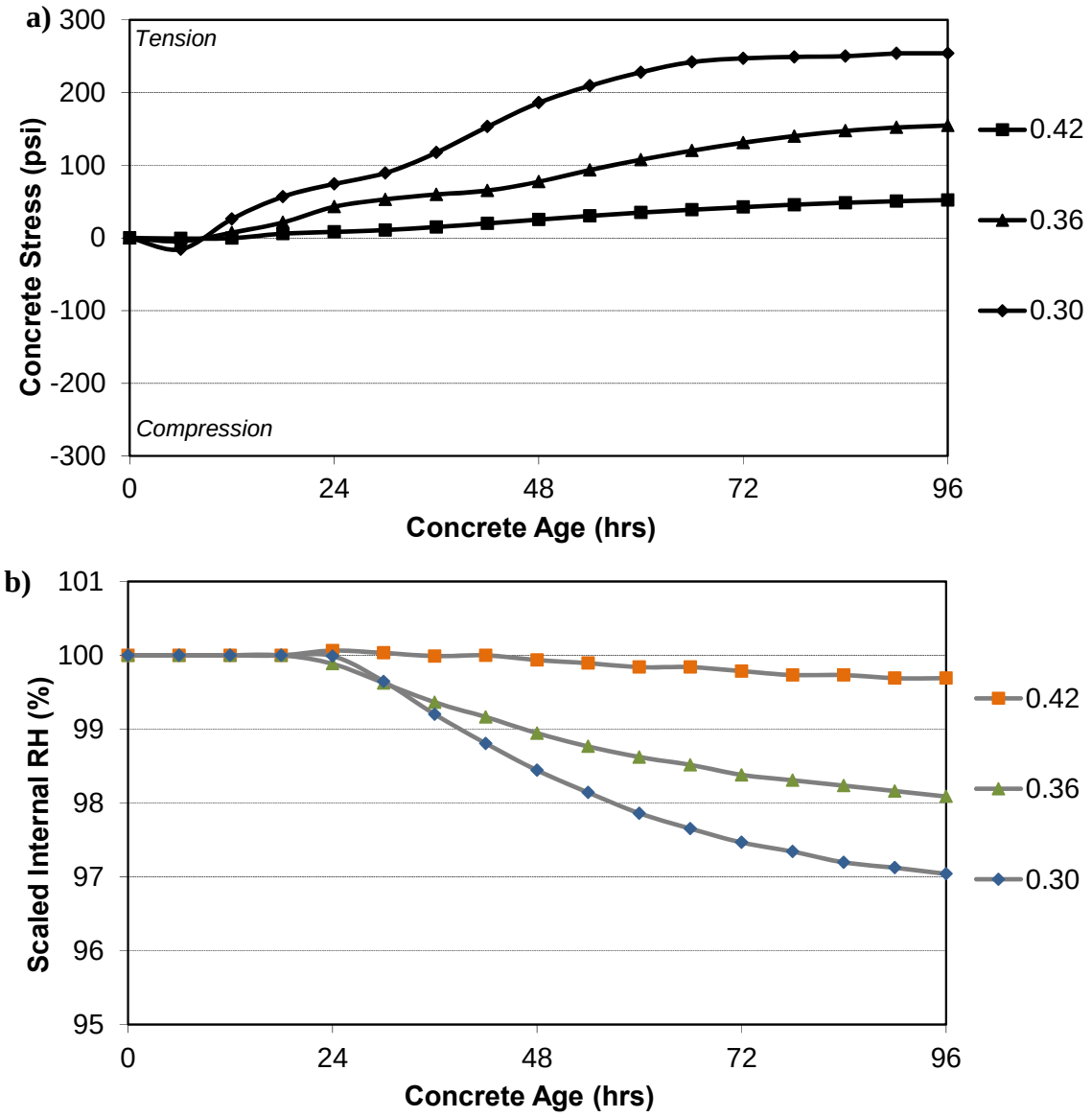

Figure 12-2: a) Isothermal stress development and b) scaled internal relative humidity of control mixtures

12.3 Autogenous Shrinkage in Mortar and Concrete

The *concrete* autogenous strain measured from the FSF and the *mortar* autogenous strain measured from the corrugated tubes are presented in Figure 12-3, where the concrete specimen are designated with a C and the mortar specimen are designated with a M. The strain of the mortar specimens are much greater than their concrete counterparts because

the capillary stresses occur in the paste fraction and are restrained by the aggregate fraction. The mortar specimen having had their coarse aggregate fractions sieved out, have reduced aggregate portions, and thus reduced internal restraint to capillary pore stresses. The expansion of the mixture with *w/c* of 0.36 concrete in the first 24 hours is due to a slight increase in temperature. The momentary loss of temperature control was due of the heat of hydration and the inability of temperature control bath to compensate adequately.

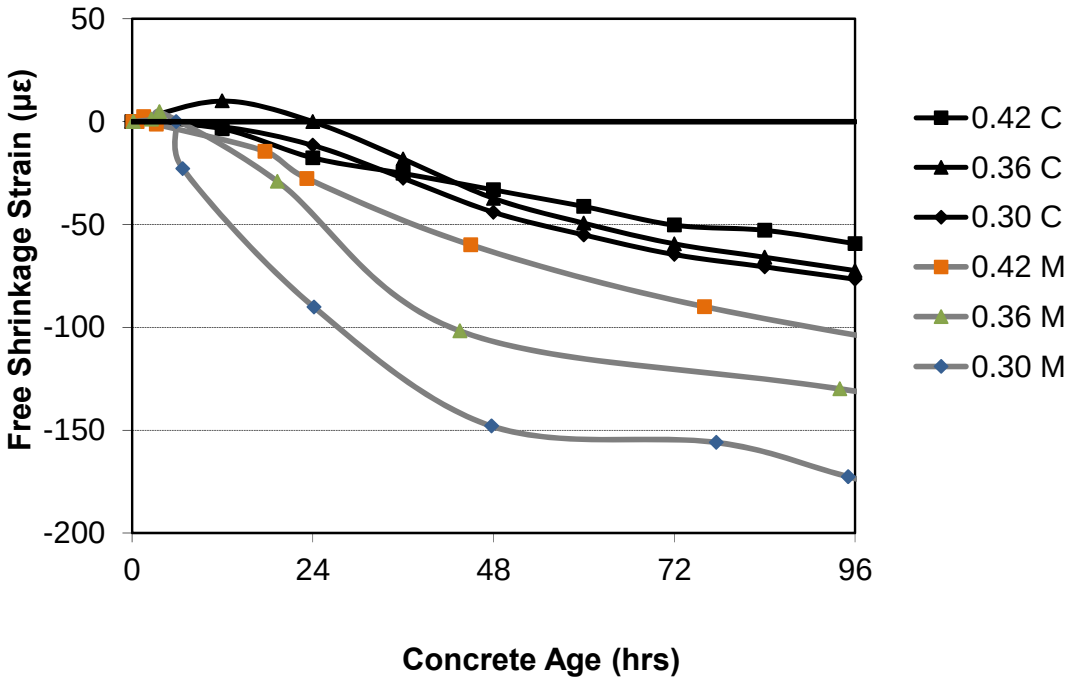

Figure 12-3: Concrete and mortar autogenous strains

12.4 Effect of Internal Curing on Mechanical Property Development

The compressive strength and splitting tensile strength of the internally cured concretes is either similar to or slightly greater than the strength of the corresponding control concrete at 7 and 28-days,as the data in Table 11-4 shows. The LWA particles are more porous and

angular than the normalweight fine aggregate, which improves the interfacial transition zone and improves the tensile bond. The modulus of elasticity of the internally cured concretes decreased slightly when compared to their control concrete counterparts. This is because the increased amount of LWA caused a decrease in density, which affects stiffness according to ACI 318 estimation equation shown in Equation 9-8. An illustration of measured modulus of elasticity compared to the ACI estimated modulus using Equation 9-8 is shown in Figure 12-4. The figure shows the estimation equation provided a reasonable fit to the modulus data and that the decrease in density corresponds to a reduction in modulus of elasticity.

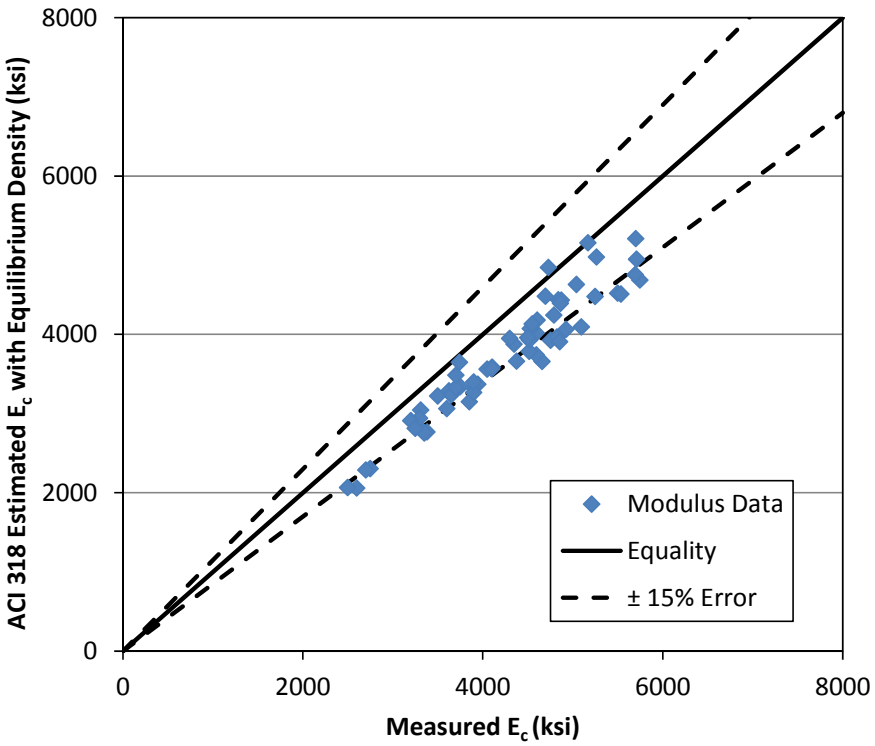

Figure 12-4: Measured modulus of elasticity compared to ACI 318 predicted

12.5 Effect of Internal-Curing Water on Cracking Tendency of Concrete

It is clear from the data in Table 11-1 and Figure 11-1b, Figure 11-2b and Figure 11-3b that the LWA internal curing delays the time to initial cracking. This improvement in cracking behavior is attributed to the *increased* tensile strength, *decreased* modulus of elasticity, and *decreased* autogenous shrinkage when compared to the non-internally cured control concrete.

The time to initial cracking of the three non-internally cured control mixtures decreases as the *w/c* decreases because the autogenous stress increases and the peak temperature increases as the *w/c* decreases. The peak temperature increases due to an increase in cement content of the lower *w/c* mixtures. Increasing the peak temperature decreases the time to cracking (Breitenbücher and Mangold 1994, Byard et al. 2010).

CHAPTER 13

PART II: CONCLUSIONS

Early-age cracking in bridge decks is a severe problem that may reduce the functional life of the structure. In this part, the effect on the cracking tendency of bridge deck concrete that results from using lightweight fine aggregate to provide internal curing was experimentally evaluated. Restrained concrete specimens were tested under temperature conditions that match those in a bridge deck, while companion specimens were tested under isothermal curing conditions. Degree of hydration was measured with semi-adiobatic calorimeter results to determine the effect of internal curing on cement hydration. The autogenous strain of concrete and mortar was measured with free shrinkage frame and corrugate tube testing techniques. Internal relative humidity was measured to determine the dependence of stress on the change in capillary pore pressures.

The results of the study support the following conclusions:

- Increasing the amount of internal-curing water available in the lightweight aggregate increases the degree of hydration.
- The Mills (1966) model predicted the degree of hydration of the non-internally cured mixtures to within 9%. It does not accurately predict the degree of hydration of the internally cured mixtures.

- The Hansen (1986) model provides poor estimates of the ultimate degree of hydration for internally cured and non-internally cured concretes.
- The compressive strength and splitting tensile strength of the internally cured concretes is similar to or slightly greater than their non-internally cured counterparts at 7 and 28-days.
- Increasing the amount of pre-wetted lightweight aggregate in the concrete systematically decreases the density and the modulus of elasticity of the concrete.
- Mortar has greater autogenous strain due to the reduced restraint provided by the coarse aggregate content to the capillary stress in the paste fraction.
- As the water-cement ratio decreases the autogenous strain and stress increases. This is due to reduced pores sizes and decreases water availability associated with lower water-cement ratio mixtures.
- Providing internal curing through pre-wetted lightweight aggregate decreases the autogenous strain of concrete and mortar compared to non-internally cured counterparts.
- The use of pre-wetted lightweight aggregates to provide internal curing in concrete can reduce or eliminate the stress development caused by autogenous shrinkage.
- The use of lightweight aggregates to provide internal curing delays the occurrence of early-age cracking in bridge deck concrete applications when compared to the normalweight control concrete. This improvement in cracking behavior is attributed to the increased tensile strength, decreased modulus of elasticity, and decreased autogenous shrinkage.

PART III

EARLY-AGE COMPLIANCE MODELING OF CONCRETE

CHAPTER 14

PART III: INTRODUCTION

Concrete at early ages behaves much differently than mature concrete. Immediately after setting, concrete undergoes a rapid change in mechanical properties. Early-age concrete has significantly different elastic and viscoelastic behavior (Emborg 1989; Westman 1999; Gutch and Rostásy 1995). For concrete placed in restrained conditions such as bridge decks, culverts, tunnels, retaining walls, and tanks, the early-age relaxation properties are essential to determine so that designers can minimize early-age cracking. By minimizing early-age cracking, the durability of structures can be improved.

Compliance models capture both instantaneous elastic response and time-dependent viscoelastic response. There are many models in literature to determine the compliance of mature concrete including the B3 (Bažant and Baweja 2000), ACI 209R-92 (ACI 209 1992), CEB MC90-99 (CEB 1999), and the GL2000 (Gardner and Lockman 2001). These models were calibrated with mature, well hardened concrete. Because of this, the initial loading age that these models were calibrated for is 1 day or later.

14.1 Background

Cracking of hardening concrete occurs when the induced tensile stress exceeds the tensile strength of the concrete. The development of in-place stresses is affected by the shrinkage, coefficient of thermal expansion, setting characteristics, restraint conditions,

stress relaxation, capillary stresses, and temperature history of the hardening concrete. The tensile strength (and strain capacity) increases as the hydration of the cementitious system progresses. The tensile strength is impacted by the cementitious materials content and type, the water-cementitious materials ratio, the aggregate type and gradation, the degree of curing (internal/external) provided, and the temperature history of the hardening concrete. Quantification of many of the mechanisms mentioned above is quite complicated at early ages, and many of these variables have complex interactions.

Early-age cracking of concrete, typically caused by thermal effects, drying shrinkage, and autogenous shrinkage, can have detrimental effects on long-term behavior and durability. Darwin and Browning (2008) reported that "by controlling early age cracking, the amount of cracking at later ages should remain low," and that early-age cracking can significantly increase the rate and amount of chloride penetration (from deicing salts), which may accelerate the corrosion rate of embedded reinforcing steel in bridge decks. Transverse bridge deck cracking occurs in most geographical locations and climates, and in many types of bridge superstructures (Krauss and Rogalla 1996). The National Cooperative Highway Research Program (NCHRP) Report 380 (Krauss and Rogalla 1996) reported the results of a survey sent to all U.S. Departments of Transportation (DOTs) and several transportation agencies overseas to evaluate the extent of deck cracking. Sixty-two percent of the responding agencies considered early-age transverse cracking to be problematic. A survey conducted by the Federal Highway Administration (FHWA) found that more than 100,000 bridges suffer from early-age cracking (FHWA 2008). Given the abundance of cracking observed in bridge decks, and

the impact of early-age cracking on long-term performance and durability, it is imperative that bridge deck concrete be proportioned and placed to minimize early-age cracking.

14.2 Objectives

The focus of this part is to model the early-age stress development of lightweight aggregate concrete. The objectives of this part are as follows:

- Model the early-age stress development from the free-shrinkage strain development to accurately predict the measured early-age stress development ,
- Perform a sensitivity analysis to determine the variables that significantly affect the early-age stress development, and
- Determine the effect of density, water-cement ratio, and curing temperature on the early-age stress development.

14.3 Research Approach

The stress development of concrete mixtures with three different water-cement ratios (*w/c*), two curing conditions, and aggregate proportions ranging from all normalweight to all lightweight aggregate was measured experimentally. The unrestrained length change of the concrete, the tensile strength, compressive strength, and modulus of elasticity development were determined. All concrete samples were cured under the same controlled temperature history. The unrestrained strain was used with the B3 compliance model (Bažant and Baweja 2000) to determine the early-age stress development. The results of the measured stress development from the rigid cracking frame were then compared to the predicted stress development. Modifications were then made to the B3

Model to account for the properties of early-age concrete and provide an accurate estimate of early-age stress development.

14.4 Outline

A summary literature review pertaining to early-age stress development, cement hydration, the maturity method, compliance modeling, and test methods to assess early-age concrete properties is presented in Chapter 15. The experimental testing program to assess early-age concrete behavior and properties is presented in Chapter 16. The modeled temperature history, the restrained stress development, free-shrinkage development, and the modeled stress development using the B3 Model are presented in Chapter 17. A discussion of modifications to the B3 Model to account for early-age stress development and results is presented in Chapter 18. The effects of lightweight aggregate, water-cement ratio, and curing temperature are discussed in Chapter 18 along with a sensitivity analysis of the model corrections factors. Discussion and results of a proposed simplified version of the Modified B3 Model are also provided in Chapter 18. The conclusions and recommendations from the test results documented in this part are presented in Chapter 19.

CHAPTER 15

PART III: LITERATURE REVIEW

The results of a literature review of early-age stress development, cement hydration, the maturity method, relaxation in concrete, viscoelastic models, engineering compliance models, and methods to assess early-age behavior are presented in this chapter.

15.1 Early-Age Stress development

Concrete at early ages develops stress due to thermal effects, autogenous shrinkage, and drying shrinkage. Development of stress due to thermal and autogenous effects will be discussed in the following sections. Because test specimens were not exposed to drying in this research, drying shrinkage will not be discussed.

15.1.1 Thermal Stresses

The development of thermal stresses can be calculated using the expression presented in Equation 15-1. For an accurate estimate of thermal stress, creep effects during early ages and over the structure's life should be accounted for in Equation 15-1 (Schindler and McCullough 2002).

$$\sigma_T = \Delta T \times \alpha_t \times E_{c,adj} \times K_r \quad \text{..... Equation 15-1}$$

where ΔT = temperature change = $T_{zero\text{-}stress}$ - T_{min} (°F),

α_t = coefficient of thermal expansion (strain/°F),

$E_{c,adj}$ = creep-adjusted modulus of elasticity (lb/in^2),

K_r = degree of restraint factor,

$T_{zero\text{-}stress}$ = concrete zero-stress temperature (°F), and

T_{min} = minimum concrete temperature (°F).

An illustration of the development of concrete temperatures and thermal stresses over time under summer placement conditions for freshly placed concrete is presented in Figure 15-1. In terms of stress development, the final-set temperature is the temperature at which the concrete begins to resist stresses that result from the restraint of external volume changes. In Figure 15-1, it can be seen that hydration causes the concrete temperature to increase beyond the setting temperature, time (A). Because the expansion of the concrete caused by the temperature rise is restrained, the concrete will be in compression when the peak temperature, time (B), is reached. When the peak temperature is reached, the hydrating paste is still developing structure, its strength is low, and high amounts of early-age relaxation may occur when the concrete is subjected to high compressive stress (Emborg 1989). The phenomenon of gradual decrease in stress when a material is subjected to sustained strain is called stress relaxation (Mehta and Monteiro 2006). As the concrete temperature subsequently decreases, the compressive stress is gradually relieved until the stress condition changes from compression to tension, time (C). The temperature at which this transient stress-free condition occurs is denoted the "zero-stress temperature". Due to the effects of relaxation, the zero-stress temperature may be significantly higher than the final-set temperature (Emborg 1989). If tensile stresses, caused by a further temperature decrease, exceed the tensile strength of the concrete, cracking will occur at time (D). Because the thermal stress is proportional to the difference between the zero-stress temperature and the cracking temperature, thermal

cracking can be minimized by decreasing the zero-stress temperature. This in turn can be accomplished by (1) minimizing the final-set temperature, (2) minimizing the peak temperature achieved during the high-relaxation phase, or (3) delaying the attainment of the peak temperature.

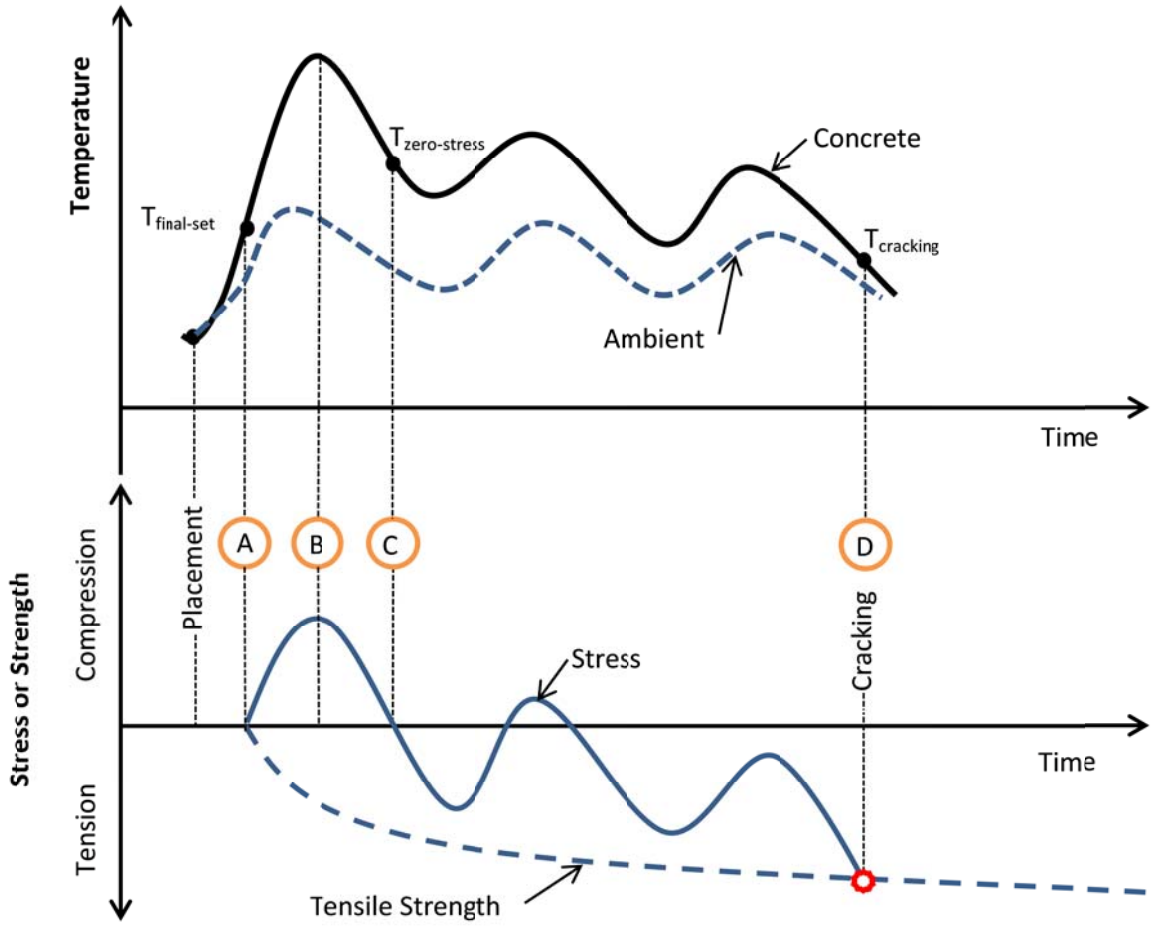

Figure 15-1: Development of early-age thermal stresses (adapted from Schindler and McCullough 2002)

15.1.2 Autogenous and Chemical Shrinkage Effects

The reaction products formed by cement hydrations occupy a smaller absolute volume than the anhydrous components (L'Hermite 1960). The reduction of the absolute volume

of the reactants due to hydration is chemical shrinkage. Before setting, this phenomenon results in a volumetric change but generates no stress because the concrete is still plastic (Holt 2001). At setting, enough hydration products have formed to provide a self-supporting skeletal framework in the paste matrix. Within the framework of solids are water-filled capillary voids. As water is consumed by the ongoing hydration process, the voids empty and capillary tensile stresses are generated, which results in volumetric shrinkage. The concrete volume change that occurs without moisture transfer to the environment or temperature change is called autogenous shrinkage. Before setting, chemical shrinkage and autogenous shrinkage are the same (Holt 2001). After setting, autogenous shrinkage is a function of capillary stresses induced by self-desiccation. Generally, autogenous shrinkage and stress development is not a concern at a *w/c* above 0.42 (Mindess, Young, and Darwin 2002; Mehta and Monteiro 2006).

Holt (2001) provided the illustration depicted in Figure 15-2 of the composition change of a sealed paste due to the cement hydration reactions, where C is the cement volume, W is the volume of water, H_y is the volume of the hydration products, and V is the volume of voids. This figure relates how the autogenous shrinkage is a portion of the chemical shrinkage. After set, the chemical shrinkage is an internal volume reduction, whereas the autogenous shrinkage is an external volume change.

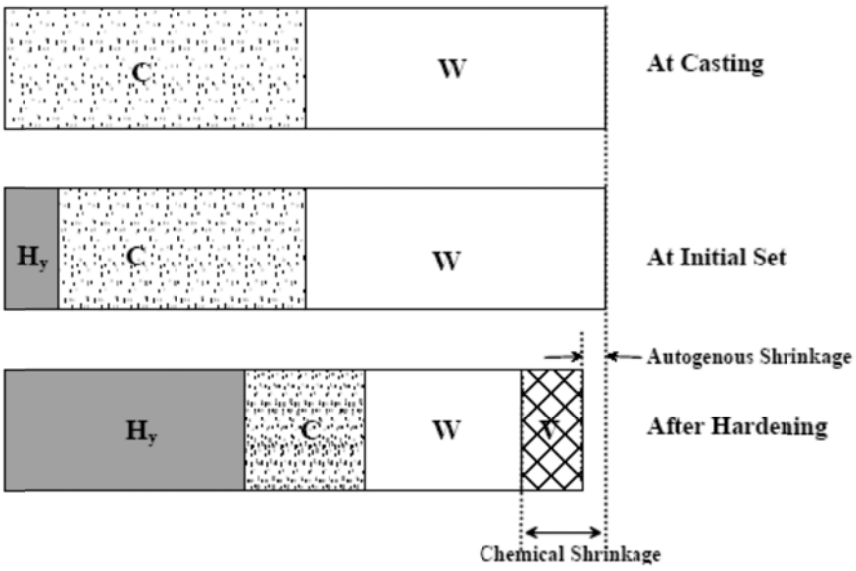

Figure 15-2: Volume reduction due to autogenous shrinkage (Holt 2001)

15.2 Early-Age Cement Hydration

When portland cement and water are combined, compounds within the cement begin to react immediately and at differing rates. The rate of cement reaction depends on the chemical makeup of the cement, the fineness of the cement grains, curing temperature and chemical admixtures (Mindess et al. 2003). The four primary compounds in cement are tricalcium silicate (C_3S), dicalcium silicate (C_2S), tricalcium aluminate (C_3A), and tetracalcium aluminoferrite (C_4AF) (Mindess et al. 2003). C_3S and C_3A hydrate more rapidly and contribute to setting (Mindess et al. 2003). When the C_3A hydrates with water and sulfates (gypsum), ettringite is formed and shown in Reaction 1 (Mindess et al. 2003). The morphology of ettringite is long needle-like crystals. As the sulfate concentration decreases over time, some of the ettringite further reacts with C_3A and water to form monosulfate hydrate as seen in Reaction 2 (Mindess et al. 2003).

C_3A + Gypsum + Water ⟶ Ettringite (Reaction 1)

C_3A + Ettringite + Water ⟶ Monosulfate Hydrate (Reaction 2)

C_3S reacts with water to form calcium silicate hydrate (C-S-H) and calcium hydrate (CH) as shown in Reaction 3. C-S-H is the main contributor to strength in hardened cement paste. The structure of C-S-H is made up of layers of plates with adsorbed water in between the layers. CH is water soluble and contributes little to strength. (Mindess et al. 2003)

C_3S + Water ⟶ C-S-H + CH (Reaction 3)

15.3 Concrete Setting and Hardening

Setting is the increase in rigidity due to the hydration of cement (Mindess et al. 2003). Initial set is considered the point at which concrete cannot be consolidated by vibration, and final set is the start of strength development (Tuthill and Cordon 1956; Sprouse and Peppler 1978). Hardening is considered the onset of appreciable strength gain (Scripture 1956). Setting and hardening occur because the products of cement hydration begin to interlock as hydration continues over time as illustrated in Figure 15-3. The direct relationship between the formation of hydration products and degree of hydration is shown in this figure. As hydration products form and interlock as a result of hydration, setting and hardening occur. There is a dormant period between initiation of hydration and setting where hydration products are being formed more slowly, and are not interlocking yet.

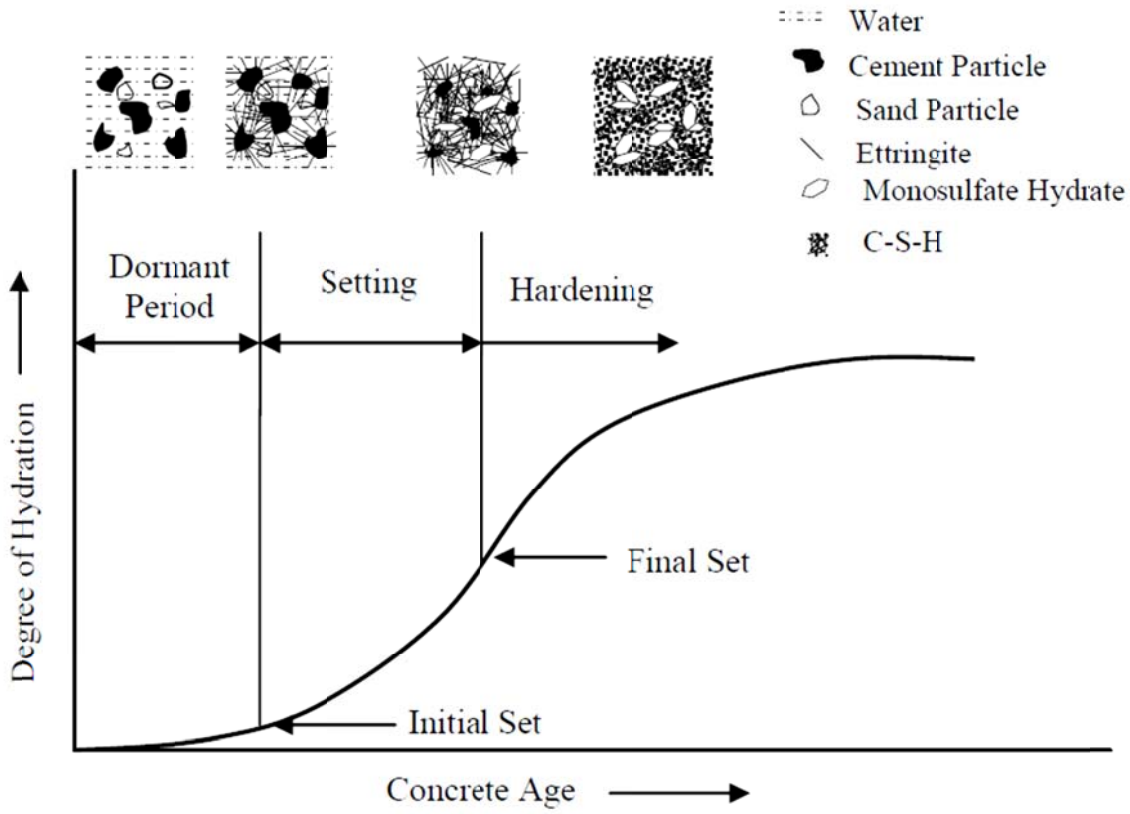

Figure 15-3: Illustration of setting and hardening of concrete (adapted from Soroka 1980 and Schindler 2004b)

15.4 Maturity Methods

The curing temperature affects the rate of hydration of the compounds in cement. Therefore, setting and strength gain are functions of both time and temperature (Pinto and Hover 1999). McIntosh (1949) first published a method to account for both time and temperature on strength development. Several functions can be used to account for the effects of time and temperature; however, the Freiesleben, Hansen, and Pedersen (1977) function, seen in Equation 15-2, based on the Arrhenius equation has been found to be more representative of the time-temperature effects of the strength development of concrete than other functions (Carino 2004).

$$t_e = \sum e^{-\frac{E}{R}\left[\frac{1}{T_c}-\frac{1}{T_r}\right]}\Delta t \quad \text{..... Equation 15-2}$$

where t_e = equivalent age at reference temperature (hours),

E = activation energy (J/mol),

T_c = average temperature of concrete during time interval Δt (K),

T_r = specified reference temperature (K),

Δt = time interval (hours), and

R = universal gas constant (J/[mol K]).

The activation energy determines the overall effect of temperature within the maturity function (Carino 2004). The activation energy can be estimated from the total content of the cement compounds, the cement fineness, and the presence of supplementary cementing materials (Schindler 2004a). The reference temperature is generally taken as 296 K (73°F) for work performed in the United States.

15.5 Relaxation in Concrete

When concrete is loaded there is an immediate elastic response. If the load is maintained there will be additional time-dependent response. This additional response is the product of the viscoelastic and viscoplastic nature of concrete. Creep is a time-dependent increase in strain under constant stress whereas relaxation is a time-dependent reduction in stress under a constant strain. Creep and relaxation effects are illustrated in Figure 15-4. Creep and relaxation occur in the paste fraction and are restrained by the aggregate fraction (Neville and Brooks 1991).

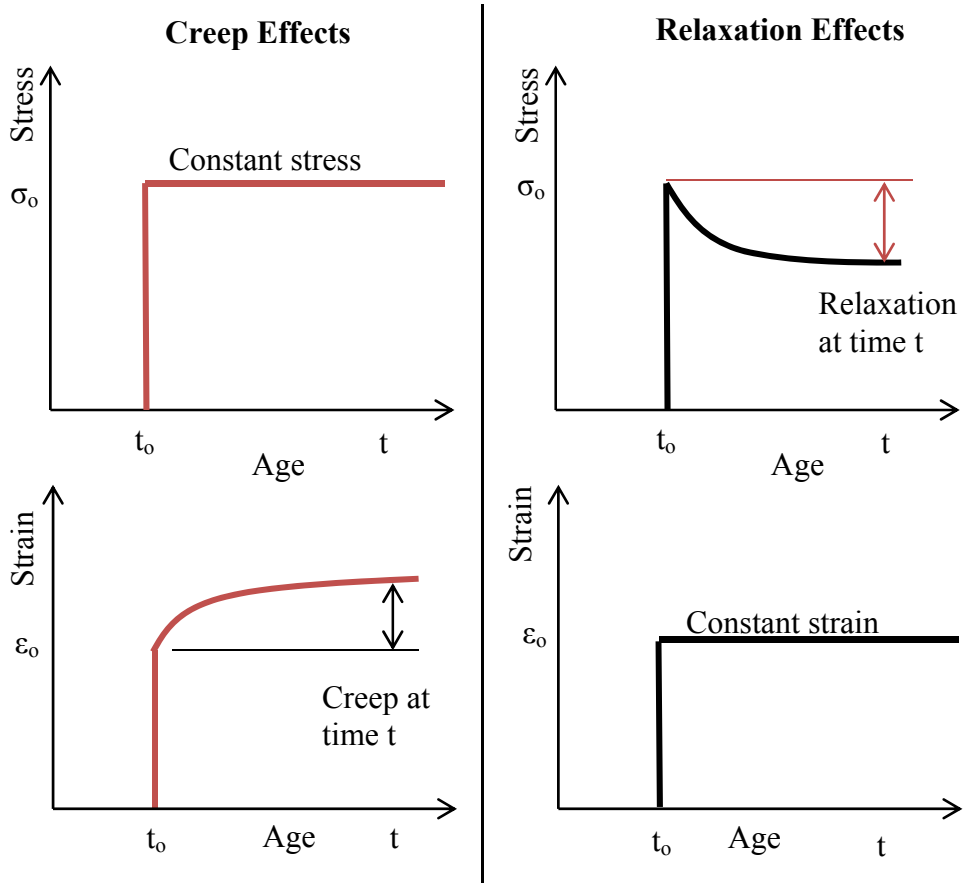

Figure 15-4: Illustration of creep and relaxation effects (adapted from Neville and Brooks 1991)

For early-age cracking, relaxation effects are beneficial in delaying the cracking time by reducing the stress development (Mehta and Monteiro 2006). Reducing the early-age stress can significantly increase the time to cracking or prevent cracking all together. A schematic of thermal stress development with and without relaxation effects is shown in Figure 15-5. The stress development with relaxation is much less and therefore the cracking time is significantly delayed as illustrated in the figure.

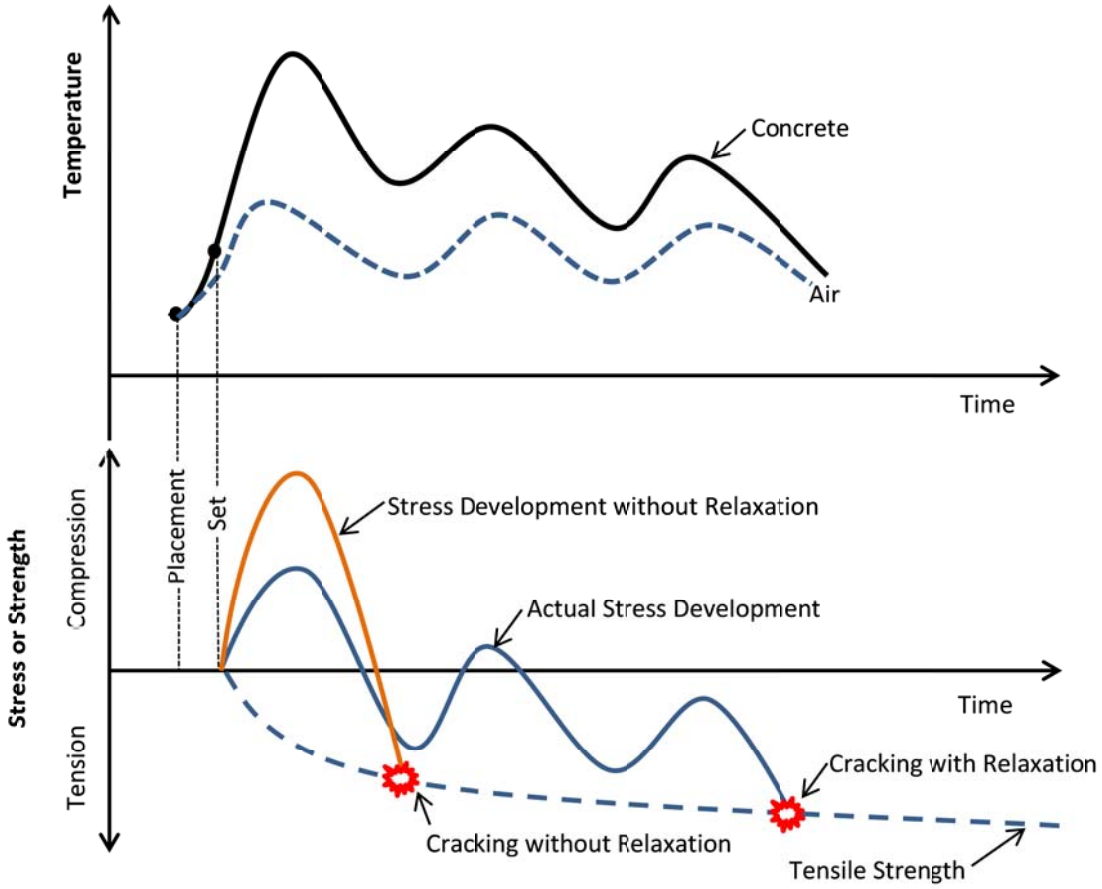

Figure 15-5: Thermal stress development with and without relaxation effects (adapted from Mehta and Monteiro 2006 and Schindler and McCullough 2002)

The time-dependent response can be expressed in terms of *compliance*, which has the units of psi^{-1}, or as a ratio of the elastic deformation which is known as a *creep coefficient*. Compliance is a unit strain per stress as show in Equation 15-3 and the creep coefficient is a ratio of time-dependent strains to instantaneous elastic strains. An illustration of creep in terms of a compliance function and in terms of a creep coefficient is shown in Figure 15-6, where $J(t,t_0)$ is the compliance term at time t as a result of loading at time t_0, E_c is the concrete elastic stiffness, σ_0 is the stress applied at time t_0, and $\Phi(t,t_0)$ is the creep coefficient at time t as a result of loading at time t_0. The compliance term encompasses both the elastic deformations and time-dependent, whereas the creep coefficient term

captures only the time-dependent deformation as shown in Figure 15-6. To give some sense of the scale of creep, after a year under sustained load, the creep coefficient is generally around two to three (Neville et al. 1983). That is to say, two to three times the elastic deformation in additional creep deformation.

$$J(t,t_0) = \varepsilon(t)/\sigma_0 \quad \text{Equation 15-3}$$

where $J(t,t_0)$ = compliance as a function of time and loading age(1/psi),

$\varepsilon(t)$ = strain at time t (in./in.), and

σ_0 = stress applied at age t_0 (psi).

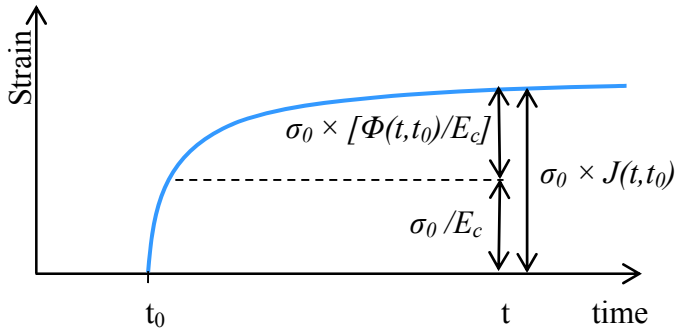

Figure 15-6: Illustration of creep in terms of compliance and creep coefficient

There is debate on what is the instantaneous elastic and time-dependent deformation (Neville et al. 1983; Bažant 1982). If concrete is loaded extremely rapidly (0.01 second) the response is considered the "pure" elastic response (Neville et al. 1983; Bažant 1982). Increasing the loading time from five seconds to two minutes can increase the strain by up to 15 % (Neville et al. 1983). The effect of load duration associated with the calculation of various elastic moduli are illustrated in Figure 15-7. Where, $J(t,t_0)$ is the compliance, Φ is the creep coefficient, and E_c and E_o represent different methods of determining elastic moduli. E_o is generally taken as the asymptotic modulus of elasticity,

which can be found by very rapidly (0.01 seconds) testing the elastic deformation of concrete (Bažant 1982). However, using a test that takes 10 minutes, instead of a rapid test, to determine the elastic modulus would yield a different elastic modulus value (E_c) and therefore creep coefficient. Because the creep coefficient is a ratio of time-dependent deformation to elastic deformation, varying the elastic deformation can significantly change the creep coefficient. The figure shows that differences in the elastic modulus can result in different creep coefficients for the same response.

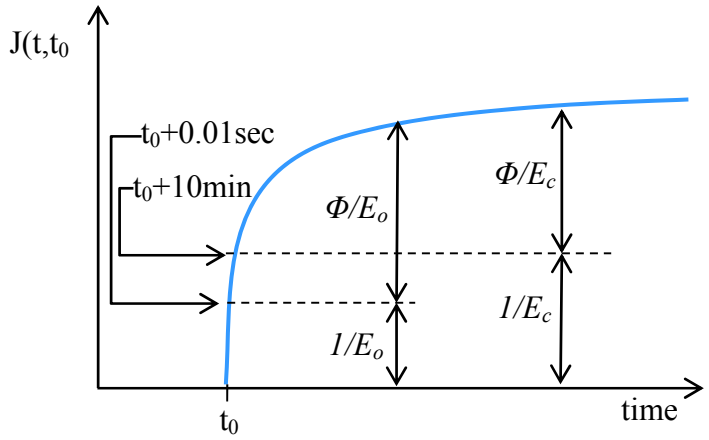

Figure 15-7: Inaccuracies related to separation of elastic and creep deformation (Adapted from Bažant 1982)

Because creep occurs in the paste, the amount of creep response varies with the degree of hydration of the paste. Because the properties of concrete change with maturity, the creep response varies greatly with the maturity of the concrete. At early ages when the paste is transitioning from a fluid to a solid, concrete exhibits a large amount of viscoelastic and elastic behavior (Emborg 1989; Westman 1999; Gutsch and Rostasy 1995).

15.5.1 Basic and Drying Creep

Many theories have been proposed as to the mechanisms that cause creep and relaxation, but none can fully account for all of the observed creep and relaxation phenomena. It is possible that creep is combination of several different mechanisms (Neville et al. 1983).

Elastic deformation is due to instantaneous, linear reversible deformations of the crystals or molecules of the concrete constitutive materials. Additional time-dependent deformation can be due to changes of position of single units or crystallographic slip; the slipping causes a rearranging of molecules and an external strain. Van der Waal's force is an attraction between adjacent particles, and is a function of the distance between the particles. If particles are not chemically bound and enough water exists between adjacent particles to reduce the Van der Waal's forces, then slip between particles is possible (Mindess et al. 2003). Slipping is not the only recognized mechanism for creep; when the C-S-H is loaded for a sustained period, the absorbed water within the layers of C-S-H is lost causing a volumetric reduction (Mehta and Montero 1996; Mindess et al. 2003). The amount of water loss is a function of the load and the time period. The total creep that occurs without loss of water to the environment is called *basic creep*. If drying is also occurring, the strain will be greater. Concrete that is exposed to both loading and drying over time will experience *drying creep*. Drying creep is an additional response greater than basic creep and unloaded drying shrinkage combined. This is because the additional loss of adsorbed water due to drying causes greater creep strains. An illustration of free drying shrinkage, basic creep, and drying creep is shown in Figure 15-8, where ε_{sh} is the drying shrinkage, ε_{bc} is basic creep, ε_{dc} is the drying creep, and ε_{tot} is the total creep.

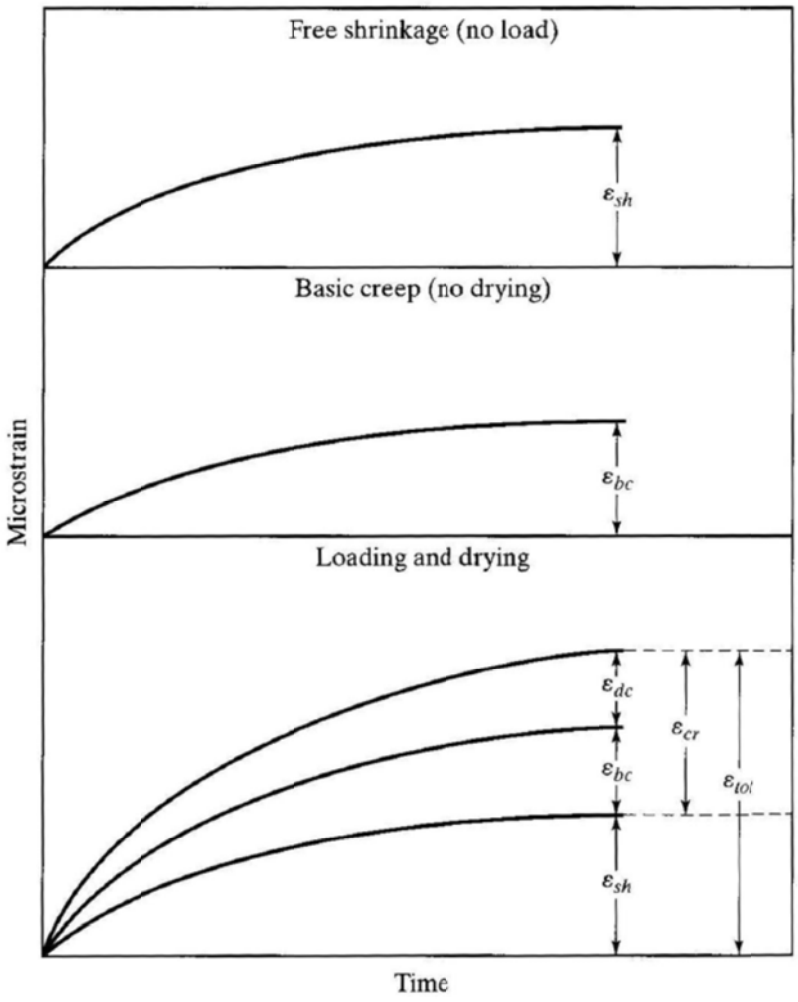

Figure 15-8: Free drying shrinkage, basic creep, and drying creep illustration (Mindess et al. 2003)

15.5.2 Recoverable and Irreversible Creep

When concrete is unloaded after a sustained loading, the concrete will exhibit an immediate recovery of the elastic deformation. Then, over time more of the strain will be recovered. However, the concrete will not recover all of the strain. During the sustained loading phase, the concrete experienced permanent deformations. This irreversible deformation is the result of removal of adsorbed water from the C-S-H and new bonds being formed in between the C-S-H layers (Mehta and Monteiro 2006). In addition to

water loss, the particles that slipped will not return to their preloaded positions, and this accounts for some of the irreversible creep. Some have argued that part of the irreversible component is the result of low-stress micro-cracking around the aggregate particles in the interfacial transition zone (Neville et al. 1983). Recoverable and irreversible creep are illustrated in Figure 15-9.

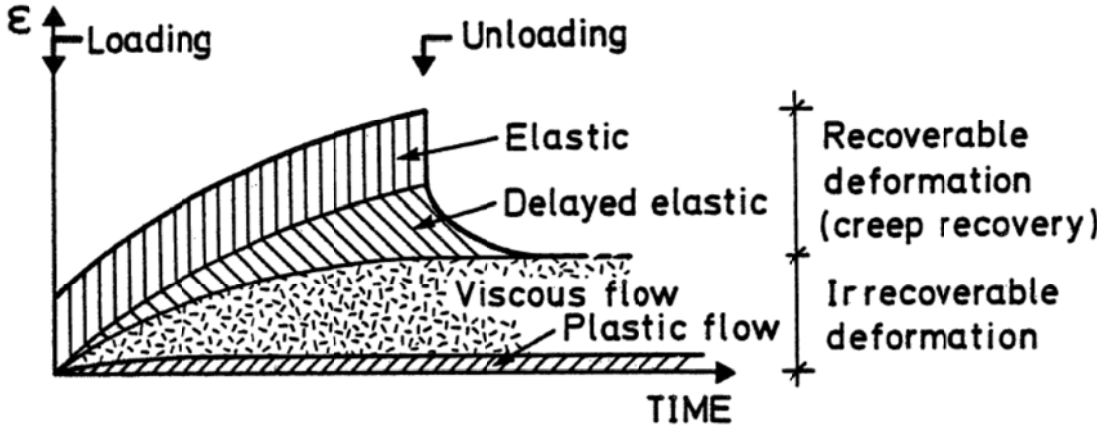

Figure 15-9: Components of creep and creep recovery (Emborg 1989)

15.5.3 Aggregate Effects on Creep

Because creep occurs in the paste and is restrained by the aggregates, the aggregate stiffness and amount plays an important role in the magnitude of the creep response. In creep behavior, the primary role of the aggregate is to restrain the creep that is occurring in the paste. Because of this, higher modulus of elasticity aggregates has reduced concrete creep response, and vice versa. Also, as the aggregate volume increases the creep is reduced. This is because the volume fraction causing creep is reduced and the volume fraction resisting creep is increased. The effect of aggregate type on creep is shown in Figure 15-10. Sandstone is the stiffest aggregate followed by gravel, granite, and finally

by limestone. The figure shows the stiffer aggregates resist the creep deformations occurring in the paste fraction more.

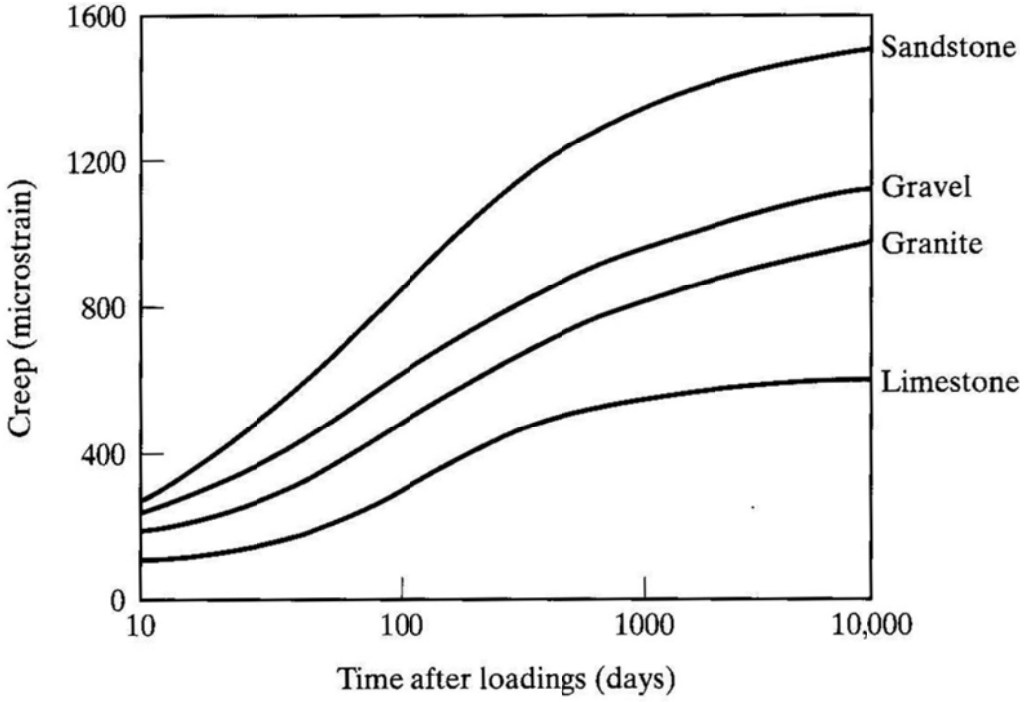

Figure 15-10: Effect of aggregate stiffness on creep (Mindess et al. 2003)

15.5.4 Superposition

Concrete behaves linear-elastically at low stress levels and non-linearly at high stress levels (Mehta and Monteiro 2006). This is true for viscoelastic behavior also. If the concrete is loaded within the linear viscoelastic range, then creep strain is proportional to the applied stress. With the principle of superposition, the sum of incremental creep responses of individual stress increments can be added to determine the strain of an element with the same stress history (McHenry 1943). An illustration of the principle of superposition is shown in Figure 15-11.

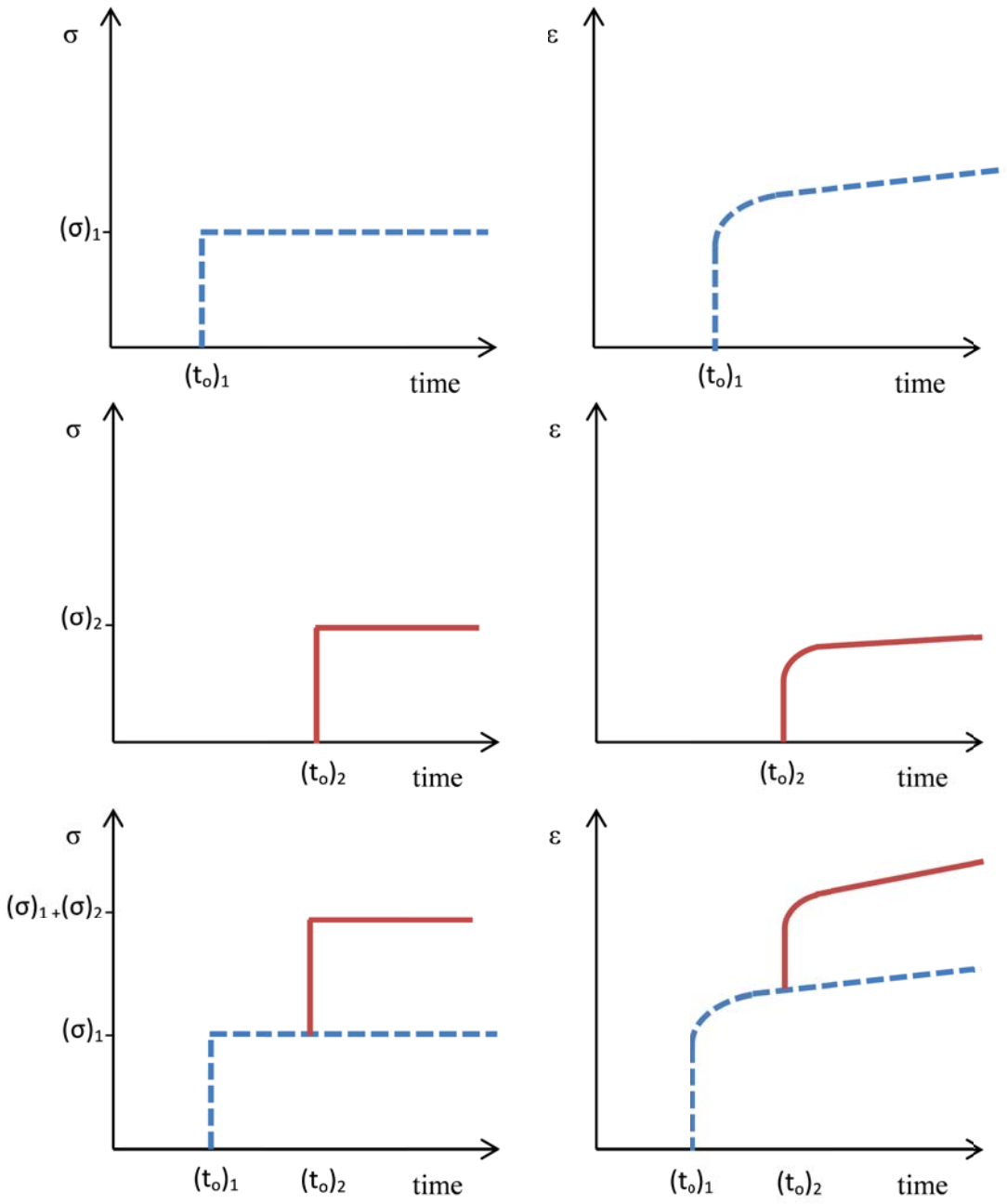

Figure 15-11 Illustration of the principle of superposition

The elastic and creep response of two elements loaded at different ages is shown in Figure 15-11. A third element loaded with the same stresses at the same times will exhibit the same behavior as the sum of the two individual elements. Because of this, the total strain

response can be estimated by adding the strain from the two individual stress cases. There is a limit at which concrete starts behaving with non-linear elastic and viscoelastic response. At that point, the principle of superposition becomes invalid because the behavior becomes non-proportional. There is a debate as to what the upper limit of proportional behavior is, but it is generally believed to be at stress-strength ratios of 40 to 60% for most mixtures, but can be as high as stress-strength ratios of 85% (Neville et al. 1983).

15.6 Viscoelastic Models

Because concrete exhibits both elastic and viscous properties, it is convenient to model stress-strain behavior with viscoelastic models. The viscoelastic behavior can be modeled with combinations of a linear spring and a linear viscous dashpot. The stress-strain behavior of a linear spring is governed by Hooke's law as defined in Equation 15-4.

$$\sigma(t) = E\varepsilon(t) \quad \text{..... Equation 15-4}$$

where $\sigma(t)$ = stress as a function of time (psi),

E = modulus of elasticity (psi), and

$\varepsilon(t)$ = strain as a function of time.

The response of the spring element is instantaneous. With a constant stress, the spring element will exhibit constant strain, and with constant strain the element will have constant stress as illustrated in Figure 15-12. The viscous dashpot is visualized by a piston with a perforated bottom displacing a viscous fluid. The behavior of a dashpot is

governed by Newton's law of viscosity and is defined in Equation 15-5 (Mehta and Monteiro 2006).

$$\dot{\varepsilon}(t) = \frac{\sigma(t)}{\eta} \quad \text{Equation 15-5}$$

where $\dot{\varepsilon}(t)$ = strain rate = $\frac{d\varepsilon}{dt}$,

$\sigma(t)$ = stress as a function of time (psi), and

η = viscous coefficient (psi × sec).

The behavior of a linear dashpot is illustrated in Figure 15-12. The constitutive relationships for a spring and dashpot are shown in Equations 15-6 and 15-7, respectively (Mehta and Monteiro 2006). For a constant stress, a dashpot will deform at a constant rate. However, for an instantaneous strain the stress response becomes infinite because a dashpot cannot undergo an instantaneous strain.

$$\sigma_E(t) = E\varepsilon_E(t) \quad \text{Equation 15-6}$$

$$\sigma_\eta(t) = \eta\dot{\varepsilon}_\eta(t) \quad \text{Equation 15-7}$$

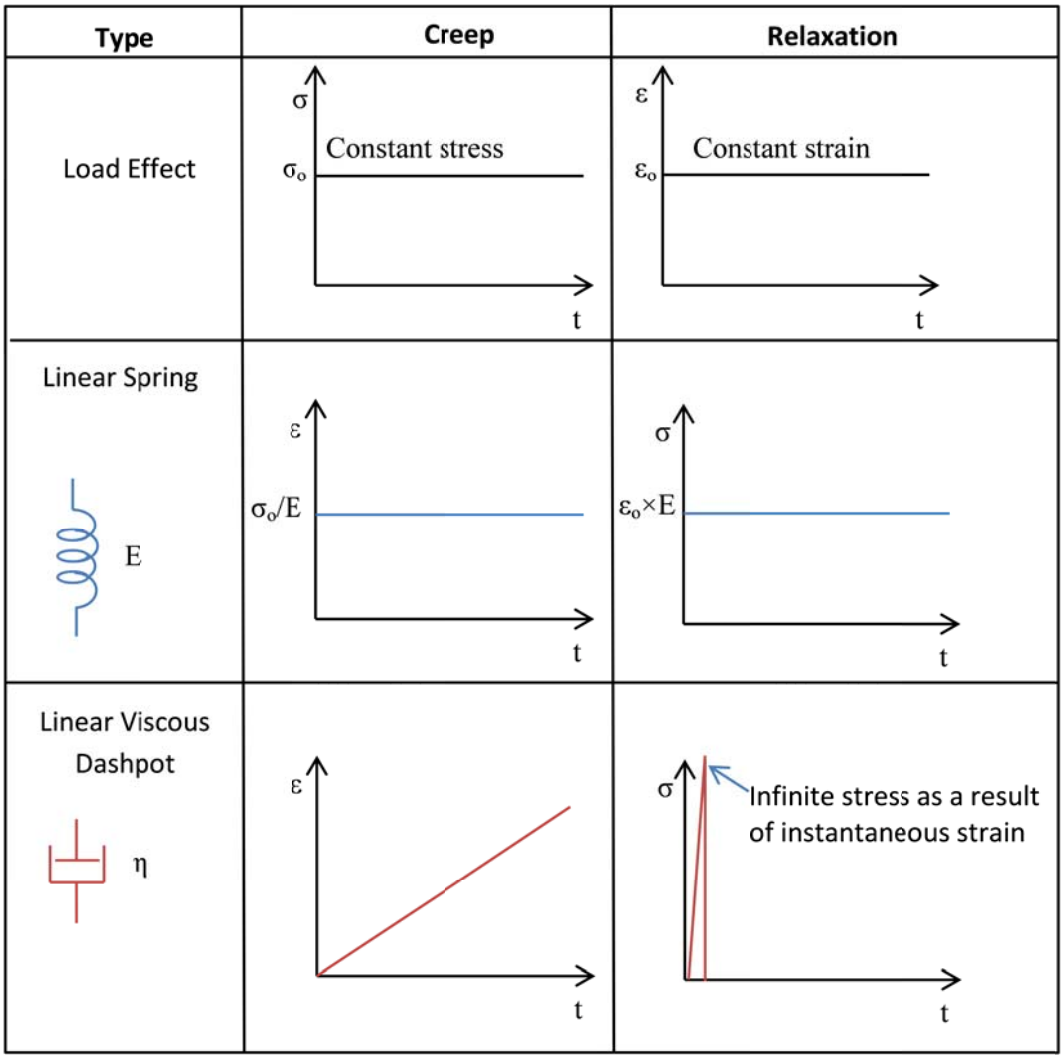

Figure 15-12: Illustration of spring and dashpot response (adapted from Mehta and Monteiro 2006)

15.6.1 Maxwell Model

More complex viscoelastic behavior can be captured by combinations of spring and dashpot elements. The Maxwell model is comprised of spring and dashpot elements linked in series as shown in Figure 15-13. Because the elements are in series, the equilibrium and compatibility equations can be expressed as Equations 15-8 and 15-9, respectively (Mehta and Monteiro 2006). With a constant load, the spring will deform instantaneously and the viscous response of the dashpot will be linear additive. The strain

response for the Maxwell model increases without bounds as shown in Figure 15-13. Under a constant strain, the Maxwell model will have an initial elastic response from the spring, then the stress will be relaxed away due to the viscous response of the dashpot. Maxwell models are generally used to account for short-term early-age relaxation behavior (Neville et al. 1983).

Equilibrium Equation: $\sigma_E(t) = \sigma_\eta(t) = \sigma(t)$ ..... Equation 15-8

Compatibility Equation: $\varepsilon(t) = \varepsilon_E(t) + \varepsilon_\eta(t)$ ..... Equation 15-9

15.6.2 Kelvin Model

The Kelvin Model combines a linear spring and a dashpot in parallel. The response of the Kelvin Model to constant stress or strain is illustrated in Figure 15-13. Equations 15-10 and 15-11 are the equilibrium and compatibility equations for the Kelvin Model, respectively (Mehta and Monteiro 2006). When a Kelvin element is subjected to an instantaneous strain, the stress response goes to infinity as illustrated in Figure 15-13. Because the spring and dashpot are in parallel, the dashpot strain response is equal to the total strain. Since no force can cause an instantaneous deformation in a dashpot, a Kelvin Model alone cannot represent relaxation response. For a constant load the dashpot will initially carry the entire load and there will be no displacement. Then, over time the viscous behavior of the dashpot will transfer load to the spring. In infinite time, the deformation will approach the elastic response of the spring (Mehta and Monteiro 2006).

Equilibrium equation: $\sigma(t) = \sigma_E(t) + \sigma_\eta(t)$ ..... Equation 15-10

Compatibility equation: $\varepsilon(t) = \varepsilon_E(t) = \varepsilon_\eta(t)$ ..... Equation 15-11

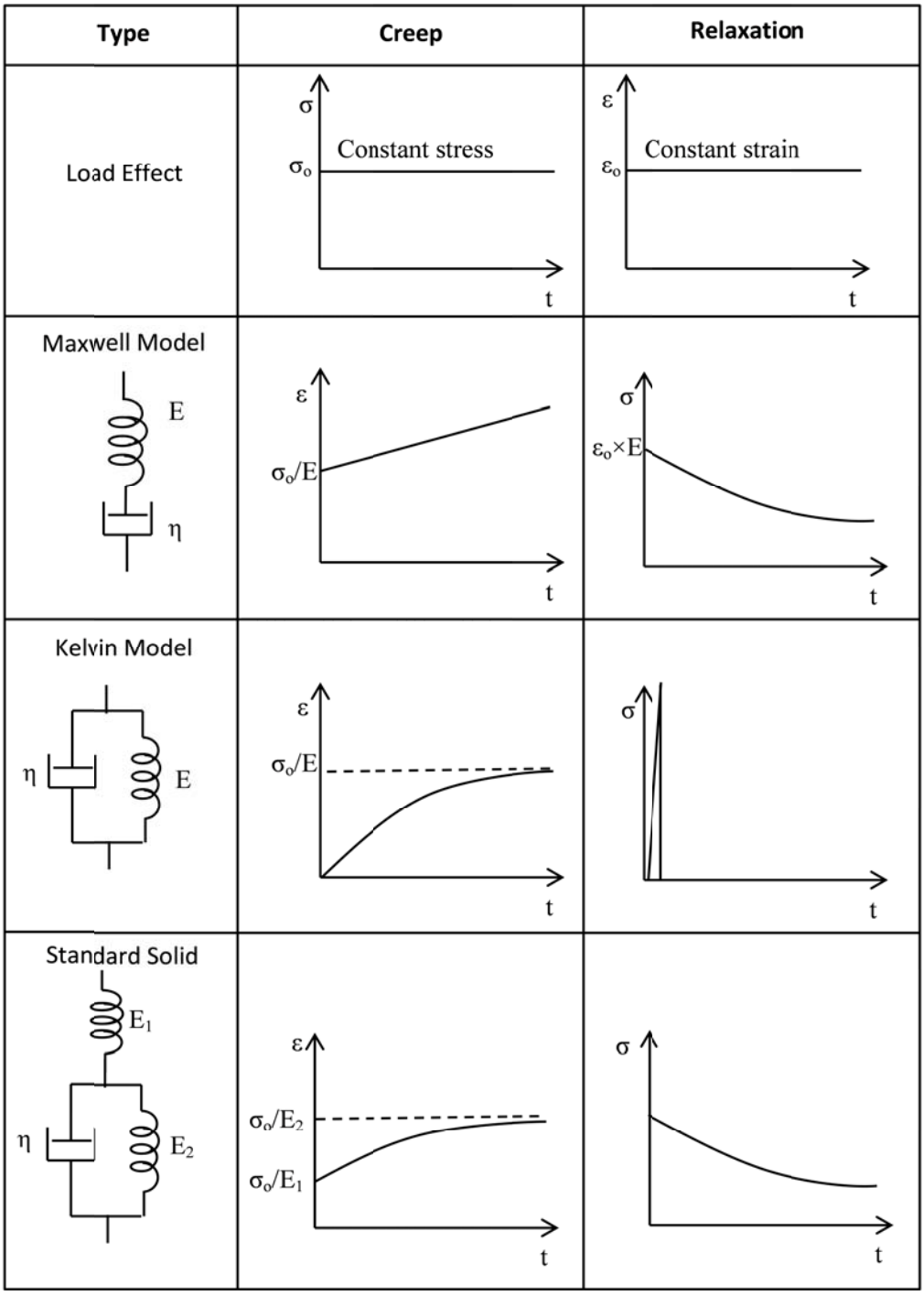

Figure 15-13: Illustration spring and dashpot combination response (adapted from Mehta and Monteiro 2006)

15.6.3 Standard Solid Model

Both the Maxwell and Kelvin models have limitations when modeling concrete behavior that can be overcome by the Standard Solid Model. The Standard Solid Model is a Kelvin element that is connected in series with a spring element. Because the spring and Kelvin elements are in series, their stresses are equal. Therefore, the strain in the Standard Solid element can be described by Equation 15-12 (Mehta and Monteiro 2006) and the creep and relaxation behavior is illustrated in Figure 15-13. The initial response of a Standard Solid to a load or strain will be dominated by the elastic response of the spring. Then, the dashpot of the Kelvin element will begin to viscously deform and transfer load to the spring of the Kelvin element. In infinite time, the response of the Standard Solid element to a constant load will be the sum of the elastic responses of the springs (Mehta and Monteiro 2006).

$$\varepsilon(t) = \frac{\sigma(t)}{E_1} + \frac{\sigma(t)}{\left(E_2 + \eta \, {}^{\partial}/_{\partial t}\right)} \quad \text{..... Equation 15-12}$$

15.7 Concrete Creep or Compliance Models

In literature there are numerous concrete creep or compliance models. This section investigates the background of some of the more recognized models. The models described in this section are limited to the ACI 209R-92 (ACI 209 1992) , GL2000 (Gardner and Lockman 2001), CEB MC 90-99 (CEB 1999), and the B3 Model (Bažant and Baweja 2000), which are discussed in ACI 209R.2 (2008). Because drying shrinkage is not included in the testing program, the drying shrinkage and drying creep will be

omitted from the summary of the models. A table of model parameters is presented in Table 15-1 where $f_{cm,28}$ is the 28-day strength of the concrete, *a/c* is aggregate-to-cement ratio by mass, cement content is the proportion of cement in the concrete, *w/c* is the water-to-cement ratio by mass, the type of cement is the cement classification as per ASTM C 150, t_c is the amount of time the sample was cured, and t_o is the age at which the concrete is loaded.

Table 15-1: Creep model parameter ranges (adapted from ACI 209 2008)

Input Variables	Model			
	ACI 209R-92	**B3 Model**	**CEB MC90-99**	**GL2000**
$f_{cm,28}$ (psi)	-	2500-10,000	2200-17,400	2320-11,900
a/c	-	2.5-13.5	-	-
Cement Content (lb/yd^3)	470-752	270-1215	-	-
w/c	-	0.35-0.85	-	-
Type of Cement (ASTM C 150)	I or II	I, II, or III	I, II, or III	I, II, or III
t_c (days)	≥ 1	≥ 1	< 14	≥ 1
t_0 (days)	≥ 7	$t_0 \geq t_c$	> 1	$t_0 \geq t_c$

15.7.1 The ACI 209 Model

The ACI 209R-92 model is an empirical model developed by Branson and Christiason (1971) with modifications by ACI committee 209. The model was initially developed for the precast/prestressed industry. Since its 1992 revision, the ACI 209 model has not been updated or revised. The model calculates the creep coefficient rather than compliance, which can introduce error due to differing values of elastic modulus and thus assumed elastic response (ACI 209 2008). The ACI 209 method calculates the ultimate creep coefficient (ϕ_u) that is adjusted to account for various environmental conditions and

mixture-specific properties captured by a gamma factor (γ_c) as shown in Equation 15-13. The method also uses a hyperbolic shaped time-rate function that asymptotically approaches the ultimate creep to account for creep over time as defined in Equation 15-14.

$$\phi_u = 2.35\,(\gamma_{c,to})(\gamma_{c,RH})(\gamma_{c,vs})(\gamma_{c,s})(\gamma_{c,\psi})(\gamma_{sh,\alpha}) \quad \text{..... Equation 15-13}$$

where $\gamma_{c,to}$ = loading age correction factor,

$\gamma_{c,RH}$ = relative humidity correction factor,

$\gamma_{c,vs}$ = volume-surface area ratio correction factor,

$\gamma_{c,s}$ = slump correction factor,

$\gamma_{c,\psi}$ = fine aggregate correction factor, and

$\gamma_{sh,\alpha}$ = air content correction factor.

$$\phi(t, t_o) = \frac{(t-t_o)^{\psi}}{d+(t-t_o)^{\psi}} \times \phi_u \quad \text{..... Equation 15-14}$$

where t = concrete age (days),

t_o = age at loading (days),

d = ACI recommends 10 for normal concrete, and

ψ = ACI recommends 0.6 for normal concrete.

15.7.2 The GL2000 Model

The GL2000 model (Gardner and Lockman 2001) is an updated version of the Atlanta 97 model (Gardner and Zhao 1993). The GL2000 model is a design-office procedure for creep and shrinkage prediction of normalweight concretes. The model can be used regardless of chemical admixture, supplementary cementing materials, curing temperature,

or casting temperature (Gardner and Lockman 2001). The initial elastic strain is calculated using the modulus of elasticity at the age of loading. The creep coefficient is based on the 28-day modulus of elasticity as shown in Equation 15-15. The creep coefficient calculation is shown in Equation 15-16. The GL2000 model calculates total compliance as the sum of the initial elastic component of compliance and the time-dependent component of compliance based on a creep coefficient approach.

$$J(t,t_0) = \frac{1}{E_{c,to}} + \frac{\phi_{28}(t,t_0)}{E_{c,28}} \quad \text{..... Equation 15-15}$$

where $J(t,t_0)$ = compliance (1/psi),

$E_{c,to}$ = modulus of elasticity at time of loading (psi),

$E_{c,28}$ = modulus of elasticity at 28 days (psi), and

$\phi_{28}(t,t_0)$ = creep coefficient.

$$\phi_{28}(t,t_0) = \Phi(t_c)\left[2\,\frac{(t-t_0)^{0.3}}{(t-t_0)^{0.3}+14} + \left(\frac{7}{t_0}\right)^{0.5}\left(\frac{(t-t_0)}{(t-t_0)+7}\right)^{0.5} + 2.5(1-1.086h^2)\left(\frac{(t-t_0)}{(t-t_0)+77\left(\frac{V}{S}\right)^2}\right)^{0.5}\right]$$

..... Equation 15-16

where $\Phi(t_c)$ = $\left[1-\left(\frac{(t-t_c)}{(t-t_c)+77\left(\frac{V}{S}\right)^2}\right)^{0.5}\right]^{0.5}$ correction for drying before loading (if $t_c = t_0$ then, $\Phi(t_c) = 1$),

V = volume of member (in.^{3}),

S = surface area of member (in.^{2}),

h = relativity humidity expressed as a ratio, and

t_c = age at the end of curing (days).

15.7.3 The CEB MC90-99 Model

The CEB MC90-99 (CEB 1999) model is intended to estimate the compliance behavior of the mean cross section of a concrete member. The CEB MC90 model was revised in 1999 for lower and higher strength concretes as is ACI 209-08. Similar to the ACI 209 model, the compliance prediction associated with the CEB MC90-99 model is hyperbolic with respect to time. It was calibrated to predict compliance in ordinary-strength concrete that is moist cured at normal temperatures for no more than 14 days. The compliance is the sum of the initial elastic response and the time-dependent response. The CEB MC90-99 model calculates the initial elastic strain based on the modulus at the loading age, but the creep coefficient is based on the 28-day modulus of elasticity. The compliance function is shown in Equation 15-17.

$$J(t,t_0) = \frac{1}{E_{c,to}} + \frac{\phi_{28}(t,t_0)}{E_{c,28}} \quad \text{..... Equation 15-17}$$

where $\phi_{28}(t,t_0)$ = $\phi_0 \beta_c(t,t_0)$,

ϕ_0 = $\phi_{RH}(h)\beta(f_{cm28})\beta(t_0)$,

$\phi_{RH}(h)$ = $\left[1 + \frac{1-h/h_0}{\sqrt[3]{0.1[(V/S)/(V/S)_0]}}\alpha_1\right]\alpha_2$,

$\beta(f_{cm28})$ = $5.3/\sqrt{f_{cm28}/f_{cm0}}$,

$\beta(t_0)$ = $\frac{1}{0.1+(t_0/t_1)^2}$,

$\beta_c(t,t_0)$ = $\left[\frac{(t-t_0)/t1}{\beta_H+(t-t_0)/t1}\right]^{0.3}$,

β_H = $150[1+(1.2\ h/h_0)^{18}]\ (V/S)/(V/S)_0 + 250\alpha_3 \leq 1500\alpha_3$,

α_1, α_2, and α_3 = correction factor based 28-day compressive strength,

f_{cm0} = 1450 psi,

$(V/S)_0$ = 2 in.,

h = relativity humidity expressed as a decimal,

h_0 = 1, and

t_1 = 1 day.

15.7.4 The B3 Model

The B3 Model (Bažant and Baweja 2000) is based on the solidification theory described in the following section. The B3 Model is a simpler and more theoretically justified compliance model than previous models proposed by Bažant and his co-workers (Bažant and Baweja 2000). The B3 Model is based on the solidification of hardening cement modeled with a Kelvin chain and linear spring. Compliance is calculated using Equation 15-18. The q_1 term is the elastic response, $C_0(t, t_0)$ is the basic creep term and $C_d(t,t_c)$ is the drying creep term. The basic creep term is presented in Equation 15-19.

$$J(t, t_0) = q_1 + C_0(t, t_0) + C_d(t, t_c) \quad \text{..... Equation 15-18}$$

$$C_0(t, t_0) = q_2 Q(t, t_0) + q_3 \ln[1 + (t - t_0)^n] + q_4 \left(\frac{t}{t_0}\right) \quad \text{..... Equation 15-19}$$

where q_1 = $0.6/E_{c,28}$ (1/psi),

q_2 = $86.814 \times 10^{-6} \times c^{0.5} f_{c,28}^{-0.9}$,

q_3 = $0.29\ (w/c)^4\ q_2$,

q_4 = $0.14 \times 10^{-6}\ (a/c)^{-0.7}$,

$$Q(t,t_0) = Q_f(t_0)\left[1+\left(\frac{Q_f(t_0)}{Z(t,t_0)}\right)^{r(t_0)}\right]^{-1/r(t_0)},$$

$$Q_f(t_0) = \left[0.086(t_0)^{2/9}+1.21(t_0)^{4/9}\right]^{-1},$$

$$Z(t,t_0) = (t_0)^{-m}\times\ln[1+(t-t_0)^n],$$

$$r(t_0) = 1.7(t_0)^{0.12}+8,$$

n = 0.1,

m = 0.5,

a/c = aggregate-cement ratio by mass,

w/c = water-cement ratio by mass, and

c = cement content (lb/yd^3).

Because the formulation of the B3 Model was based on physical phenomena, each term has a physical meaning and is therefore easier to comprehend than other models proposed by Bažant and his co-workers. The physical meanings of each term in Equation 15-18 and 15-19 are provided below. The aging viscoelastic term represents an age dependent viscoelasticity and the non-aging viscoelastic term is an age independent viscoelasticity. A graphical illustration of the magnitude and contribution of each term is provided in Figure 15-14 for a bridge deck mixture loaded at one day. From the results shown in this figure it can be seen that the total response is initially dominated by the aging viscoelastic and elastic responses. Over time, the plastic flow response begins to significantly contribute to the overall behavior. For this mixture, the non-aging viscoelastic response is negligible.

q_1 ⟶ Elastic compliance component (1/psi)

$q_2 Q(t, t_0)$ ⟶ Aging viscoelastic compliance component (1/psi)

$q_3 \ln[1 + (t - t_0)^n]$ ⟶ Non-aging viscoelastic compliance component (1/psi)

$q_4 \left(\frac{t}{t_0}\right)$ ⟶ Plastic flow compliance component (1/psi)

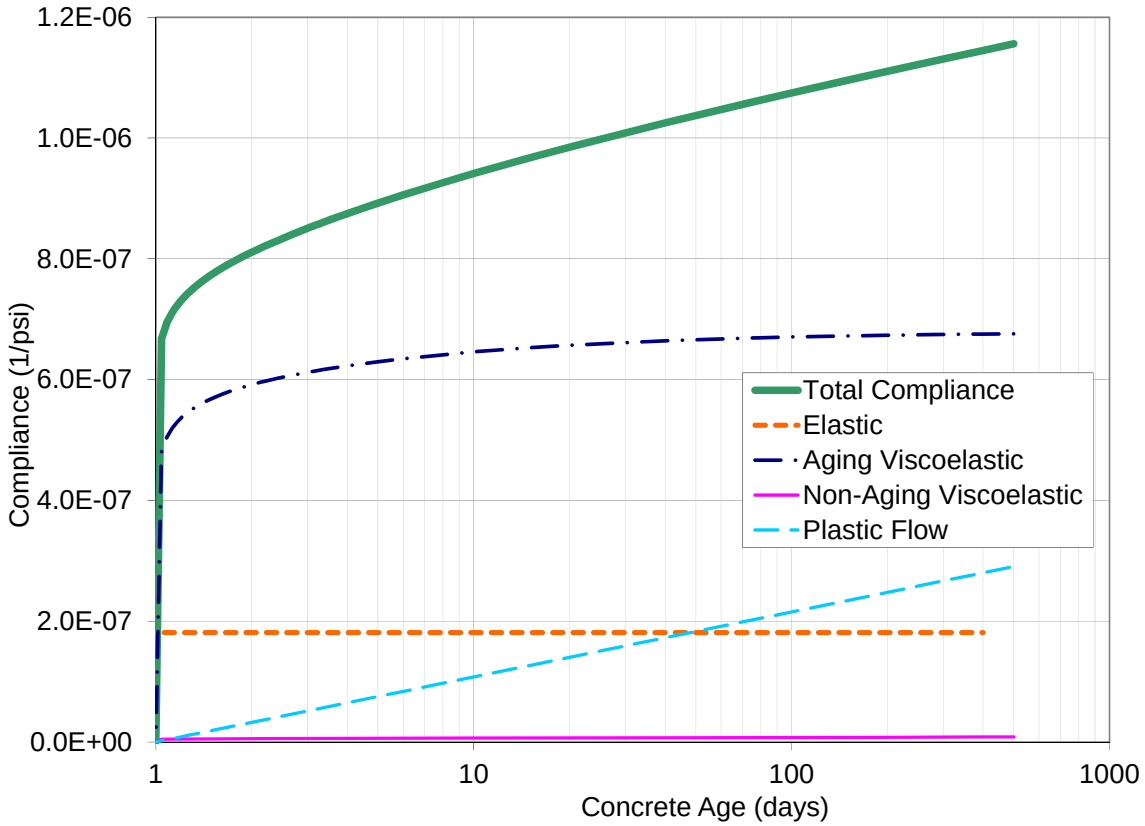

Figure 15-14: Components of B3 Model (bridge deck concrete with t_0=1 day)

Unlike other models, the elastic response of the B3 Model is treated as a constant with respect to age. Since the elastic response is the immediate strain under very short load durations (1 μs), Bažant and Prasannan (1989a) state that the results from *elastic modulus tests* represents both elastic and creep behavior. Because of this Bažant and Prasannan (1989a) state: "We nevertheless take the view that age-dependence of E(t) is a

complication that is both unnecessary and thermodynamically objectionable." The modulus used in the B3 Model is the asymptotic modulus, which can be estimated as the measured 28-day modulus divided by 0.6 (Bažant and Baweja 2000).

15.7.4.1 *Solidification Theory*

The solidification theory (Bažant and Prasannan 1989a; Bažant and Prasannan 1989b) is a physically justified model that describes the cement hydration as growth of a load-bearing volume fraction. This micro-mechanical solidification is modeled with a Kelvin chain as shown in Figure 15-15. A Kelvin chain is Kelvin elements linked in series. As the concrete ages more Kelvin elements are added to account for the decreasing viscoelastic behavior of the aging concrete. The total strain of the solidifying element is described by Equation 15-20 (Bažant and Prasannan 1989b).

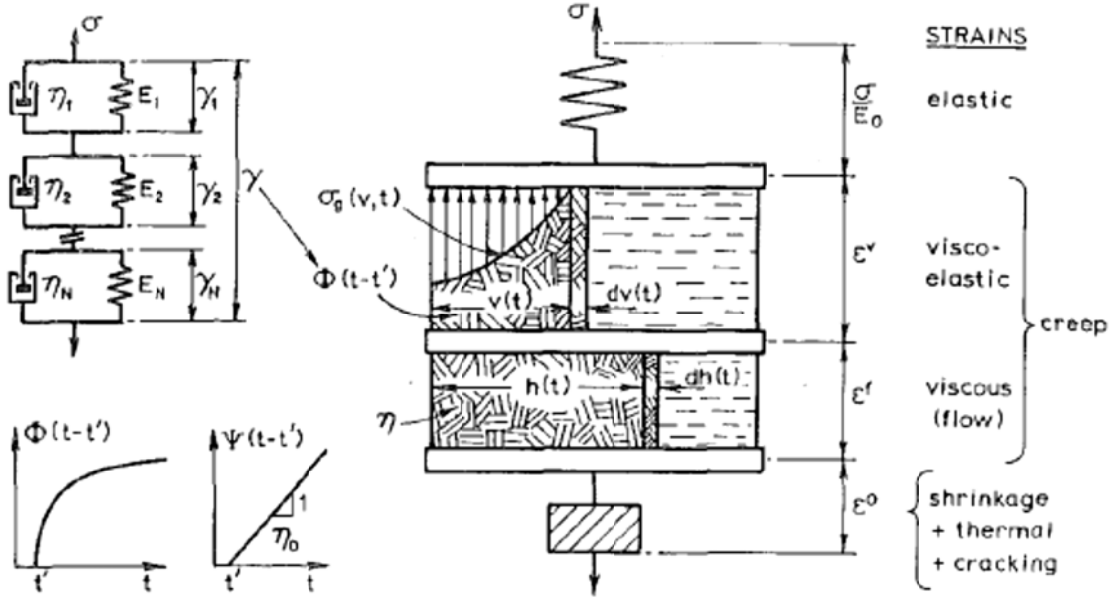

Figure 15-15: Compliance model from solidification theory (Bažant and Prasannan 1989a)

$$\varepsilon = \frac{\sigma}{E_0} + \varepsilon_v + \varepsilon_f + \varepsilon_0 \quad \text{..... Equation 15-20}$$

where $\frac{\sigma}{E_0}$ = the instantaneous elastic response,

ε_v = the viscoelastic response,

ε_f = the plastic flow, and

ε_0 = strain due to thermal dilation, drying, and cracking.

The complete derivation of the compliance function based on the solification theory can be found in Bažant and Prasannan (1989a). It was found that the formulation of the aging viscoelastic response did not have a closed form solution; therefore, an approximation solution was determined with errors generally less than 0.5%.

15.7.4.2 *Early-Age Behavior of the B3 Model*

The B3 Model was not calibrated or designed to account for the behavior of concrete loaded before one day. However, for crack prediction modeling it is necessary to determine the amount of relaxation that occurs from the onset of setting. It has been found that the B3 Model does not accurately predict the relaxation behavior of concrete loaded prior to one day due to a lack of viscoelastic response (Østergaard et al. 2001). This lack of early-age viscoelastic response was corrected by Østergaard et al. (2001)with a modified q_2 term as shown in Equation 15-21. The q_5 term is referred to as the structural set time, and should correspond to the transition from liquid viscoelastic to solid viscoelastic response (Østergaard et al. 2001). If q_5 is set equal to the age at loading (t_0) then the modified q_2 approaches infinity; therefore, q_5 should be less than t_0.

$$q'_2 = q_2\left(\frac{t_0}{t_0 - q_5}\right)$$ ..... Equation 15-21

where q_5 = structural setting time (days).

The advantage of a correction in the form of Equation 15-21 is that the effect is quickly diminishing, which leaves the B3 Model virtually unmodified at later ages as shown in Figure 15-16. The early-age viscoelastic response will be increased greatly by the q_2 modification, but after three days the modified q_2 is virtually the same as the unmodified q_2 as illustrated in the figure.

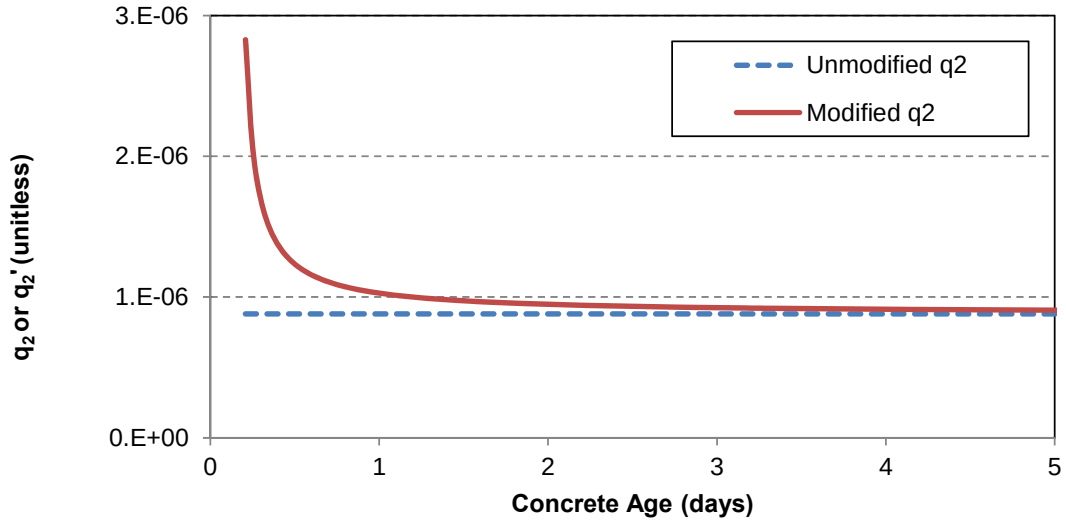

Figure 15-16: Effect of q_2 modification (with q_5 = 0.25 days)

15.8 Methods to Assess Early-Age Concrete Behavior

15.8.1 Restrained Stress Development

The rigid cracking frame (RCF), shown in Figure 15-17, is comprised of two mild steel crossheads and two 4-in. diameter Invar steel sidebars. The test setup was adapted from the configuration developed by Dr. Rupert Springenschmid as documented by RILEM Technical Committee 119 (1998). The RCF test is a relative index of cracking sensitivity.

According to Springenschmidand Breitenbücher (1998), a mixture with increased cracking time and decreased cracking temperature will have improved cracking performance in the field. This increased performance may be in the form of increased crack spacing, decreased crack widths or fewer cracks.

a)

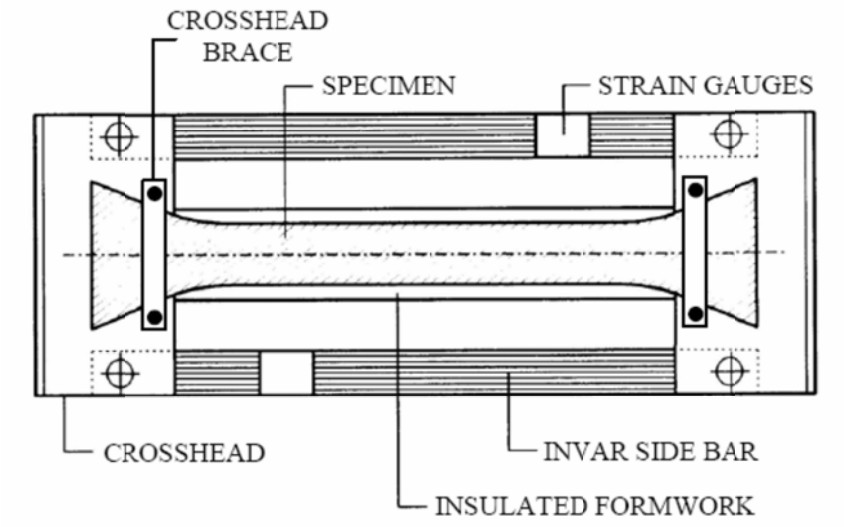

b)

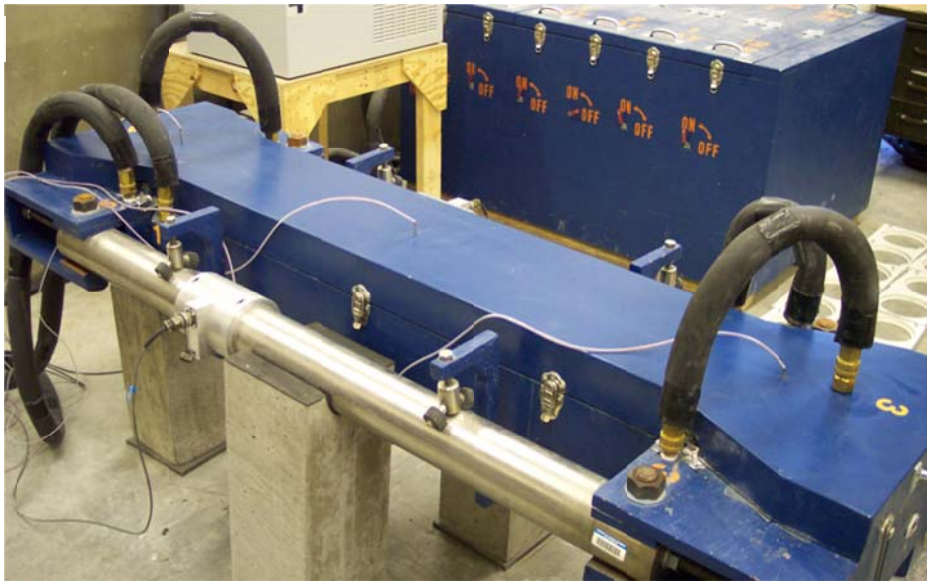

Figure 15-17: Rigid cracking frame test setup: a) Schematic of test (Mangold 1998) b) Actual equipment used

Fresh concrete is consolidated in the RCF, and the stress development of the concrete is measured continuously until cracking occurs. The 6 × 6 × 49 in. concrete

specimen is restrained by dovetailed crossheads at each end. The dovetail is gradually tapered to reduce stress concentrations and is lined with teeth that grip the concrete. To further prevent slippage of the concrete, crosshead braces are used at the end of the crosshead to restrain opening of the crosshead as the concrete goes into tension. The formwork shown includes 0.5-in. diameter copper tubing throughout. A mixture of water and ethylene glycol is circulated from a temperature-controlled water bath through the formwork to control the curing temperature of the concrete sample. The formwork of the RCF is lined with sheeting to reduce friction between the concrete and the form and to seal the concrete specimen on all surfaces. Because of the presence of the sealed plastic layer around the concrete specimen, no moisture is lost and drying shrinkage effects do not contribute to the stress development while the forms are in place.

When concrete in the RCF starts to hydrate and volume changes due to temperature and autogenous shrinkage effects develop, the Invar steel bars provide restraint against movement and stress develops in the concrete. The concrete's stress development is monitored using strain gauges mounted on the Invar bars, that are calibrated to the bar forces, which equilibrate the concrete stresses.

The RCF captures the stress due to thermal and autogenous effects; therefore, the stress developed by the RCF under a match-cured condition is a function of the concrete's coefficient of thermal expansion, temperature history, modulus of elasticity, autogenous shrinkage, and relaxation.

It been observed that the cracking frame stress at failure is less than the splitting tensile strength measured on molded concrete cylinders (Meadows 2007). This is due to the test specimen size, the rate of loading, and the type of loading (Meadows 2007). The

section of concrete subjected to the highest tensile stress is much larger in the cracking frame than in a 6 × 12 in. cylinder. The larger volume of concrete subjected to the highest tensile stress in the cracking frame provides a higher probability of a flaw in the sample and therefore it has a lower apparent tensile strength. In addition, the rate of loading can affect the strength results. Slow load rates yield lower apparent strength and conversely higher load rates yield higher apparent strength (Wight and MacGregor 2009). The splitting tensile strength specimens were loaded to failure in less than 5 minutes, whereas the cracking frames were loaded for 23 - 109 hours, thus the concrete in the cracking frame will exhibit a lower apparent tensile strength. In addition, the cracking frame is a direct tension test; whereas the splitting tension is an indirect tension test. Meadows (2007) reports that the ratio of cracking frame stress at failure to splitting tensile strength generally falls between 50 to 80 %.

15.8.2 Unrestrained Length Change Assessment

Bjøntegaard (1999) developed a free-shrinkage frame (FSF) to determine the unrestrained uniaxial length change of a curing *concrete* specimen. A FSF similar to the one developed by Bjøntegaard was constructed at Auburn University and is shown in Figure 15-18. The FSF consists of a box that is thermally controlled with 0.5-in. diameter copper tubing, and a supporting Invar steel frame. The box serves as the formwork for the freshly placed concrete and the system to match cure the concrete to any temperature profile. A 6 × 6 × 24 in. concrete specimen is cast with two sacrificial steel plates connected with an Invar rod to a linear variable displacement transducer (LVDT) to measure linear expansion and contraction. The fresh concrete is placed on a double layer of plastic sheeting with a lubricant in between to minimize friction, which facilitates free movement of the concrete

specimen. The plastic layer also seals the specimen, so that no moisture is lost. Therefore drying shrinkage effects do not contribute to the free movement measured in the FSF. When concrete in the FSF is cured to a specified temperature history, the measured strain is a function of thermal and autogenous effects.

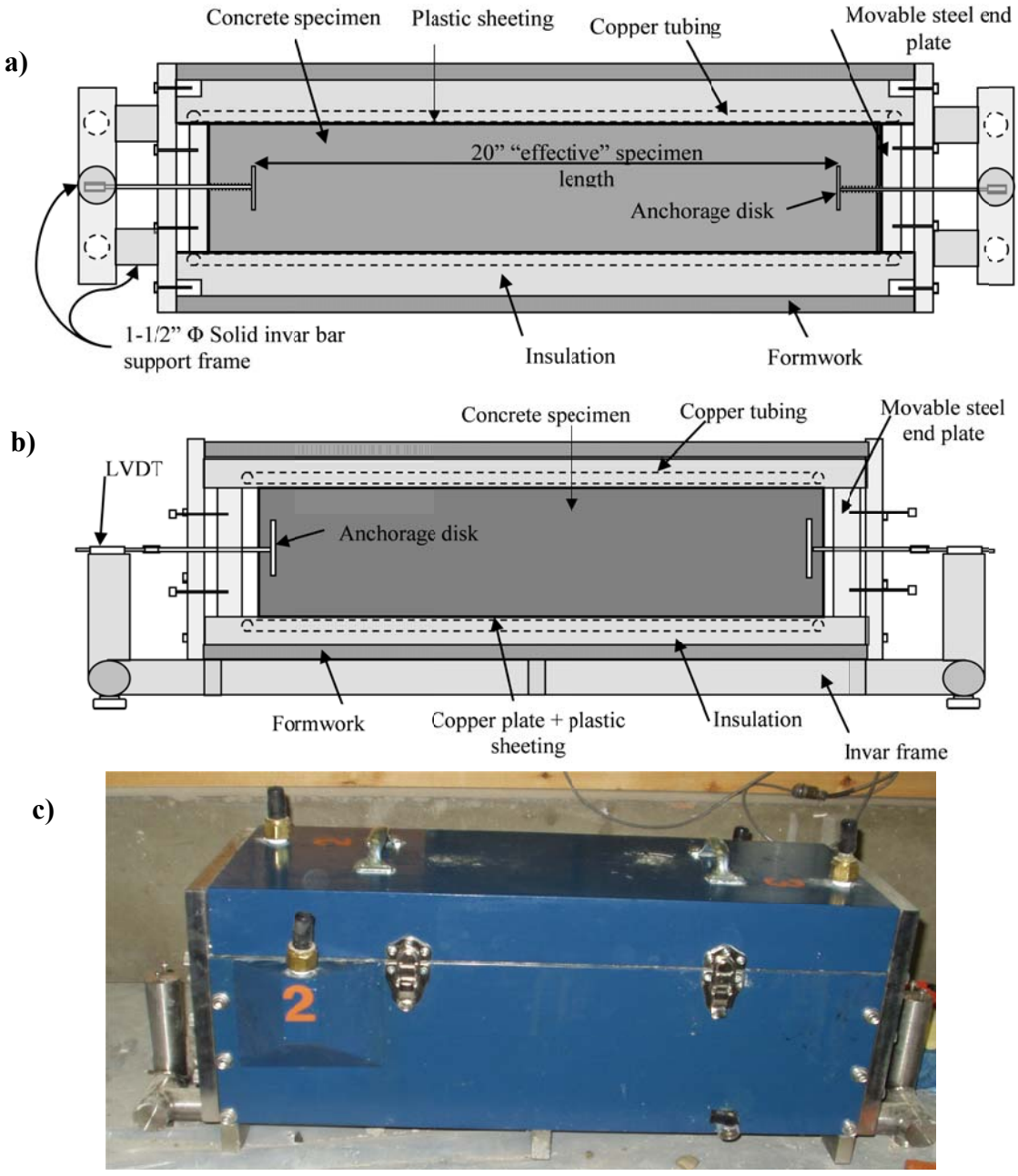

Figure 15-18: Free-shrinkage frame test setup: a) Plan view schematic of test equipment, b) Section view schematic, and c) Actual equipment used

When the concrete is placed, the movable steel end plates support the fresh concrete ends. When initial set is reached, the movable end plates are released and moved back to allow expansion beyond the initial specimen size. Initial set is determined from penetration resistance as per ASTM C 403. The mortar sample for setting is match-cured to the same temperature history of the FSF. The end plates in position prior to placement are shown in Figure 15-18a, and the end plates drawn back after setting are shown in Figure 15-18b.

CHAPTER 16

PART III: EXPERIMENTAL PROGRAM

16.1 Experimental Program

Concretes proportioned with varying amounts and types of lightweight aggregates and *w/c* were tested to determine their early-age stress development using RCF testing techniques. Temperature profiles were modeled to determine the temperature history that concrete in an 8-in. thick bridge deck would experience under both summer and fall placement scenarios. Concrete in the RCF was match-cured to modeled temperature conditions as schematically shown in Figure 16-1. Free shrinkage and mechanical property testing were performed on match-cured concrete specimens also, as shown in Figure 16-1.

Curing temperatures have a major impact on the rate of hydration, rate of development of mechanical properties, and the rate of stress development in concrete. Stress development data collected at typical laboratory temperatures often do not represent the worst-case scenario, as it is well known that early-age cracking is exacerbated under warm-weather conditions (Schindler and McCullough 2002). Each mixture with *w/c* of 0.42 was thus tested under the following two placement scenarios:

- **Summer placement scenario**: Concrete placement temperature ≈ 95 °F, and ambient air temperature cycling between 85 and 95 °F.
- **Fall placement scenario**: Concrete placement temperature ≈ 73 °F, and ambient air temperature cycling between 70 and 77 °F.

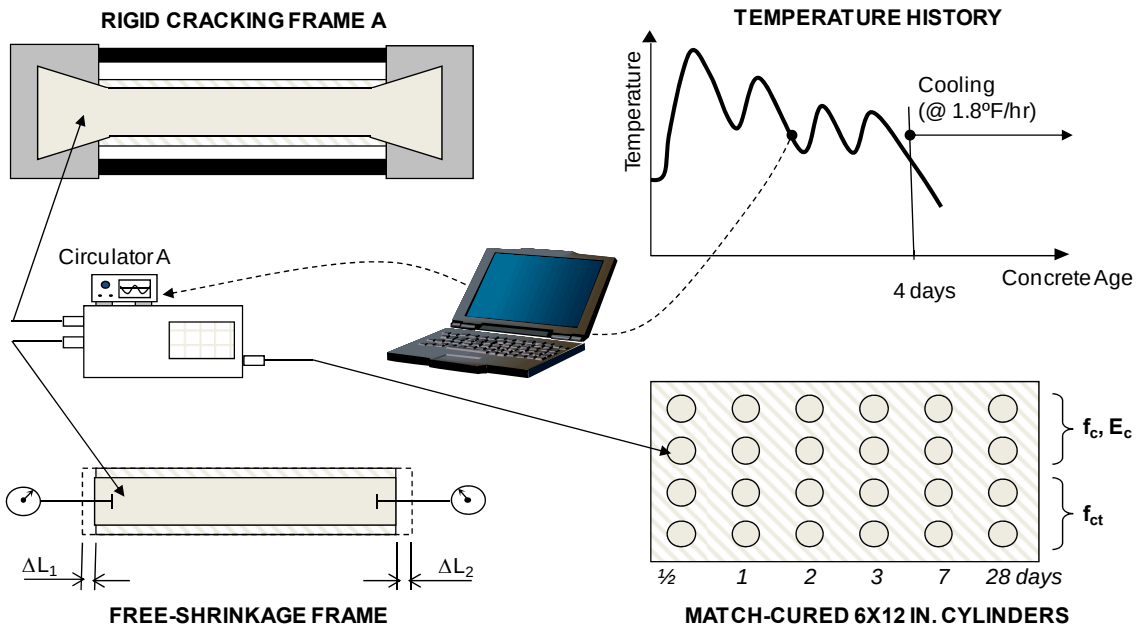

Figure 16-1: Match curing testing setup

The use of these two placement scenarios allows one to determine the effect of placement and curing temperature on the cracking sensitivity of the lightweight aggregate and control concrete mixtures. The ConcreteWorks software program (Poole et al. 2006) was used to predict the concrete temperature history of each specific mixture as it would develop in an 8-in. thick bridge deck for both summer and fall placement scenarios. The development of the temperature profile is discussed in Section 16.4.

All constituent materials for the summer placement scenario were placed in an environmental chamber and preconditioned so that the fresh concrete temperature would be approximately 95 °F. All the constituent materials for the fall placement scenario were conditioned at room temperature so that the fresh concrete temperature would be approximately 73 °F.

After 96 hours, the modeled temperature profile essentially followed the prevailing diurnal cycle typical of the simulated placement month. The temperature peaks and valleys were the same from day-to-day because the effect of the cement hydration had dissipated and only environmental effects affected the temperature change of the concrete at this age. Therefore, if cracking had not occurred before 96 hours it was not likely to occur without additional temperature decrease. If cracking had not occurred at 96 hours, the temperature was decreased by 1.8 °F/hr until the onset of cracking, which is also the practice used by Breitenbücher and Mangold (1994).

16.2 Materials

16.2.1 Normalweight Aggregates

Siliceous ASTM C 33 No. 67 river gravel was used as the control coarse aggregate. The normalweight fine aggregate was a siliceous river sand. Both aggregate types were obtained from the quarry of Martin Marietta Materials located in Shorter, Alabama. An ASTM C 33 No. 67 crushed limestone from Tuscumbia, Alabama was used to determine the effect of stiffness of normalweight aggregate on relaxation properties. The aggregates were sampled and sieve analyses were performed to obtain the gradations as per ASTM C 136. Samples were also obtained for specific gravity and absorption capacity testing of the coarse and fine aggregate as per ASTM C 127 and ASTM C 128, respectively. The sieve analysis results for all aggregates are presented in Appendix A. The specific gravity and absorption capacity for the normalweight coarse and fine aggregates are shown in Table 16-1.

Table 16-1: Normalweight aggregate material properties

Item	Siliceous Coarse Aggregate	Limestone Coarse Aggregate	Siliceous Fine Aggregate
Supplier	Martin Marietta	Martin Marietta	Vulcan Materials
Source	Shorter, AL	Tuscumbia, AL	Shorter, AL
Gradation (ASTM C 33)	No. 67	No. 67	-
Absorption (%)	0.52	0.90	0.41
Bulk-specific gravity (SSD)	2.63	2.64	2.61
Fineness Modulus	-	-	2.45

16.2.2 Lightweight Aggregates

The lightweight aggregates were selected to represent those available in different regions of the United States and to include the three raw materials used in the United States for LWA: shale, clay, and slate. Three sources of lightweight coarse aggregates and four sources of lightweight fine aggregates were used. The aggregates were sampled and sieve analyses were performed to obtain the gradations as per ASTM C 136. The gradations of the aggregates can be found in Appendix A. Relative density and absorption testing of the lightweight material was performed using ASTM C 128. For the lightweight fine aggregates, Provisional Method 2 of ASTM C 128 (the rubber mat method) was used to determine when the sample was at the surface dry condition. The source location, type, and properties of each of the fine lightweight aggregates are shown in Table 16-2. The source location, type, and properties of each of the lightweight coarse aggregate are shown in Table 16-3. Two gradations of *clay* fine aggregates were used; the coarser gradation is called "*Maximizer*" as per the terminology used by this supplier. In addition, two *slate* fine aggregates were used. The coarser fine aggregate is labeled "D Tank" and the other is "MS 16" fine aggregate. Because LWA never reach saturation, the term saturated surface

dry is inappropriate (ESCSI 2007). Because of this, the relative density and absorption calculations are presented for the pre-wetted surface dry (SD) condition after at least 7 days of preconditioning.

Table 16-2: Lightweight fine aggregate source and material properties

Item	Lightweight Fine Aggregate Type					
	Slate		Clay		Shale	
Supplier	Stalite		TXI		Buildex	TXI
Source	Gold Hill, NC		Frazier Park, CA		New Market, MO	Streetman, TX
Gradation	0 to #4	0 to #4	0 to #4	0 to 3/8 in.	0 to #4	0 to #4
Absorption (SD) (%)	9.0	9.0	19.0	19.0	19.3	24.5
Relative Density (SD)	1.84	1.84	1.81	1.81	1.80	1.80
Fineness Modulus	2.83	3.37	3.07	4.32	2.99	3.35

Table 16-3: Lightweight coarse aggregate source and material properties

Item	Lightweight Coarse Aggregate Type		
	Slate	Clay	Shale
Supplier	Stalite	TXI	Buildex
Source	Gold Hill, NC	Frazier Park, CA	New Market, MO
Gradation (ASTM C330)	#4 to 3/4 in.	#4 to 3/8 in.	#4 to 1/2 in.
Absorption (SD) (%)	6.4	25.5	32.0
Bulk-specific gravity (SD)	1.52	1.72	1.59

16.2.3 Portland Cement

An adequate quantity of Type I portland cement was donated by TXI Inc. to complete all testing associated with this project. The properties of the portland cement are shown in Table 16-4.

Table 16-4: Portland cement properties

C_3S	C_2S	C_3A	C_4AF	Free CaO	SO_3	MgO	Blaine Fineness
60.3 %	18.2 %	5.4 %	11.3 %	0.9 %	2.6 %	1.3 %	351 m^2/kg

16.3 Mixture Proportions

Twenty-eight combinations of various mixtures and curing conditions were used to develop an early-age stress prediction model. Mixtures were evaluated with river gravel (RG) and limestone (LS) coarse aggregates. Also, internal curing (IC), sand-lightweight (SLW), and all-lightweight (ALW) mixtures with expanded clay, shale, or slate LWA were evaluated. Mixtures with *w/c* of 0.42, 0.36, and 0.30 were tested also. All of the mixtures with *w/c* of 0.42 were tested at two different simulated placement seasons fall (Fall) and summer (Sum). For convenience a mixture identification system is used to refer to a specific type of mixture and placement season. The identification system used is as follows

w/c	Aggregate Type	LWA Mixture Type	(Simulated Placement Season)
0.42	RG	IC	(Fall)
0.36	LS	SLW	(Sum)
0.30	Shale	ALW	
	Clay		
	Slate		

Example: **0.42 Clay SLW (Sum),** represents the sand-lightweight mixture with a *w/c* of 0.42, made with expanded clay lightweight aggregate, and placed under simulated summer conditions.

The mixtures with *w/c* of 0.36 and 0.30 were tested with only river gravel coarse and were match cured only to the fall placement scenario. A control and two IC mixtures were tested with *w/c* of 0.36 and 0.30. Only the expanded shale fine aggregate from Streetman, Texas was used to replace the normalweight fine aggregate to provide internal

curing for the mixtures with *w/c* of 0.36 and 0.30. Two different levels of internal curing were provided: a low-level (ICM) and a high-level (ICH).

The 0.42 RG mixture is a typical bridge deck mixture that meets the specification requirements of the Alabama Department of Transportation. The 0.42 IC mixtures are similar to the normalweight mixture, except that a fraction of the normalweight fine aggregate was replaced with lightweight fine aggregate. The IC mixture was initially proportioned using the method proposed by Bentz, Lura, and Roberts (2005). However, it was found that the ASTM C 567 calculated equilibrium density of the IC mixture was below 135 lb/ft^3, which did not allow the mixture to be classified as "normalweight concrete" as per the AASHTO LRFD Bridge Design Specifications (2007). It was desired that the mixture be in the "normalweight concrete" category. Because of this, the maximum replacement of normalweight fine aggregate with lightweight fine aggregate was determined to obtain a calculated equilibrium density of 135 lb/ft^3. The IC mixtures thus contained *less* LWA than required by the method proposed by Bentz et al. (2005).

The SLW mixture was proportioned using lightweight coarse aggregate and normalweight fine aggregate. The ALW mixture used both lightweight fine and coarse aggregate. The cement content for the SLW and ALW mixtures was increased to increase the paste content to improve the workability and pumpability of these lightweight concrete mixtures.

The mixtures with *w/c* of 0.36 and 0.30 mixtures have the same paste, fine aggregate, and coarse aggregate volumes as the mixtures with *w/c* of 0.42. The cement contents were increased accordingly to provide correct paste volumes for each *w/c*. The

normalweight sand was replaced with different amounts of lightweight aggregate to provide different levels of internal curing.

The slump and air contents were specified to be 4.0 ± 1.0 in. and 5.5 ± 1.5 %, which are typical values for bridge deck construction in the southeastern region of the United States. For this project, the measured density of the concrete was produced to be ± 1 lb/ft^3 of the calculated density after correcting for the measured air content of each batch.

The proportions of the mixtures made with normalweight aggregates are presented in Table 16-5. The proportions of the mixtures with expanded clay, shale and slate lightweight aggregate are presented in Table 16-6, Table 16-7, and, Table 16-8, respectively. The proportions of the internal curing mixtures with *w/c* of 0.36 and 0.30 are shown in Table 16-9.

Table 16-5: Normalweight aggregate mixtures

Item	0.42 RG	0.42 LS	0.36 RG	0.30 RG
Water Content (lb/yd^3)	260	260	238	218
Cement Content (lb/yd^3)	620	620	677	738
SSD River Gravel Coarse Aggregate (lb/yd^3)	1,761	0	1,761	1,761
SSD Limestone Coarse Aggregate (lb/yd^3)	0	1,760	0	0
SSD Normalweight Fine Aggregate (lb/yd^3)	1,210	1,211	1,210	1,210
Target Total Air Content (%)	5.5	5.5	5.5	5.5
Water-Cement Ratio (*w/c*)	0.42	0.42	0.36	0.30

Table 16-6: Clay lightweight aggregate mixtures with *w/c* of 0.42

Item	0.42 Clay IC	0.42 Clay SLW	0.42 Clay ALW
Water Content (lb/yd^3)	260	276	276
Cement Content (lb/yd^3)	620	658	658
SSD River Gravel Coarse Aggregate (lb/yd^3)	1,761	0	0
SD Clay Lightweight Coarse Aggregate (lb/yd^3)	0	1,029	948
SSD Normalweight Fine Aggregate (lb/yd^3)	878	1,316	0
SD Clay Lightweight Maximizer (lb/yd^3)	230	0	0
SD Clay Lightweight Fine Aggregate (lb/yd^3)	0	0	998
Target Total Air Content (%)	5.5	5.5	5.5
Water-Cement Ratio (*w/c*)	0.42	0.42	0.42

Table 16-7: Shale lightweight aggregate mixtures with *w/c* of 0.42

Item	0.42 Shale IC	0.42 Shale SLW	0.42 Shale ALW
Water Content (lb/yd^3)	260	276	276
Cement Content (lb/yd^3)	620	658	658
SSD River Gravel Coarse Aggregate (lb/yd^3)	1,761	0	0
SD Shale Lightweight Coarse Aggregate (lb/yd^3)	0	933	948
SSD Normalweight Fine Aggregate (lb/yd^3)	878	1,354	0
SD Shale Lightweight Fine Aggregate (lb/yd^3)	230	0	908
Target Total Air Content (%)	5.5	5.5	5.5
Water-Cement Ratio (*w/c*)	0.42	0.42	0.42

Table 16-8: Slate lightweight aggregate mixtures with *w/c* of 0.42

Item	0.42 Slate IC	0.42 Slate SLW	0.42 Slate ALW
Water Content (lb/yd^3)	260	276	276
Cement Content (lb/yd^3)	620	658	658
SSD River Gravel Coarse Aggregate (lb/yd^3)	1,761	0	0
SD Slate Lightweight Coarse Aggregate (lb/yd^3)	0	875	896
SSD Normalweight Fine Aggregate (lb/yd^3)	818	1,381	0
SD Slate Lightweight D Tank Fine Aggregate (lb/yd^3)	276	0	0
SD Slate Lightweight MS 16 Fine Aggregate (lb/yd^3)	0	0	945
Target Total Air Content (%)	5.5	5.5	5.5
Water-Cement Ratio (*w/c*)	0.42	0.42	0.42

Table 16-9: Internal curing mixtures with *w/c* of 0.36 and 0.30

Item	0.36 ICM	0.36 ICH	0.30 ICM	0.30 ICH
Water Content (lb/yd^3)	238	238	218	218
Cement Content (lb/yd^3)	677	677	738	738
SSD River Gravel Coarse Aggregate (lb/yd^3)	1,761	1,761	1,761	1,761
SD TXI Shale Fine Aggregate (lb/yd^3)	184	275	188	253
SSD Natural Sand (lb/yd^3)	956	823	940	867
Target Total Air Content (%)	5.5	5.5	5.5	5.5
Water-Cement Ratio (*w/c*)	0.36	0.36	0.30	0.30

16.4 Temperature Modeling

The temperature profile that an in-place concrete element experiences is a function of the geometry of the element, the concrete mixture proportions, the chemical composition of the cementing materials, the placement temperature, the thermal conductivity of the

aggregate, and environmental effects such as ambient temperature, wind speed, and incoming solar radiation.

To assess the effect of placement and curing temperature, the concrete modeling software ConcreteWorks (Poole et al. 2006) was used to determine the temperature profile that an 8-inch thick bridge deck constructed on stay-in-place metal forms would experience. Two placement scenarios were investigated: summer and fall conditions. Bridge deck temperatures for summer and fall placements were determined for Montgomery, Alabama on construction dates of August 15 and October 15, respectively. Semi-adiabatic calorimetry was used to determine the hydration parameters of each mixture (Schindler and Folliard 2005). Using the hydration parameters, as well as the placement date, city, bridge geometry, aggregate type, thermal diffusivity, mixture proportions, placement temperature, wind speed, ambient relative humidity, and percent cloud cover, two concrete temperature profiles were generated for each simulated placement season. Note that this practice captures the unique temperature profile that each mixture would experience due to its own heat of hydration and thermal properties should it be placed in an 8-inch thick bridge deck. The match-cured temperature profile used for each mixture is thus unique to that mixture.

The mixtures were tested at each of the temperature scenarios to evaluate the effect of placement temperature and curing temperature on time to initial cracking. When summer scenarios mixtures were tested, the raw materials were placed in an environmental chamber and conditioned to obtain fresh concrete temperatures of approximately 95 °F.

16.5 Test Methods

16.5.1 Restrained Stress Development

Each mixture was placed in the RCF and was match cured to a temperature profile developed to reflect the temperature profile of an 8-in. thick concrete bridge deck constructed under summer or fall placement conditions. The development of the temperature profile is discussed in Section 16.4. If the specimen had not cracked after 96 hours, the concrete was cooled at a rate of 1.8 °F/hr to induce cracking, which is also the practice used by Breitenbücher and Mangold (1994). Since the response of the specimen was still measured after cooling was started, this approach still allows one to assess the behavior of the concrete up until cracking occurs. The stress development of a specimen in the RCF cured under match-cured conditions is a function of its coefficient of thermal expansion, temperature history, modulus of elasticity, autogenous shrinkage, and relaxation.

16.5.2 Free-Shrinkage Frame

Each mixture was tested in the FSF and cured using the same match-cured temperature profile that was used for the RCF, as shown in Figure 16-1. The FSF captured the strain the concrete would experience if it was unrestrained. The strain measured is a function of autogenous shrinkage, coefficient of thermal expansion, and temperature history of the concrete.

16.5.3 Mechanical Properties

For each mixture and placement scenario, twenty-four 6 × 12 in. cylinders were cast as per ASTM C 192. The cylinders were match cured using the same temperature history as the RCF and the FSF, as shown in Figure 16-1. The cylinders were tested for compressive strength, splitting tensile strength, and modulus of elasticity as per ASTM C 39, ASTM C 496, and ASTM C 469, respectively at ½ , 1, 2, 3, 7, and 28 days. Two cylinders were first tested to determine the splitting tensile strength of the concrete. From the splitting tensile strength, 40 % of the compressive strength was estimated, which was used for modulus of elasticity testing. The same two cylinders used for modulus of elasticity testing were used for compressive strength testing. After the modulus of elasticity testing was completed, the two cylinders were then tested to failure to determine the compressive strength of the concrete. In no instance was the upper load limit used for modulus of elasticity testing greater than 40 % of the actual compressive strength of the tested sample.

16.6 Early-Age Compliance Modeling with the B3 Model

Using the equivalent-age maturity function, modeled temperature history, and the activation energies calculated from the cement composition (Schindler 2004a), the free-shrinkage frame, rigid cracking frame, and mechanical property results were corrected for curing temperature effects. Activation energy of 41,520 J/mol and reference temperature of 276 °K (73°F) were used as maturity function constants.

An illustration of the compatibility of a cross-section of the rigid cracking frame and a concrete specimen in *tension* is shown in Figure 16-2. As the concrete in the RCF undergoes a temperature decrease the combined thermal strain (ε_T), and autogenous strain

(ε_A) are restrained, which leads to strain in the RCF (ε_{RCF}). The amount of strain in the RCF will be a function of the concrete area to side bar area ratio, and concrete stiffness to side bar stiffness ratio. Using the sign convention where tensile elongation is positive and compressive contraction is negative, the resulting strain of the concrete specimen will be the sum of the thermal and autogenous effects minus the strain in the RCF. Therefore, the stress captured by the RCF is a function of the thermal strain (ε_T), autogenous strain (ε_A), the strain of the RCF specimen (ε_{RCF}), and the amount of relaxation.

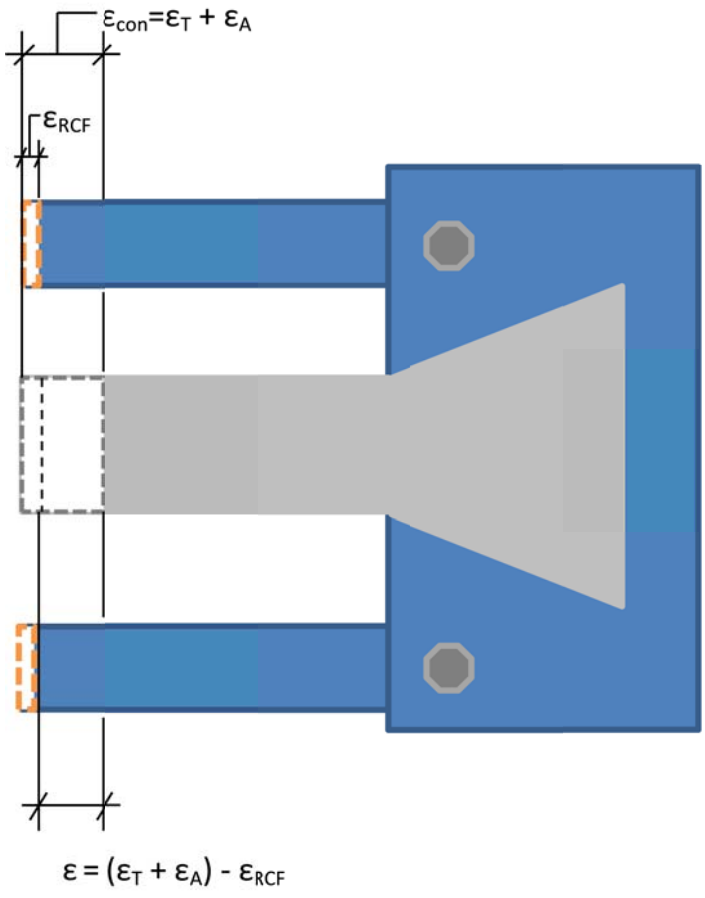

Figure 16-2: Rigid cracking frame compatibility

The strain captured by the FSF (ε_{FSF}) is the combined thermal (ε_T) and autogenous (ε_A) strains as expressed in Equation 16-1. Because the RCF was not fully restrained, the RCF concrete specimen experiences some strain and this strain was captured by the strain gauges on the side bars. If the frame was fully restrained, Equation 15-20 would be equal to zero; however because it is not, Equation 15-20 can be written as Equation 16-2. Where, ε_{RCF} is negative because it is a contraction. Rearranging Equation 16-2, and realizing that ε_0 is equal to the strain in the FSF (ε_{FSF}), Equation 16-2 can be written as Equation 16-3. Realizing that the elastic response (1/E), the viscoelastic response, and the plastic flow response is captured by the compliance term of the B3 Model, Equation 16-3 can be further simplified into Equation 16-4 to calculate the stress development.

$$\varepsilon_{FSF} = \varepsilon_T + \varepsilon_A \quad \text{..... Equation 16-1}$$

where

ε_{FSF} = strain measured from the free-shrinkage frame (in./in.),

ε_T = strain due to thermal effects (in./in.), and

ε_A = strain due to autogenous effects (in./in.).

$$-\varepsilon_{RCF} = \frac{\sigma}{E_0} + \varepsilon_v + \varepsilon_f + \varepsilon_0 \quad \text{..... Equation 16-2}$$

where $\frac{\sigma}{E_0}$ = the instantaneous elastic response,

ε_v = the viscoelastic response,

ε_f = the plastic flow, and

ε_0 = strain due to thermal dilation, drying, and cracking.

$$-\varepsilon_{RCF} = \sigma \frac{1}{E_0} + \varepsilon_v + \varepsilon_f + \varepsilon_{FSF} \quad \text{Equation 16-3}$$

$$\sigma = \frac{\varepsilon_{FSF} - \varepsilon_{RCF}}{J(t,t_0)} \quad \text{Equation 16-4}$$

where

σ = calculated stress development (psi), and

ε_{RCF} = strain of the rigid cracking frame specimen (in./in.).

$J(t, t_0)$ = compliance function (1/psi).

Compliance is a function of time (t) and time at loading (t_0). The compliance function was calculated using the B3 Model and loading ages in one-hour steps as a function of time until the stress-to-strength ratio of 70 % was reached. At stress-to-strength ratios above 70 % the response becomes non-proportional; thus, superposition becomes invalid (Neville et al. 1983). With the compliance function known in one-hour loading age increments, the compliance term is a function of only time. An illustration of the compliance functions for different loading ages, as a function of time, are shown in Figure 16-3. The effect of different time step lengths is investigated in the following chapter. Starting at initial set, the free-shrinkage frame results were discretized into the change in strain over one-hour time steps ($\Delta\varepsilon_{FSF}$). The strain of RCF concrete specimen measured from the side bar strain gages were also determined over the same one-hour time step ($\Delta\varepsilon_{RCF}$). The total change in strain over the one-hour time step is the change in FSF strain ($\Delta\varepsilon_{FSF}$) minus the change in RCF strain ($\Delta\varepsilon_{RCF}$), as expressed in Equation 16-5. The strain change increments were divided by the compliance function for that loading

age, to determine the stress response as a function of time for each strain increment. Using the principle of superposition, the response of all the strain increments were calculated by summing the response of the strain increments at a time and those previously as illustrated in Figure 16-4 and expressed in Equation 16-6.

$$\Delta\varepsilon(t_0) = \Delta\varepsilon_{FSF} - \Delta\varepsilon_{RCF} \quad \text{..... Equation 16-5}$$

$$\sigma(t_n) = \sum\left[\frac{\Delta\varepsilon(t_{0,1})}{J(t_n,t_{0,1})} + \frac{\Delta\varepsilon(t_{0,2})}{J(t_n,t_{0,2})} + \cdots + \frac{\Delta\varepsilon(t_{0,n})}{J(t_n,t_{0,n})}\right] \quad \text{..... Equation 16-6}$$

where $\sigma(t_n)$ = stress at time n (psi),

$J(t_n, t_{0,1})$ = compliance function at time *n* for loading at time one (1/psi), and

$\Delta\varepsilon(t_{0,1})$ = one hour strain increment at time one from the free-shrinkage frame (in./in.).

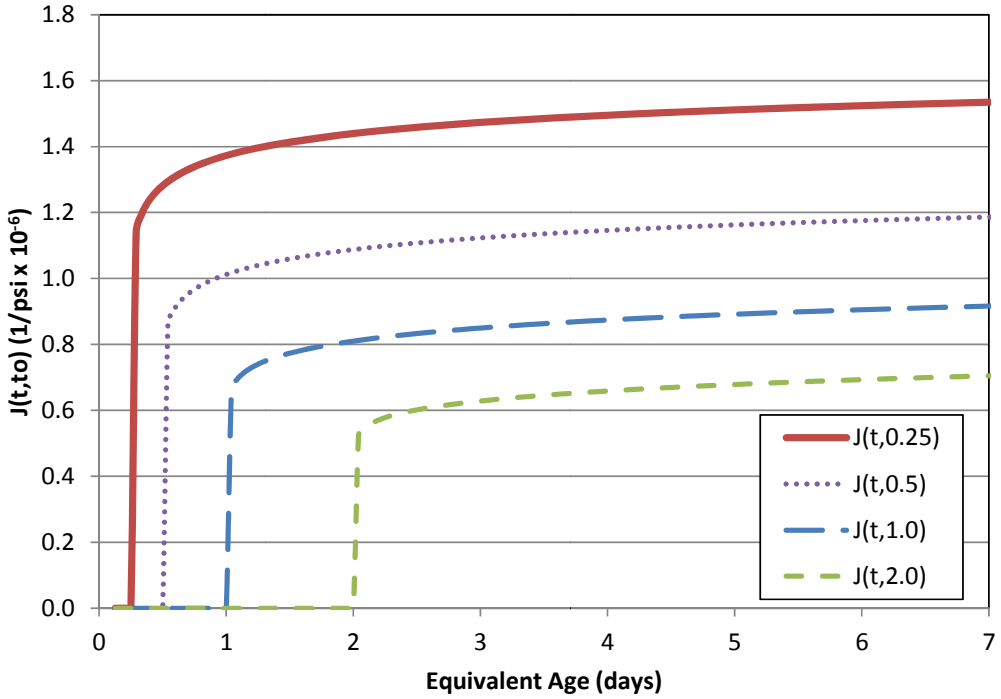

Figure 16-3: Calculated compliance function for various loading ages as a function of time

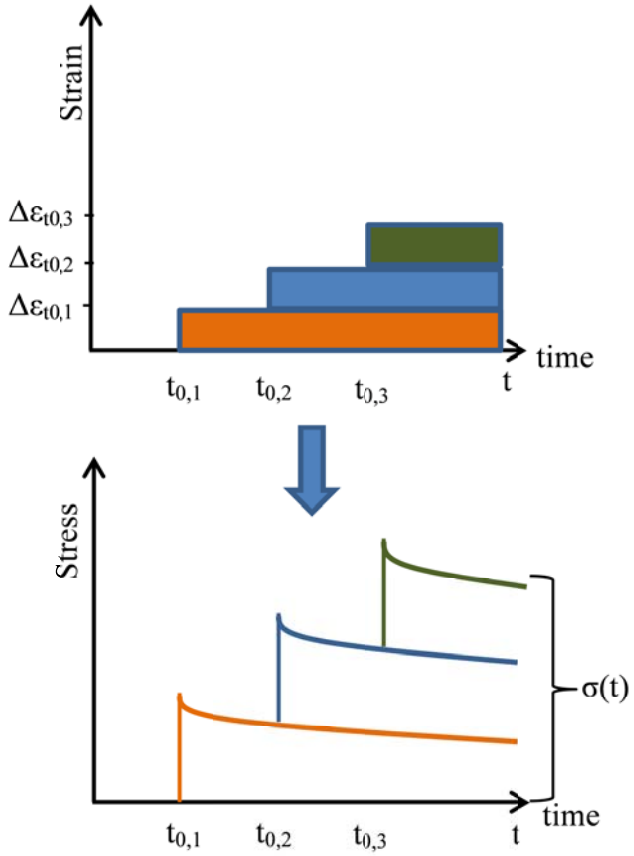

Figure 16-4: Illustration of superposition of stress relaxation

CHAPTER 17

PART III: EXPERIMENTAL RESULTS

The results collected from the experimental work performed for this part are presented in this chapter. A discussion of the results and a method to improve the predictions of the B3 Model is presented in Sections 18.1 and 18.2, respectively. The modified B3 Model results and a discussion of the findings are presented in Sections 18.3 and 18.4, respectively. The effect of density, water-cement ratio, and curing temperature on relaxation using the Modified B3 Model is shown in Section 18.5. A sensitivity analysis of the modification parameters is provided in Section 18.6. A simplified modified B3 Model is proposed and discussed in Section 18.7. A summary of the work performed in this part and conclusions are provided in Chapter 19.

The complete temperature profile, rigid cracking frame, and free-shrinkage results can be seen in Parts I and II. Results that represent typical behavior are presented in this part.

17.1 Curing Temperatures

The temperature modeling results for the slate mixtures with *w/c* of 0.42 for the fall and summer placement scenarios are shown in Figure 17-1. The results are shown in terms of

actual age and are truncated at the time of cracking. These results are typical for the other types of lightweight aggregate concrete.

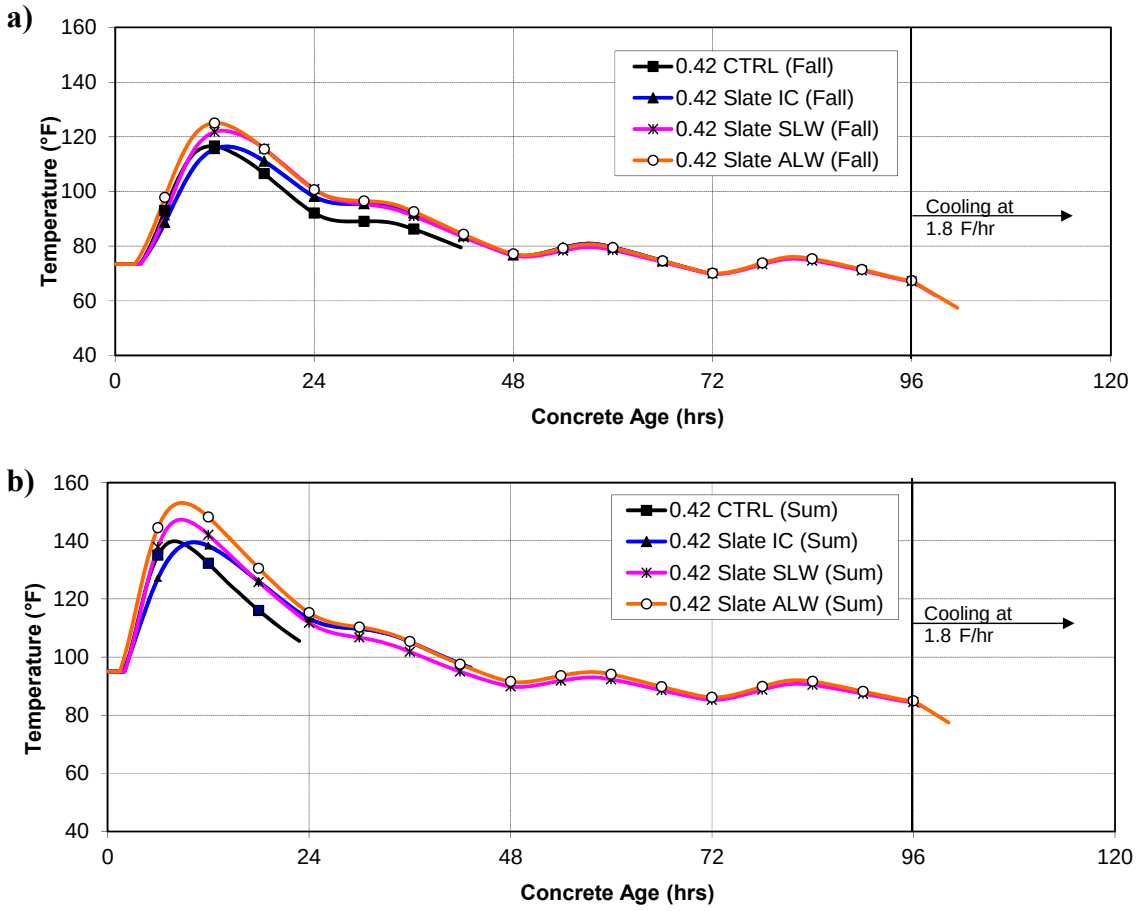

Figure 17-1: Modeled temperature profiles of slate lightweight mixtures and normalweight mixtures for a) fall and b) summer placement scenarios

17.2 Rigid Cracking Frame Results

The rigid cracking frame results for the normalweight and slate lightweight mixtures with *w/c* of 0.42 for the fall and summer placement scenarios are shown in Figure 17-2. The data are truncated after cracking. Only the slate data are shown; however, the behavior of the other aggregate sources is similar and can be viewed in Parts I and II.

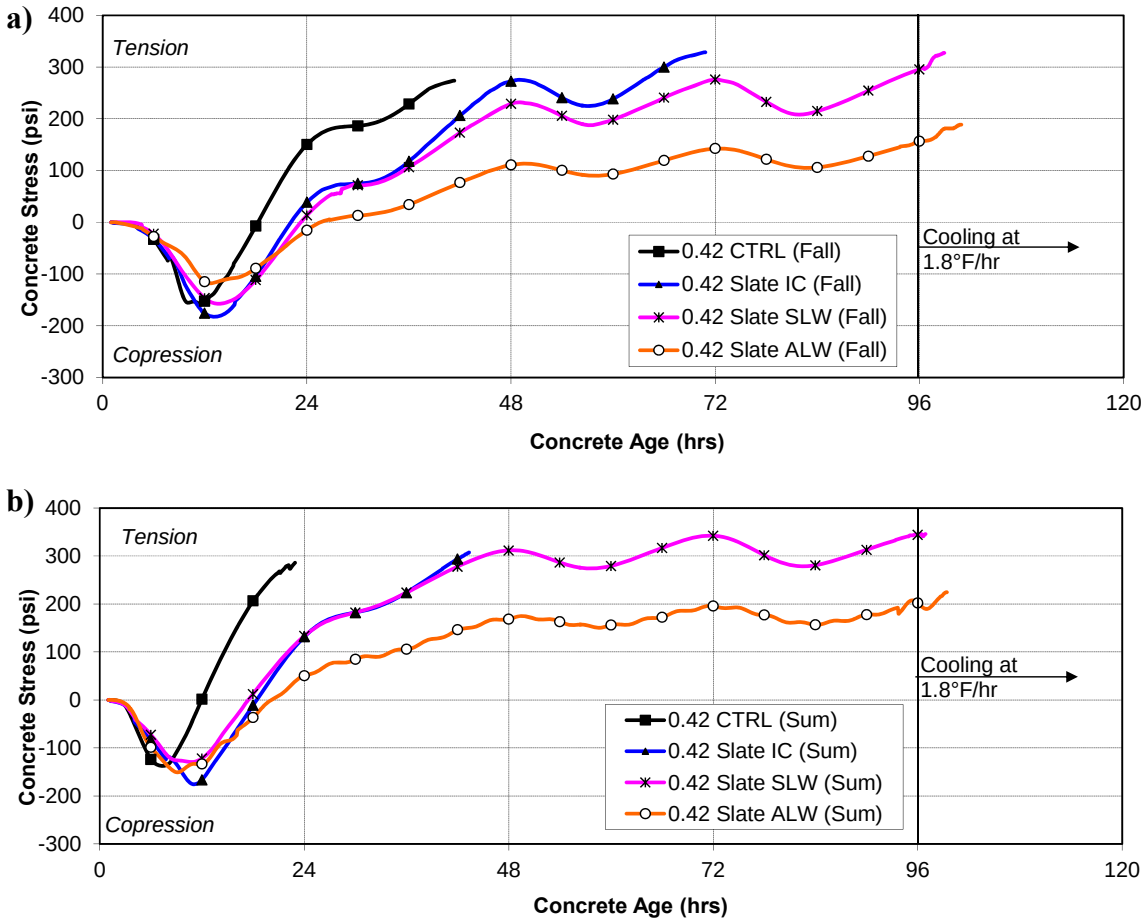

Figure 17-2: Rigid cracking frame results of slate lightweight mixtures normalweight mixtures for a) fall and b) summer placement scenarios

17.3 Free-shrinkage frame Results

The free-shrinkage frame results for the normalweight and slate lightweight mixtures with *w/c* of 0.42 for the fall and summer placement scenarios are shown in Figure 17-3. The data are truncated at the time of cracking and start at the initial set time of each mixture.

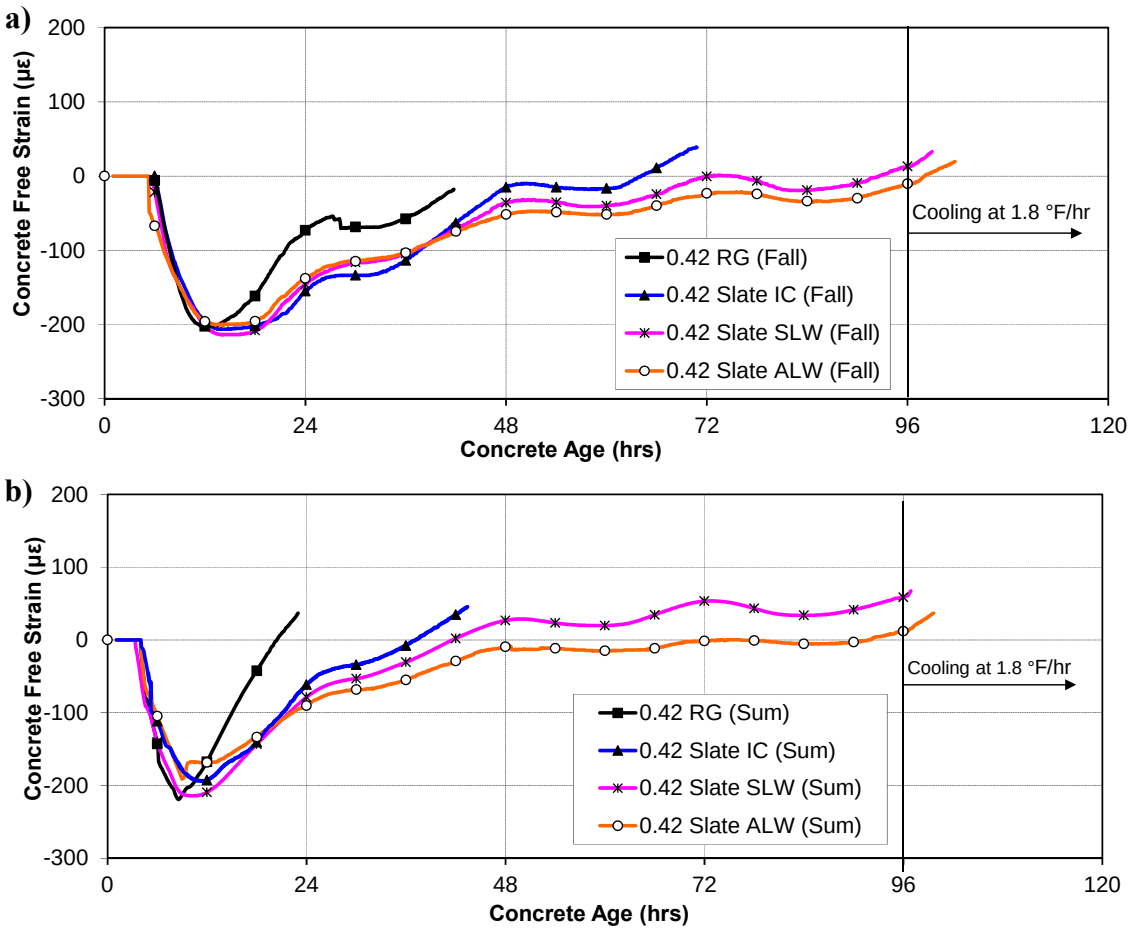

Figure 17-3: Free-shrinkage frame results of expanded slate lightweight mixtures and normalweight mixtures for a) fall and b) summer placement scenarios

17.4 Mixture Properties

Two batches were required for each mixture due to the size of the laboratory concrete mixer. The first batch was for the rigid cracking frame and free-shrinkage frame specimens and the second batch was for the cylindrical specimens for mechanical property development testing. The results of the slump, total air content, and density of the mixtures with river gravel and expanded slate aggregates are presented in Table 17-1. The coefficient of thermal expansion (CTE) test was only performed on samples from the mixtures with fall placement scenarios and is summarized in Table 17-1.

Table 17-1: Fresh and hardened test results of mixtures with normalweight and expanded slate aggregate and *w/c* of 0.42

Mixture and Placement Scenario	Batch No.	Fresh Concrete Test Results				Hardened CTE (με/°F)
		Slump (in.)	Temp. (°F)	Air (%)	Density (lb/ft^3)	
0.42 RG (Fall)	1	3.25	74	5.00	143.8	6.2
	2	4.50	73	6.25	141.9	
0.42 RG (Sum)	1	2.50	100	4.75	143.0	-
	2	2.00	100	5.25	141.9	
0.42 Slate IC (Fall)	1	3.25	74	5.75	137.8	5.9
	2	3.50	75	5.75	138.6	
0.42 Slate IC (Sum)	1	2.00	97	4.50	140.6	-
	2	2.50	97	4.75	140.1	
0.42 Slate SLW (Fall)	1	3.50	74	4.50	119.0	5.1
	2	3.75	74	4.50	119.2	
0.42 Slate SLW (Sum)	1	2.00	97	4.25	119.8	-
	2	2.50	95	4.25	120.0	
0.42 Slate ALW (Fall)	1	5.00	70	5.00	104.0	4.3
	2	4.50	68	5.25	103.8	
0.42 Slate ALW (Sum)	1	2.25	92	4.50	104.3	-
	2	2.50	95	4.25	104.8	

17.5 Mechanical Property Development

The compressive strength, splitting tensile strength, and modulus of elasticity development were measured by testing cylinders match cured to the bridge deck temperature profile for each mixture and placement scenario. A regression analysis was performed on the discrete data points with the exponential function recommended by ASTM C 1074. The resulting best-fit curves for each property are shown in Figure 17-4 and Figure 17-5 for fall and summer placement scenarios, respectively. The average of the two test cylinders for each mechanical property is summarized in Appendix B.

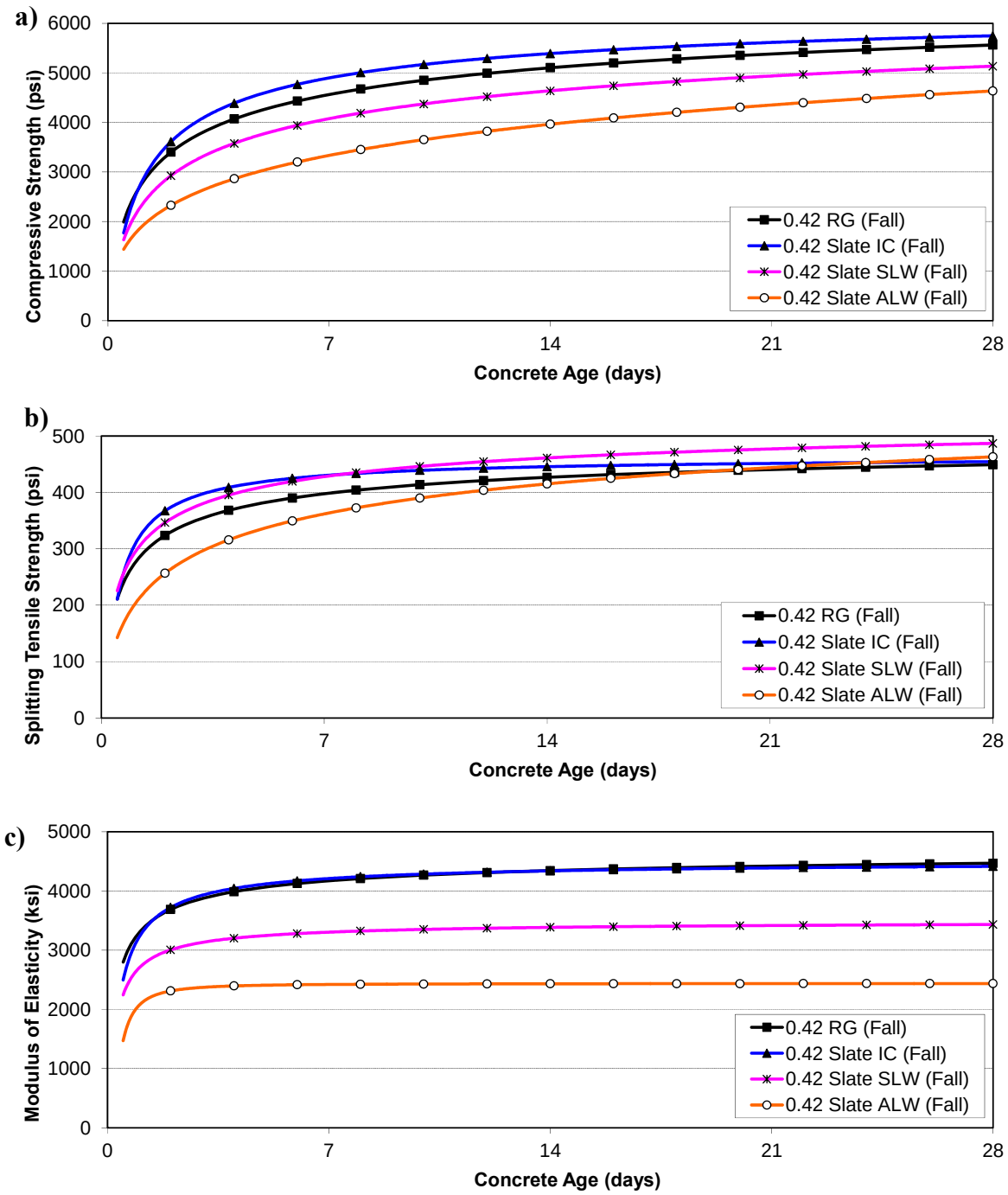

Figure 17-4: Fall placement scenario a) compressive strength, b) modulus of elasticity, and c) splitting tensile strength of 0.42 *w/c* normalweight and expanded slate lightweight aggregate mixtures.

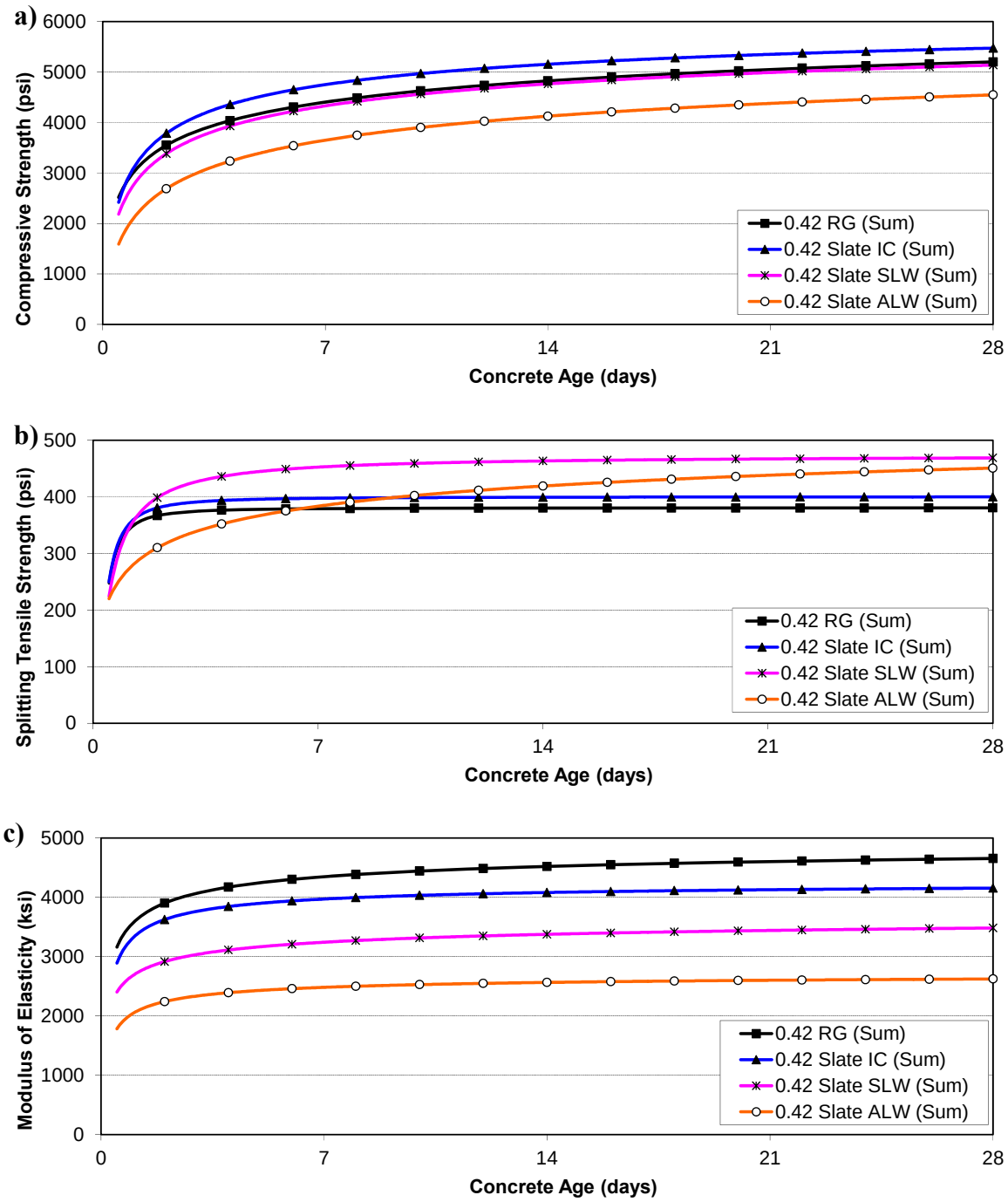

Figure 17-5: Summer placement scenario a) compressive strength, b) modulus of elasticity, and c) splitting tensile strength of normalweight and expanded slate lightweight aggregate mixtures.

17.6 B3 Model Results

The stress development from the B3 compliance model using the free-shrinkage data and the measured stress development in terms of equivalent age for the 0.42 LS (Fall) mixture are shown in Figure 17-6. The splitting tensile strength development was scaled by a factor equal to the ratio of stress measured at cracking to the cylinder splitting tensile strength at the same equivalent age. This was done so that the stress development and strength development coincide at cracking. For example, the cracking stress for the 0.42 LS (Fall) mixture was 379 psi at 6.1 days of equivalent age. The splitting tensile strength at 6.1 days of equivalent age was 429 psi. Thus, the splitting tensile strength development was scaled by 0.88 to determine the strength development relative to the stress at cracking. The scaled tensile strength development is shown in Figure 17-6.

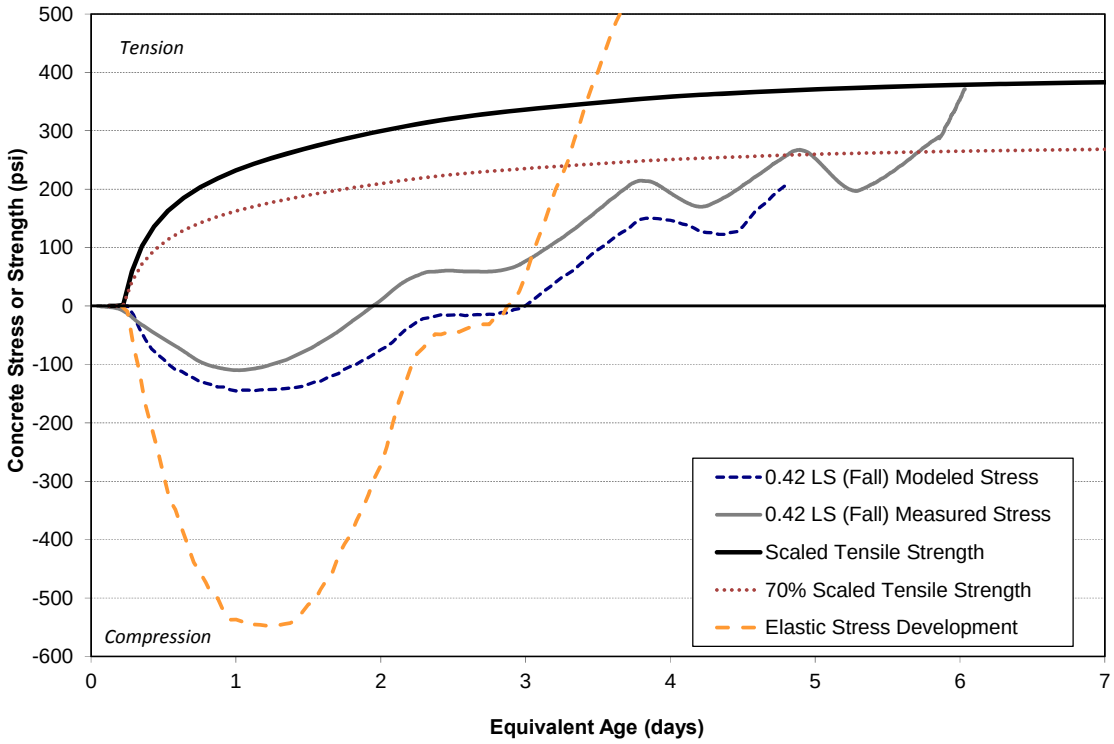

Figure 17-6: B3 Modeled stress development, measured stress development, elastic stress development, and scaled strength of 0.42 LS (Fall) mixture

The data in Figure 17-6 shows the modeled stress development truncated when the measured stress development reaches the scaled stress-to-strength ratio of 70 %. To illustrate the stress development without relaxation effects, the elastic stress development is also shown in the figure. The data illustrates that the modeled stress development using only elastic effects would be significantly inaccurate compared to measured stress development.

The stress predictions with the unmodified B3 Model for the fall placement scenario for the 0.42 RG, 0.42 LS, 0.42 Slate IC, 0.42 Slate SLW, and 0.42 Slate ALW mixtures can be seen in Figure 17-7 to Figure 17-11. The data are truncated when the measured stress reaches 70 % of the stress-to-scaled-strength ratios. This approach was used due to the significant nonlinear behavior of concrete at higher stress to strength ratios which is not accounted for in the B3 model. The 70 % stress to scaled strength ratio is illustrated in Figure 17-6 for the 0.42 LS (Fall) mixture. The measured and the B3 Model's predicted stress developments are generally parallel and offset; however, above 70 % the measured and modeled stress begin to converge due to the additional nonlinear behavior of the measured stress shown in Figure 17-6.

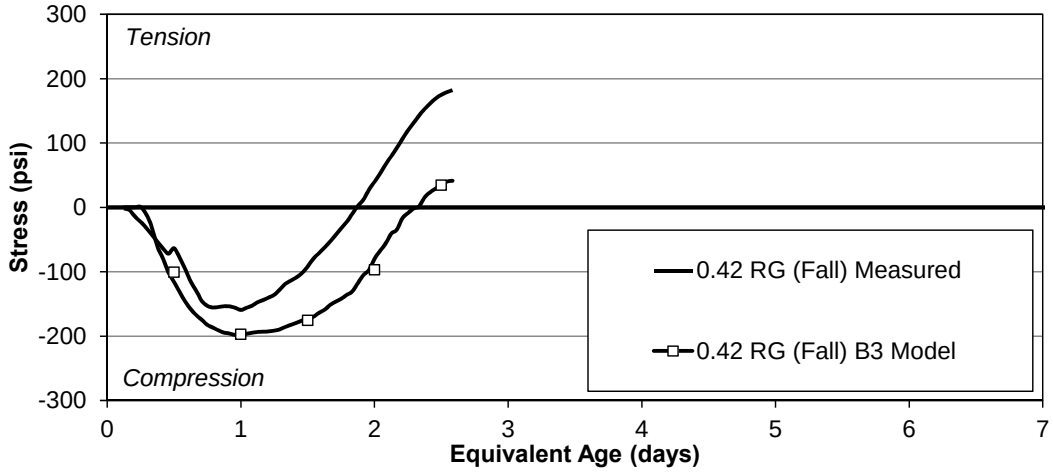

Figure 17-7: B3 Modeled and measured stress development for the 0.42 RG (Fall) mixture

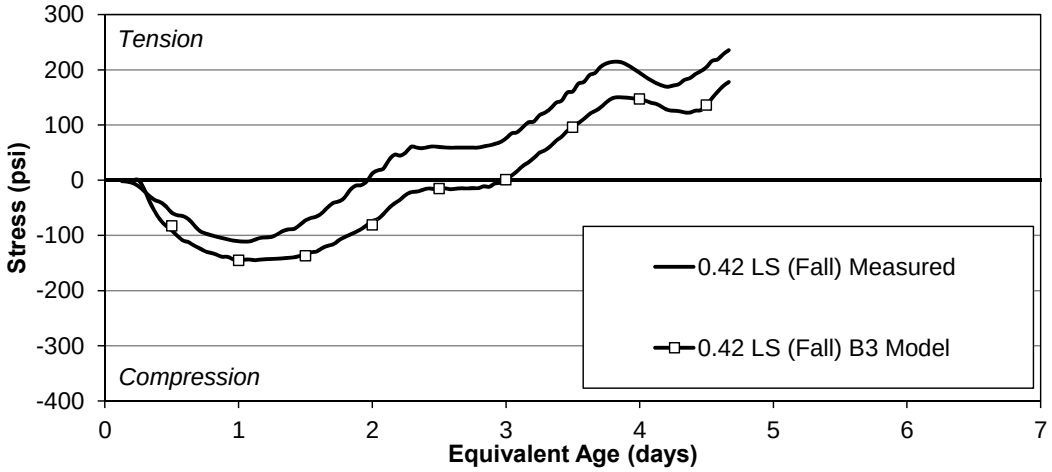

Figure 17-8: B3 Modeled and measured stress development for the 0.42 LS (Fall) mixture

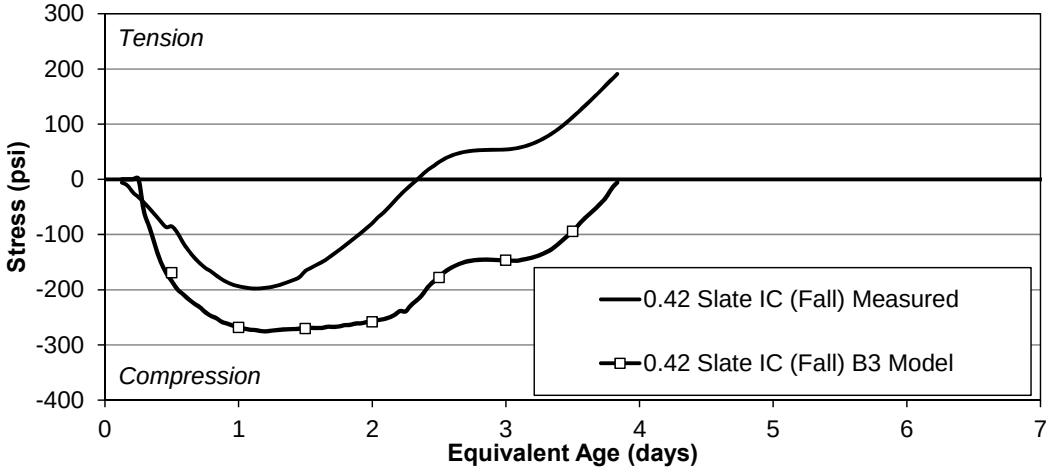

Figure 17-9: B3 Modeled and measured stress development for the 0.42 Slate IC (Fall) mixture

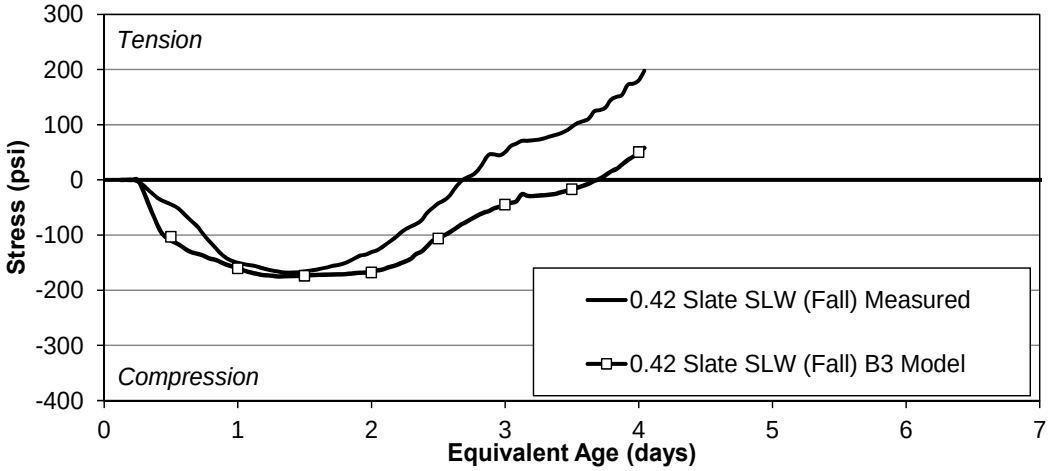

Figure 17-10: B3 Modeled and measured stress development for the 0.42 Slate SLW (Fall) mixture

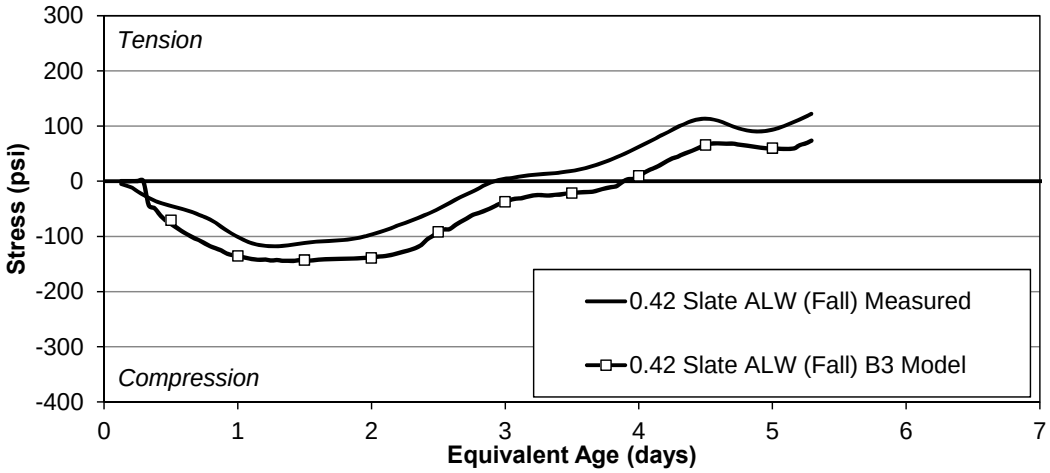

Figure 17-11: B3 Modeled and measured stress development for the 0.42 Slate ALW (Fall) mixture

CHAPTER 18

DISCUSSION OF RESULTS AND DEVELOPMENT OF THE MODIFIED B3 MODEL

The stress predictions obtained with the B3 Model are discussed in Section 18.1. Based on the ability of the B3 Model to predict the measured stress, modifications to the B3 Model were made to more accurately predict the early-age behavior, which is discussed in Section 18.2. The stress predictions using the resulting Modified B3 Model are presented in Section 18.3. This is followed by a discussion of the results in Section 18.4. Using the Modified B3 Model, the effect of density, and *w/c* on relaxation are investigated and discussed in Section 18.5. A sensitivity analysis of the Modified B3 Model is performed and discussed in Section 18.6. A simplified method to find the constants for the Modified B3 Model is proposed in Section 18.7.

18.1 Discussion of B3 Model Results

The B3 Model generally overpredicts the early-age *compressive* stress development caused by early-age hydration as shown in Figure 17-7 to Figure 17-11. This is because the model was not calibrated or designed to predict the behavior of concrete before one day, which is the period where the modulus of elasticity is rapidly changing and the concrete behavior is highly viscoelastic. This lack of calibration at early ages leads to an

inaccurately early-age elastic and viscoelastic response. The lack of the B3 Model's ability to account for early-age compressive stress lead to higher than measured compressive stress development, and this in turn caused a delay in the predicted time at zero-stress and lower tensile stress development.

The measured stress development versus B3 Model stress development for all mixtures at one-hour increments are plotted in Figure 18-1, where a negative value is a compressive stress and a positive value is a tensile stress. Because concrete starts behaving nonlinearly at higher stress to strength ratios, the data points that were above 70% stress to scaled strength were omitted from Figure 18-1. The figure illustrates that because the B3 Model overpredicts the compressive stress development and underpredicts the tensile stress development, most of the data points are below the line of equality.

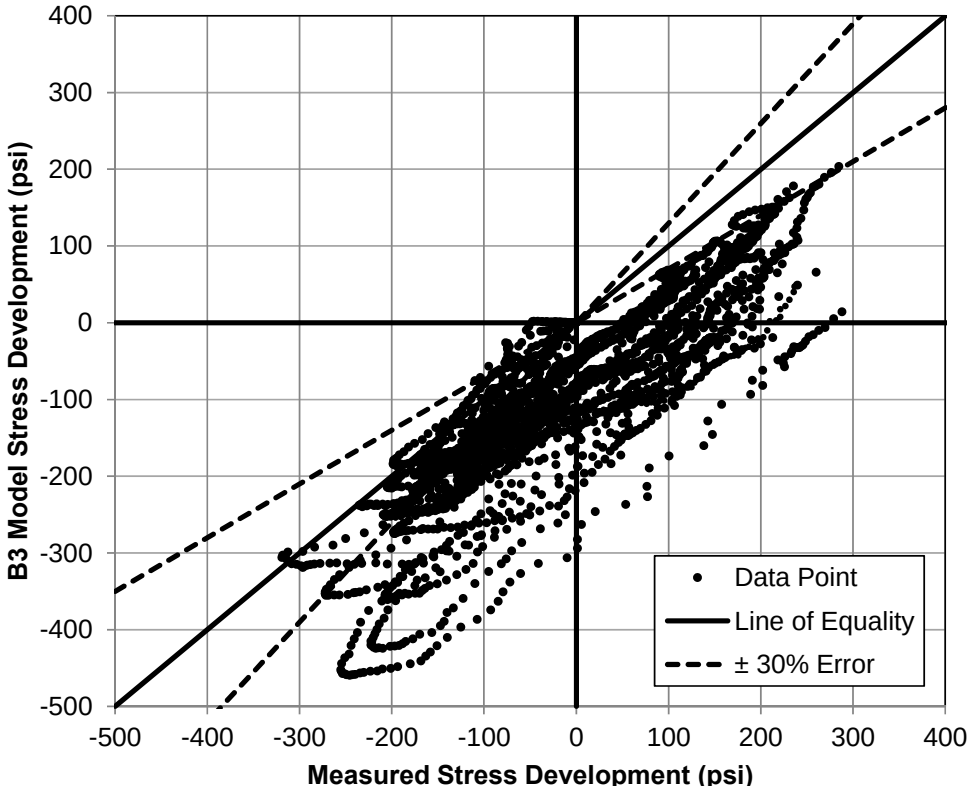

Figure 18-1: Measured versus modeled stress development for unmodified B3 Model

The coefficient of determination (r^2) of the modeled and measured stress development was calculated for each mixture. The coefficient of determination is expressed in Equation 18-1 (Scheaffer et al. 2010). The coefficient of determination is a way to quantify the goodness of fit of a predicted data set to a measured data set, where 1.0 is a perfect fit. The unbiased estimate of the standard deviation of the absolute error (S_j), shown in Equation 18-2 (McCuen 1985), was also calculated for the stress development of the B3 Model prediction and the measured stress. When the measured stress reached a stress to scaled strength ratio of 70%, the data were truncated. The r^2 and S_j of the mixtures are shown in Table 18-1. The measured free-strain data from the 0.42 Clay ALW (Sum), 0.42 Shale SLW (Fall), and 0.42 Shale ALW (Fall) mixtures were determined to be erroneous, so they were omitted from the analysis. The r^2 and S_j of all of the data collected give a measure of how well the B3 Model predicts the measured stress.

$$r^2 = 1 - \frac{SS_{err}}{SS_{tot}} \quad \text{Equation 18-1}$$

where r^2 = coefficient of determination (unitless),

SS_{err} = sum of the squared error = $\sum(y_i - f_i)^2$,

SS_{tot} = sum of squares total = $\sum(y_i - \bar{y})^2$,

y_i = predicted value (psi),

$\bar{y}$ = mean observed data (psi), and

f_i = observed data (psi).

$$S_j = \sqrt{\frac{1}{n-1}\sum_i^n \Delta_i^2} \quad \text{Equation 18-2}$$

where S_j = unbiased estimate of the standard deviation (psi),

n = number of data points (unitless), and

Δ_i = absolute error (psi).

Table 18-1: The coefficient of determination and unbiased estimation of standard deviation for the B3 Model's predicted stress compared to measured stress

Mixture	Placement Scenario	Coefficient of Determination, r^2	Unbiased Estimation of Standard Deviation of Absolute Error, S_j (psi)
		Original B3 Model	Original B3 Model
0.42 RG	Fall	0.21	88
	Summer	0.33	89
0.42 LS	Fall	0.77	61
	Summer	0.75	140
0.42 Slate IC	Fall	-0.53	160
	Summer	0.73	66
0.42 Slate SLW	Fall	0.45	73
	Summer	0.53	78
0.42 Slate ALW	Fall	0.72	41
	Summer	0.90	43
0.42 Clay IC	Fall	0.01	110
	Summer	0.58	75
0.42 Clay SLW	Fall	-0.3	85
	Summer	0.61	109
0.42 Clay ALW	Fall	-0.97	93
0.42 Shale IC	Fall	-0.55	23
	Summer	0.83	132
0.42 Shale SLW	Summer	-0.26	117
0.42 Shale ALW	Summer	0.88	43
0.36 RG	Fall	0.49	123
0.36 ICM	Fall	0.45	106
0.36 ICH	Fall	-0.02	153
0.30 RG	Fall	0.43	126
0.30 ICM	Fall	-0.65	241
0.30 ICH	Fall	0.17	182
Total Data		**0.25**	**107**

The r^2 value of 0.25 for all the data indicates that 25 % of the sum of the squares of the deviation of the predicted values, about their mean, is attributable to the relation between the measured and predicted stress (Scheaffer et al. 2010). The S_j of 101 psi for all of the collected data indicates a relatively large standard deviation in error between the predicted stress of the B3 Model and the measured stress development.

18.2 Development of the Modified B3 Model

As discussed in Section 18.1, the B3 Model underestimates the amount of early-age relaxation and overestimates the early-age elastic response, thus causing an increase in predicted compressive stress at early ages and reduced tensile stress at later ages. Others have suggested this is due to a lack of early-age viscoelastic response (Østergaard et al. 2001). However, early-age concrete exhibits both high viscoelastic properties and rapidly changing elastic properties (Emborg 1989). The elastic response of the B3 Model is treated as a constant equal to the asymptotic modulus of elasticity, which Bažant estimates as the 28-day modulus of elasticity divided by 0.6 as shown in Equation 15-19. This may be acceptable for sufficiently hardened concrete; however the modulus of elasticity at early ages is changing rapidly (Emborg 1989; Westman 1999). The elastic modulus for the 0.42 LS is shown versus the asymptotic modulus used in the B3 Model in Figure 18-2. Using the asymptotic modulus of elasticity leads to falsely high early-age stress predictions because the actual elastic response is much less. Because of this, the function developed by Østergaard et al. (2001) was used to adjust the B3 Model's lack of viscoelastic response and a correction of the same mathematical form was used to modify the elastic properties. The early-age viscoelastic modification developed by Østergaard et

al. (2001) and the proposed early-age elastic modification are shown in Equations 18-1 and 18-2, respectively. Both modified responses will decrease the stress development that results from an early-age loading.

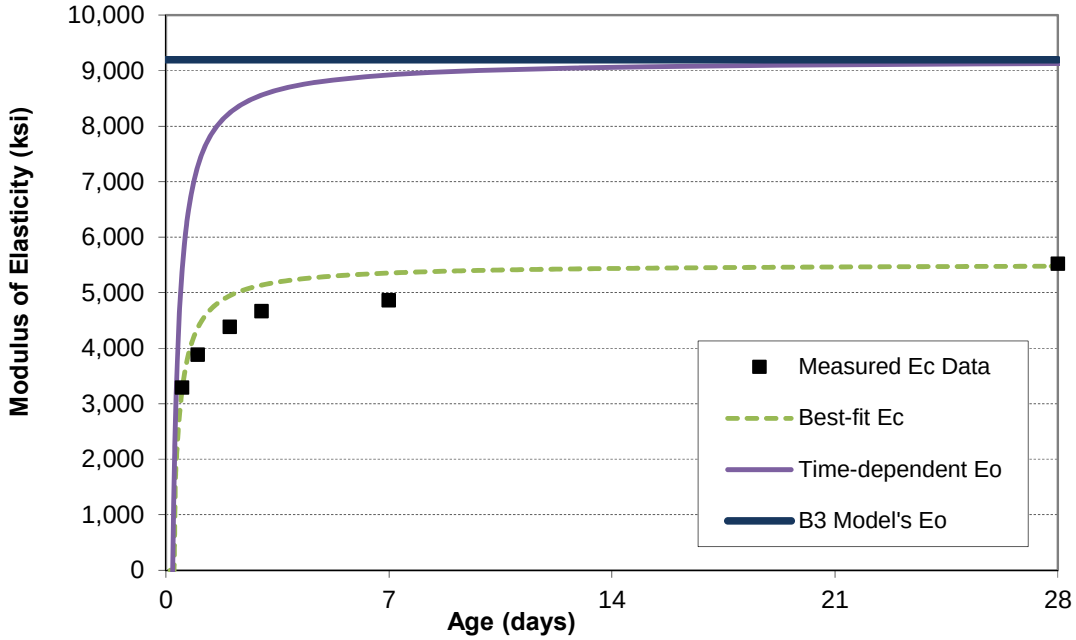

Figure 18-2: Illustration of modifications made to the elastic behavior of the B3 Model for 0.42 LS mixture

$$q_2' = q_2\left[\frac{t_0}{t_0 - q_5}\right] \quad \text{..... Equation 18-1}$$

$$q_1' = q_1\left[\frac{t_0}{t_0 - q_6}\right] = \frac{0.6}{E_{c,28}}\left[\frac{t_0}{t_0 - q_6}\right] \quad \text{..... Equation 18-2}$$

where q_1' = modified elastic compliance (1/psi),

q_2' = modified aging viscoelastic compliance (1/psi),

q_5 = factor for early-age viscoelastic behavior (days), and

q_6 = factor for early-age elastic behavior (days).

Similar to q_5, q_6 cannot be greater than the setting time because the response approaches infinity when the loading age (t_0) equals q_6. A modification in the form of Equations 18-1 and 18-2 quickly diminishes leaving the model virtually unchanged at later ages. If the elastic and creep terms of the B3 Model as expressed in Equations 15-18 and 15-19 are combined and drying effects are omitted, then the B3 Model can be expressed as Equation 18-3. Then, the modified B3 Model can be expressed as Equation 18-4.

$$J(t,t_0) = q_1 + q_2 Q(t,t_0) + q_3 \ln(1 + (t - t_0)^n) + q_4 \left(\frac{t}{t_0}\right) \text{..... Equation 18-3}$$

where q_1 = Elastic compliance = $\frac{0.6}{E_{c,28}}$ (1/psi),

$q_2 Q(t,t_0)$ = Aging viscoelastic compliance (1/psi),

$q_3 \ln(1 + (t - t_0)^n)$ = Non-aging viscoelastic compliance (1/psi), and

$q_4 \left(\frac{t}{t_0}\right)$ = Plastic flow compliance (1/psi).

$$J(t,t_0) = q_1 \left[\frac{t_0}{t_0 - q_6}\right] + q_2 \left[\frac{t_0}{t_0 - q_5}\right] Q(t,t_0) + q_3 \ln(1 + (t - t_0)^n) + q_4 \left(\frac{t}{t_0}\right) \text{ ..Equation 18-4}$$

where q_5 = age factor for early-age viscoelastic behavior in equivalent age (days), and

q_6 = age factor for early-age elastic behavior in equivalent age (days).

The effect of increasing q_6 on the elastic component of compliance (q_1') is shown in Figure 18-3. Increasing q_6 results in a greater elastic component of compliance at early ages; and at later ages, approached the unmodified elastic compliance component. The stress predicted from increased elastic component of compliance will be reduced compared to the unmodified elastic compliance component. The effect of increasing q_5 on

the modified age-dependent viscoelastic component of compliance [q_2' $Q(t,t_0)$]is shown in Figure 18-4. Increasing q_5 leads to increased viscoelastic response, which leads to more stress being relaxed and reduced predicted stress when compared to the unmodified viscoelastic response.

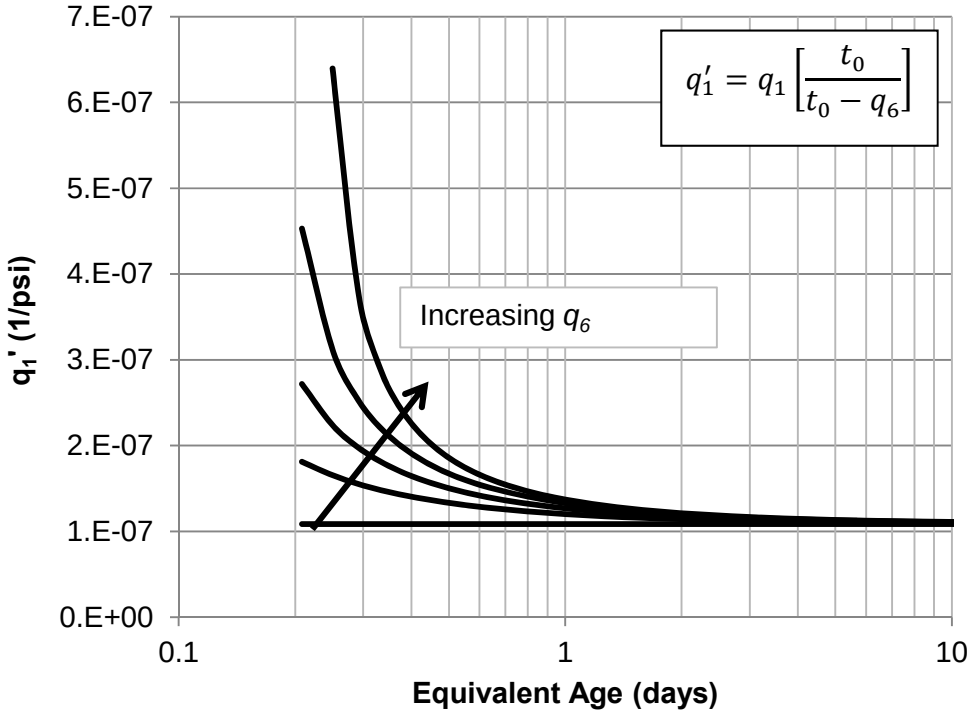

Figure 18-3: Effect of increasing q_6 on modified elastic response

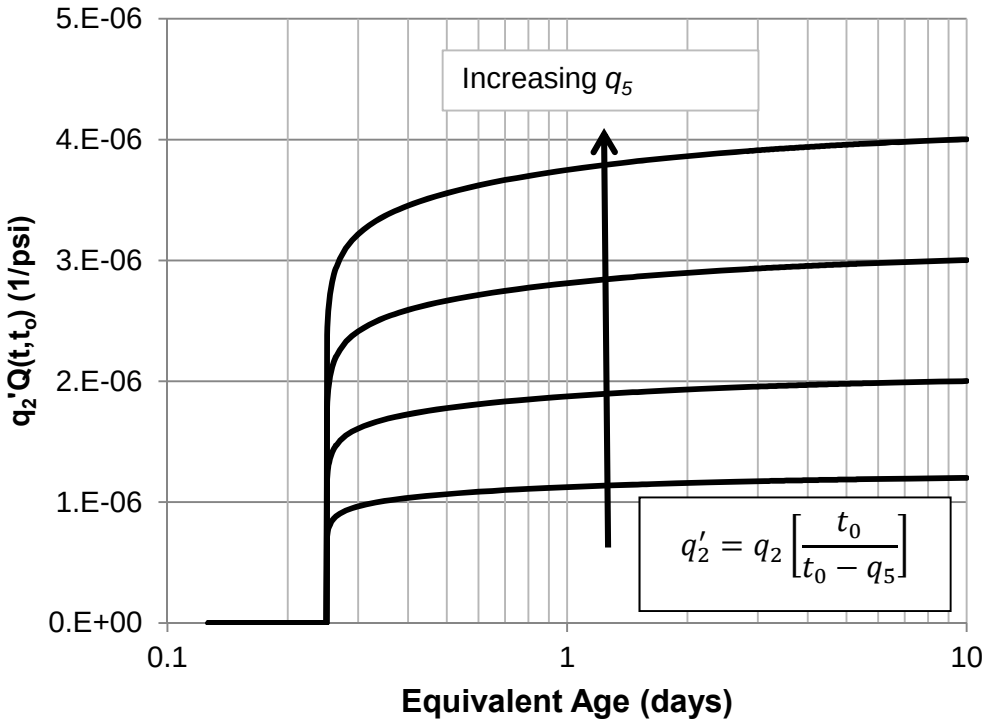

Figure 18-4: Effect of increasing q_5 on the modified viscoelastic response

The effect of the new q_1' and q_2' on compliance [$J(t,t_0)$] is shown in Figure 18-5. The unmodified compliance at a loading age of 0.25 days [$J(t,0.25)$] and 2.0 days [$J(t,2.0)$] as a function of equivalent age are shown in this figure. For this illustration, the modifiers q_5 and q_6 were both set equal to the time just before initial set in equivalent age, which is their maximum allowable value. The effect on compliance of only the viscoelastic response modified (q_2') and then both viscoelastic (q_2') and elastic modification (q_1') are shown. At the 0.25-day loading age, the effects of the modifications on compliance are significant, whereas the effect on the 2-day loading is insignificant as shown in Figure 18-5. The effect of the viscoelastic modification is greater than the effect of only the elastic modification. The change in response provided by the q_1' adjustment decreases the elastic stress development. The change in response provided by the q_2'

adjustment increases the stress relaxation. Both modified responses will decrease the stress development that results from an early-age loading.

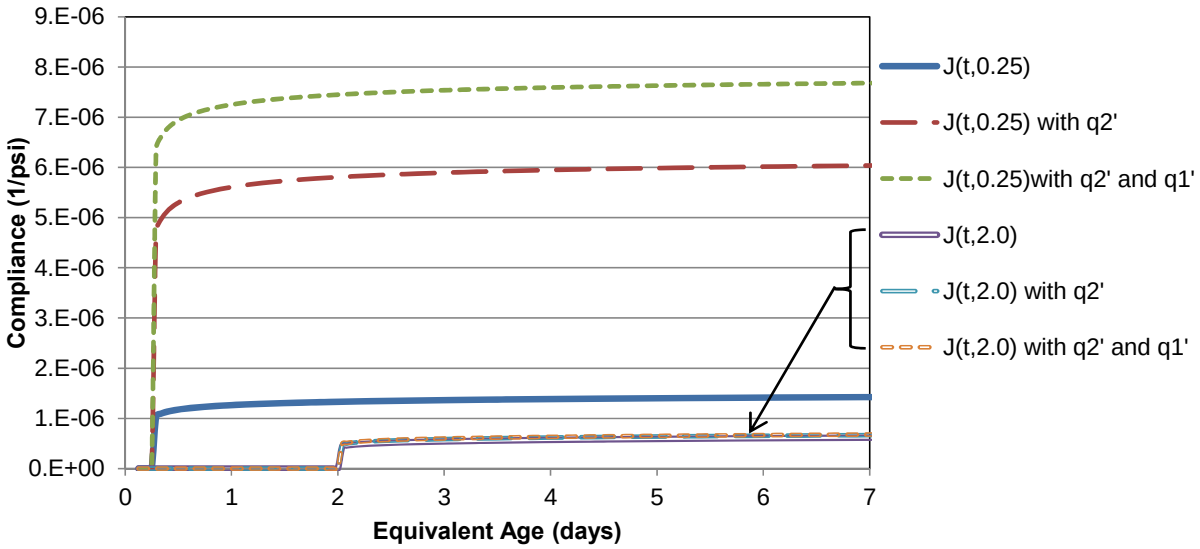

Figure 18-5: Effect of q_1' and q_2' corrections on calculated compliance

To solve for the most appropriate q_5 and q_6 values, the measured stress was compared to the modeled stress. The analysis to determine the most appropriate modifying terms was done in terms of equivalent age (t_e). The q_5 and q_6 term were solved for separately. The elastic modifier was solved for first to represent the development of early-age modulus of elasticity. An illustration of the modulus modification is shown in Figure 18-2. The figure shows the discrete data points and the best-fit modulus data. The best-fit modulus was determined using a regression analysis minimizing the error between the discrete data points, and the modifying equation expressed in Equation 18-2 using the measured 28-day modulus. This result was then scaled by a factor of 0.6^{-1} to determine the time-dependent asymptotic modulus (E_0). The unmodified E_0 is also shown for

comparison. The time-dependent E_0 approaches the unmodified E_0 at later ages as illustrated in Figure 18-2.

The q_5 term was then solved for by minimizing the error between stress development of the elastic modified B3 Model results and the measured stress development. Therefore, the selected viscoelastic modifier, q_5, provided the least error when compared to the measured stress development. The maximum allowable value of q_5 and q_6 was set equal to initial set as measured by ASTM C 403 in terms of equivalent age. Only the data with a stress to scaled strength ratio of less than 70 % were used to determine the best-fit value of q_5.

18.3 Evaluation of the Modified B3 Model Results

The results of the Modified B3 Model are presented in this section with a discussion of the behavior associated with the model. The stress predicted with the Modified B3 Model, the unmodified B3 Model, and the measured stress development for the 0.42 RG (Fall), 0.42 LS (Fall), 0.42 Slate IC (Fall), 0.42 Slate SLW (Fall), and 0.42 Slate ALW (Fall) results are presented in Figure 18-6 to Figure 18-10. The complete Modified B3 Model results can be found in Appendix C. The data are truncated at the stress to corrected strength ratio of 70 %. A scatter plot of the measured versus Modified B3 Model stress development is presented in Figure 18-11. The values of q_5 and q_6 along with the measured initial set of each mixture and placement scenario are presented in terms of equivalent age (t_e) in Table 18-2. According to Pinto and Hover (1999), setting times in equivalent age for a mixture will be the same regardless of curing temperature; therefore only one set setting time for each mixture is shown.

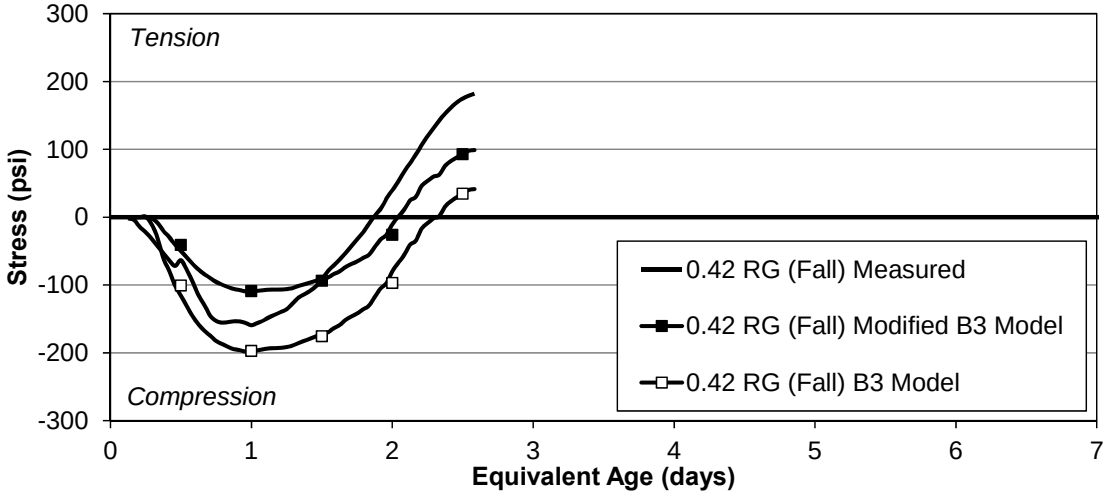

Figure 18-6: Measured, B3 Modeled, and Modified B3 Modeled stress development for 0.42 RG (Fall)

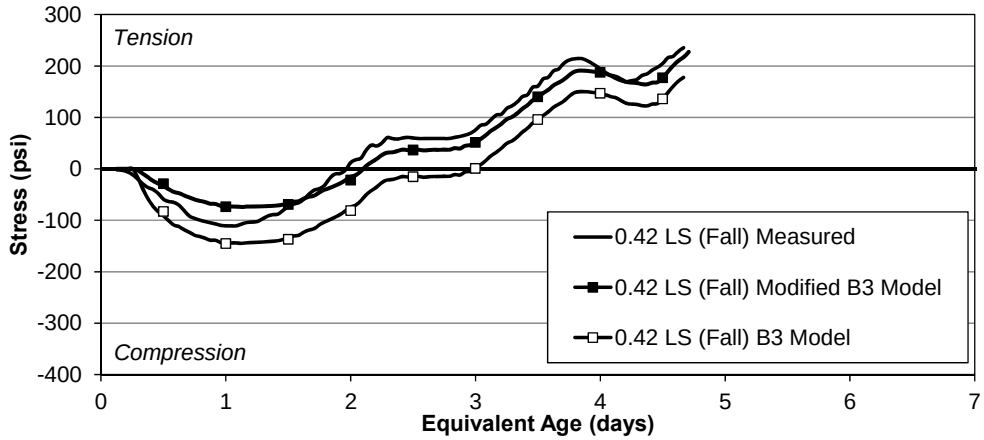

Figure 18-7: Measured, B3 Modeled, and Modified B3 Modeled stress development results for 0.42 LS (Fall)

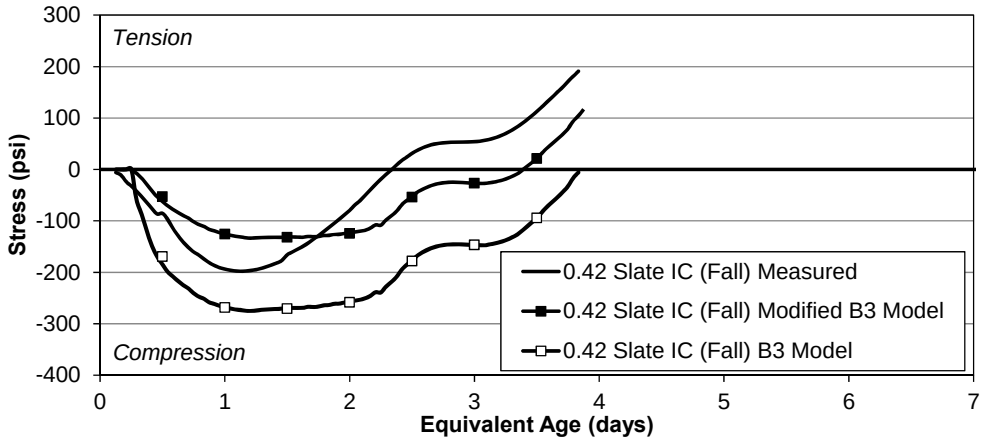

Figure 18-8: Measured, B3 Modeled, and Modified B3 Modeled stress development for 0.42 Slate IC (Fall)

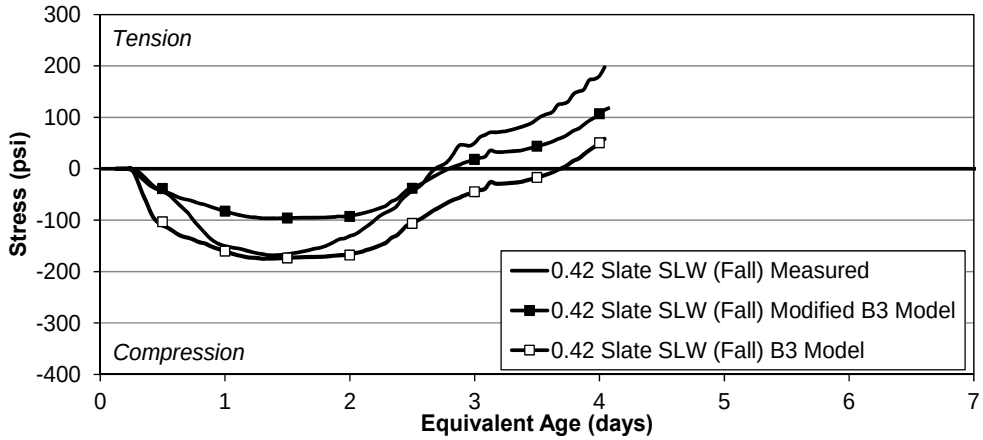

Figure 18-9: Measured, B3 Modeled, and Modified B3 Modeled stress development for 0.42 Slate SLW (Fall)

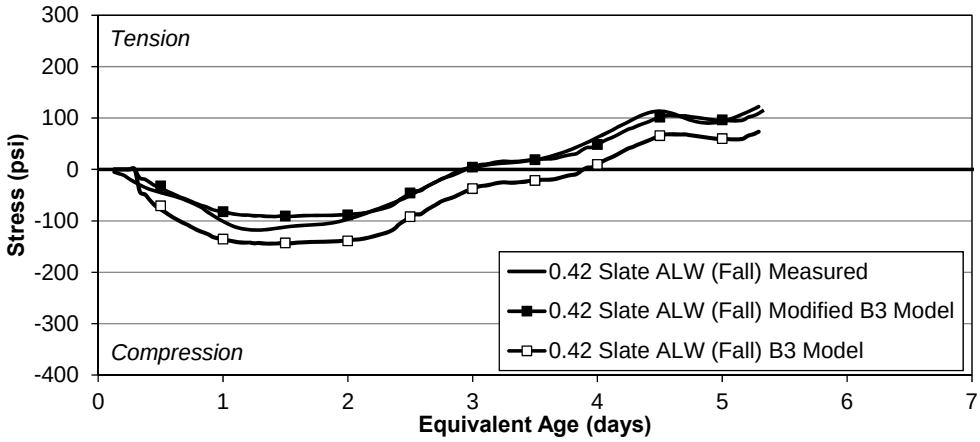

Figure 18-10: Measured, B3 Modeled, and Modified B3 Modeled stress development for 0.42 Slate ALW (Fall)

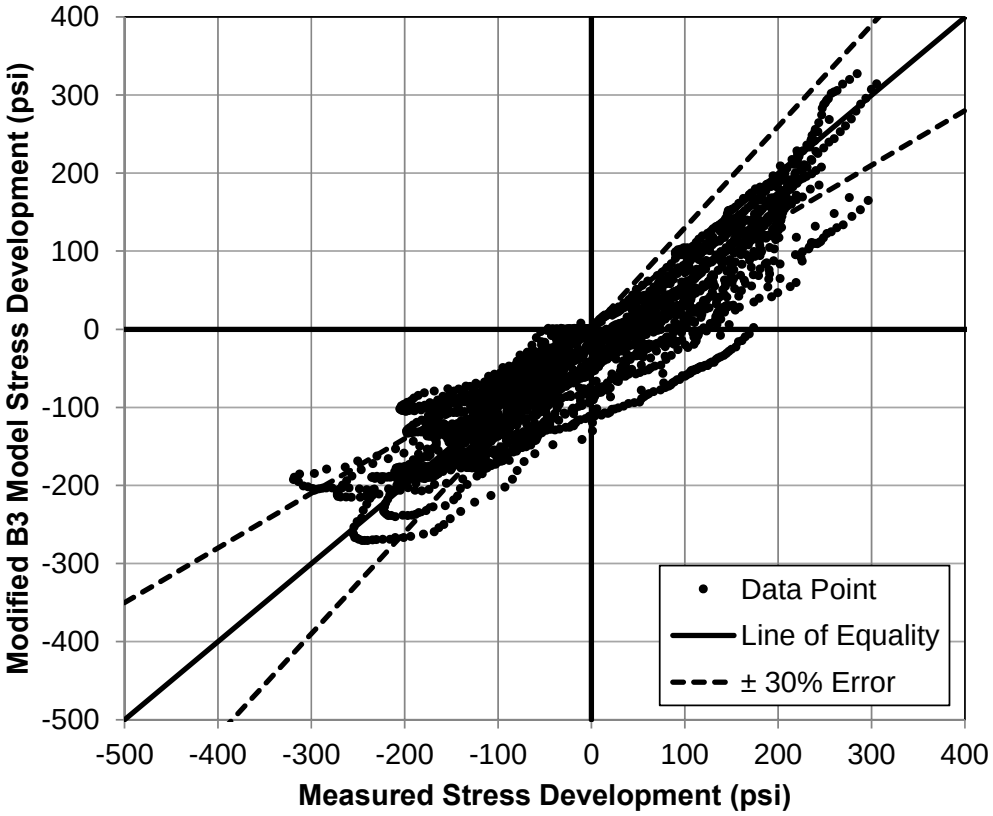

Figure 18-11: Measured versus Modified B3 Model stress development

Table 18-2: q_5 and q_6 correction factor values and measured setting times

Mixture	Placement Scenario	Equivalent Age (Days)			
		q_5	q_6	Initial Set	Final Set
0.42 RG	Fall	0.19	0.20	0.20	0.29
	Summer	0.20	0.20		
0.42 LS	Fall	0.21	0.21	0.21	0.28
	Summer	0.00	0.21		
0.42 Slate IC	Fall	0.21	0.21	0.21	0.30
	Summer	0.21	0.21		
0.42 Slate SLW	Fall	0.20	0.20	0.20	0.29
	Summer	0.20	0.20		
0.42 Slate ALW	Fall	0.18	0.17	0.19	0.31
	Summer	0.19	0.19		
0.42 Clay IC	Fall	0.22	0.22	0.22	0.30
	Summer	0.22	0.17		
0.42 Clay SLW	Fall	0.23	0.23	0.23	0.35
	Summer	0.23	0.21		
0.42 Clay ALW	Fall	0.22	0.22	0.22	0.36
0.42 Shale IC	Fall	0.00	0.21	0.21	0.30
	Summer	0.21	0.17		
0.42 Shale SLW	Summer	0.22	0.22	0.22	0.33
0.42 Shale ALW	Summer	0.23	0.23	0.23	0.37
0.36 RG	Fall	0.17	0.17	0.17	0.21
0.36 ICM	Fall	0.20	0.20	0.20	0.33
0.36 ICH	Fall	0.18	0.18	0.18	0.26
0.30 RG	Fall	0.15	0.09	0.15	0.22
0.30 ICM	Fall	0.18	0.16	0.18	0.27
0.30 ICH	Fall	0.19	0.17	0.19	0.29

Note: Activation energy of 41520 J/mol and reference temperature of 276°K (73°F) were used as maturity function constants

18.4 Discussion of the Modified B3 Model

The coefficient of determination and the unbiased estimation of standard deviation of absolute error of the B3 Model and Modified B3 Model results compared to the measured stress development are provided in Table 18-3. As discussed in Section 18.1, the B3 Model generally underpredicts the early-age viscoelastic relaxation and overpredicts the elastic stress development. The early-age stress developments predicted with the Modified B3 Model are illustrated in Figure 18-6 to Figure 18-10. The modified early-age viscoelastic and elastic responses reduced the predicted compressive stress development due to greater viscoelastic relaxation and reduced elastic stress development. The increased viscoelastic response caused more stress to be relaxed and the decreased elastic stress was due to the reduced early-age modulus of elasticity causing less stress per unit of strain. Both the viscoelastic response and elastic response combine to reduce the early-age compressive stress.

The later-age tensile stress prediction from the Modified B3 Model was also improved. The increased early-age compressive stress response decreased the time to zero stress and provide a much closer estimate to the later-age tensile stress development. The improvement of the Modified B3 Model compared to the unmodified B3 Model is quantified in Table 18-3. The r^2 of the whole data set improved from 0.25 to 0.79 and the S_j from all the data improved from 107 psi to 57 psi. This improvement in r^2 and S_j quantifies that the Modified B3 Model provides an improved fit of the measured data when compared to the original B3 Model.

Table 18-3: Coefficient of determination and unbiased estimation of standard deviation of absolute error B3 Model and the Modified B3 Model

Mixture	Placement Scenario	Coefficient of Determination, r^2		Unbiased Estimation of Standard Deviation of Absolute Error, S_i (psi)	
		Unmodified B3 Model	Modified B3 Model	Unmodified B3 Model	Modified B3 Model
0.42 RG	Fall	0.21	0.77	88	47
	Summer	0.33	0.83	89	48
0.42 LS	Fall	0.77	0.98	61	23
	Summer	0.75	0.97	140	109
0.42 Slate IC	Fall	-0.53	0.73	160	68
	Summer	0.73	0.96	66	37
0.42 Slate SLW	Fall	0.45	0.83	73	48
	Summer	0.53	0.96	78	46
0.42 Slate ALW	Fall	0.72	0.97	41	12
	Summer	0.90	0.90	43	34
0.42 Clay IC	Fall	0.01	0.97	110	73
	Summer	0.58	0.83	75	37
0.42 Clay SLW	Fall	-0.3	0.58	85	45
	Summer	0.61	0.67	109	84
0.42 Clay ALW	Fall	-0.97	0.46	93	44
0.42 Shale IC	Fall	-0.55	0.41	23	24
	Summer	0.83	0.96	132	76
0.42 Shale SLW	Summer	-0.26	0.88	117	77
0.42 Shale ALW	Summer	0.88	0.92	43	27
0.36 RG	Fall	0.49	0.95	123	38
0.36 ICM	Fall	0.45	0.84	106	65
0.36 ICH	Fall	-0.02	0.97	153	23
0.30 RG	Fall	0.43	0.78	126	80
0.30 ICM	Fall	-0.65	0.69	241	96
0.30 ICH	Fall	0.17	0.94	182	43
Total Data Set		**0.25**	**0.79**	**107**	**57**

18.5 Compliance Behavior

To compare the relaxation response of the concretes, the elastic response must be normalized. This was done by using the same elastic response for all the mixtures and comparing the modified early-age compliance functions. With the elastic response equal

the differences in the data are due to the relaxation response only. As illustrated in Figure15-14, the aging viscoelastic term has near vertical shape after loading. Because of this shape, some of the figures in the following sections appear to have different elastic responses. However, it should be noted that this behavior is due to the aging viscoelastic term.

18.5.1 Effect of Aggregate Stiffness on Relaxation

The Modified B3 Model compliance functions with normalized elastic response for loading at 0.5 day and 1.0 day of equivalent age for the fall placement scenario concretes with expanded slate lightweight aggregate and *w/c* of 0.42 are shown in Figure 18-12 and Figure 18-13, respectively. The elastic normalized compliance response of mixtures with lightweight coarse aggregate is greater than that of the mixtures with normalweight coarse aggregate. This is to be expected, because the less stiff lightweight aggregate cannot resist the relaxation occurring in the paste as well as the stiffer normalweight coarse aggregate. It has been reported by Mindess et al. (2003) and Neville et al. (1983) that aggregates with reduced stiffness has increased time-dependent response.

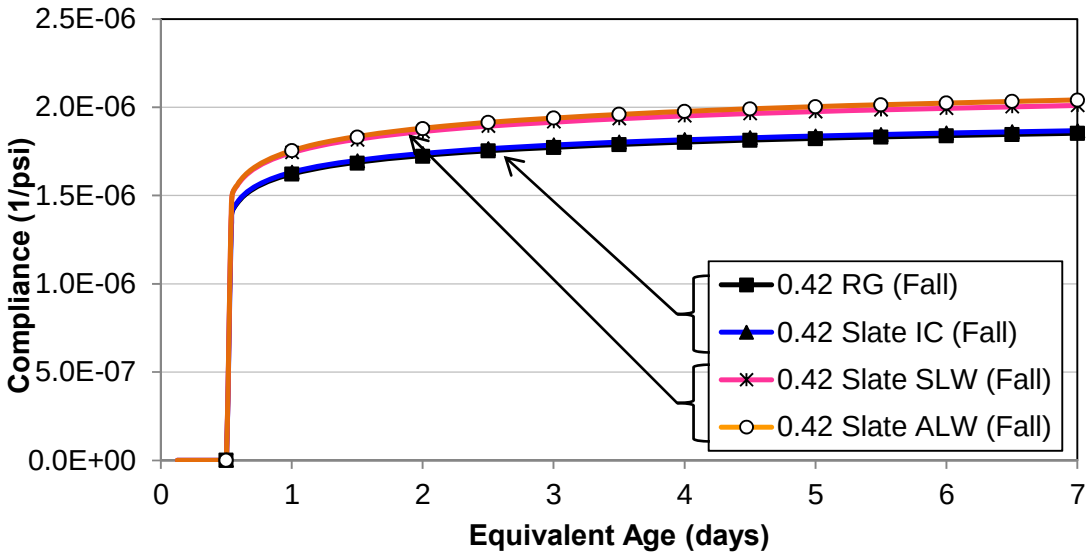

Figure 18-12: Compliance with normalized elastic response of normalweight and slate lightweight mixtures with *w/c* of 0.42 loaded at 0.5 day

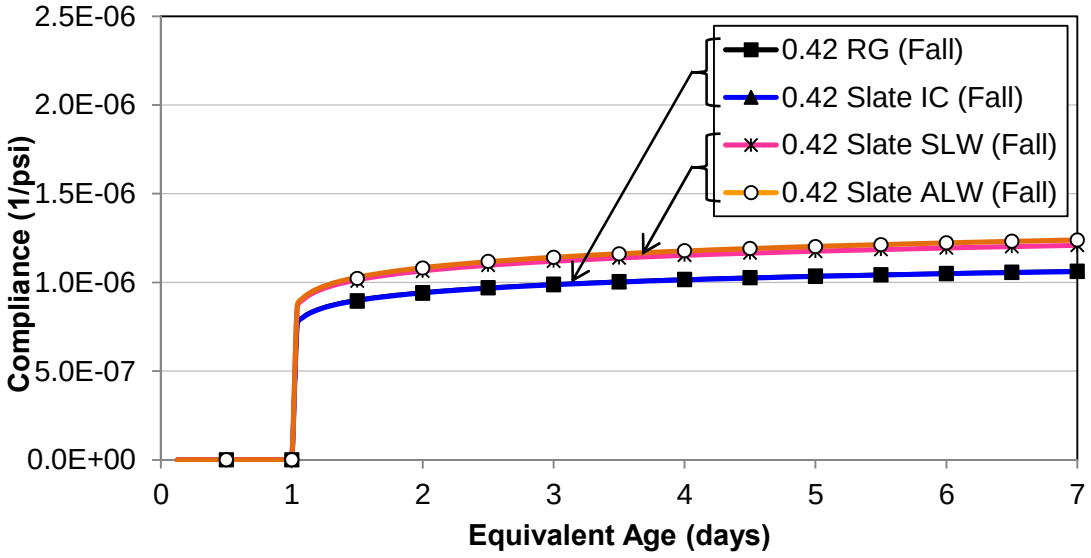

Figure 18-13: Compliance with normalized elastic response of normalweight and slate lightweight mixtures with *w/c* of 0.42 loaded at 1 day

18.5.2 Effect of Water-Cement Ratio on Relaxation

The effect of *w/c* on relaxation can be evaluated from the data shown in Figure 18-14 where the compliance of mixtures with normalweight aggregates and *w/c* of 0.42, 0.36,

and 0.30 are shown at 0.5-day loading. The response of the 0.42 RG (Fall) mixture is the greatest followed by the 0.36 RG (Fall) mixture and finally the 0.30 RG (Fall) mixture. The aggregate and paste volumes of these mixtures are equal. For the mixtures with *w/c* of 0.36 and 0.30, the cement contents were increased and the water contents were decreased to provide an equal volume of paste and this lead to an increase in paste quality without an increase in paste volume. Therefore, with equal aggregate resistance to relaxation, the reduction in compliance response is due to the higher quality paste. This result matches the findings reported by Neville et al. (1983).

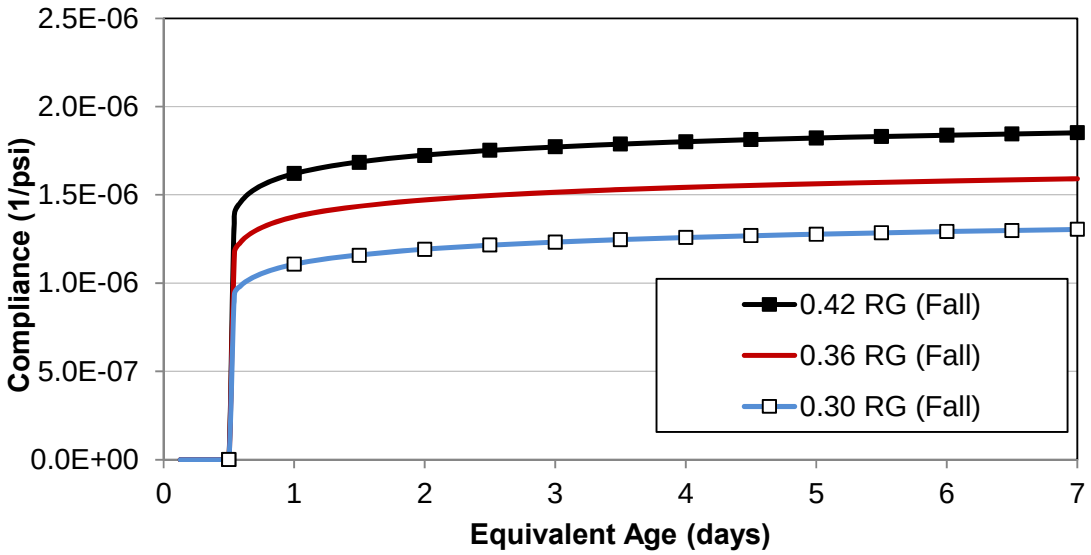

Figure 18-14: Compliance with normalized elastic response of normalweight aggregate mixtures with *w/c* of 0.42, 0.36, and 0.42 loaded at 0.5-day

18.5.3 Effect of Curing Temperature on Relaxation

The effect of curing temperature on relaxation is illustrated in Figure 18-15, where the elastic normalized compliance for mixtures with *w/c* of 0.42 and normalweight aggregates are shown at a 1.0-day loading age for the fall and summer placement scenarios. The figure shows the compliance response of the mixtures to be virtually the same. The use of

the equivalent-age maturity functions seems to account for the effect of curing temperature on compliance behavior.

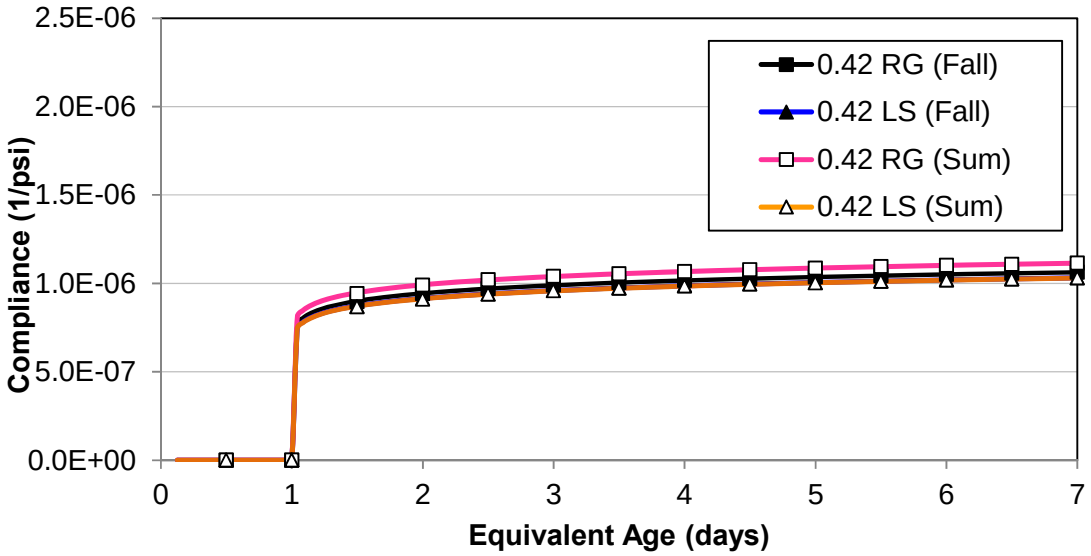

Figure 18-15: Compliance with normalized elastic response of normalweight aggregate mixtures with *w/c* of 0.42 loaded at 1.0-day for summer and fall placement scenarios

18.6 Sensitivity Analysis of the Modified B3 Model

To determine the sensitivity of compliance to changes in q_5 and q_6 an analysis was performed. This was done by varying the values of q_5 and q_6 from their minimum value of zero to their maximum value which is equal to the equivalent age just before initial set. At q_5 and q_6 values equal to zero the B3 Model is unmodified because the modifying expressions shown in Equations 18-1 and 18-2 will both equal one. The sensitivity of the correction factor was investigated and the results are illustrated in Figure 18-16 to Figure 18-20. The setting time of the mixture shown is 0.2 days of equivalent age. The compliance function for 0.25-, 0.5-, 1.0- and 2.0-day loading ages are shown in the figures. The compliance for various values of q_5 and q_6 at a loading age of 0.25 days and age of 7 days [J(7.0,0.25)] is summarized in Table 18-4, and the data summarized in the

table is illustrated in Figure 18-21. The loading age of 0.25 days was used because the effects of the correction factors are best illustrated at early ages.

The modifying term q_5 was varied why setting q_6 equal to zero and the effect on compliance was determined and is illustrated in Figure 18-21a). The early-age viscoelastic correction factor q_5 was varied from zero to 0.2 days equivalent age. The effect of change in q_5 is nonlinear as shown in Figure 18-21a). The closer to setting time (0.20 days in this case) the greater effect on compliance a change in q_5 has. For example, changing q_5 from zero to 0.15 increases the compliance response 121 % and changing q_5 from 0.15 to 0.20 days increases compliance 324 % from the unmodified compliance as shown in Table 18-4. Similar effects can be seen in Figure 18-21b) for q_6; however the magnitude of change in compliance is much less than for q_5. Changing q_6 from zero to 0.15 days increases compliance by 16 %, whereas a change from 0.15 days to 0.2 days leads to a 72 % change. Like q_5, the effect on compliance of a change in q_6 is increased the closer the value is to setting (0.20 days) as shown in Table 18-4. The sensitivity of compliance to early-age viscoelastic and elastic corrections is greater the closer their values are to initial setting time. As previously mentioned, the effect of the correction factors diminishes over time leaving the later-age B3 Model unmodified as illustrated in Figure 18-18 to Figure 18-20 where the data show that at 1-day loading the compliance terms for varying q_5 to be very similar.

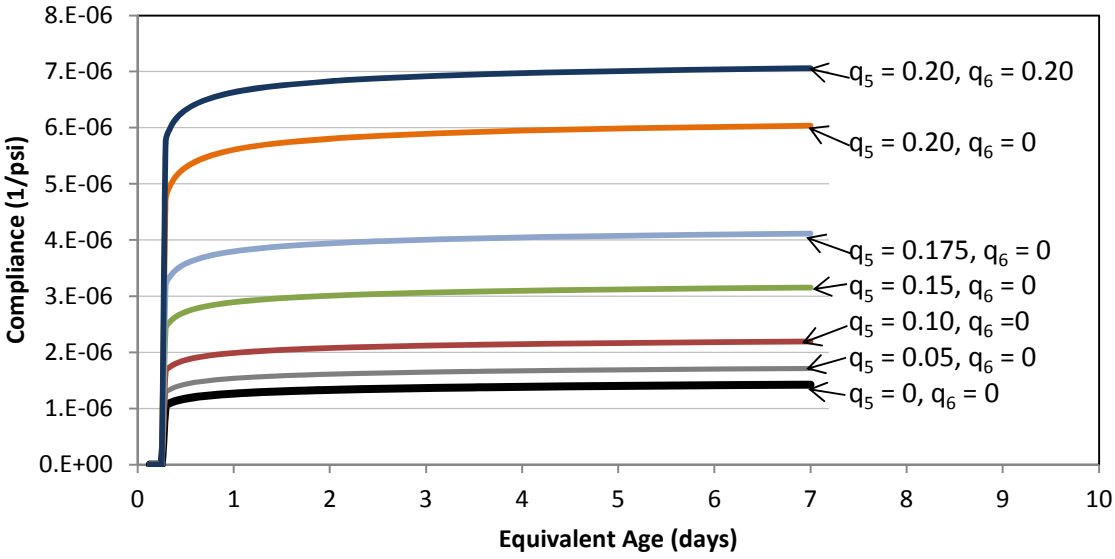

Figure 18-16: Compliance sensitivity of q_5 term, with t_0=0.25 days

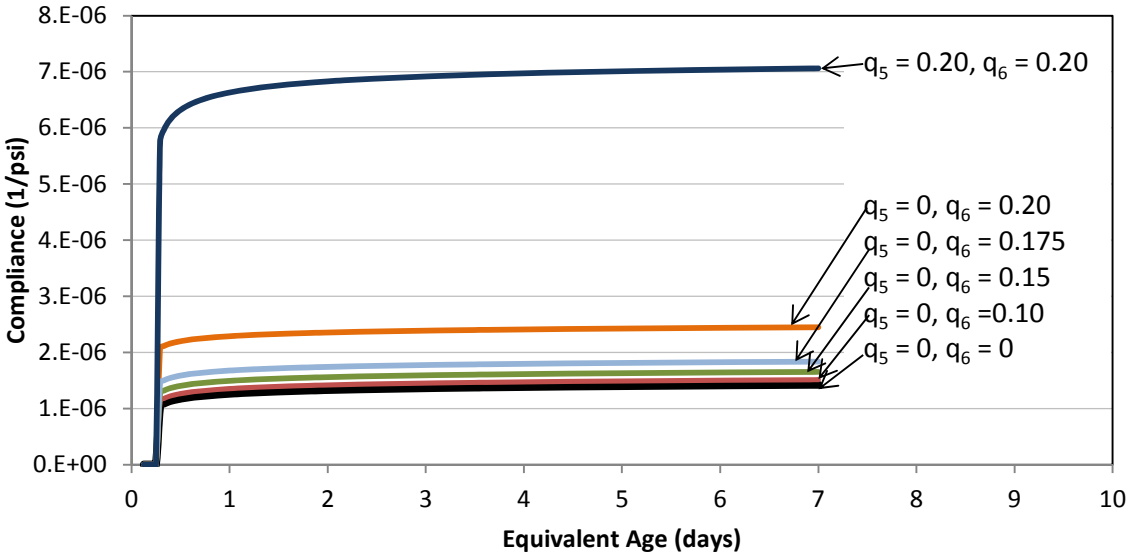

Figure 18-17: Compliance sensitivity of q_6 term, with t_0=0.25 days

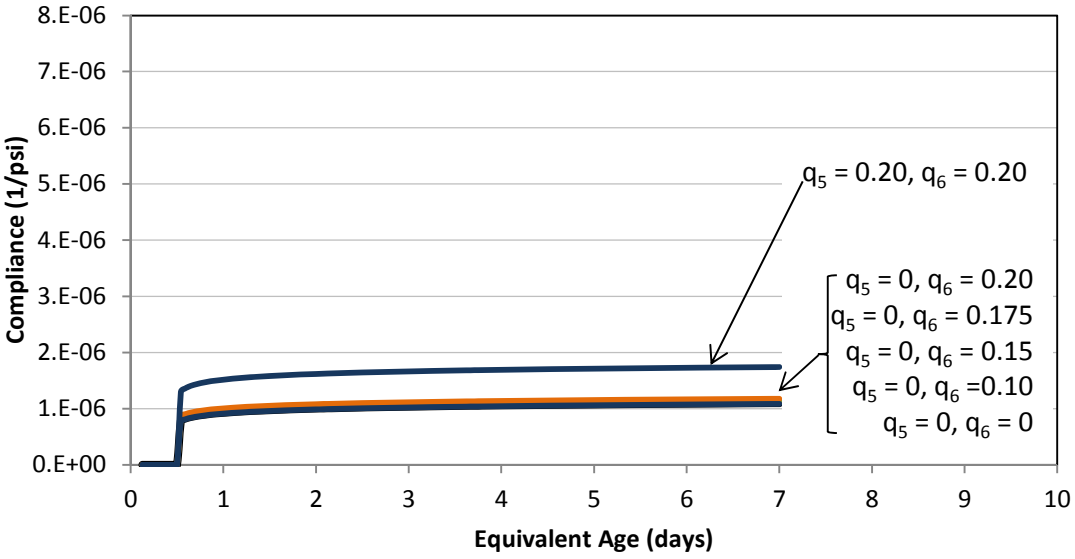

Figure 18-18: Compliance sensitivity of q_6 term, with t_0=0.5 days

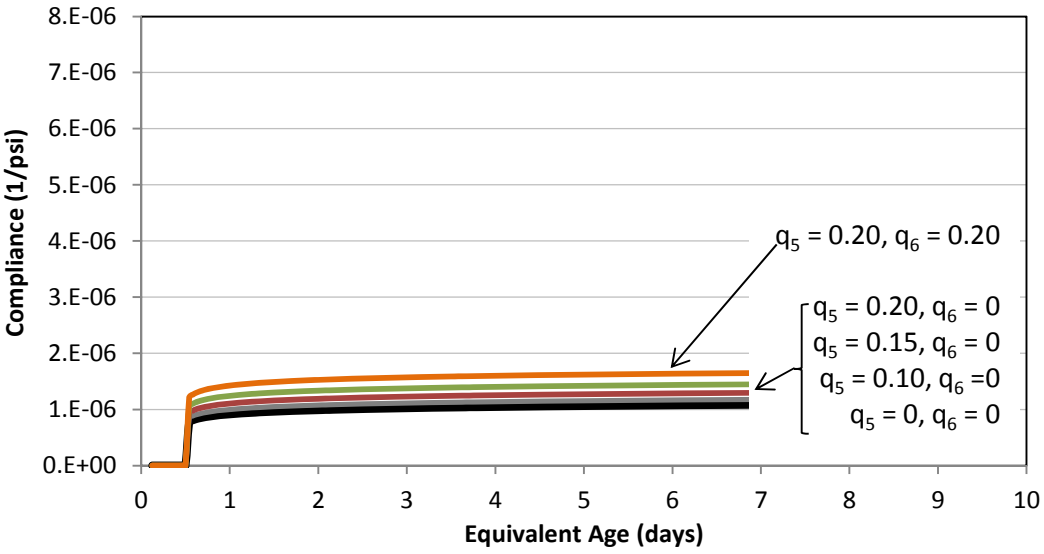

Figure 18-19: Compliance sensitivity of q_5 term, with t_0=0.5 days

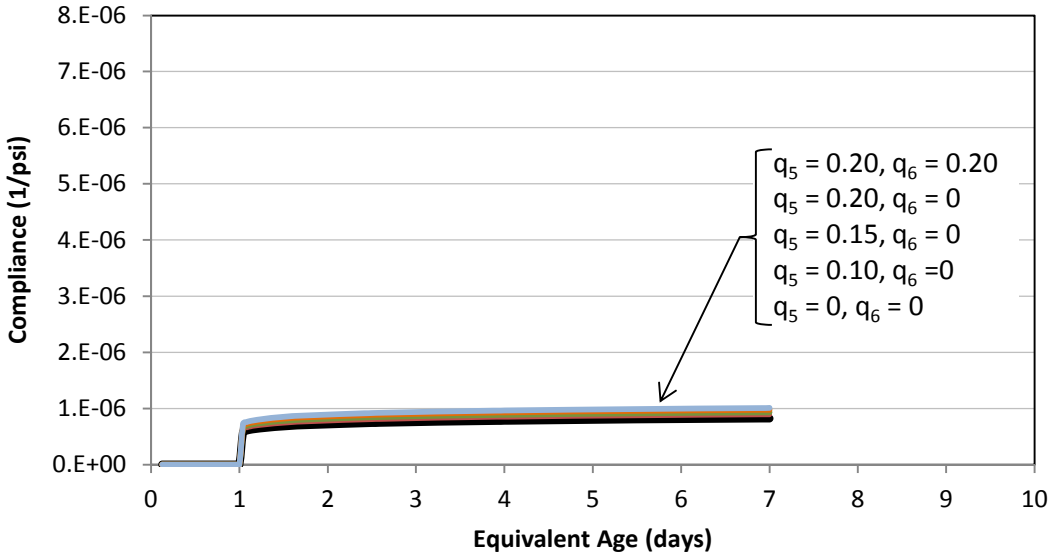

Figure 18-20: Compliance sensitivity of q_5 term, with t_0=1.0 days

Table 18-4: Compliance for various correction factor values at loading age of 0.25 day and age of 7 days

Correction Factor Values		J(7.0,0.25) (1/psi)	Difference from Unmodified B3 Model (%)
q_5 (days)	q_6 (days)		
0.000	0.000	1.42E-06	-
0.000	0.100	1.51E-06	6
0.000	0.150	1.65E-06	16
0.000	0.175	1.84E-06	29
0.000	0.200	2.45E-06	72
0.050	0.000	1.71E-06	20
0.100	0.000	2.19E-06	54
0.150	0.000	3.15E-06	121
0.175	0.000	4.11E-06	189
0.200	0.000	6.04E-06	324
0.200	0.200	7.06E-06	396

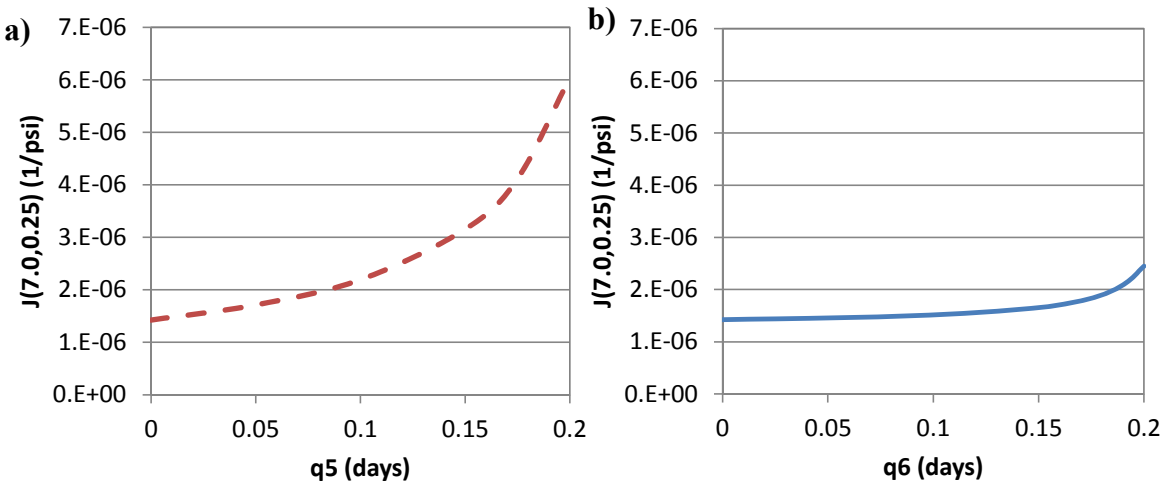

Figure 18-21: Effect of a) varying q_5 and, b) varying q_6 on compliance with a loading age of 0.25 days and age of 7 days

18.7 Development of the Simplified Modified B3 Model

The q_5 and q_6 correction factors for each mixture plotted with the initial set time in terms of equivalent age are shown in Figure 18-22 and Figure 18-23, respectively. The data illustrate how the values of the q_5 and q_6 terms are generally near the initial setting equivalent age. Therefore, a Simplified Modified B3 Model was developed where the q_5 and q_6 values are assumed to be just before initial set equivalent age. Thus, the Simplified Modified B3 Model only requires the original input data and the initial set time to calculate early-age compliance.

The unbiased estimation of standard deviation of absolute error was calculated and the coefficient of determination for the Simplified Modified B3 model and is presented in Table 18-5 along with the results for the Modified B3 Model. The data indicate that using the simplified approach, setting the q_5 and q_6 correction factor values equal to just before the set time, had no effect on the r^2 or S_j of the total data set to two significant digits, and only slightly affected the prediction accuracy for some of the individual data sets.

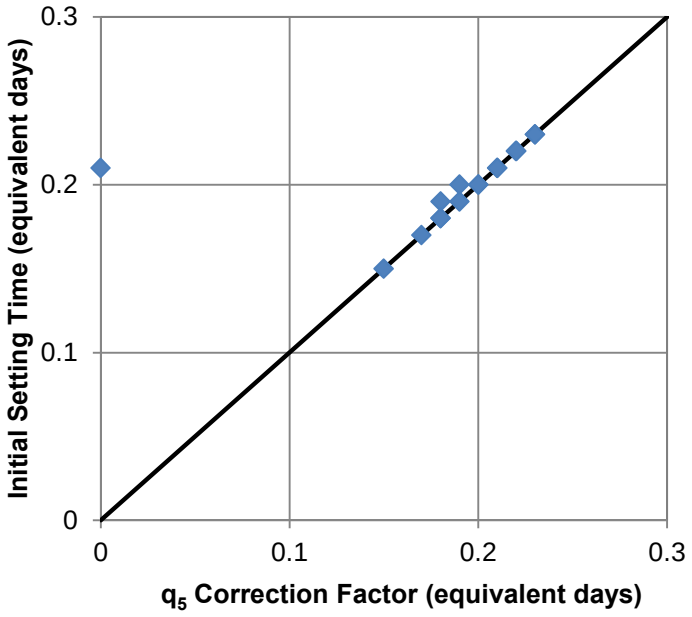

Figure 18-22: q_5 correction factor versus initial setting time

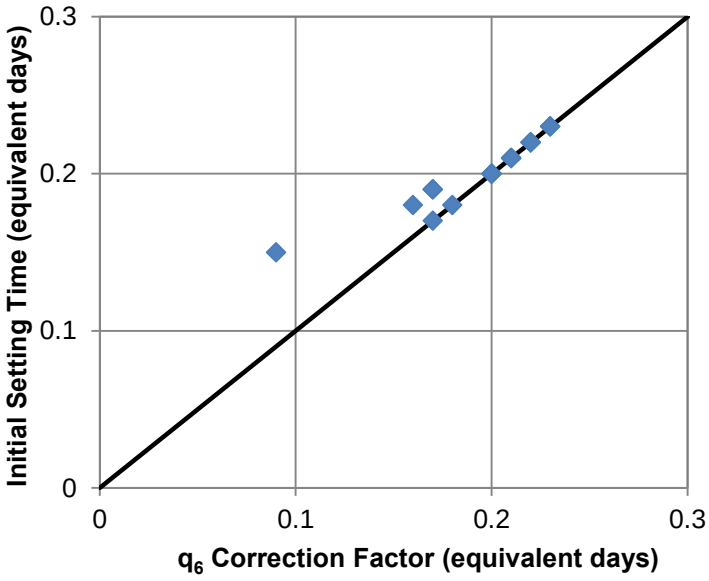

Figure 18-23: q_6 correction factor versus initial setting time

Table 18-5: Coefficient of determination and unbiased estimation of standard deviation of absolute error of Simplified Modified B3 Model and the Modified B3 Model

Mixture	Placement Scenario	Coefficient of Determination, r^2		Unbiased Estimation of Standard Deviation of Absolute Error, S_i (psi)	
		Simplified Modified B3 Model	Modified B3 Model	Simplified Modified B3 Model	Modified B3 Model
0.42 RG	Fall	0.77	0.77	47	47
	Summer	0.83	0.83	48	48
0.42 LS	Fall	0.96	0.96	23	23
	Summer	0.97	0.97	109	109
0.42 Slate IC	Fall	0.73	0.73	68	68
	Summer	0.96	0.96	37	37
0.42 Slate SLW	Fall	0.83	0.83	48	48
	Summer	0.96	0.96	46	46
0.42 Slate ALW	Fall	0.97	0.97	14	12
	Summer	0.90	0.90	34	34
0.42 Clay IC	Fall	0.97	0.97	73	73
	Summer	0.83	0.83	40	37
0.42 Clay SLW	Fall	0.58	0.58	45	45
	Summer	0.67	0.67	84	84
0.42 Clay ALW	Fall	0.46	0.46	44	44
0.42 Shale IC	Fall	0.41	0.41	79	76
	Summer	0.96	0.96	29	29
0.42 Shale SLW	Summer	0.88	0.88	77	77
0.42 Shale ALW	Summer	0.91	0.92	28	27
0.36 RG	Fall	0.95	0.95	38	38
0.36 ICM	Fall	0.84	0.84	65	65
0.36 ICH	Fall	0.97	0.97	23	23
0.30 RG	Fall	0.78	0.78	80	80
0.30 ICM	Fall	0.68	0.69	98	96
0.30 ICH	Fall	0.94	0.94	42	43
Total Data Set		**0.79**	**0.79**	**57**	**57**

18.8 Time Step Analysis

A time step of 60-minute was used for this testing program. This time step was chosen because, the 24-hour stress oscillations caused by the diurnal temperature cycle could

easily be captured by a 60-minute time step. However, if the frequency of the stress oscillations were shorter, then a shorter time set may be required to capture the changes in stress.

The 0.42 LS (Fall) and 0.42 Slate ALW (Fall) mixtures were used to illustrate the effect of the length of the time step on the coefficient of determination (r^2) and the unbiased estimate of standard deviation of absolute error (S_j) because of their different stiffness and because the Modified B3 Model predicts their stresses accurately. The modeling spreadsheet was setup to analyze the same data set with a 20, 40, 60 and 120-minute time step lengths, the S_j and r^2 were determined for the modeled and predicted stress values, and are shown in Table 18-6. The data show that there is not a significant loss in precision when a 60-minute time step is used compared to a 20-minute time step. These results illustrate, that the use of a 60-minute time step captures the change in stress with sufficient accuracy.

Table 18-6: Time step analysis results

Mixture	Statistical Indicator	Time Step Length			
		20 min	**40 min**	**60 min**	**120 min**
0.42 LS (Fall)	r^2	0.980	0.978	0.975	0.964
	S_j (psi)	20.8	21.9	23.3	28.5
0.42 Slate ALW (Fall)	r^2	0.986	0.984	0.980	0.962
	S_j (psi)	10.9	11.5	12.3	13.8

CHAPTER 19

PART III: CONCLUSIONS

19.1 Summary of Work

Early-age compliance modeling of concrete was examined in this part. This was accomplished by measuring the early-age stress development of concrete with varying densities, lightweight aggregate types, water-cement ratios, and temperature histories. The stress development was modeled using the B3 compliance model (Bažant and Baweja 2000) and the measured free-shrinkage strain of the concrete. The measured stress development was compared to the stress development predicted by the B3 compliance model. The B3 compliance model did not adequately predict the response of the concrete at early ages due to low viscoelastic response and high elastic stress development used by the model. Modifications were made to the B3 Model to better account for the early-age viscoelastic and elastic response. The effects of aggregate stiffness, water-cement ratio, and curing temperature on early-age relaxation were examined. The sensitivity of compliance to changes in the early-age viscoelastic and elastic correction factors was investigated. A Simplified Modified B3 Model was developed that uses the equivalent age at initial set as model inputs. The Simplified Modified B3 Model can be used to estimate the early-age stress development without the need to have rigid cracking frame data to calibrate the modification factors associated with the Modified B3 Model.

19.2 Conclusions

The results presented Part III support the following conclusions:

- The B3 Model underestimates the early-age relaxation response.
- A viscoelastic modifying term (q_5), introduced by Østergaard et al. (2001) and shown in Equation 18-1, more accurately accounts for the high amount of relaxation of concrete at early ages by increasing the viscoelastic response.
- The constant asymptotic modulus of the B3 Model, leads to high early-age elastic stress development compared to measured stress development. A proposed elastic response modifying term (q_6), shown in Equation 18-2, more accurately accounts for the changing stiffness of early-age concrete.
- The early-age modifications recommended in the Modified B3 Model have diminishing effectiveness and the later age predictions are virtually unchanged with regards to the original B3 Model.
- The contribution of the elastic and viscoelastic components of the Modified B3 Model provides a better fit when compared to measured stress development at early ages.
- Using the Modified B3 Model, it was found that the stiffer aggregates reduced the compliance response. Lightweight aggregates provided increased stress relaxation leading to reduced early-age stress development.
- Using the Modified B3 Model, with constant aggregate and paste volumes, decreasing the water-cement ratio decreased the compliance response.

- Curing temperature had little effect on the Modified B3 Model results, and the use of the equivalent-age maturity function accounts for the effects of temperature on compliance.
- The sensitivity of the Modified B3 Model compliance function to change in the early-age modifiers (q_6 and q_5) is more significant the closer their values are to initial setting, which is their maximum possible value.
- The Simplified Modified B3 Model provides an estimation of early-age stress development without a significant loss of accuracy.

CHAPTER 20

CONCLUSIONS AND RECOMMENDATIONS

20.1 Summary of Work

Early-age cracking of concrete is a severe problem that may reduce the functional life of concrete. In this project, the early-age behavior of lightweight aggregate concrete was investigated. This was done in three parts 1) assessment of early-age stress and mechanical property development, 2) evaluation of internal curing and autogenous shrinkage stress, and 3) performing early-age compliance modeling. Expanded shale, clay, and slate lightweight coarse and fine aggregates were evaluated in this study.

For part one normalweight, internal curing (IC), sand-lightweight (SLW), and all-lightweight (ALW) concretes were made in the laboratory and their early-age behavior evaluated. The normalweight concrete used is a typical mixture used in bridge deck applications in the Southeastern United States with a water-cement ratio of 0.42. The IC mixture is similar to the normalweight mixture, except that a fraction of the normalweight fine aggregate was replaced with pre-wetted lightweight fine aggregate. The amount of lightweight aggregate added to the IC mixture was selected to obtain a concrete with an equilibrium density of 135 lb/ft^3, which allows this mixture to be classified as "normalweight concrete" as per the AASHTO LRFD Bridge Design Specifications (2007).

Each concrete was made and cured under conditions that simulate summer and fall placement conditions in the southeastern parts of the United States. Ten different concretes were produced and tested at two different curing conditions. Additionally, for each mixture and placement condition, 24 cylinders were cast and tested for compressive strength, splitting tensile strength, and modulus of elasticity to assess the development of these properties over time. The coefficient of thermal expansion of the hardened concrete was also assessed with a test setup similar to that required by AASHTO T 336 (2009).

For part two, the effect on the cracking tendency of bridge deck concrete that results from using lightweight fine aggregate to provide internal curing was experimentally evaluated. Restrained concrete specimens were tested under temperature conditions that match those in a bridge deck, while companion specimens were tested under isothermal curing conditions. Degree of hydration was obtained from semi-adiabatic calorimeter results to determine the effect of internal curing on cement hydration. The autogenous strain of concrete and mortar was measured with free-shrinkage frame and corrugate tube testing techniques. Internal relative humidity was measured to determine the dependence of stress on the change in capillary pore pressures.

The early-age compliance modeling of concrete was examined in part three. This was accomplished by measuring the early-age stress development of concrete with varying densities, lightweight aggregate types, water-cement ratios, and temperature histories. The stress development was modeled using the B3 compliance model (Bažant and Baweja 2000) and the measured free-shrinkage strain of the concrete. The measured stress development was compared to the stress development predicted by using the B3 compliance model. The B3 compliance model did not adequately predict the response of

the concrete at early ages due to low viscoelastic relaxation and high elastic stress development used by the model. Modifications were made to the B3 Model to better account for the early-age viscoelastic and elastic response. The effects of aggregate stiffness, water-cement ratio, and curing temperature on early-age relaxation were examined. The sensitivity of compliance to changes in the early-age viscoelastic and elastic correction factors was investigated. A Simplified Modified B3 Model was developed that uses the equivalent age at initial set as model inputs. The Simplified Modified B3 Model can be used to estimate the early-age stress development without the need to have rigid cracking frame data to calibrate the modification factors associated with the Modified B3 Model.

20.2 Conclusions

The focus of part one was to investigate the early-age stress development and cracking tendency of lightweight aggregate concrete. The research presented in part one supports the following conclusions:

- Increasing the amount of pre-wetted lightweight aggregate in the concrete systematically decreases the density and thus the modulus of elasticity of the concrete. By using the *fresh* density and Equation 3-2 found in ACI 318 (2008), the density and compressive strength can be used to estimate, with reasonable accuracy, the modulus of elasticity of all the concretes made with lightweight aggregate.
- In general, the compressive strength of the internal curing concretes was slightly higher at all ages than that of the normalweight control concrete. The compressive

strength development of the sand-lightweight concretes was similar to that of the normalweight control concrete. Whereas, the compressive strength for the all-lightweight concretes were approximately 13 to 19 % lower when compared to that of the normalweight control concrete.

- All internal curing and sand-lightweight concretes exhibited an increase in splitting tensile strength when compared to the normalweight control concrete.
- The slate all-lightweight concrete has a decreased splitting tensile strength up to an age of approximately 7 days when compared to the normalweight control concrete. Whereas, both the clay and shale all-lightweight concretes have a similar or slightly increased splitting tensile strength when compared to the normalweight control concrete. The difference in the splitting tensile strength results of the all-lightweight concretes may be related to the particle packing of the slate all-lightweight mixture used in this study.
- The equations of ACI 207.2R (1995) and ACI 207.1R to estimate the splitting tensile both provide accurate estimates for all of the concretes made with lightweight aggregate.
- The ACI 318 (2008) and AASHTO (2007) lightweight modification factor (λ factor) to estimate the splitting tensile strength from a known compressive strength is very conservative for the lightweight aggregate concretes tested in this study.
- Increasing the amount of pre-wetted lightweight aggregate in the concrete systematically decreases the coefficient of thermal expansion. There is a reduction of 15 % and 30 % in coefficient of thermal expansion for the sand-lightweight and

all-lightweight concretes, respectively, when compared to the normalweight control concrete.

- Increasing the amount of lightweight aggregate in the mixture decreases the concrete's thermal diffusivity, which resulted in an increase in peak hydration temperatures.
- Higher placement and curing temperatures result in higher thermal stresses. Decreasing the placement and curing temperature can reduce tensile stresses and delay cracking.
- The time to cracking for all concretes made with LWA when placed under *summer* placement conditions is *greater* than the time to cracking of the normalweight concrete when placed under *fall* conditions. This indicates that the use of pre-wetted LWA may be especially beneficial during summer time placement conditions to minimize the occurrence of cracking at early ages in bridge deck applications.
- The use of pre-wetted lightweight aggregates in concrete can reduce or eliminate the stress development caused by autogenous shrinkage. The decrease in autogenous stresses is due to internal curing, because water is desorbed from the lightweight aggregates to fill capillary voids formed by chemical shrinkage.
- Internal curing concrete made with pre-wetted lightweight aggregate experienced *reduced* stress development due to autogenous shrinkage effects when compared to the normalweight concrete. Since the sand-lightweight and all-lightweight concretes can supply more internal curing water, they cause a greater reduction in tensile stresses due to autogenous shrinkage effects than the internal curing

concretes. The sand-lightweight and all-lightweight concretes used in this study completely prevented the development of tensile stresses due to autogenous shrinkage effects.

- The use of lightweight aggregates to produce internal curing concretes with a density of 135 lb/ft^3 delays the occurrence of cracking at early ages in bridge deck concrete applications when compared to the normalweight control concrete. This improvement in cracking behavior is attributed to the *increased* tensile strength and *decrease* in modulus of elasticity, coefficient of thermal expansion, and autogenous shrinkage of the internal curing concretes when compared to the normalweight control concrete.
- The use of sand-lightweight and all-lightweight concretes significantly delays the occurrence of cracking at early ages in bridge deck concrete applications when compared to the normalweight control concrete. Although the sand-lightweight and all-lightweight concretes experience greater peak temperatures, the significant reduction in coefficient of thermal expansion and modulus of elasticity lead to a significant overall delay in early-age cracking in bridge deck concrete applications.
- When compared to a normalweight control concrete, the introduction of lightweight aggregates in concrete effectively delays the occurrence of cracking at early ages in bridge deck applications.

The focus of part two was to investigate the effect of different amount of internal cuing on degree of hydration, internal relative humidity, autogenous shrinkage of concrete, and

mortar, and stress development due to autogenous shrinkage of concrete. The data collected in part two support the following conclusions.

- Increasing the amount of internal-curing water available in the lightweight aggregate increases the degree of hydration.
- The Mills (1966) model predicted the degree of hydration of the non-internally cured mixtures to within 9 %. It does not accurately predict the degree of hydration of the internally cured mixtures.
- The Hansen (1986) model provides poor estimates of the ultimate degree of hydration for internally cured and non-internally cured concretes.
- The compressive strength and splitting tensile strength of the internally cured concretes is similar to or slightly greater than their non-internally cured counterparts at 7 and 28 days.
- Increasing the amount of pre-wetted lightweight aggregate in the concrete systematically decreases the density and the modulus of elasticity of the concrete.
- Mortar has greater autogenous strain due to the reduced restraint provided by the coarse aggregate content to the capillary stress in the paste fraction.
- As the water-cement ratio decreases the autogenous strain and stress increases. This is due to reduced pores sizes and decreased water availability associated with lower water-cement ratio mixtures.
- Providing internal curing through pre-wetted lightweight aggregate decreases the autogenous strain of concrete and mortar compared to non-internally cured counterparts.

- The use of pre-wetted lightweight aggregates to provide internal curing in concrete can reduce or eliminate the stress development caused by autogenous shrinkage.
- The use of lightweight aggregates to provide internal curing delays the occurrence of early-age cracking in bridge deck concrete applications when compared to the normalweight control concrete. This improvement in cracking behavior is attributed to the increased tensile strength, decreased modulus of elasticity, and decreased autogenous shrinkage.

The focus of part three was modeling of early-age stress development. The results presented in part three support the following conclusions.

- The B3 Model underestimates the early-age relaxation response.
- A viscoelastic modifying term (q_5), introduced by Østergaard et al. (2001) and shown in Equation 18-1, more accurately accounts for the high amount of relaxation of concrete at early ages by increasing the viscoelastic response.
- The constant asymptotic modulus of the B3 Model, leads to high early-age elastic stress development compared to measured stress development. A proposed elastic response modifying term (q_6), shown in Equation 18-2, more accurately accounts for the changing stiffness of early-age concrete.
- The early-age modifications recommended in the Modified B3 Model have diminishing effectiveness and the later age predictions are virtually unchanged with regards to the original B3 Model.

- The contribution of the elastic and viscoelastic components of the Modified B3 Model provides a better fit when compared to measured stress development at early ages.
- Using the Modified B3 Model, it was found that the stiffer aggregates reduced the compliance response. Lightweight aggregates provided increased stress relaxation leading to reduced early-age stress development.
- Using the Modified B3 Model, with constant aggregate and paste volumes, decreasing the water-cement ratio decreased the compliance response.
- Curing temperature had little effect on the Modified B3 Model results, and the use of the equivalent-age maturity function accounts for the effects of temperature on compliance.
- The sensitivity of the Modified B3 Model compliance function to change in the early-age modifiers (q_6 and q_5) is more significant the closer their values are to initial setting, which is their maximum possible value.
- The Simplified Modified B3 Model provides an estimation of early-age stress development without significant loss of model accuracy

20.3 Recommendations for Future Research

The following recommendations are given for future research:

1. It is possible that the difference in splitting tensile strength results of the all-lightweight concretes is related to differences in the particle packing the all-lightweight mixtures evaluated. The effect of particle packing on the properties of all-lightweight concrete should be evaluated to determine its effect.

2. The thermal properties of the concretes made with lightweight aggregates were back-calculated from semi-adiabatic calorimeter results and were thus not directly measured. If it is deemed necessary to model the in-place temperature of various types of lightweight concretes, then it is recommended that the thermal properties of these concretes be determined by standardized ASTM test methods.
3. The experimental program used in this study did not evaluate the effect that the use of lightweight aggregate will have on drying shrinkage or concrete and its effect on the long-term performance of bridge decks should be evaluated.
4. The degree of hydration was determined indirectly from semi-adiabatic calorimeter test results. The degree of hydration should be confirmed with isothermal calorimetry or by methods to determine chemically bound water.
5. The Modified B3 Model was determined through best-fit of the data assuming superposition was valid. The early-age compliance of specimen with singular loading ages and stress should be determined to further calibrate the modifications.
6. The research focused on the stress development of bridge deck concrete. The effect of lightweight aggregates on early-age stress development of mass concrete, precast concrete, and concrete pavement applications should also be investigated.

REFERENCES

AASHTO T 336. 2009. *Standard Method of Test for Coefficient of Thermal Expansion of Hydraulic Cement Concrete*. Washington DC, American Association of State Highway and Transportation Officials.

AASHTO. 2007. *LRFD Bridge Design Specifications*. 4th Edition with 2009 interim revisions. Washington DC, American Association of State Highway and Transportation Officials.

ACI 318. 2008. *Building Code Requirements for Structural Concrete and Commentary*. Farmington Hills, MI, American Concrete Institute.

ACI 207.1R. 1996. *Mass Concrete*. Farmington Hills, MI, American Concrete Institute.

ACI 207.2R. 1995. *Effect of Restraint, Volume Change, and Reinforcement on Cracking of Mass Concrete.* Farmington Hills, MI, American Concrete Institute.

ACI 209.2 R. 2008. *Guide for Modeling and Calculating Shrinkage and Creep in Hardened Concrete.* Farmington Hills, MI, American Concrete Institute.

ACI 209R. 1992. *Prediction of Creep, Shrinkage, and Temperature Effects in Concrete Strucures.* Farmington Hills, MI, American Concrete Institute.

ACI 211.1R. 1991. *Standard Practice for Selecting Proportions for Normal, Heavyweight, and Mass Concrete*. Farmington Hills, MI, American Concrete Institute.

Bažant, Z.P. 1982. Mathamatical Models for Creep and Shrinkage of Concrete. *In Creep and Shrinkage in Concrete Structures.* eds. Z.P. Bažant and F.H. Wittmann. John Wiley and Sons. pp. 163-258.

Bažant, Z.P., and S. Baweja. 1995. Creep and Shrinkage Prediction Model for Analysis and Design of Concrete Structures-Model B3. *Materials and Structures.* Vol. 28, pp. 357-365.

Bažant, Z.P., and S. Baweja. 2000. Creep and Shrinkage Prediction Model for Analysis and Design of Concrete Structures (B3). *The Adam Neville Symposium: Creep and Shrinkage-Structural Design Effects,* ACI SP-194. ed. A. Al-Manaseer American Concrete Institute, Farmington Hills, MI, pp. 1-83.

Bažant, Z.P., and L.J. Najjarr. 1972. Nonlinear Water Diffusion in Nonsaturated Concrete. *Materials and Structures.* Vol. 5, pp. 3-22.

Bažant, Z.P, and S. Prasannan. 1989a. Solidification Theory for Concrete Creep I: Formulation. *ASCE Journal of Engineering Mechanics.* Vol. 115, No. 8, pp. 1691-1703.

Bažant, Z.P, and S. Prasannan. 1989b. Solidification Theory for Concrete Creep I: Verification. *ASCE Journal of Engineering Mechanics.* Vol. 115, No. 8, pp. 1704-1725.

Bentz, D.P., P. Lura, and J.W. Roberts. 2005. Mixture Proportioning for Internal Curing. *Concrete International,* Vol. 27, No. 2, pp. 35-40.

Bentz, D. P., and J.W. Weiss. 2011. "Internal Curing: A 2010 State-of-the-Art Review." NIST, Gaithersburg, MD.

Bjøntegaard, Ø. 1999. *Thermal Dilation and Autogenous Deformation as Driving Forces to Self-Induced Stresses in High Performance Concrete*. Doctoral Thesis. Norwegian University of Science and Technology, Division of Structural Engineering. Trondheim, Norway.

Branson, D. E., and M. L. Christiason. 1971. Time Dependent Concrete Properties Related to Design-Strength and Elastic Properties: Creep and Shrinkage. In *Creep, Shrinkage, and Temperature Effects*, SP-27, American Concrete Institute, Farmington Hills, MI. pp. 257-277.

Breitenbücher, R., and M. Mangold. 1995. Minimization of Thermal Cracking in Concrete at Early Ages. In RILEM Proceedings 25, *Thermal Cracking in Concrete at Early Ages*, ed. R. Springenschmid, London, E & FN Spon, pp. 205-212.

Byard, B. E., and A.K. Schindler. 2010. *Cracking Tendency of Lightweight Concrete.* Highway Research Center, Research Report, Auburn, AL.

Byard, B.E., A.K. Schindler, and R.W. Barnes. 2010. Cracking Tendency of Lightweight Concrete in Bridge Deck Applications, *Proceedings of the Concrete Bridge Conference*, Phoenix, AZ.

Byard, B.E, A.K. Schindler, R.W. Barnes, and A. Rao. 2010. Cracking Tendency of Bridge Deck Concrete, *Journal of the Transportation Research Board*, TRR No. 2164, pp. 122-131.

Carino, N.J. 2004. *The Maturity Method.* In Handbook on Nondestructive Testing of Concrete, 2nd ed., ed. V.M. Malhotra and N.J. Carino, 5.1-5.47. West Conshocken, Pennsylvania: ASTM International.

Castro, J., L. Keiser, M. Golias, and W.J. Weiss. 2011. Absorption and Desorption of Fine Lightweight Aggregate for Applications to Internally Cured Concrete Mixtures. *Cement and Concrete Composites,* Vol. 33, No 10, pp. 1001-1008.

CEB. 1999. *Structural Concrete: Textbook on Behaviour, Design, and Performance. Updated Knowledge of the CEB/FIP Model Code 1990.* Fib Bulletin 2 V. 2, Federation Internationale du Béton, Lausanne, Switzerland. pp. 37-52.

Chandra, S., and L. Berntsson. 2002. *Lightweight Aggregate Concrete.* Noyes Publications, Norwich, NY.

Coussy, O. 2010. *Mechanics and Physics of Porous Solids*. Wiley, John and Sons. Hoboken, NJ.

Darwin, D., and J. Browning. 2008. Construction of Low Cracking High Performance Concrete Bridge Decks: Field Experience. *Proceedings of the Concrete Bridge Conference*, St. Louis, MO. May 4-7.

Delatte, N., D. Crowl, E. Mack, and J. Cleary. 2008. Evaluating High Absorptive Materials to Improve Internal Curing of Concrete. In ACI SP 256, *Internal Curing of High-Performance Concretes,* ed. D. Bentz and B. Mohr. Farmington Hills, MI.

Emborg, M. 1989. *Thermal Stresses in Concrete Structures at Early Ages*. Doctoral Thesis. Luleå University of Technology. Luleå, Sweden.

ESCSI. 2007. *Reference Manual for the Properties and Applications of Expanded Shale, Clay and Slate Lightweight Aggregate*. ESCSI, Salt Lake City, UT.

FHWA. 2008. *Cast-in-Place High Performance Concrete.* Federal Highway Administration High Performance Concrete Website,

http://knowledge.fhwa.dot.gov/cops/hpcx.nsf/home?openform&Group=HPC%20Cast-in-Place%20Construction&tab=WIP, accessed 2008.

Freiesleben Hansen, P., and J. Pederson. 1977. Maturity Computer for Controlled Curing and Hardening of Concrete. *Nordisk Betong.* Vol.1, No. 19, pp.19-34.

Harmon, K.S. 2000. Physical Characteristics of Rotary Kiln Expanded Slate Lightweight Aggregate, *Proceeding of the 2nd International Symposium on Structural Lightweight Aggregate Concrete*, Kristiansand, Norway, June 18-22, pp. 574-583.

Gardner, N. J., and M. J. Lockman. 2001. Design Provisions for Drying Shrinkage and Creep of Normal Strength Concrete. *ACI Materials Journal*, Vol. 98, No. 5, pp. 159-167.

Gardner, N.J., and J.W. Zhao. 1993. Creep and Shrinkage Revisited. *ACI Materials Journal*, Vol. 90, No. 3, pp. 236-246.

Golias, M.E. 2010. *The Use of Soy Methyl Ester-Polystyrene Sealants and Internal Curing to Enhance Concrete Durability*. Masters Thesis, Purdue University, Purdue, IN.

Grasley, Z.C. 2003. *Measuring and Modeling the Time-Dependent Response of Cementitious Materials to Internal Stresses.* Ph.D. Thesis. University of Illinois at Urbana-Champaign. Urbana, IL.

Gutch, A. and F. S. Rostásy. 1995. Young Concrete Under High Tensile Stresses – Creep, Relaxation, and Cracking. In RILEM Proceedings 25, *Thermal Cracking*

in Concrete at Early Ages, ed. R. Springenschmid, London, E & FN Spon, pp. 111-118.

Hammer, T.A. 1999. Test Methods for Linear Measurements of Autogenous Shrinkage Before Setting. In *Autogenous Shrinkage of Concrete*. ed. Ei-ichi Tazawa, E & FN Spon, London, pp. 143-154.

Hansen, T. C. 1986. Physical Structure of Hardened Cement Paste: A Classical Approach. *Materials and Structures*, Vol. 10, No3, pp. 423-436.

Henkensiefken, R. 2008. *Internal Curing in Cementitious Systems made using Saturated Lightweight Aggregate.* Masters Thesis. Purdue University. Purdue, IN.

Holt, E. 2001. *Early Age Autogenous Shrinkage of Concrete*. Doctoral Thesis. The University of Washington in Seattle. Seattle, WA.

Jensen, O. M., and P. F. Hansen. 2001. Water-Entrained Cement-Based Materials - I. Principles and Theoretical Background. *Cement and Concrete Research*, Vol. 31, No. 4, pp.647-654.

Krauss, P.D., and E.A. Rogalla. 1996. *Transverse Cracking in Newly Constructed Bridge Decks*. NCHRP Report 380, Transportation Research Board, National Research Council, Washington, D.C.

L'Hermite, R.G. 1960. Volume Changes of Concrete. *Fourth International Symposium on the Chemistry of Cement.* Wahsington D.C. pp. 659-702.

Lamond, J.F., and J.H. Pielert. 2006. *Significance of Tests and Properties of Concrete and Concrete-Making Materials*. ASTM Publication STP 169D. American Society of Testing Materials, West Conshohocken, PA.

Lura, P. 2003. *Autogenous Deformation and Internal Curing of Concrete.* Doctoral Thesis. Technical University of Delft. Delft, The Netherlands.

Lura, P., D.P. Bentz, D.A. Lange, K. Kovler, and A. Bentur. 2004. Pumice Aggregates for Internal Water Curing. *Proceedings of International RILEM Symposium on Concrete Science and Engineering: A Tribute to Arnon Bentur*. Evanston, IL. March 22-24, pp.137-151.

Maggenti, R. 2007. From Passive to Active Thermal Control. *Concrete International,* Vol. 29, No. 2, pp. 24-30.

Mangold, M. 1998. Methods for Experimental Determination of Thermal Stresses and Crack Sensitivity in the Laboratory. In RILEM Report 15, *Prevention of Thermal Cracking in Concrete at Early Ages*, ed. R. Springenschmid, London, E & FN Spon, pp. 26-39.

McCuen, R.H. 1985. *Statistical Methods for Engineers*, Prentice-Hall. Upper Saddle River, NJ.

McHenry, D. 1943. A New Aspect of Creep in Concrete and its Application to Design. *Proceedings of the American Society of Testing Materials*. Vol. 43. pp. 1069-1084.

McIntosh, J.D. 1949. Electrical Curing of Concrete. *Magazine of Concrete Research.* Vol. 1, No. 1, pp. 21-28.

Meadows, J.L. 2007. *Early-Age Cracking of Mass Concrete Structures.* Master Thesis. Auburn University. Auburn, AL.

Mehta, P.K., and P.J.M. Monteiro. 2006. *Concrete: Microstructure, Properties, and Materials*. 3rd Edition, McGraw-Hill, Inc. New York, NY.

Mills, R. H. 1966. Factors Influencing Cessation of Hydration in Water-Cured Cement Paste. *Proceedings of the Symposium on Structure of Portland Cement Paste and Concrete*, Highway Research Board, Washington, DC, 406-424.

Mindess, S., J.F. Young, and D. Darwin. 2002. *Concrete*. 2nd Edition, Prentice Hall, Upper Saddle River, NJ.

Neville, A.M., and J.J. Brooks. 1991. *Concrete Technology*. Revised Edition, Pearson, Edinburgh Gate, England.

Neville, A.M., W.H. Dilger, and J.J. Brooks. 1983. *Creep of Plain and Structural Concrete*. Construction Press, Essex, England.

Østergaard, L., D.A. Lange, S.A. Altoubat, and H. Stang. 2001. Tensile Basic Creep of Early-Age Concrete Under Constant Load. *Cement and Concrete Research*. Vol. 31, pp. 1895-1899.

Pinto, R, and K.C. Hover. 1999. Application of Maturity Approach to Setting Times. *ACI Materials Journal*. Vol. 96, No.6, pp.686-691.

Poole, J.L, K.A. Riding, R.A. Browne, and A.K. Schindler. 2006. Temperature Management of Mass Concrete Structures. *Concrete Construction Magazine*.

RILEM 42 CEA. 1981. Properties of Set Concrete at Early Ages: State of the Art Report. Materials and Structures, Vol. 14, No.84, pp. 399-450.

RILEM Technical Committee 119-TCE. 1998. Testing of the Cracking Tendency of Concrete at Early Ages in the Cracking Frame Test. In RILEM Report 15, *Prevention of Thermal Cracking in Concrete at Early Ages*, ed. R. Springenschmid, London, E & FN Spon, pp. 315-339.

RILEM Technical Committee 196-ICC. 2007. *Internal Curing of Concrete*. ed. K. Kovler and O.M. Jensen, Bagneux, RILEM Publications S.A.R.L.

Sakyi-Bekoe, K.O. 2008. *Assessment of the Coefficient of Thermal Expansion of Alabama Concrete.* Masters Thesis. Auburn University. Auburn, AL.

Scheaffer, R.L., M.S. Mulekar, and J.T. McClave. 2010. *Probability and Statistics for Engineers,* 5th Edition. Brooks/Cole, Boston, Massachusetts.

Schindler, A.K. 2004a. Effect of Temperature on Hydration of Cementitious Materials. *ACI Materials Journal*. Vol. 101, No. 1, pp. 72-81.

Schindler, A.K. 2004b. Prediction of Concrete Setting. Proceedings of the *RILEM International Symposium on Advances in Concrete through Science and Engineering*, eds. J. Weiss, K. Kovler, J. Marchand, and S. Mindess, RILEM Publications SARL, Evanston, Illinois.

Schindler, A.K., and K.J. Folliard. 2005. Heat of Hydration Models for Cementitious Materials. *ACI Materials Journal*, Vol. 102, No. 1, pp. 24-33.

Schindler, A.K., and B.F. McCullough. 2002. The Importance of Concrete Temperature Control During Concrete Pavement Construction in Hot Weather Conditions. *Journal of the Transportation Research Board*, TRR No. 1813, pp. 3-10.

Scripture, E.W. 1956. Setting Time. In *Significance of Tests and Properties of Concrete and Concrete Aggregates*, STP 169, pp. 53-60. Philadelphia, Pennsylvania: ASTM International.

Sokora, E.W. 1980. *Portland Cement Paste and Concrete.* New York: Chemical Publishing Co., Inc.

Sprouse, J.H. and R.B. Peppler. 1978. *Setting Time.* In *Significance of Tests and Properties of Concrete and Concrete-Making Materials,* STP 169B, pp. 105-121. Philadelphia, Pennsylvania: ASTM International.

Tuthill, L.H. and W.A. Cordon. 1955. Properties and Uses of Initially Retarded Concrete. *Journal of the American Concrete Institute* Vol. 52, No. 2. pp. 273-286.

Van Breugel, K. 1997. *Simulation of Hydration and Formation of Structure in Hardening Cement Based Material*. Ph.D. Thesis. Delft University, Delft, Netherlands.

Weakley, R.W. 2009. *Evaluation of Semi-Adiabatic Calorimetry to Quantify Concrete Setting.* Master of Science Thesis. Auburn University, AL.

Westman, G.1999. *Concrete Creep and Thermal Stresses: New Creep Models and their Effect on Stress Development.* Doctoral Thesis. Luleå University of Technology. Luleå, Sweden.

Wight, J.K., and J.G. MacGregor. 2009. *Reinforced Concrete.* 5th Edition Prentice Hall, Upper Saddle River, NJ.

APPENDIX A: AGGREGATE GRADATIONS

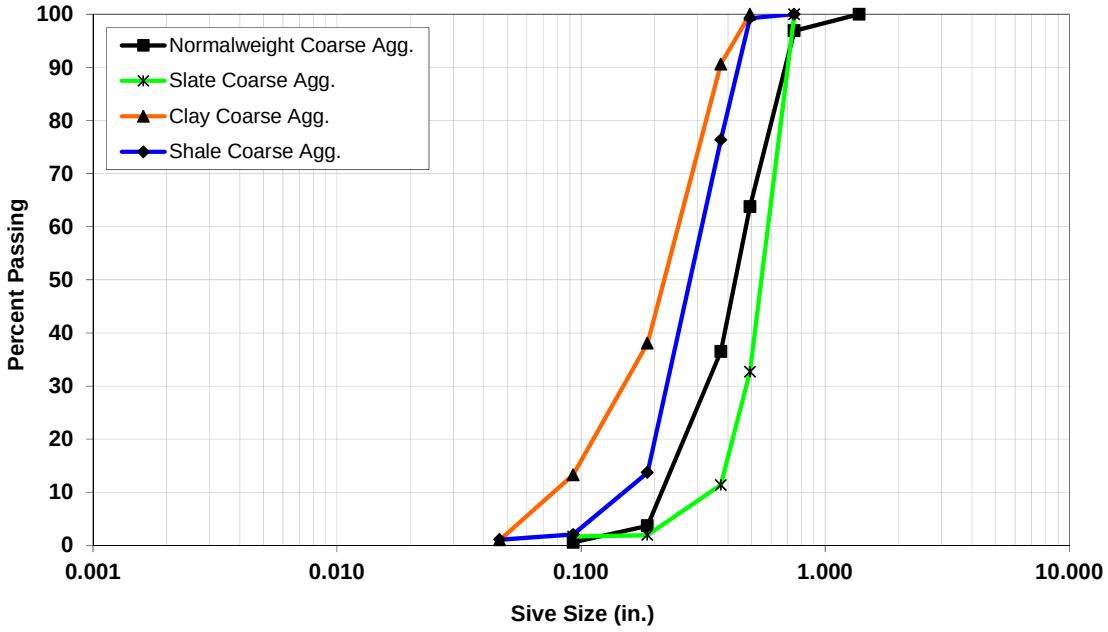

Figure A-1: Coarse aggregate gradations

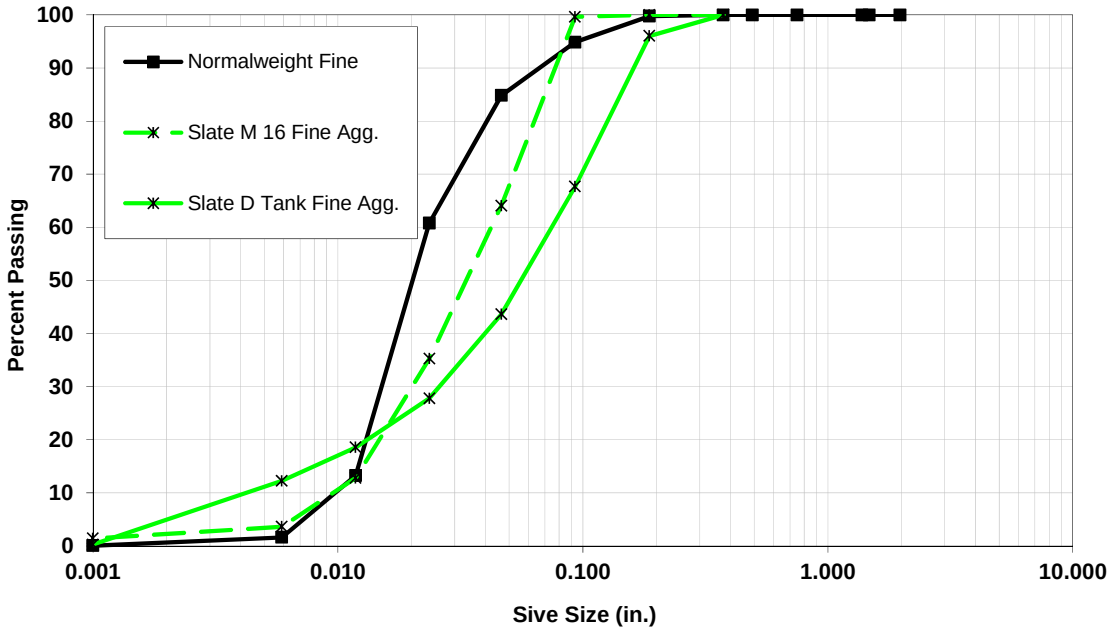

Figure A-2: Slate fine aggregate gradations

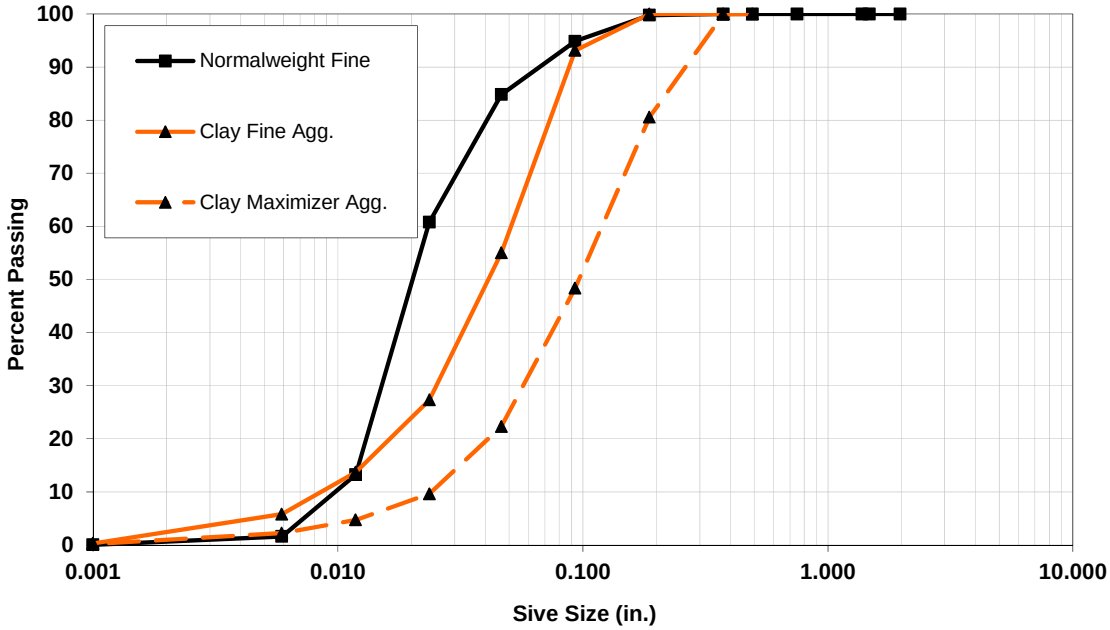

Figure A-3: Clay fine aggregate gradations

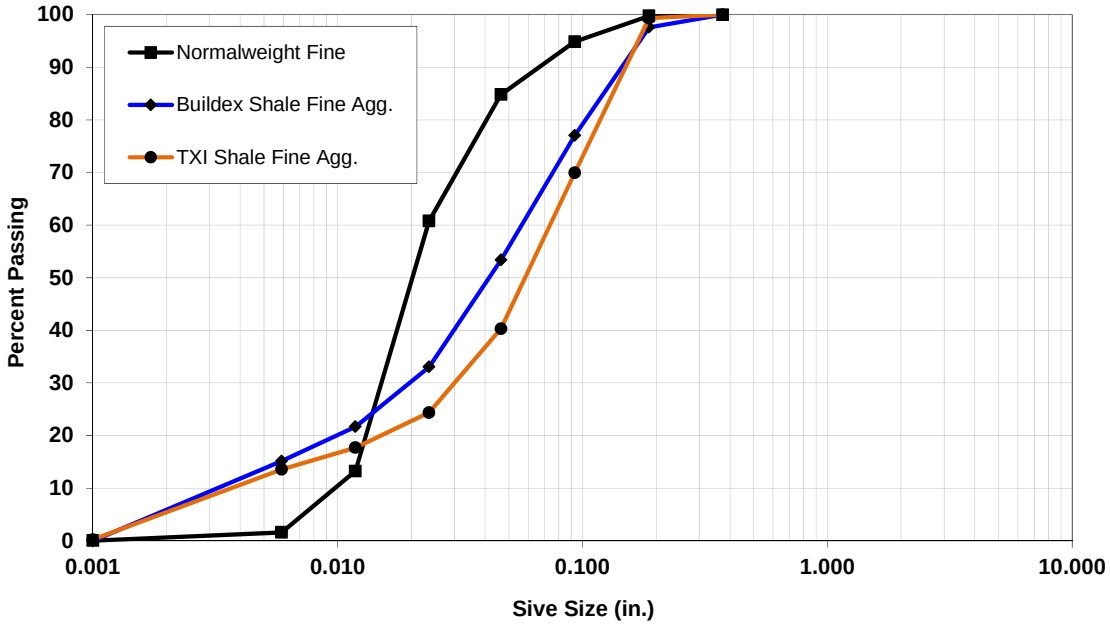

Figure A-4: Shale fine aggregate gradations

APPENDIX B: MECHANICAL PROPERTIES

Table B-1: Compressive strength results

Compressive Strength (psi)						
Mixture	**Match-Cured Concrete Age (days)**					
	1/2	**1**	**2**	**3**	**7**	**28**
Control RG (Fall)	1770	2890	3690	3720	4230	5700
Control RG (Sum)	2330	3210	3750	3820	4100	5310
Slate IC (Fall)	1590	2950	3700	3980	4740	5840
Slate IC (Sum)	2300	3280	3830	4210	4490	5580
Slate SLW (Fall)	1590	2280	3050	3470	4170	5140
Slate SLW (Sum)	2090	2980	3380	3540	4410	5130
Slate ALW (Fall)	1180	1960	2560	2930	2820	4760
Slate ALW (Sum)	1540	2130	2670	3250	3400	4610
Clay IC (Falll)	1950	3160	3900	4130	4530	5820
Clay IC (Sum)	2450	3570	4110	4620	4980	5640
Clay SLW (Falll)	1090	2240	3050	3240	3850	5020
Clay SLW (Sum)	2050	3140	3510	3710	4160	5380
Clay ALW (Falll)	1370	2280	2620	2930	3300	4860
Clay ALW (Sum)	1750	2730	3470	4240	3810	4490
Shale IC (Falll)	1580	2830	3500	3870	4310	5610
Shale IC (Sum)	2380	3380	4080	4300	4510	5640
Shale SLW (Falll)	1370	2460	2920	3260	3720	5040
Shale SLW (Sum)	1970	2620	3470	3680	3970	4920
Shale ALW (Falll)	800	2040	2750	2960	3690	4780
Shale ALW (Sum)	1670	2590	2920	3240	3530	4320
0.42 LS (Fall)	1090	3100	3840	4300	4830	6080
0.42 LS (Sum)	1910	3100	3840	4300	4830	5630
0.36 RG (Fall)	2935	4232	4875	4975	5300	6435
0.36 ICM (Fall)	2780	4420	4810	5245	5675	6890
0.36 ICH (Fall)	2760	4095	4835	5165	5565	6960
0.30 RG (Fall)	4830	6115	6570	6760	7330	8115
0.30 ICM (Fall)	4355	5725	6445	6435	7030	8120
0.30 ICH (Fall)	3595	5520	5995	6685	7815	8860

Table B-2: Splitting tensile strength results

Tensile Strength (psi)						
Mixture	**Match-Cured Concrete Age (days)**					
	1/2	**1**	**2**	**3**	**7**	**28**
Control RG (Fall)	200	280	345	355	385	465
Control RG (Sum)	245	340	370	360	355	410
Slate IC (Fall)	205	320	360	395	420	465
Slate IC (Sum)	245	355	390	350	385	430
Slate SLW (Fall)	200	330	350	370	430	495
Slate SLW (Sum)	225	330	410	425	425	485
Slate ALW (Fall)	170	270	340	375	375	385
Slate ALW (Sum)	210	270	325	350	350	460
Clay IC (Falll)	235	345	405	410	455	505
Clay IC (Sum)	250	310	370	440	405	460
Clay SLW (Falll)	130	275	365	385	440	530
Clay SLW (Sum)	230	370	345	410	475	510
Clay ALW (Falll)	165	270	335	355	430	505
Clay ALW (Sum)	215	295	355	390	435	480
Shale IC (Falll)	215	345	405	420	465	455
Shale IC (Sum)	230	370	415	400	460	505
Shale SLW (Falll)	200	325	405	430	430	500
Shale SLW (Sum)	250	360	405	425	440	520
Shale ALW (Falll)	105	265	340	355	430	445
Shale ALW (Sum)	205	325	365	380	415	485
0.42 LS (Fall)	230	355	435	425	370	450
0.42 LS (Sum)	230	355	435	425	415	500
0.36 RG (Fall)	330	425	450	475	475	485
0.36 ICM (Fall)	305	505	515	495	515	565
0.36 ICH (Fall)	315	395	455	495	495	525
0.30 RG (Fall)	505	550	575	575	600	600
0.30 ICM (Fall)	465	525	540	580	620	665
0.30 ICH (Fall)	365	530	555	545	555	610

Table B-3: Modulus of elasticity results

Modulus of Elasticity (ksi)						
Mixture	**Match-Cured Concrete Age (days)**					
	1/2	**1**	**2**	**3**	**7**	**28**
Control RG (Fall)	2750	3300	3900	3750	4050	4550
Control RG (Sum)	3150	3550	4000	4150	4150	4750
Slate IC (Fall)	2500	3250	3850	3900	4100	4500
Slate IC (Sum)	2850	3400	3650	3650	3950	4200
Slate SLW (Fall)	2200	2800	3000	3250	3150	3500
Slate SLW (Sum)	2300	2800	3000	3000	3100	3550
Slate ALW (Fall)	1450	2100	2300	2300	2450	2450
Slate ALW (Sum)	1750	2100	2250	2350	2400	2650
Clay IC (Falll)	2700	3200	3650	3700	3700	4300
Clay IC (Sum)	3000	3600	3900	4000	4350	4250
Clay SLW (Falll)	1500	2100	2350	2400	2650	2800
Clay SLW (Sum)	2000	2300	2500	2550	2750	2850
Clay ALW (Falll)	1200	1600	1600	1700	1700	2050
Clay ALW (Sum)	1350	1650	1900	2050	1850	2000
Shale IC (Falll)	2600	3350	3600	3500	3900	4350
Shale IC (Sum)	3100	3450	4000	4000	3950	4250
Shale SLW (Falll)	1800	2400	2550	2650	3000	3200
Shale SLW (Sum)	2200	2500	2750	2750	2950	3400
Shale ALW (Falll)	1200	1900	2000	2050	2200	2350
Shale ALW (Sum)	1600	1900	1950	2050	2000	2150
0.42 LS (Fall)	3290	3880	4385	4665	4865	5520
0.42 LS (Sum)	3290	3880	4385	4665	4865	4940
0.36 RG (Fall)	3310	4660	4755	4825	5095	5535
0.36 ICM (Fall)	3270	4105	4595	4855	4925	5250
0.36 ICH (Fall)	3380	3945	4375	4515	4520	4865
0.30 RG (Fall)	4595	5500	5745	5695	5710	5700
0.30 ICM (Fall)	3740	4605	4840	4875	5040	5265
0.30 ICH (Fall)	3625	4530	4790	4695	4730	5170

APPENDIX C: MEASURED AND MODELED STRESS DEVELOPMENT

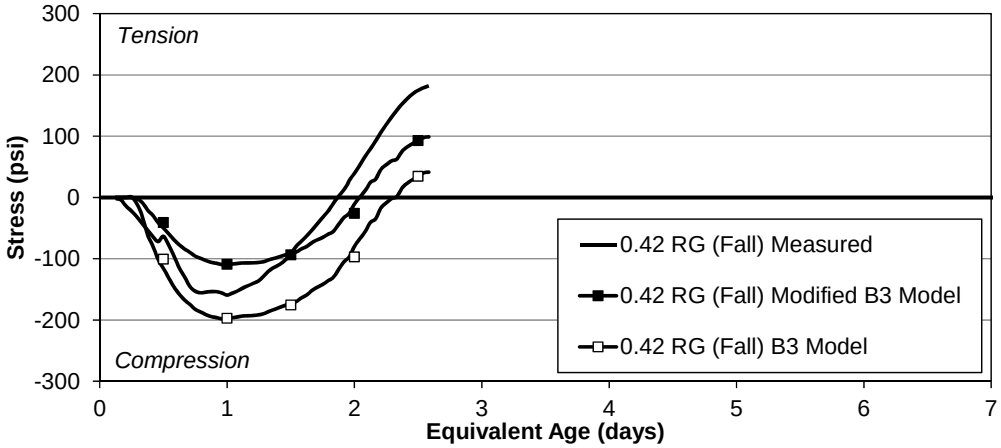

Figure C-1: Measured, B3 Modeled, and Modified B3 Modeled stress development for 0.42 RG (Fall)

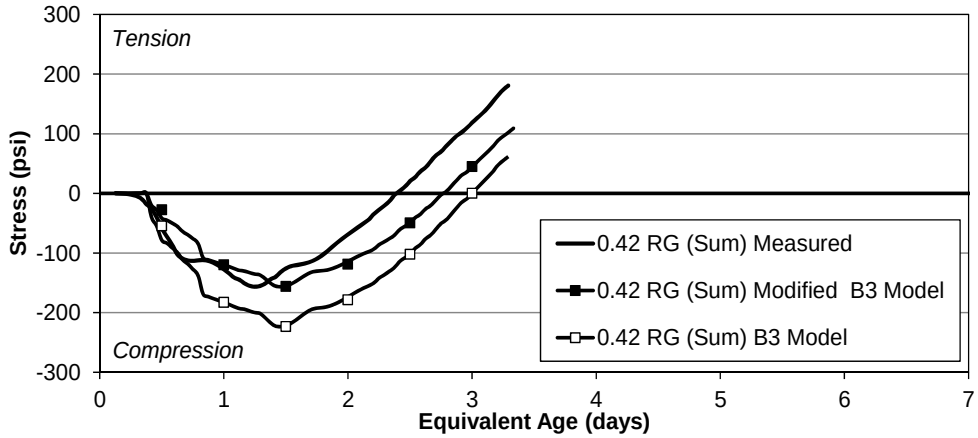

Figure C-2: Measured, B3 Modeled, and Modified B3 Modeled stress development for 0.42 RG (Sum)

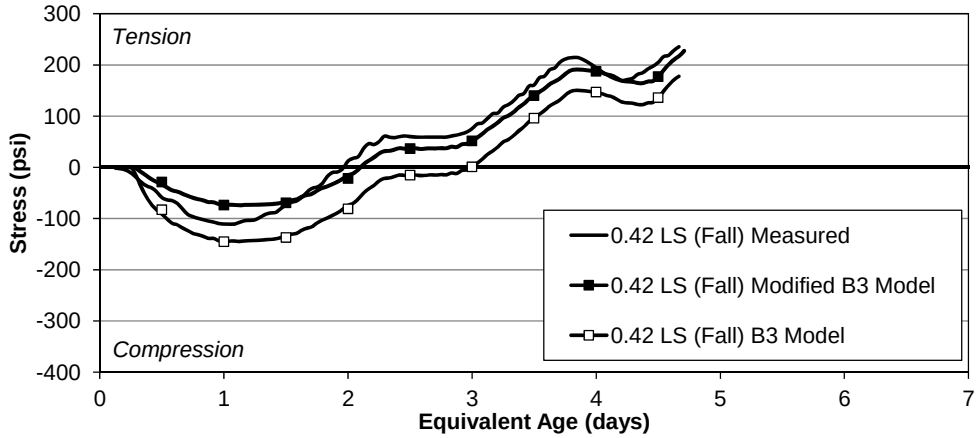

Figure C-3: Measured, B3 Modeled, and Modified B3 Modeled stress development for 0.42 LS (Fall)

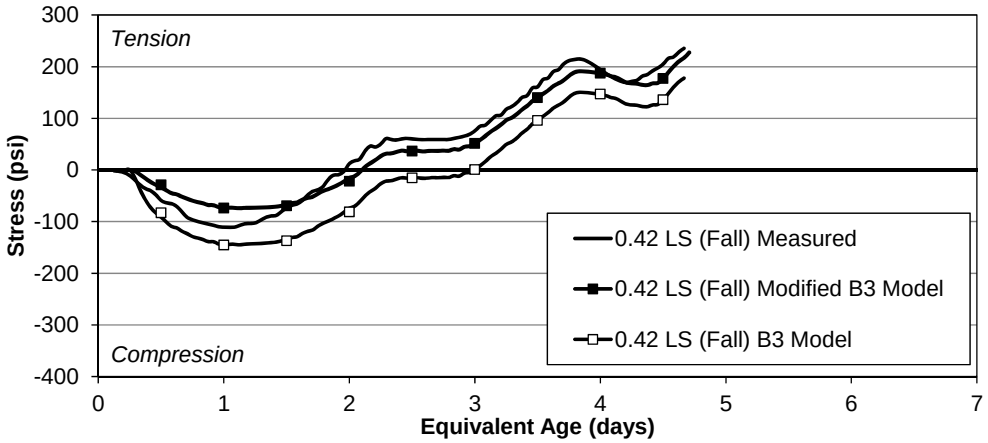

Figure C-4: Measured, B3 Modeled, and Modified B3 Modeled stress development for 0.42 LS (Sum)

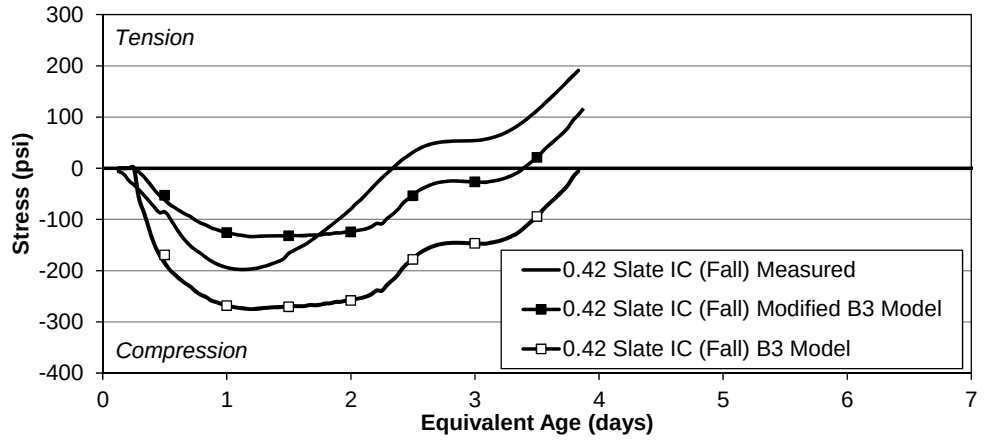

Figure C-5: Measured, B3 Modeled, and Modified B3 Modeled stress development for 0.42 Slate IC (Fall)

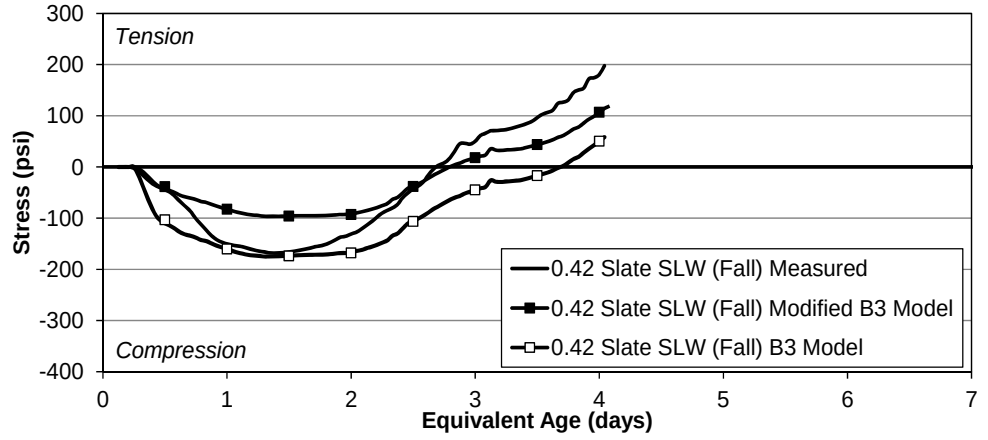

Figure C-6: Measured, B3 Modeled, and Modified B3 Modeled stress development for 0.42 Slate SLW (Fall)

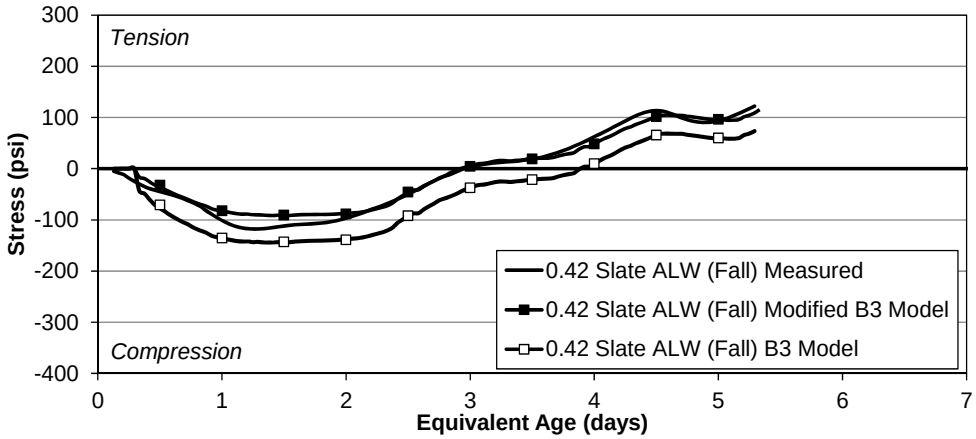

Figure C-7: Measured, B3 Modeled, and Modified B3 Modeled stress development for 0.42 Slate ALW(Fall)

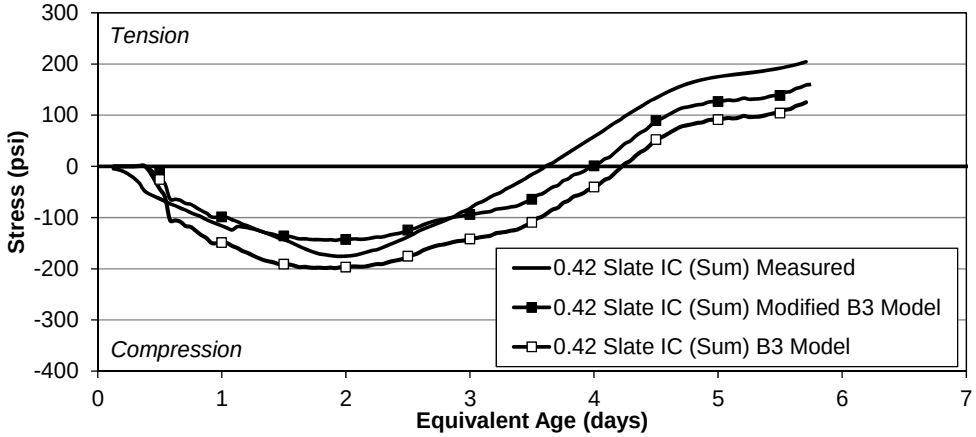

Figure C-8: Measured, B3 Modeled, and Modified B3 Modeled stress development for 0.42 Slate IC (Sum)

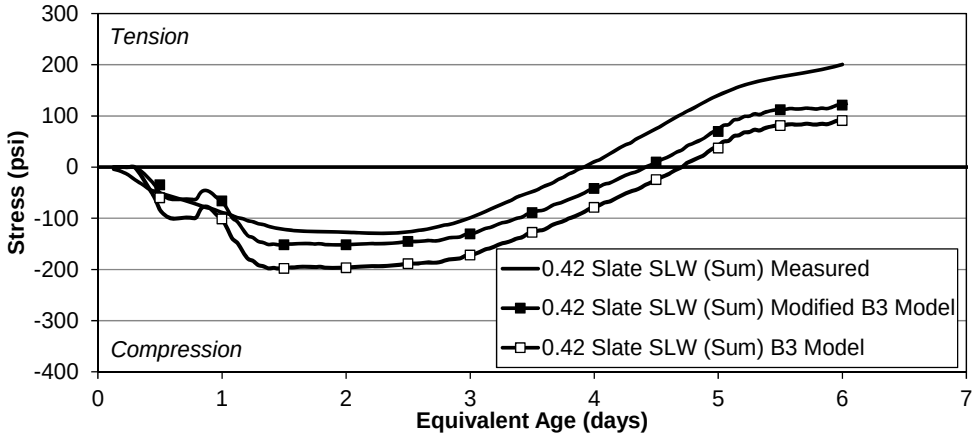

Figure C-9: Measured, B3 Modeled, and Modified B3 Modeled stress development for 0.42 Slate SLW (Sum)

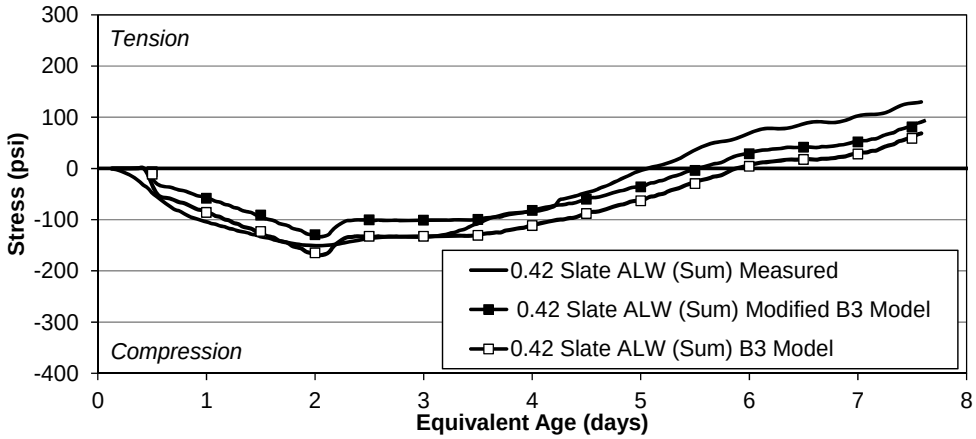

Figure C-10: Measured, B3 Modeled, and Modified B3 Modeled stress development for 0.42 Slate ALW (Sum)

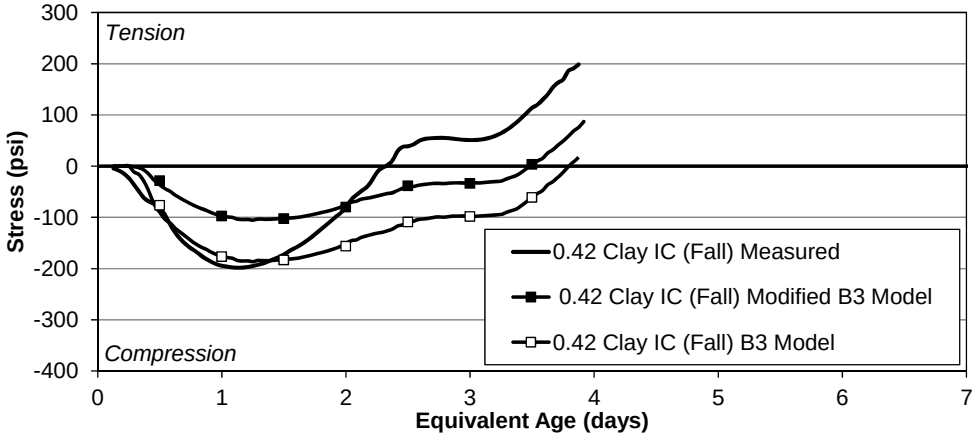

Figure C-11: Measured, B3 Modeled, and Modified B3 Modeled stress development for 0.42 Clay IC (Fall)

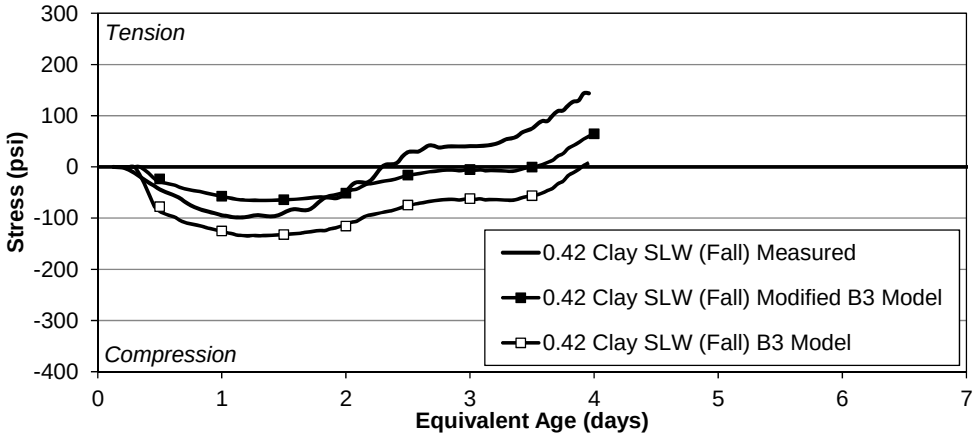

Figure C-12: Measured, B3 Modeled, and Modified B3 Modeled stress development for 0.42 Clay SLW (Fall)

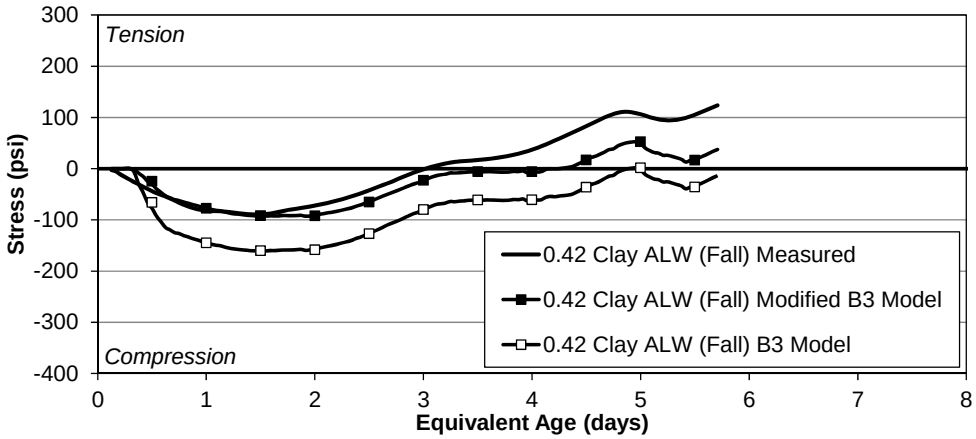

Figure C-13: Measured, B3 Modeled, and Modified B3 Modeled stress development for 0.42 Clay ALW (Fall)

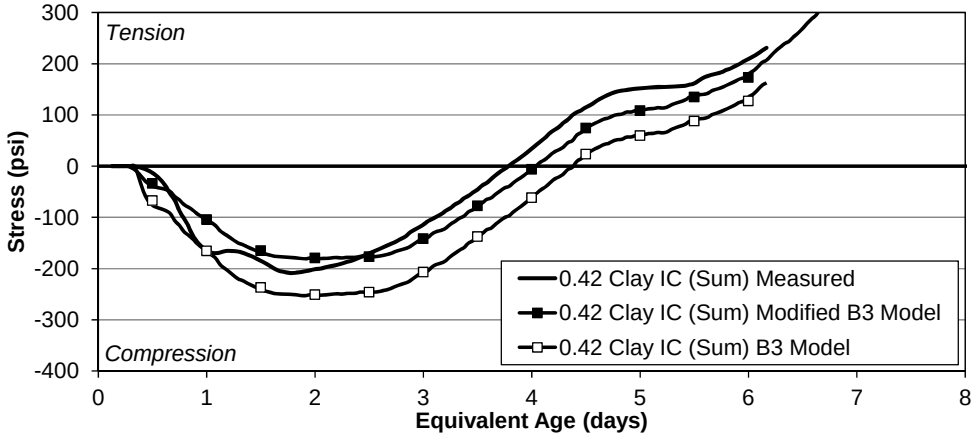

Figure C-14: Measured, B3 Modeled, and Modified B3 Modeled stress development for 0.42 Clay IC (Sum)

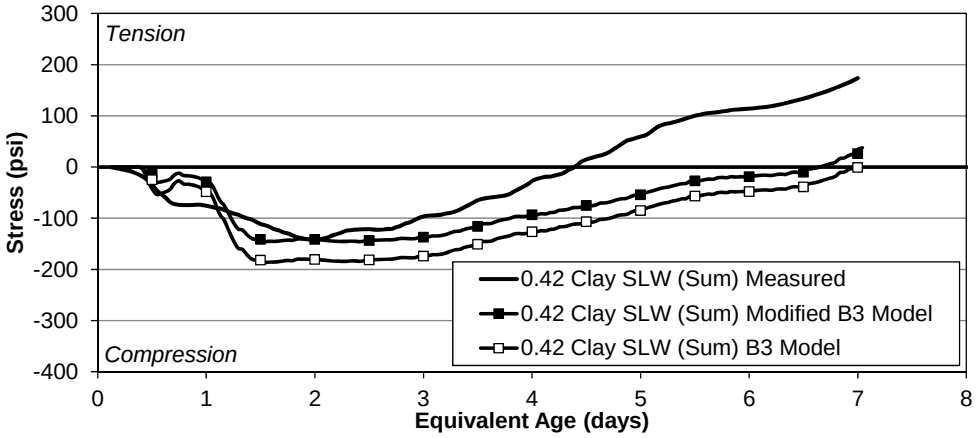

Figure C-15: Measured, B3 Modeled, and Modified B3 Modeled stress development for 0.42 Clay SLW (Sum)

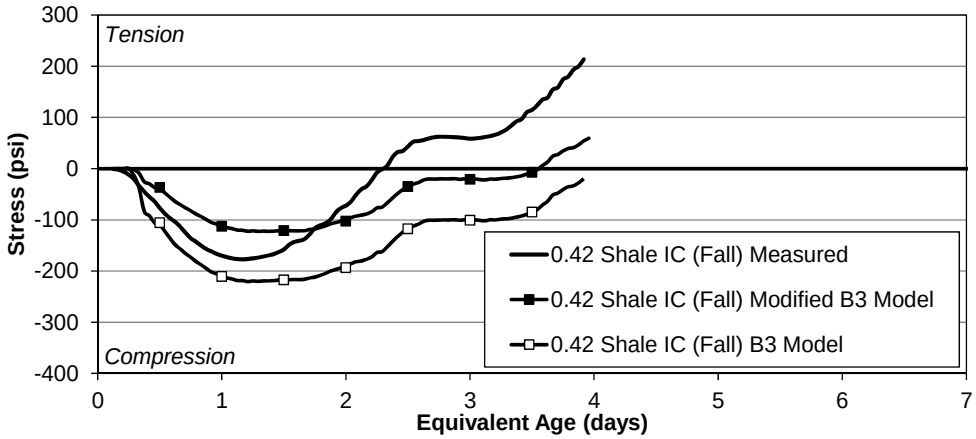

Figure C-16: Measured, B3 Modeled, and Modified B3 Modeled stress development for 0.42 Shale IC (Fall)

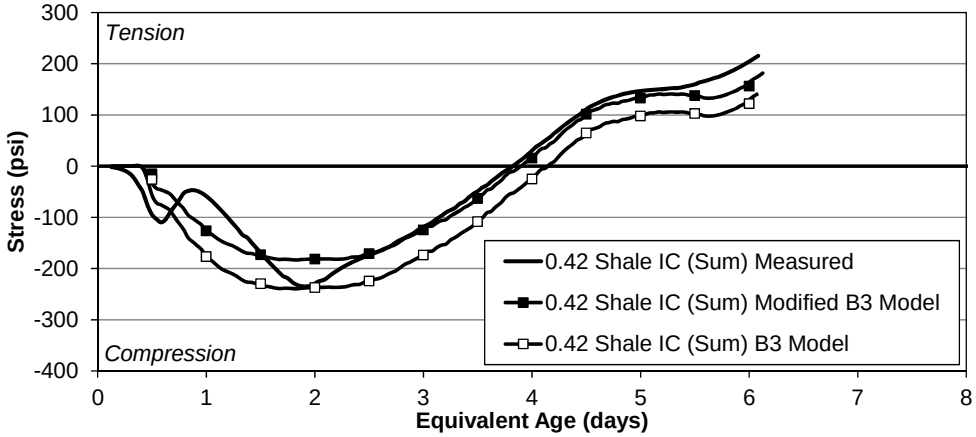

Figure C-17: Measured, B3 Modeled, and Modified B3 Modeled stress development for 0.42 Shale IC (Sum)

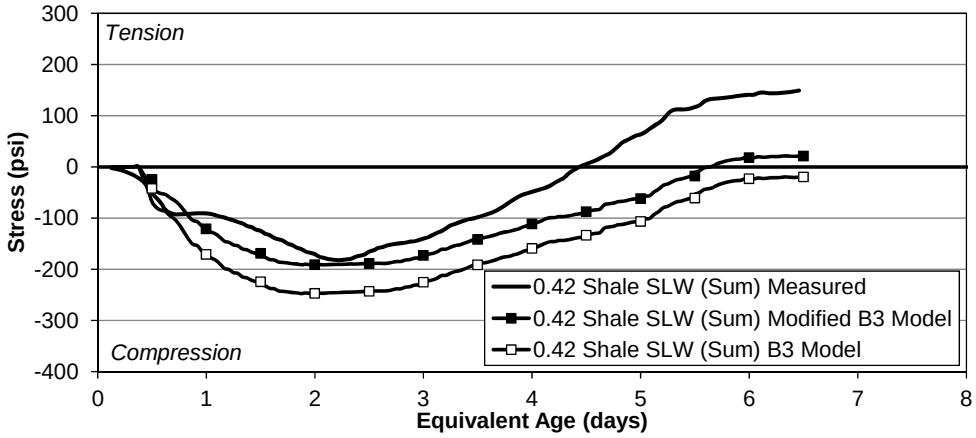

Figure C-18: Measured, B3 Modeled, and Modified B3 Modeled stress development for 0.42 Shale SLW (Sum)

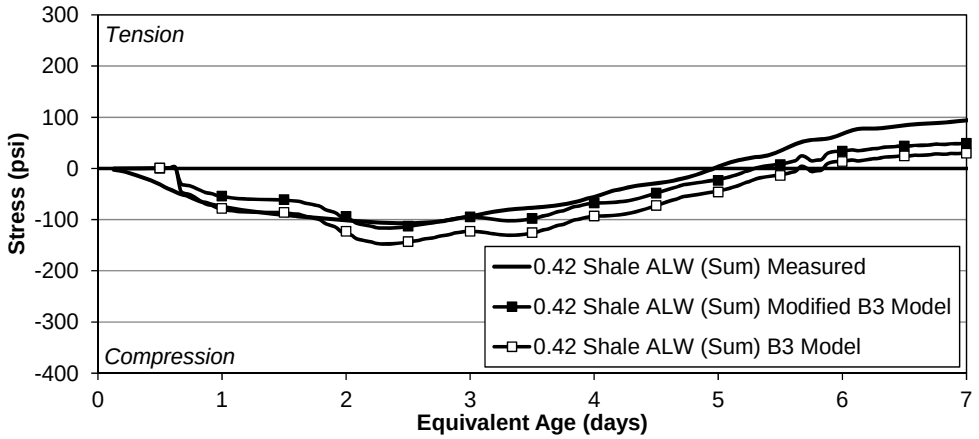

Figure C-19: Measured, B3 Modeled, and Modified B3 Modeled stress development for 0.42 Shale ALW (Sum)

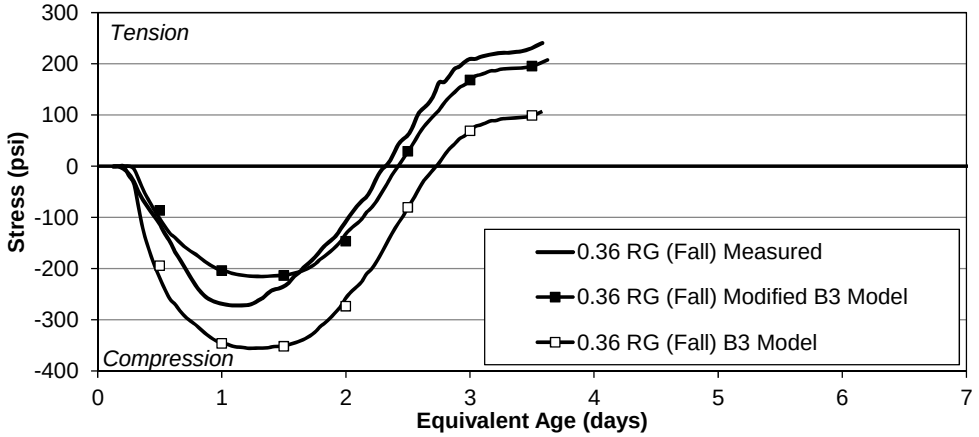

Figure C-20: Measured, B3 Modeled, and Modified B3 Modeled stress development for 0.36 RG (Fall)

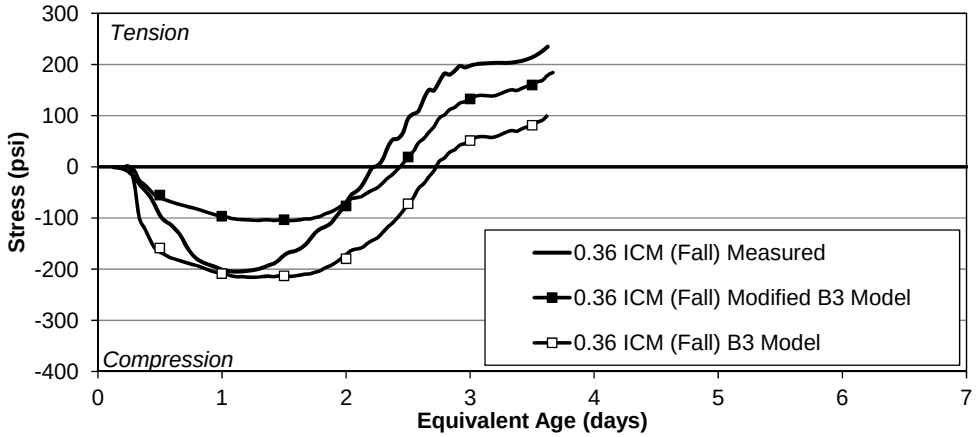

Figure C-21: Measured, B3 Modeled, and Modified B3 Modeled stress development for 0.36 ICM (Fall)

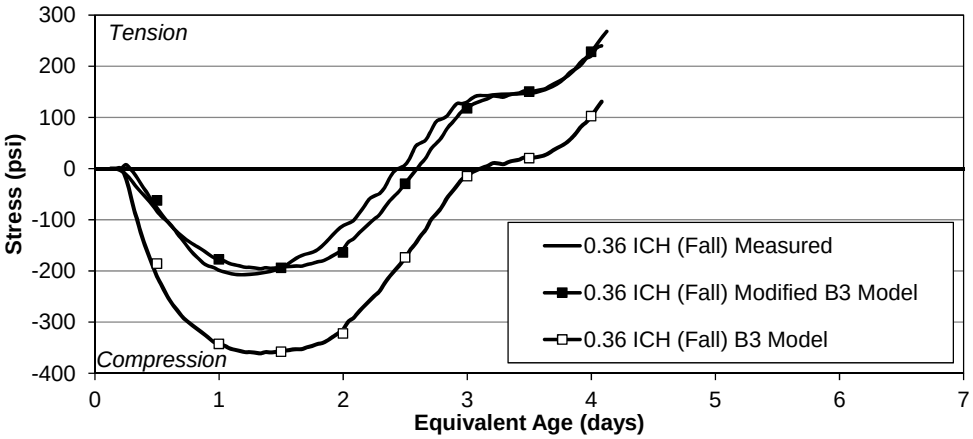

Figure C-22: Measured, B3 Modeled, and Modified B3 Modeled stress development for 0.36 ICH (Fall)

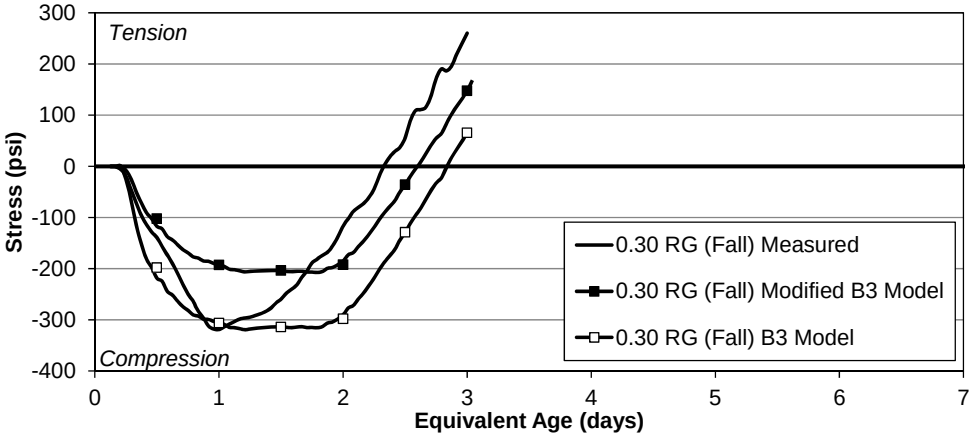

Figure C-23: Measured, B3 Modeled, and Modified B3 Modeled stress development for 0.30 RG (Fall)

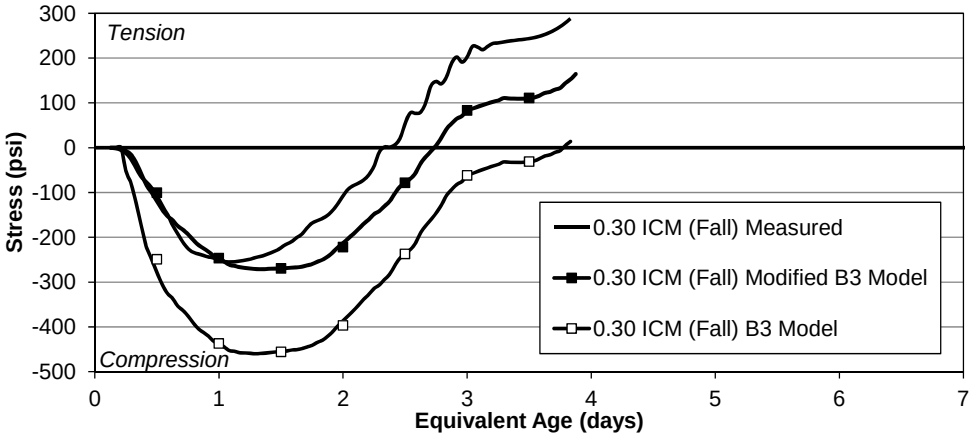

Figure C-24: Measured, B3 Modeled, and Modified B3 Modeled stress development for 0.30 ICM (Fall)

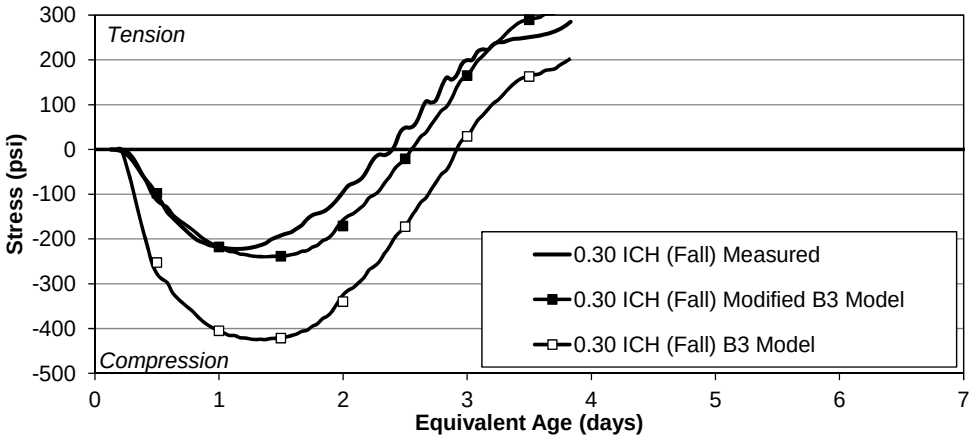

Figure C-25: Measured, B3 Modeled, and Modified B3 Modeled stress development for 0.30 ICH (Fall)